Final Report

INTRODUCTION OF FRACTURE RESISTANCE TO THE DESIGN AND EVALUATION OF OPEN GRADED FRICTION COURSES IN FLORIDA

UF Project No.: 00054539

Contract No.: BD545-53

Submitted to:

Florida Department of Transportation
605 Suwannee Street
Tallahassee, FL 32399

Dr. Reynaldo Roque, P.E.
Chulseung Koh
Yu Chen
Xingsong Sun
George Lopp

Department of Civil and Coastal Engineering
College of Engineering
365 Weil Hall, P.O. Box 116580
Gainesville, FL 32611-6580
Tel: (352) 392-9537 extension 1458
Fax: (352) 392-3394

July 2009

DISCLAIMER

"The opinions, findings and conclusions expressed in this publication are those of the authors and not necessarily those of the Florida Department of Transportation.

Prepared in cooperation with the State of Florida Department of Transportation."

SI* (MODERN METRIC) CONVERSION FACTORS

APPROXIMATE CONVERSIONS TO SI UNITS

Symbol	When You Know	Multiply By	To Find	Symbol
	LENGTH			
in	inches	25.4	millimeters	mm
ft	feet	0.305	meters	m
yd	yards	0.914	meters	m
mi	miles	1.61	kilometers	km
	AREA			
in^2	square inches	645.2	square millimeters	mm^2
ft^2	square feet	0.093	square meters	m^2
yd^2	square yards	0.836	square meters	m^2
ac	acres	0.405	hectares	ha
mi^2	square miles	2.59	square kilometers	km^2
	VOLUME			
fl oz	fluid ounces	29.57	milliliters	ml
gal	gallons	3.785	liters	l
ft^3	cubic feet	0.028	cubic meters	m^3
yd^3	cubic yards	0.765	cubic meters	m^3

NOTE: Volumes greater than 1000 l shall be shown in m^3.

	MASS			
oz	ounces	28.35	grams	g
lb	pounds	0.454	kilograms	kg
T	short tons (2000 lb)	0.907	megagrams	Mg
	TEMPERATURE (exact)			
°F	Fahrenheit temperature	5(F-32)/9 or (F-32)/1.8	Celcius temperature	°C
	ILLUMINATION			
fc	foot-candles	10.76	lux	l
fl	foot-Lamberts	3.426	candela/m^2	cd/m^2
	FORCE and PRESSURE or STRESS			
lbf	poundforce	4.45	newtons	N
psi	poundforce per square inch	6.89	kilopascals	kPa

APPROXIMATE CONVERSIONS FROM SI UNITS

Symbol	When You Know	Multiply By	To Find	Symbol
	LENGTH			
mm	millimeters	0.039	inches	in
m	meters	3.28	feet	ft
m	meters	1.09	yards	yd
km	kilometers	0.621	miles	mi
	AREA			
mm^2	square millimeters	0.0016	square inches	in^2
m^2	square meters	10.764	square feet	ft^2
m^2	square meters	1.195	square yards	yd^2
ha	hectares	2.47	acres	ac
km^2	square kilometers	0.386	square miles	mi^2
	VOLUME			
ml	milliliters	0.034	fluid ounces	fl oz
l	liters	0.264	gallons	gal
m^3	cubic meters	35.71	cubic feet	ft^3
m^3	cubic meters	1.307	cubic yards	yd^3
	MASS			
g	grams	0.035	ounces	oz
kg	kilograms	2.202	pounds	lb
Mg	megagrams	1.103	short tons (2000 lb)	T
	TEMPERATURE (exact)			
°C	Celcius temperature	1.8C + 32	Fahrenheit temperature	°F
	ILLUMINATION			
lx	lux	0.0929	foot-candles	fc
cd/m^2	candela/m^2	0.2919	foot-Lamberts	fl
	FORCE and PRESSURE or STRESS			
N	newtons	0.225	poundforce	lbf
kPa	kilopascals	0.145	poundforce per square inch	psi

* SI is the symbol for the International System of Units. Appropriate rounding should be made to comply with Section 4 of ASTM E380.

(Revised August 1992)

Technical Report Documentation Page

1. Report No.	2. Government Accession No.	3. Recipient's Catalog No.
Final		

4. Title and Subtitle	5. Report Date
Introduction of Fracture Resistance to the Design and Evaluation of Open Graded Friction Courses in Florida	July 2009
	6. Performing Organization Code 0054539
7. Author(s) Reynaldo Roque, Chulseung Koh, Yu Chen, Xingsong Sun, and George Lopp	8. Performing Organization Report No.
9. Performing Organization Name and Address University of Florida Department of Civil and Coastal Engineering 365 Weil Hall P.O. Box 116580 Gainesville, FL 32611-6580	10. Work Unit No. (TRAIS)
	11. Contract or Grant No. BD-545 #53
12. Sponsoring Agency Name and Address Florida Department of Transportation Research Management Center 605 Suwannee Street, MS 30 Tallahassee, FL 32399	13. Type of Report and Period Covered Final 6/17/05-4/30/09
	14. Sponsoring Agency Code

15. Supplementary Notes

16. Abstract

A dog-bone direct tension test (DBDT) to accurately determine tensile properties of asphalt concrete, including OGFC, was conceived, developed and validated. Resilient modulus, creep, and strength tests were performed at multiple temperatures on dense-graded and OGFC mixtures produced two aggregates with both the newly developed DBDT and existing Superpave IDT. Excellent correspondence was observed between properties determined from each type of test, indicating that fundamental properties can be accurately determined using either test. Differences in strain rate between the two tests resulted in expected differences in strength and failure strain. Creep compliance was highly correlated between the two tests but was lower for IDT than for DBDT, which can be attributed to the higher confinement in IDT. It was concluded that DBDT compliance is more appropriate for uniaxial stress states, while IDT compliance is more appropriate for biaxial stress states. Continued use of Superpave IDT was recommended because it is much more practical. A composite specimen (OGFC on HMA) direct tension fracture test was developed to evaluate the effects of OGFC and interface conditions on top-down cracking performance. Results indicated that use of polymer modified bonding agents can significantly improve cracking resistance of pavements with OGFC. Continuum and micro-mechanics based FEM models developed to predict cracking performance of composite mixtures indicated that traditional OGFC accelerates development of top-down cracking and should not be assigned a structural benefit in pavement design. The modeling results also indicated the benefit of polymer-modified bonding agents. The benefits of using micro-mechanics to optimize OGFC design were illustrated. Recommendations were made for continued development and validation of testing and modeling of composite systems to optimize OGFC design.

17. Key Word	18. Distribution Statement
OGFC, Superpave IDT, Direct Tension Test, DBDT, Bonded Interlayer, Multi-Scale Analysis	No restrictions. This document is available to the public through the National Technical Information Service, Springfield, VA, 22161

19. Security Classif. (of this report)	20. Security Classif. (of this page)	21. No. of Pages	22. Price
Unclassified	Unclassified		

Form DOT F 1700.7 (8-72) Reproduction of completed page authorized

ACKNOWLEDGMENTS

The authors would like to acknowledge and thank the Florida Department of Transportation (FDOT) for providing technical and financial support and materials for this project. Special thanks go to engineers and technicians of the Bituminous Section of the State Materials Office for their contributions in terms of their expert knowledge, experience, and constructive advice throughout the course of this work. Their efforts are sincerely appreciated and clearly made a positive impact on the quality of the research.

EXECUTIVE SUMMARY

This study was conducted to evaluate the effects of open graded friction course (OGFC) mixture on top-down cracking resistance of asphalt pavement. Since its introduction, OGFC as a surface layer has provided unique functions such as quick drainage due to high air void, increase in skid resistance, and reduction in pavement noise. However, the tensile properties of this mixture, which may play a strong role in the top-down cracking performance of asphalt pavement, have not been properly evaluated. In addition, the effect of using bonded interface (e.g., Novabond tack coat) on performance has not been properly investigated. Stress development at the top of the asphalt structural layer may be significantly affected by the material properties/characteristics of open graded asphalt mixture and interface conditions with the underlying structural layer. Therefore, it is necessary to accurately and reliably determine the fracture properties of open graded asphalt mixture and to assess the effect of bonded interface to determine their overall contribution to top-down cracking resistance of the pavement structure.

A dog-bone direct tension test (DBDT), associated components and sub-assemblies to accurately determine tensile properties of asphalt concrete, including OGFC, was conceived, developed and validated. DBDT has some advantages over other tension testing systems. The primary advantage of DBDT over other direct tension test systems is the fact that the failure plane is known a priori so that failure limits can be measured directly on that plane. Also, DBDT can be used to test both laboratory gyratory compacted specimens and field cores. Proper data reduction, analysis methods, and correction factors were developed based on three dimensional finite element analysis to account for non-uniform stress, strain, and rotation effects. The newly developed DBDT and existing Superpave IDT were used to perform resilient modulus, creep, and strength tests at multiple temperatures on dense-graded and OGFC mixtures produced with two aggregates. Tensile properties of dense and open graded asphalt mixture were successfully

obtained and both testing systems provided reasonable and consistent test results with respect to temperature and aging. Excellent correspondence was observed between properties determined from each type of test, indicating that fundamental properties can be accurately determined using either test. Differences in strain rate between the two tests resulted in expected differences in strength and failure strain. Creep compliance was highly correlated between the two tests but was lower for IDT than for DBDT, an effect that was attributed to the higher confinement in IDT. It was concluded that DBDT compliance is more appropriate for uniaxial stress states, while IDT compliance is more appropriate for biaxial stress states. That provides additional reason why conditions at the surface are more conducive to top-down cracking. Continued use of Superpave IDT was recommended because it is much more practical.

Additional FEM analyses and initial tests performed on composite specimens (OGFC on HMA) revealed that testing and interpretation of composite specimens involved unique challenges that had to be overcome to obtain relevant results. It was determined that although the dog-bone configuration is ideal for uniform specimens composed of a single mixture, it was not suitable for testing composite specimens; the dog-bone specimen results in excessively non-uniform and complex stress states in composite specimens. Therefore, a new direct tension test for composite specimens was conceived and specimen and loading conditions were investigated to simulate top-down cracking behavior. A composite specimen direct tension fracture test was developed to evaluate the effects of OGFC and interface conditions on top-down cracking performance. Results indicated that use of polymer modified bonding agents can significantly improve cracking resistance of pavements with OGFC.

Finite element method was used to perform both continuum analysis and multi-scale analysis, involving the combined use of continuum and micro-mechanics, to develop models of

OGFC on HMA, including the interface between them. In the multi-scale approach, a finite element model was used to predict the global pavement response, which defined the boundary conditions for the micro mechanical model used to predict the local response of the OGFC and the bonded interface. Predictions from both modeling approaches, using OGFC and HMA properties obtained from tests performed in this study, indicated that traditional OGFC with conventional tack coat accelerates development of top-down cracking compared to pavements with no OGFC. The primary reason for reduced cracking performance is that OGFC has much lower fracture energy than dense graded HMA. The modeling results also indicated the benefit of polymer-modified bonding agents. The benefits of using micro-mechanics to optimize OGFC design were illustrated. The composite mixture tests and the numerical modeling were in excellent agreement.

Recommendations were made for continued development and validation of testing and modeling of composite systems to optimize OGFC design. The need to evaluate effects of aging, moisture, and healing on pavement systems with OGFC surfaces was also emphasized.

TABLE OF CONTENTS

LIST OF TABLES

LIST OF FIGURES

CHAPTER 1
INTRODUCTION

1.1 Background

Since its introduction to the United States in the 1940s, open graded friction course (OGFC) or porous/permeable friction course (PFC) has been used primarily as a functional layer that does not increase structural load bearing capacity. The function of this layer includes increasing skid resistance of pavement surface through increased macro and micro texture, quick water drainage with high air void contents, and reduction in pavement noise. With these functional advantages, open graded friction course has attained global attention. In 1978, NCHRP reported that 15 states in the US were using OGFC extensively and several additional states were considering the use of OGFC (Halstead, 1978). Since that time, several state DOTs have initiated an implementation program for OGFC that included work related to its design and construction. Kandhal and Mallick (1998) reported that 19 of 50 highway agencies contacted, including the state of Florida, indicated they were using OGFC. However, several problems were reported with OGFC mixtures, including premature oxidation, early raveling, stripping of the underlying layers, reduction of the OGFC benefits by time through plugging of the surface pores, difficulties during snow and ice removal, and construction difficulties. Furthermore, most if not all open graded friction course mixture design guidelines are empirical in nature. Asphalt content is determined to produce a minimum VMA (Voids in the Mineral Aggregate) at a sufficiently high effective asphalt film thickness to ensure adequate durability of the mixture. Evaluation of this kind mixture has primarily focused on its function such as skid resistance, permeability and

durability. Existing design processes and evaluation methods do not accommodate pavement performance-based criteria (e.g. top-down cracking) for OGFC. However, open graded friction courses may play a key role in top-down cracking performance of pavement. There is suggestive evidence that a good quality and well bonded OGFC results in better top-down cracking performance of the overall pavement. In addition, it seems evident that cracks that develop either in the OGFC or the HMA structural layer can be effectively arrested and/or deterred with appropriate interface conditions between the OGFC and the underlying structural layer by reducing the rate of creep and damage of the composite system.

Surface initiated longitudinal cracking, which is often called top-down cracking, is now recognized as a common distress mode in asphalt pavement. Previously, it was generally thought that load-associated cracking initiated only at the bottom of asphalt layer, and then propagated to the surface (bottom-up cracking). Top-down cracking is predominantly parallel to the asphalt pavement centerline and located in the vicinity of the wheel paths. For years, many researchers all over the world have endeavored to define the underlying mechanisms of top-down cracking. Prior research has indicated that top-down cracking is initiated by critical tensile stresses in the surface of the asphalt pavement due to non-uniform contact stress by modern radial truck tires (Myers et al., 1998; Baladi et al., 2002). These cracks then propagate downward by the combined effects of both load and temperature (Dauzats and Rampal, 1987; Kim, 2005). Many other factors have been associated with this mode of failure as will be discussed in section 2.3. However, the effects of open graded friction course mixtures on the development of this mode of failure have not yet been fully identified or verified. As mentioned earlier, it seems fairly evident that top-down cracking can be affected by the properties and characteristics of open graded friction course mixtures because they are directly exposed to surface tensile stress

induced by traffic loading, thermal stresses, and environmental effects. Thus, it is necessary to properly evaluate fracture resistance of OGFC and bonded interface condition in order to acquire more insight regarding their effect on top-down cracking of pavement.

To date, very little work has been done to evaluate and characterize fracture resistance of open graded asphalt mixture. There are currently several laboratory test methods available to evaluate fracture resistance of asphalt mixture as will be described in section 2.4. Superpave IDT has been widely used to evaluate fracture resistance of dense graded asphalt mixtures. However, there is a concern that the open graded nature of OGFC mixtures may require a modified testing protocol from that used for dense graded mixtures. Previous research by Varadhan (2004) has shown a region of high damage under the loading strips during Superpave IDT testing of open graded asphalt mixtures. In order to overcome this effect, specimen thickness and loading rate during strength testing was increased. However, a study is needed to optimize the test conditions needed to ensure that consistent fracture properties of open graded asphalt mixtures can be obtained with the Superpave IDT. In particular, the effects of temperature need to be evaluated. Based on the experience of the researchers, a lower test temperature will likely minimize the potential problem with localized damage under the loading strips in the Superpave IDT test. As for the bonded interface, only limited work has also been performed on a suitable fracture performance test and test conditions that can characterize its effect on top-down cracking.

Therefore, there is a clear need to identify evaluation methods that allow for the characterization and optimization of fracture resistance of open graded asphalt mixture and interface condition. To achieve this purpose, it is necessary to accurately and reliably determine the fracture properties of open graded asphalt mixture and assess effect of bonded interface to identify the overall contribution to cracking resistance of the total pavement structure.

1.2 Hypothesis

In Florida, it is estimated that top-down cracking accounts for more than 90% of cracking in pavements. According to Florida specification, a friction course is required on most state roads and highways, so it appears that the effect of friction course mixtures and interface condition may play a significant role in the development of the top-down cracking. Dense graded friction courses can be handled as a dense graded structural mix but open graded friction courses are another mater, as indicated in the previous discussion. Hence, the following hypotheses formed the basis for this study.

- Properties and characteristics of OGFC mixture/interface condition have an influence on top-down cracking performance of pavement.
- Fundamental tensile properties of dense and open graded asphalt mixture (i.e., independent of specimen geometry) can be obtained at intermediate temperatures (-10°C to 10°C) using either the Superpave IDT or uniaxial direct tension test.
- Multi-scale FEM analysis is more helpful in explaining reason and achieving understanding with respect to top-down cracking mechanism of the asphalt pavement.

1.3 Objectives

The primary objectives of this research study were as follows:

- Identify an appropriate testing system to accurately and reliably measure relevant tensile properties of open graded asphalt mixtures and dense graded asphalt mixtures in general.

- Develop a dog-bone direct tension test (DBDT), associated components and data interpretation methods for evaluating tensile properties of open graded asphalt mixtures and describe potential benefits of the dog-bone direct tension test system.
- Evaluate tensile properties of open graded asphalt mixture, as well as dense graded asphalt mixture in general with both Superpave IDT and DBDT
- Compare the tensile properties from both proposed direct tension test and Superpave IDT to investigate the fundamental tensile properties of asphalt mixtures and to optimize the use of Superpave IDT for open graded asphalt mixtures.
- Identify key properties and characteristics of thin surface courses that may affect top-down cracking performance to evaluate the contribution of the OGFC to the cracking resistance of the HMA pavement structure.
- Develop a test and analysis system to evaluate the effect of interface conditions on the overall fracture performance of pavement system with OGFC/PFC mixtures.
- Develop a numerical model of different mixture structure to generate the stress distribution for different crack length.
- Develop a multi-scale model of different mixture structure to evaluate the effects of mixture components to the stress distribution, which will affect the growth of crack in the structure.
- Use the Florida HMA fracture mechanics to evaluate the contribution of the OGFC layer and the bond between the OGFC layer and underlying asphalt concrete to the resistance of top-down cracking.

1.4 Scope

This study was initiated because the effect of OGFC and bonded interface condition on the top-down cracking performance has not been extensively investigated. A detailed literature review also revealed that no appropriate test method has been available to determine tensile properties of open graded asphalt mixture and to evaluate fracture resistance of bonded interface. Accurate determination of the tensile properties of dense graded asphalt mixture and reliable assessment of fracture behavior on composite specimen made up of open graded and dense graded asphalt mixture with various interface conditions may allow for clearer understanding of the top-down cracking mechanism. In order to assess their relative contribution to the cracking resistance on overall fracture performance, it is necessary to obtain fracture properties of dense graded and open graded asphalt mixture individually. Also, there is need to evaluate the fracture behavior of composite specimen to verify the contribution of the individual components and the interface condition. Evaluation of the effect of friction course and interface condition on top-down cracking performance may be complicated by combination of aggregates, binders and additives, aging, traffic loading, thermal stress, and many other environmental factors. In order to reduce the level of complication and increase relevancy, this study is primarily focused on well-controlled samples produced in the laboratory.

Regarding individual mixture tests, two mixture types were evaluated for each gradation. Resilient modulus, creep compliance, and strength tests were performed using Superpave IDT and the dog-bone direct tension test developed in this study. Tests were performed at the following temperatures: -10°C, 0°C, 5°C and 10°C. Two aging conditions were used: short term oven aging (STOA) and long term oven aging (LTOA). HMA fracture mechanics model was

used to analyze test results and to make it possible to evaluate fracture resistance of the asphalt mixtures tested.

In order to develop specimen preparation and testing protocols for composite specimen direct tension test, two Superpave dense graded asphalt mixtures were used to evaluate possible damage to the dense graded asphalt mixture induced during the OGFC compaction process. One Superpave dense graded mixture and two open graded mixtures were examined to evaluate the effect of interface conditions.

As for the numerical modeling, two types of FEM models were developed: a continuum model and a multi-scale model. The continuum model was useful for capturing the stress distribution of the pavement structure with different mixtures and conditions while multi-scale model provided more specific information on the effects of the mixture components and conditions on the stress distribution and performance. HMA fracture mechanics was used to determine the relationship of crack length and the load cycles for both models. The contribution of OGFC and bonded interface to the resistance of top-down cracking was evaluated based on the crack growth rate.

1.5 Research Approach

This study focused primarily on identifying the effect of open graded friction course mixture and interface condition on top-down cracking performance of asphalt pavement. For that purpose, an appropriate test method to accurately and reliably obtain tensile properties of open graded asphalt mixtures was conceived and identified. Also, a new test system for evaluating composite specimens, which consists of an open graded and dense graded asphalt mixture with various interface conditions, was developed. For numerical modeling, the finite element

modeling (FEM) was used for continuum and multi-scale analysis. The approach used involved the following steps:

- Review previous research on open graded friction course, bonded interface pavement systems, top-down cracking mechanism, and existing methods to obtain tensile properties of asphalt mixture for assessing top-down cracking performance.
- Develop and validate a dog-bone direct tension test (DBDT) and associated data interpretation method and investigate its feasibility and accuracy for determining tensile properties of asphalt mixtures.
- Conduct laboratory tests using Superpave IDT and DBDT on dense and open graded asphalt mixtures subjected to various conditions to evaluate tensile properties.
- Conceive and develop a direct tension test for composite specimens and identify appropriate testing conditions (e.g. specimen, loading conditions etc.) to simulate the top-down cracking in the composite specimen mixture.
- Perform laboratory tests using the newly developed direct tension test for composite specimen to evaluate the effect of the interface condition on top-down cracking performance.
- Develop and analyze a continuum and multi-scale FEM model to evaluate how the characteristics of OGFC and the interface condition affect the top-down cracking resistance.

The entire research program was accomplished as shown in Figure 1-1, starting with problem identification and a comprehensive worldwide literature review. Most of the research

effort was focused on three main tasks: laboratory test for evaluation of individual mixture; laboratory test for evaluation of composite mixture; and numerical modeling.

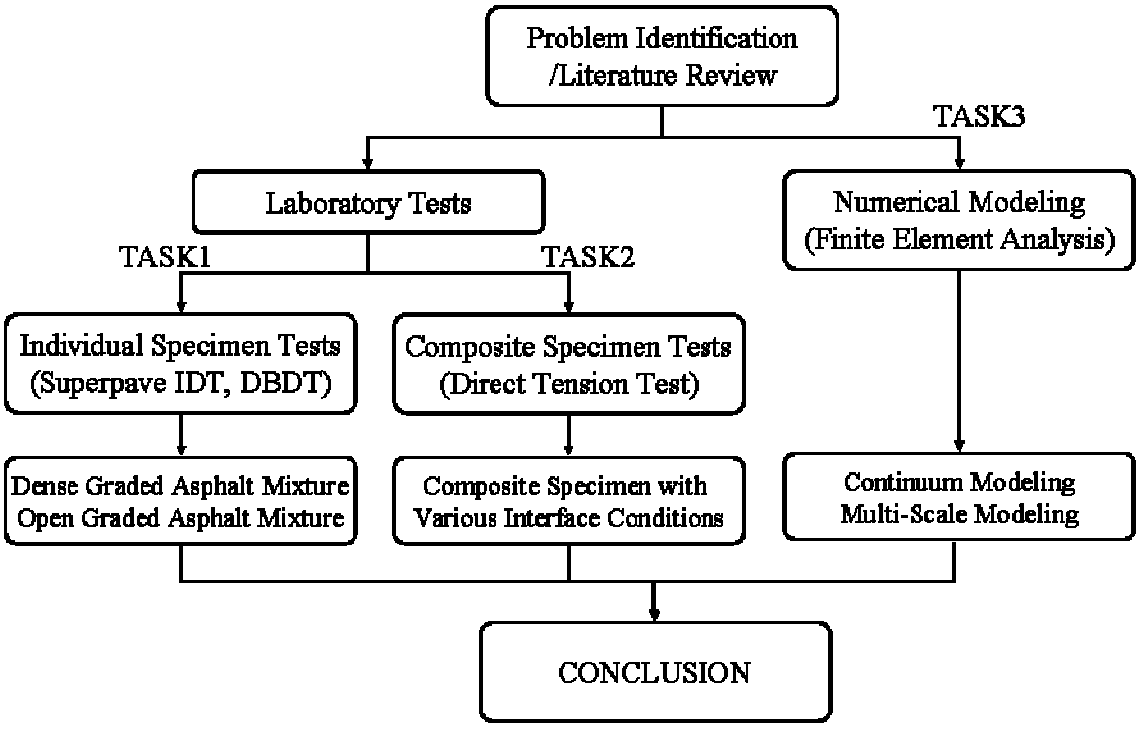

Figure 1-1 Research Approach

In laboratory tests, dense graded and open graded asphalt mixtures were tested and evaluated individually using both Superpave IDT and the DBDT developed as part of this study. Also, composite mixture with various interface conditions were evaluated using a new direct tension test developed in this study. Continuum and multi-scale finite element analyses were conducted to gain a more comprehensive understanding of the effect of open graded mixture and bonded interface condition on cracking behavior. The microstructure of the mixture was modeled in the multi-scale analysis. The effects of the mixture components on stress distribution were evaluated. The HMA fracture mechanics model was used to evaluate the fracture performance of

the different structures based on numerical analysis. Fundamental mixture/interface response and numerical analysis modeling provided useful information for cracking performance of the asphalt pavement.

CHAPTER 2
LITERATURE REVIEW

2.1 Evaluation of Open-Graded Friction Course

2.1.1 Introduction

Various agencies around the world have used open graded friction course. Different terminologies have been used to describe this type of mixtures as shown in Table 2-1 (Suresha et al., 2009). Although there are slight difference between open graded friction course (OGFC) in the US and porous asphalt (PA) in other countries, their functions are the same. Therefore, OGFC, PA and open graded asphalt mixture (OGAM) will be referred to interchangeably in this report.

Table 2-1 Terminologies for Open Graded Surface Friction Course (after Suresha et al., 2009)

Country	Agency	Terminology	References
United States of America	American Society for Testing and Materials (ASTM)	Open-Graded Friction Course (OGFC)	ASTM (2004)
	Federal Aviation Administration (FAA)	Porous Friction Course (PFC)	FAA (2005)
Australia	Australian Asphalt Pavement Association (AAPA)	Open-Graded Asphalt (OGA)	AAPA (2004)
New Zealand	Transit New Zealand (TNZ)	Porous Asphalt (PA)	TNZ (2007)
South Africa	Southern African Bitumen Association (Sabita)	Porous Asphalt (PA)	Sabita (1995)
Japan	Japan Highway Public Corporation (JHPC)	Porous Asphalt (PA)	Asahi and Kawamura (2000)

Open graded asphalt mixture is distinctly different than dense graded asphalt mixture. As expected from its name, it is designed to contain about 15-25% air voids, preferably interconnected. In order to gain relatively higher air voids, open graded asphalt mixture uses a uniform gradation. The aggregate gradation is made up of mostly a single coarse aggregate size with relatively low fine aggregate and filler. Asphalt contents for this mixture are slightly higher that dense graded asphalt mixture (Cooley et al., 2000).

2.1.2 Functions and Durability

Alvarez et al. (2006) summarized advantages and disadvantages of OGFC. They reported that advantages of OGFC could be divided into three areas: safety, environment, and economy. In order for this layer to achieve its functions, it should have proper air void content (15-25%), consequently, surface texture evaluation might be needed to clarify the distinction between OGFC and other pavement types. McDaniel et al. (2004) used the Circular Texture Meter (CTM) that is equipped with a charge coupled device (CCD) laser displacement sensor to measure the surface profile. They showed that OGFC has significantly greater texture depth than dense graded conventional surface (more than four times), indicating that OGFC has more surface air void contents. Other researchers also addressed higher macro surface texture depth of OGFC (Perez-Jimenez and Gordillo, 1990; Wang and Flintsch, 2007). These characteristics essentially allow for quick water drainage from the pavement during and shortly after rainfall. Thus, OGFC can improve traffic safety even when pavement is wet (Ruiz et al., 1990; van der Zwan et al., 1990). Kandhal and Mallick (1998) also mentioned from their survey that 85 percent of states that use or have used OGFC in the United States gave OGFC a higher than “good” rating in terms of safety. In addition, fast drainage of water keeps the pavement from accumulating water on the surface which would cause hydroplaning, prevents splash and spray behind vehicles (van

Heystraeten and Moraux, 1990), and decreases glare from the pavement by diffusing reflection of light (van der Zwan et al., 1990). On the other hand, dense graded asphalt layer is much less permeable and thus water during rainfall tends to drain over the surface, which may cause reduction in skid resistance in wet weather and increase a potential for hydroplaning. From the environmental point of view, it has been widely reported that OGFC can reduce traffic noise. Perez-Jimenez and Gordillo (1990) found that OGFC has a beneficial effect on noise reduction both outside and inside of a vehicle. Recently, McDaniel et al. (2004) have also observed that OGFC reduced pavement noise compared with dense graded asphalt mixture by 3.6 dB and 4.2 dB with pass-by and close proximity noise measurements, respectively. Moreover, noise reduction capability in the pavement itself provides economic savings since the use of other provisions such as noise barriers might be decreased or not needed.

However, disadvantages of this layer, however, have also been reported by many researchers. Raveling, which is defined as progressive disintegration of HMA layer due to dislodgement of aggregate particles, is one of the main problems (Swart, 1997; Huber, 2000). During the 1990s, improvements in binder (modified binder) and gradation improved OGFC performance in terms of raveling (Huber, 2000; Mallick et al., 2000; McDaniel and Thornton, 2005). Perez-Jimenez and Cordillo (1990) reported that open graded asphalt mixture with polymeric binder exhibited higher resistance to disintegration. Another problem associated with open graded surface is clogging of pores with time. Clogging pores gradually reduce the functional effectiveness of OGFC. Based on 20-years trials, Bowskill and Colwill (1997) pointed out that the lifetime of open graded asphalt is limited by clogging and by accelerated hardening of the binder. Based on multi-year monitoring in the US, Kowalski et al. (2009) stated that an increase in noise with time could be explained by clogging of the surface pores. However,

Kraemer (1997) stated that it is important not to regard the reduction of hydraulic and acoustic surface properties as a failure when it would simply mean that such asphalt gradually turns into non-porous surfacing and still affords good surface characteristics.

2.1.3 Structural Capacity

OGFC is a relatively thin asphalt layer placed on the structural dense graded layer. Open graded friction courses are generally considered to have no or little structural contribution in current structural design systems because it is unclear whether the relatively low stiffness and open graded mixture of OGFC significantly contributes to structural capacity. Therefore, it is important to evaluate structural capacity of OGFC, especially as it affects top-down cracking.

In general, it has been observed that the stiffness of open graded asphalt mixture is about 50 to 80 percent less than conventional dense graded asphalt mixture. Therefore, OGFC has less ability to distribute load-induced stresses than dense graded asphalt mixture. Argentina adopted a 50 percent structural capacity for OGFC in their pavement design system based on the resilient modulus test that showed roughly 60 percent of the conventional mixture (Bolzan et al., 2001). van Heystraeten and Moraux (1990) summarized the results of research conducted by the Belgian Road Research Center (BRRC). Based on modulus tests, they reported the structural contribution of OGFC lies between 73 and 79 percent of that of a wearing course in conventional dense asphalt concrete. In the Netherlands, van der Zwan et al. (1990) showed that the initial dynamic modulus of open graded asphalt mixture is approximately 80 percent of that of dense asphalt concrete. Consequently the effective structural contribution is about 80 to 90 percent with multilayer elastic analysis. However, they also stated aging, stripping and temperature retaining of OGFC affects structural integrity. Considering these combined effects, they concluded that depending on the thickness of the structure, OGFC can be expected to contribute about 50

percent of the equivalent bearing capacity achievable with dense asphalt concrete. Verhaeghe et al. (1994) concluded that open graded asphalt mixture is not suitable for use as strengthening layers because of its poorer mechanical properties compared with conventional dense asphalt. They also observed that the use of polymer modified binder results in a significant increase in the fatigue resistance of OGFC.

Khalid and Walsh (1996) also reported the lower modulus value of open graded asphalt than conventional dense graded asphalt mixtures. McDaniel et al. (2004) conducted the frequency sweep test using the Superpave Shear Test (SST). They reported lower stiffness values in open graded mixtures tested in the laboratory, indicating that there is very little mastic to stiffen the mixture. However, other researchers have pointed out that reduction in modulus should not always mean corresponding reduction in structural capacity. Poulikakos et al. (2006) developed a fatigue evolution model using elastic layer theory. On the basis of results of their model, they concluded that the modulus value of the open graded asphalt does not have a strong effect on the horizontal strain at the bottom of the asphalt layer and thus does not have a strong influence on the design life of the structure if underlying pavement structure remains the same. Similarly, Toppeiner (1993) mentioned that the use of 60 to 75 percent structural layer coefficients for OGFC compared with for dense graded asphalt is conservative, since similar structural contributions can be obtained from well designed OGFC. Moreover, he added that structural layer coefficient based on the resilient modulus can underestimate the structural contribution of open graded asphalt mixture. In Spain, based on the analysis of the reinforcement capacity and the reduction in deflection induced by OGFC and dense graded asphalt layer, they have determined that both dense graded layer and OGFC have similar structural capacity

(Alvarez et al., 2006). Oregon Department of Transportation also applies a similar structural coefficient for both layers on the basis of the deflection measurements (Kandhal, 2002).

According to a research in New Zealand, average lifetime of OGFC is 10.5 years, which is relatively short compared with that of dense graded asphalt layer, 16.2 years (Bartley consultants, 1999). Similarly, van der Zwan et al. (1990) reported the service life of OGFC is 10 years in the Netherlands. They also emphasized that OGFC is sensitive to mechanical damage in the first year after installation. Voskuilen et al. (2004) mentioned damage in the initial stage is one of the causes of shorter service life in OGFC. However, the use of modified binder provided the benefits to enhance the initial strength, but they indicated that modified binder does not necessarily guarantee the longer service life. Nevertheless, it is believed that modified binders increase the service life of OGFC by increasing the cohesion and adhesion in the asphalt mixture and by increasing the binder film thickness without the binder drainage during construction.

2.1.4 Closure

A review of literature revealed that most research on the evaluation of OGFC has focused on its functionality, durability and structural integrity based on conventional fatigue (bottom-up cracking). Relatively little research to date had been carried out on top-down cracking resistance of open graded asphalt mixture. Given its position top of the pavement system, open graded friction course may play an important role to either resist or accelerate top-down cracking, which is induced by surface tensile stress. More comprehensive evaluation on the tensile properties of OGFC is necessary to properly assess its effect on fracture resistance and top-down cracking in flexible pavement.

2.2 Bonded Interlayer in Pavement System

The asphalt concrete pavement system is a layered structure. In mechanistic design methods for pavement systems, the procedures are generally based on stresses and strains computed with the assumption that either the layers are fully bonded or fully unbonded. For OGFC, the effects of bond are not just limited to effects of full or partial bonding. Since the OGFC is a porous friction course with high void ratio, it is easy for a bonding agent to permeate into the OGFC structure, thereby enhancing material properties. An evaluation of the ten year performance of ground tire rubber in an open graded friction course on SR 16 in Bradford County indicates that increased binder content from ground tire rubber modification of the friction course can reduce longitudinal wheel path cracking. Based on this study, there is a high likelihood that bonded friction course process could significantly extend the cracking performance of open graded mixes in Florida by providing more polymer modified asphalt as a bonding agent for friction course.

Another case that represents the bond effects is Novachip, which was used in evaluation of open-graded and bonded friction courses in Florida by Birgisson et al. (2006). Novachip consists of a layer of hot precoated aggregate over a polymer-modified binder spray application. Tests have shown that Novachip has much higher DCSE and FE than conventional OGFC.

Unpublished work performed by Roque at University of Florida has shown that bonded interface between the OGFC mixture and the underlying structural mixture reduces the rate of creep and damage of the composite system. However, only limited work has been performed on the development of a suitable fracture performance test that can characterize the benefits of OGFC and the bonded interface. Therefore, a study is needed to define and optimize the test conditions needed to obtain consistent fracture properties of OGFC mixtures. It is also necessary to develop a research-based direct tension test to accomplish the goals of this project.

2.3 Top-Down Cracking Mechanism

2.3.1 Introduction

It is now well recognized that load-related top-down cracking, which initiates at the surface of the pavement and propagates downward, commonly occurs in hot mix asphalt pavements. This phenomenon has been reported to occur in many parts of the United States (Roque and Ruth, 1990; Myers et al., 1998; Myers, 2000; Uhlmeyer et al., 2000; Myers et al., 2001; Svasdisant et al., 2002; Schorsch et al., 2003; Kim, 2005) as well as in Europe (Molenaar, 1984; Dauzats and Rampal., 1987; Gerritsen et al., 1987; Nunn, 1998; De Freitas et al., 2005), Japan (Matsuno and Nishizawa, 1992; Himeno et al., 1997; Komoriya et al., 2001; Uchida et al., 2002) and other countries (Wambura et al., 1999; Raju et al., 2008).

Previously, research on asphalt pavement cracking performance has generally focused on the traditional fatigue mechanism that considers failure which initiates at the bottom of the asphalt surface layer. Conventional multi-layer analysis of pavements subject to a uniformly distributed load would always yield maximum tensile stresses and strains to occur at the bottom of the asphalt concrete layer. Also, traditional fatigue approach assumes there is an average condition over the life of the pavement, where an equal amount of damage is done by each wheel load applied for that condition. Interestingly enough, however, contradictions associated with this approach have been raised by many researchers. Francken (1979) found that rest periods significantly increase the fatigue life of asphalt mixtures. This appears to indicate that asphalt concrete has the potential to heal, or that the actual failure mode is not a true fatigue phenomenon. Both of these ideas negate the validity of conventional fatigue mechanism. Roque and Ruth (1990) also contradicted this approach by indicating that fatigue parameters generally

do not consider the effects of temperature changes, rest periods, and age-hardening when they explained the critical condition concept.

Top-down cracking clearly cannot be explained by this traditional fatigue mechanism. As indicated above, pavement modeling as a linear-elastic multilayer system with homogeneous materials and a circular, uniformly distributed vertical loading will not predict maximum tensile stresses and/or strains to occur near the pavement surface.

2.3.2 Influencing Factors on Top-Down Cracking

For years, many researchers have made efforts to identify fundamental mechanisms that may lead to top-down cracking initiation and propagation. A detailed review of this work is presented below.

It is well accepted that near surface tensile stress and/or strain induced by non-uniform contact stress between the tire and asphalt surface layer may cause top-down cracking. Based on multiple computer models using measured tire-pavement interface stresses, Myers et al. (1998) indicated that this mode of distress may be initiated by high surface tensile stresses due to non-uniform contact stress between the ribs of radial truck tires and the surface of the asphalt layer. One of their interesting findings is that the radial truck tires behave very differently than bias-ply truck tire. Consequently, the location where the tensile stresses are acting is under the treads of the tire rather than at the tire edges. Researches presented by Jacobs (1995) and De Beer et al. (1997) indicate that most significant tension is found under the widest tread. Nunn (1998) also concluded that surface initiated cracking (top-down cracking) in the UK was caused by horizontal tensile stresses at the surface generated by truck tires. Wide based tires generated the highest tensile stress. In fact, much work on top-down cracking resulted in similar conclusion (Himeno et al., 1997; Baladi et al., 2002).

Thermal effects also induce surface tensile stress. Dauzats and Rampal (1987) reported that thermal stress in the asphalt surface course may initiate top-down cracking, which is then propagated by traffic loads. Myers et al. (1998) also indicated that significant thermal stresses that can contribute to the initiation and propagation of surface cracks can develop near the surface of the pavement. More recent work by Kim (2005) showed that although top-down cracking performance in Florida was most strongly affected by traffic loading, thermal effects also appeared to affect performance.

In the study presented herein, most efforts were concentrated on effects of open graded surface friction course mixtures and interface condition on top-down cracking. In Florida, the top pavement layer often consists of a thin Open Graded Friction Course (OGFC) designed to quickly remove the surface water during rain events. The performance of these porous surface mixtures are certainly more severely affected by environmental exposure issues than underlying dense graded mixtures. They are directly exposed to UV radiation, intense heat and due to their inherent higher air void content, they are prone to oxidation, environmental leaching and are more susceptible to sudden dramatic temperature changes from rainfall. These combined effects most likely cause accelerated asphalt binder hardening. Through the analysis of field data and laboratory test results, Svasdisant et al. (2002) concluded that pavements with higher asphalt surface modulus due to aging would have higher potential for top-down cracking. They reported that because of increased exposure to sunlight and oxygen, age hardening mainly affects the surface course while the lower courses are less affected. Aging increases the stiffness of binder with corresponding effect on the asphalt mixtures (Bell et al., 1991) and higher air voids generally accelerates aging (Martin et al., 1990). This seems to imply that higher air void contents of open graded asphalt mixtures might severely accelerate age-hardening. Some

researchers have stated that this aging issue might be one of cause of top-down cracking (Wambura et al., 1999; Uchida et al., 2002; De Freitas et al., 2003). Another interesting issue associated with environmental condition was presented in Japan. Matsuno and Nishizawa (1992) reported that top-down cracking is absent in shadowy areas such as under bridges and appears mostly in areas exposed to extensive solar radiation. Based on analysis using finite element method, they concluded that traffic loads cause high tensile strains in hot pavements. Similarly, based on multi year survey, Komoriya et al. (2001) reported that surface initiated cracking grew faster with longer exposure to the sunshine and that high rainfall is prone to the generation of surface longitudinal cracks. They also emphasized the surface material in stating that fine graded mixture is more resistant to surface longitudinal cracks than coarse graded mixture, which supports the finding reported by De Freitas et al. (2005).

It is also noted that stiffness gradients might make contribution to top-down cracking. It is well known that stiffness in the asphalt concrete layer is non-uniform because of induced temperature gradients, age-hardening and pavement cooling rates (Roque et al., 1988). Stiffness gradients in the asphalt concrete layer had significant effects on near-surface tensile response, which are not considered in traditional fatigue approaches (Myers, 2000; Myers et al., 2001).

Secondary effects for cracking at the asphalt surface might be related to construction quality, including effects of segregation and poor compaction (Gerritsen et al., 1987; Chang et al., 2002; Schorsch et al., 2003; De Freitas et al. 2005).

2.3.3 Characteristics of Top-Down Cracking

Gerritsen et al. (1987) reported that pavements in the Netherlands were experiencing premature cracking in the wearing courses, and cracks did not extend into the lower asphalt layer. Uhlmeyer et al. (2000) similarly observed that surface initiated cracking often stops at the

interface between the wearing course and the underlying layer (around 50 mm). They also reported that the crack width is around 3 to 4 mm at the surface and closed with depth. Myers et al. (1998) made similar observations and explained that tensile stresses dissipate quickly with depth.

Literature from many countries concurs that top-down cracking is predominantly parallel to the asphalt pavement centerline and located in the vicinity of the wheel paths (Gerristen et al., 1987; Matsuno and Nishzawa, 1992; Schorsch et al., 2003). However, researchers from different countries reported different ages at which this mode of failure initiated: the Netherlands (Gerristen et al., 1987), soon after construction; Japan (Matsuno and Nishzawa, 1992), from 1 to 5 years; France (Dauzats and Rampal, 1987), from 3 to 5 years; the state of Washington in US (Uhlmeyer et al., 2000) from 3 to 8 years; the state of Florida in US (Myers et al,. 1998), from 5 to 10 years; UK (Nunn, 1998), even after 10 years.

Matsuno and Nishzawa (1992) conducted finite element analysis on two typical pavement cross sections and concluded the pavement cross section had little effect on surface tensile strain. However, Nunn (1998) and Uhlmeyer et al. (2000) found top-down cracking was observed in thicker asphalt pavement while Bensalem et al. (2000) observed top-down cracking in mostly thin asphalt layer.

2.3.4 Closure

It seems obvious that there is a fundamentally close relationship between top-down cracking and properties of surface materials since surface mixtures are directly exposed to the surface tensile stress induced by both traffic loading and environmental conditions. However, studies on top-down cracking have not included the effect of open graded friction course mixtures. Recently, there has been a growing recognition that these open graded mixtures may be

the “first front” in resisting top-down cracking. Myers et al. (1998) concluded that this type of cracking is in fact primarily related to mixture composition. Specifically, more fracture resistant asphalt mixtures are needed to mitigate top-down cracking. This seems to indicate the need to better characterize and determine properties of open graded asphalt mixture and to evaluate their effect on top-down cracking performance.

2.4 Asphalt Mixture Tests in Tension Mode

2.4.1 Introduction

Very little work to date has been reported on the testing and characterization of fracture resistance of open graded asphalt mixtures. The laboratory mixture evaluation tests required are of course dependent on the mechanisms determined to drive top-down cracking performance. In addition, it was reported that the only way to determine asphalt mixture properties is to measure them directly since they cannot be obtained reliably from the relationship with current asphalt binder properties (Roque et al., 1997). Asphalt mixture tests must provide accurate information on the damage and fracture properties of the HMA mixture. In the case of top-down cracking, it is extremely important that these properties be obtained using a tensile mode of loading, as it has been shown that damage and fracture primarily develop in the presence of tensile stresses.

Determination of tensile properties are critical for evaluating top-down cracking mechanisms, since the cracks appear to develop mostly in opening mode, fracture mode I (Myers, 2000), indicating that tension is at least partially, if not predominantly responsible for the development of cracks. There are currently several tests which are being used to measure the tensile properties of asphalt mixture in the laboratory: Superpave IDT (Roque and Buttlar, 1992; Buttlar and Roque, 1994; Roque et al., 1997), hollow cylinder test (Buttlar et al., 1999; Buttlar et

al., 2004), disk-shaped compact tension test (Wagoner et al., 2005; Wagoner et al., 2006), semi-circular beam test (Li and Marastreanu, 2004; Huang and Shu, 2005), and uniaxial direct tension test (Haas, 1973; Bolzan and Huber, 1993; Kim et al., 2002). Each of these testing modes offers advantages and disadvantages from the standpoint of practicality as well as their ability to provide accurate damage and fracture properties. A complete review was performed to identify an appropriate measurement system for determining fracture properties of open graded asphalt mixtures and/or asphalt mixture in general.

2.4.2 Superpave Indirect Tension Test (Superpve IDT)

Currently, Superpave IDT test is widely used to evaluate the tensile properties of dense graded asphalt mixtures. Superpave IDT best represents a biaxial state of stress at the bottom of the asphalt layer. The Superpave IDT loading configuration results in fairly uniform tensile stresses perpendicular to the direction of the applied load. A key advantage of the Superpave IDT over the other testing systems is that the failure plane is known a priori; it is almost always along the vertical diametral plane (Roque and Buttlar, 1992). Thus, measurements can be obtained on the failure plane at the time of failure. This results in the potential for very accurate determination of mixture failure limits. Roque et al. (1997) developed the measurement and data analysis systems employed in the Superpave IDT, which overcame the interpretation problems typically associated with this test. From a practical point of view, the test is relatively simple in nature using compressive loads through loading strips. One disadvantage of the Superpave IDT is that test results are more difficult to analyze because of the more complex stress states that develop within the test specimen. Also, tensile response depends strongly on Poisson's ratio. In addition, local failure can occur due to shear fracture under the loading strips at higher temperatures, particularly in open-graded mixtures. These problems are exacerbated for thin

specimens (e.g., thin wearing courses). Based on the authors' experience using the Superpave IDT test on open-graded mixtures, it appears that surface air void content and aggregate structure may have an effect on the test results at relatively high test temperatures. Similar problems can be expected with SMA mixtures. These effects can be expressed more generally as localized damage under the loading strips. Figure 2-1 shows Superpave IDT in the environmental chamber.

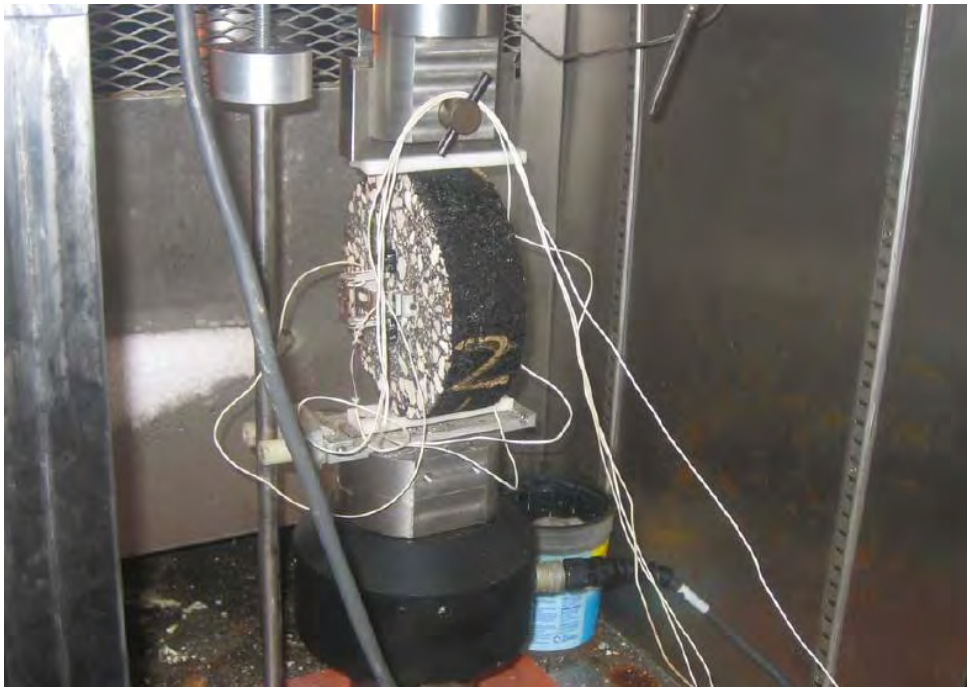

Figure 2-1 Superpave IDT

2.4.3 Hollow Cylinder Tension Test (HCT)

Recently, hollow cylinder testing has been proposed for the determination of tensile properties of asphalt mixtures (Buttlar, 1999). Figure 2-2 presents a sample for hollow cylinder tension test. Hollow cylinder tests offer near uniform stress fields around the entire

circumference of the cylinder without the alignment problems presented by the direct tension test. As a consequence, there is no significant stress concentration.

Figure 2-2 Hollow Cylinder Tension Test Sample

However, the test requires relatively thick specimens (approximately 150 mm), which may make it a problem when properties need to be obtained from field cores from thin surface layers associated with top-down cracking problems on open graded asphalt mixtures. In addition, the plane of failure is arbitrary in this test, which makes it difficult or impossible to obtain measurements on the failure plane at the instant of failure. As Buttlar et al. (1999) mentioned in their paper, this test has innate problems such as density gradient problems and wall thickness determination with respect to aggregate particle size. Coring the gyratory compacted sample to produce hollow test sample makes this test less practical.

2.4.4 Disk-Shaped Compact Tension Test (DCT)

As a fracture toughness test, disk-shaped compact tension test has been developed to be able to test cylindrical cores obtained from the field as well as compacted in the laboratory (Wagoner et al., 2005). Figure 2-3 shows disk-shaped compact tension test. This test is a common fracture test specified in ASTM E 399 for metallic materials.

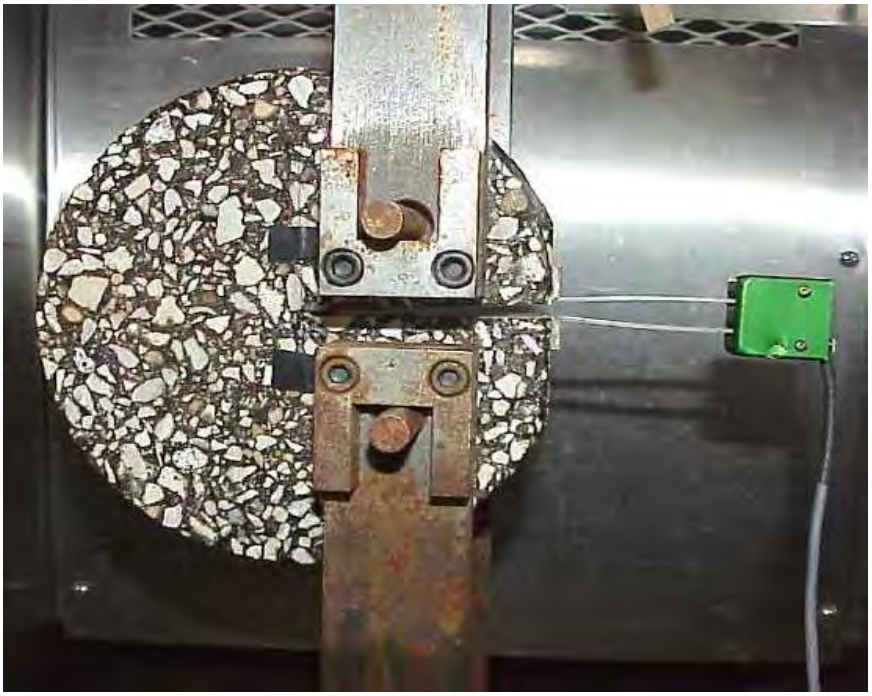

Figure 2-3 Disk-Shaped Compact Tension Test

However, application to asphalt mixtures still has not been established. Also the test is primarily suitable for determination of fracture toughness, and not other properties. Compact tension test could produce erroneous results if the crack front deviates from a straight (pure Mode 1) crack path. It could happen in the asphalt mixture due to aggregate particles deflecting the crack around an aggregate and/or eccentric loading. The stress distribution around the holes used for loading is unknown, and premature rupture could occur at the loading holes. Sample

preparation must go through several stages including slicing, drilling holes for loading, slicing flat edge at the notch mouth, and producing a suitable notch. These steps also make this test less practical.

2.4.5 Semi-Circular Bending Test (SCB)

Semi-circular bending test has been used to measure the fracture resistance of asphalt mixtures (Li and Marasteanu, 2004; Huang and Shu, 2005). Figure 2-4 shows semi-circular bending test. Originally, single-edge notched beam test (SEB) was utilized to obtain fracture toughness in fracture mechanics (Anderson, 2005). In the asphalt community, this test was modified to apply to asphalt mixture because it is not easy to obtain the specimen for SEB from the field and in the laboratory.

Figure 2-4 Semi-Circular Bending Test

However, use of the semi-circular bending test resulted in other problems. The SCB test arrangement for asphalt mixture is a 150 mm in diameter semi-circle supported by two rollers with a span of 120 mm which leads to a relatively short fracture ligament. The initial ligament length should be as large as possible to produce reliable fracture properties. The fundamental measurement of tensile strength is a difficulty in beam testing due to neutral axis shifting and stress redistribution after the initiation of tensile fracture.

2.4.6 Uniaxial Direct Tension Test

Haas (1973) stated that the stiffness modulus of an asphalt mixture should be obtained using a direct tension approach. The typical uniaxial direct tension test for asphalt mixtures uses a cylindrical specimen that is bonded to end caps of the same or slightly larger diameter as shown in Figure 2-5. In theory, the uniaxial direct tension test benefits from the uniform stress and strain fields in the middle of the specimen, but in practice, evaluation of asphalt mixtures is difficult due to the many detrimental effects associated with this method. Bolzan and Huber (1993) summarized the following disadvantages:

- Stress concentration near the ends of the samples has been observed in many experiments.
- Sample failure can occur due to misalignment.
- Sample preparation requires a long time and a skilled operator/technician.
- The failure plane is presumed to occur at the center of the specimen perpendicular to the vertical axis, but in practice, it may occur at any locations over the specimens.
- This test has had some difficulty in obtaining repeatability

Furthermore, it might not be possible to do this test on field cores since it would consist of several layers. That may not be thick enough to make cylindrical specimens for this test.

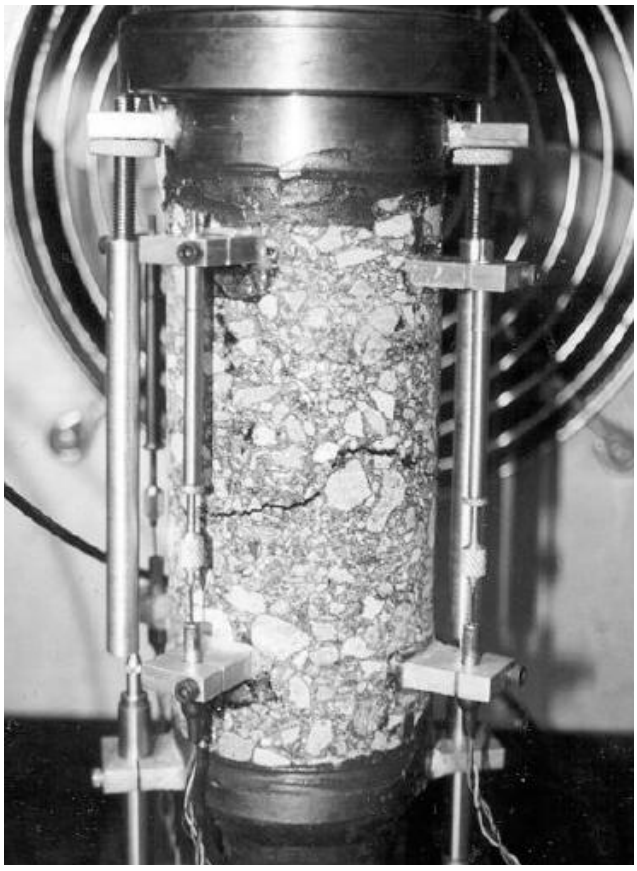

Figure 2-5 Uniaxial Direct Tension Test

2.4.7 Closure

In summary, none of existing test methods, including Superpave IDT, provides a suitable method for obtaining tensile properties of open graded asphalt mixture. Thus, it is necessary to develop a test method and system which mitigates the disadvantages of existing tests and at the same time, meets the following requirements: a direct tension mode test; can be performed on gyratory compacted specimens or field cores; can test samples of various thickness (thin or thick); and can be used on all mixture types (dense-graded, open-graded).

CHAPTER 3
DEVELOPMENT OF DOG-BONE DIRECT TENSION TEST

3.1 Introduction

A mechanical test to evaluate the tensile properties of asphalt mixture is necessary in mixture design, quality control, and thus pavement design. As mentioned in the literature review, because the existing direct tension test is unsuitable for evaluating the tensile properties of asphalt mixtures, a Dog-Bone Direct Tension test (DBDT) was conceived to overcome its disadvantages and to provide appropriate tensile properties of asphalt mixture. The DBDT provides some potential advantages including the fact that the failure plane is known a priori, which means failure limits can be measured directly on the failure plane. Due to DBDT specimen geometry, stress concentrations near the ends of specimen are less critical, and the location where failure is likely to occur is maximized. The DBDT specimens can be produced by simply coring opposing sides from slices or disks obtained from cylindrical laboratory samples or field cores. Development and evaluation efforts for the DBDT are described in the following sections. The intent behind the development of this direct tension test is for it to provide a comparison to the more easily performed Superpave IDT test. Thus, the new direct tension test should be viewed as a research tool, rather than a production test.

3.2 Development of Dog-Bone Direct Tension Test

The primary objective of this section is to describe the design, development and evaluation of a new direct tension test system that was conceived for determining tensile properties of asphalt mixtures.

3.2.1 Two Dimensional Finite Element Analysis

Two dimensional finite element method (FEM) analyses were conducted to determine optimum width of the specimen, coring radius, and coring overlap considering stress distributions at both the centerline of the specimen and the area near the loading heads. Stress distributions of the centerline and headline of the specimen were checked to ensure higher enough stress concentration at edge of a specimen, thereby increasing potential for failure at the center of the specimen and not near the loading heads (problem with traditional specimens). Simultaneously, the stress distributions across the centerline should be as uniform as possible to guarantee stress concentration over a large enough area to capture a representative portion of the mixture. Coring radii (r) and coring overlaps (x) were variables used for analysis to optimize the specimen geometry as presented in Figure 3-1.

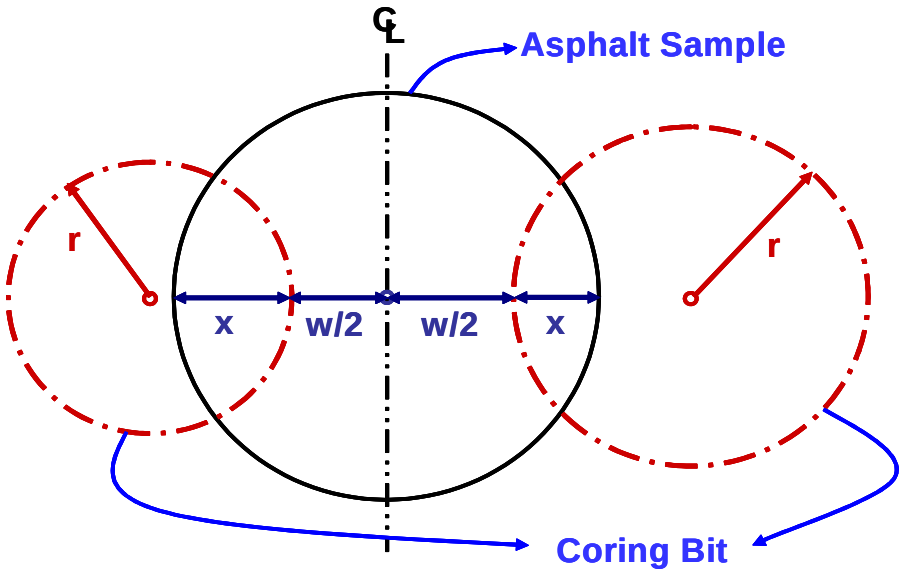

Figure 3-1 Coring Radius (r) and Coring Overlap (x)

Figure 3-2 shows two dimensional finite element mesh and its coordinate. Based on the predicted stress distributions for two-inch wide specimens, a coring radius of 3 inches and a coring overlap of 2 inches produced centerline stresses that were reasonably uniform and considerably greater than stresses near the loading heads (headline). Analysis results for this case are summarized in Table 3-1.

This final specimen geometry results in a large enough cross section for testing without sacrificing the integrity of the mixture. As indicated in this table, a significant stress difference between the centerline and the headline of the specimen was observed. The stress concentration at the centerline should cause the specimen to break in this region, thereby compensating for any density gradients in gyratory compacted specimens as previously exposed by researchers (Harvey et al., 1991; Shashidhar, 1999, Chehab et al, 2000). As also shown in Figure 3-3, the percent difference in the computed stress along the centerline is around 30%. However, this 30% increase in stress between the outer edge and center of the specimen is about the same as that observed for Superpave IDT specimens from which material properties have been determined successfully (Roque and Buttlar, 1992). The key to success is to have the gages directly on the planes of maximum stress. Therefore, measurements are obtained in the center of the edges of the specimen as well as on the specimen faces.

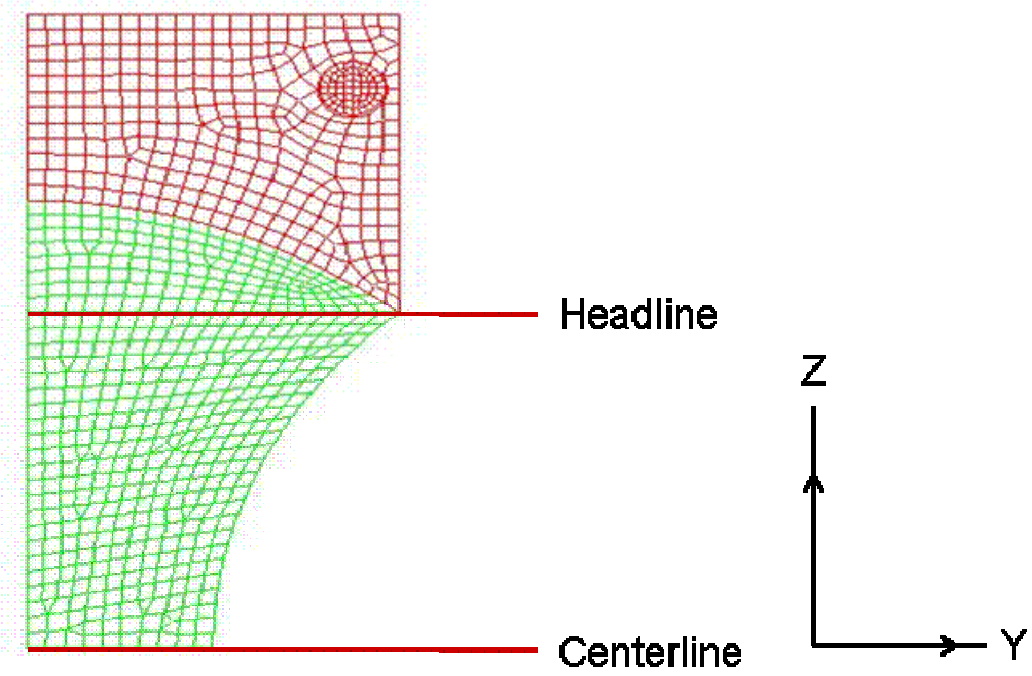

Figure 3-2 2-D FEM Mesh and Coordinates

Table 3-1 Analysis Results for Determining DBDT Sample Geometry

Various Coring Overlaps with Fixed Coring Radius (3 in)				
Coring Overlap (in)	0.5	1.0	1.5	2.0
% Difference of Stress on Center Line (%)	20.39	27.04	28.02	31.31
Stress Difference between Center Line and Head Line (%)	20.14	20.26	26.62	43.17
Various Coring Radii with Fixed Coring Overlap (2 in)				
Coring Radius (in)	1.5	2.0	2.5	3.0
% Difference of Stress on Center Line (%)	61.17	46.42	37.39	31.31
Stress Difference between Center Line and Head Line (%)	50.59	48.54	45.91	43.17

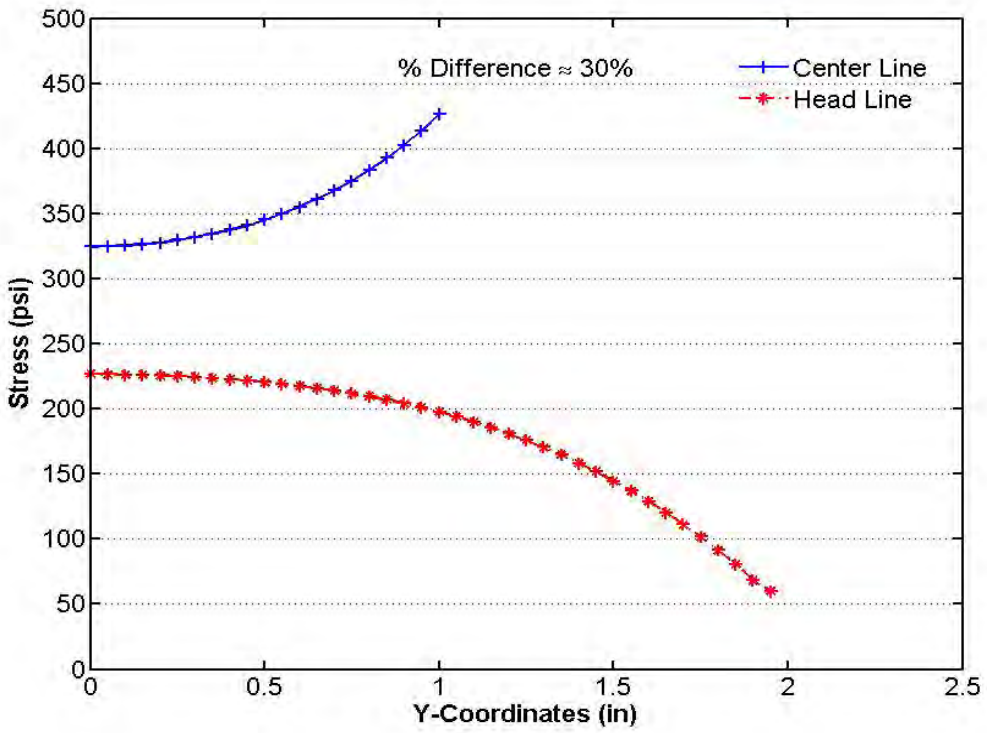

Figure 3-3 Stress Distribution on Centerline and Headline (3 in coring radius and 2 in coring overlap)

3.3 Dog-Bone Direct Tension Testing System

After thorough analysis and discussion, a DBDT prototype system was proposed, designed and built. The complete system is composed of several pieces, including a specimen coring jig, specimen loading heads, strain gage sensors and attachment kits, a dual cylinder tensile load equalizer, and a PC controlled servo-hydraulic load frame with an integrally mounted environmental chamber. All shop drawings of components and subassemblies were generated during prototype development. The various components of the DBDT system that were designed, developed, and/or procured are described in this section. An asphalt concrete specimen instrumented with the new DBDT system and ready for testing in the loading frame is shown in Figure 3-4.

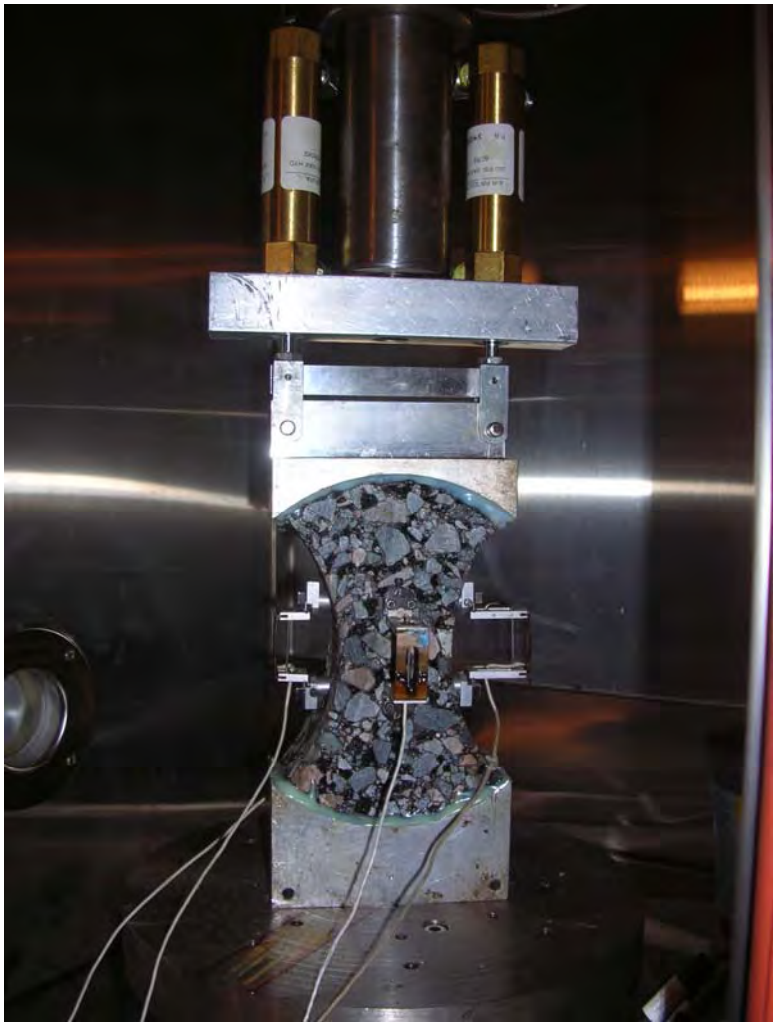

Figure 3-4 Dog-Bone Direct Tension Test Prototype

The proposed system was designed to properly perform three types of mixture tests: resilient modulus, creep compliance, and tensile strength tests, which provide the properties needed to fully define fracture behavior using the HMA fracture model developed at the University of Florida (Zhang et al., 2001; Roque et al., 2004a).

3.3.1 Coring Process

A coring jig was designed and built to make dog-bone shaped asphalt specimens. The opposing sides of the specimen were cored with the coring jig shown in Figure 3-5.

The coring barrel of the coring machine pushes down onto an asphalt specimen on the coring fixture, which has grooves at its base to accommodate the coring barrel after it goes through the base of the specimens. The coring jig has three bearings to prevent the coring barrel from chattering and wavering as well as hold it during the coring process.

The coring fixture was fitted with an adjustable round shaped steel block, which restrains the specimen laterally to accommodate different diameter specimens. A hex key causes the block to move the specimen laterally such that the specimen is exactly centered on the coring fixture. The steel block is reversible so that both sides of the specimen can be cored without readjustment.

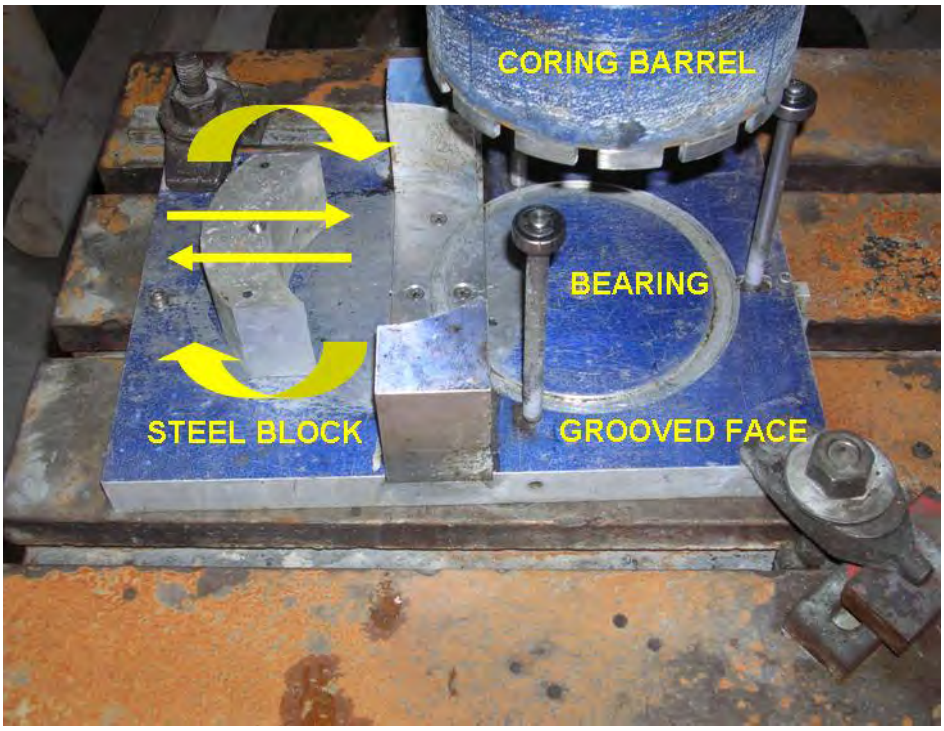

Figure 3-5 Coring Jig

3.3.2 Bonding Specimen to Loading Heads

Suitable loading heads were designed to prevent eccentricity due to bending or misalignment. The system can be used with any independent loading frame including the MTS system. Loading heads were machined from 6061-T6 aluminum with V-grooved specimen contact surfaces to increase the bonding strength between the loading heads and the specimens as shown in Figure 3-6. Also, the upper loading head has two holes through which the load is applied with loading pins.

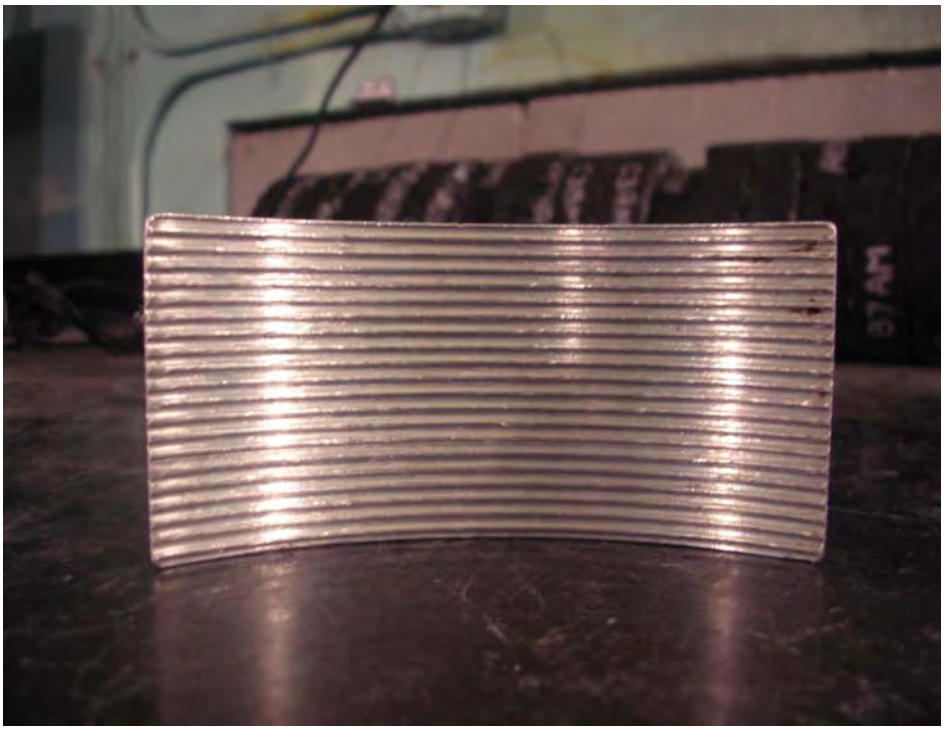

Figure 3-6 Loading Head with Grooved Contact Surface

To make the loading head usable for specimen of various thicknesses, a series of shim stocks were employed as shown in Figures 3-7 and 3-8. If the thickness of a specimen is not the same as that of loading heads, a series of shim stocks can be placed beneath either the specimen or the loading head in order to eliminate eccentricity due to bending or poor alignment. The upper and lower loading heads were connected with distance-adjustable two alignment bars as shown in Figures 3-7 and 3-8. These also help to ensure good alignment during bonding process.

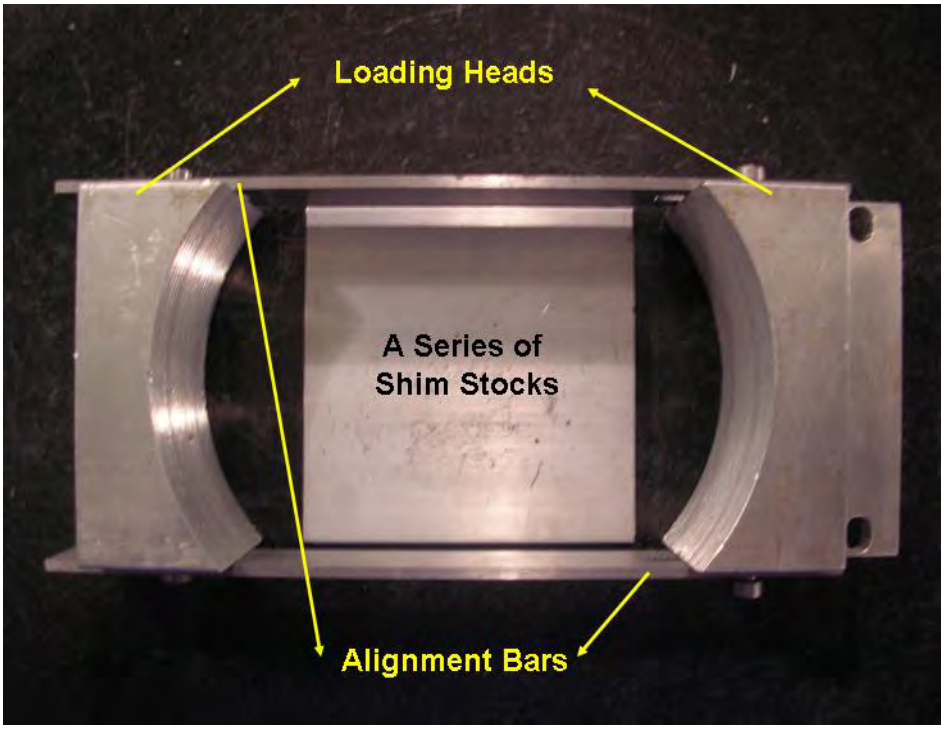

Figure 3-7 Loading Heads with Alignment Bars and Shim Stocks

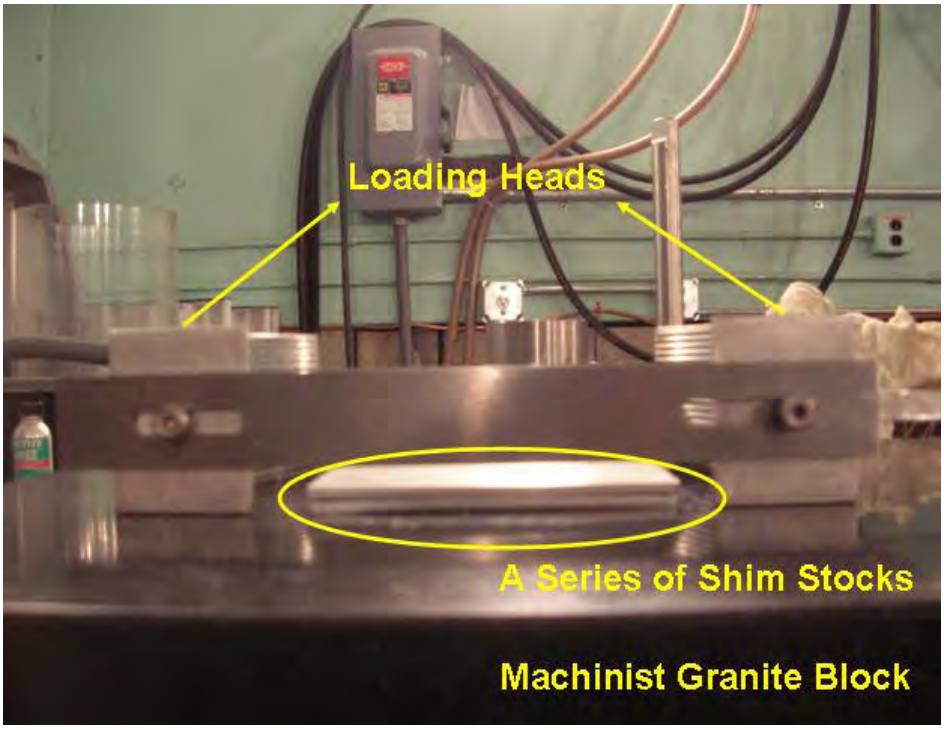

Figure 3-8 Loading Heads with a Series of Shim Stocks

An area of concern was the bond between a specimen and the loading heads. Similar to the uniaxial direct tension test, this interface can make or break the test. Several epoxies and adhesives from different manufactures were procured and evaluated to determine which chemistry provided sufficient bond strength and practicality. The final selection was based on working time, curing time, and ultimate tensile strength. Detailed properties of the bond agent selected are shown in Table 3-2. This bond agent consists of two materials: resin and hardener. Figure 3-9 shows the bond agent and mixing nozzle. The ratio of resin to hardener is two to one by volume. The entire bonding process was performed on a machinist granite block to provide a flat reference surface as shown in Figure 3-10.

Table 3-2 Characteristics of LOCTITE Hysol Product E-20HP

Physical Properties (25°C)	
Dielectric Strength (Volts/Mil)	500
Tensile Strength, ASTM D 638 (psi)	5,700
Tensile Elongation, ASTM D 638 (%)	8
Hardness, ASTM D 1706 (Shore D)	80
Glass Transition Temperature, T_g, (°C)	60
Curing Properties (25°C)	
Working Life (min)	20
Tack Free Time (min)	40

Figure 3-9 Bonding Agent Gun with Mixing Nozzle

Figure 3-10 Machinist Granite Block

3.3.3 Strain Gage Mounting System

Four extensometers were used to measure on-specimen deformations. Two of the sensors are placed at the center of the specimen's flat faces and the other two are placed at the center of curved edges. The extensometers placed on the faces are the most appropriate for determination of resilient modulus and creep compliance. Since the edge measures deformation in the immediate vicinity of maximum tensile stress, they can detect the instant when the material fractures and are most appropriate to determine failure limits (i.e., strength, failure strain, fracture energy etc.). Detailed stress analysis based on finite element method will be discussed in the section 3.5.1.

At first, it was difficult to place and attach the aluminum gage points at the exact position planned, especially at the curved edges of the specimen. Longer gage points with an angle were conceived and prepared for both edges as shown in Figures 3-11 and 3-12. The same gage points

used for IDT specimens were used for the flat faces. Also, simple templates shown in Figures 3-13 and 3-14 were designed and machined to mount gage points precisely at the center of test specimen's face and edge considering the curvature of a specimen. Placement of the gage points with these templates guarantees that the gage points on one face or edge of the specimen are perfectly aligned with gage points on the other face or edge. Gage point spacing of 1.5 in was used. The longer angled gage points were formed to be more effective for use on the specimen's curved edges.

Figure 3-15 shows a specimen after attaching gage points on faces and edges. Knife edges are affixed on the gage points using a set screw. The extensometers are then clipped onto these knife edges to measure both face and edge deformations. Extensometers are designed to rely on a minimum spring force to maintain contact with knife edges mounted to gage points glued on the specimen. This is the same system currently in use for Superpave IDT. Knife edges were also modified to simplify their placement onto the gage points for edges as shown in Figures 3-16 and 3-17.

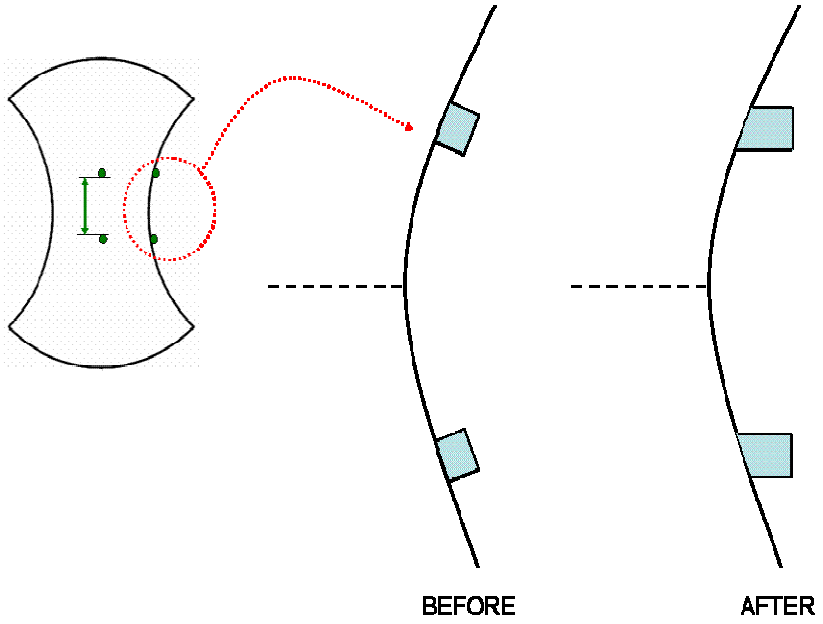

Figure 3-11 Gage Point Positioning on Edge

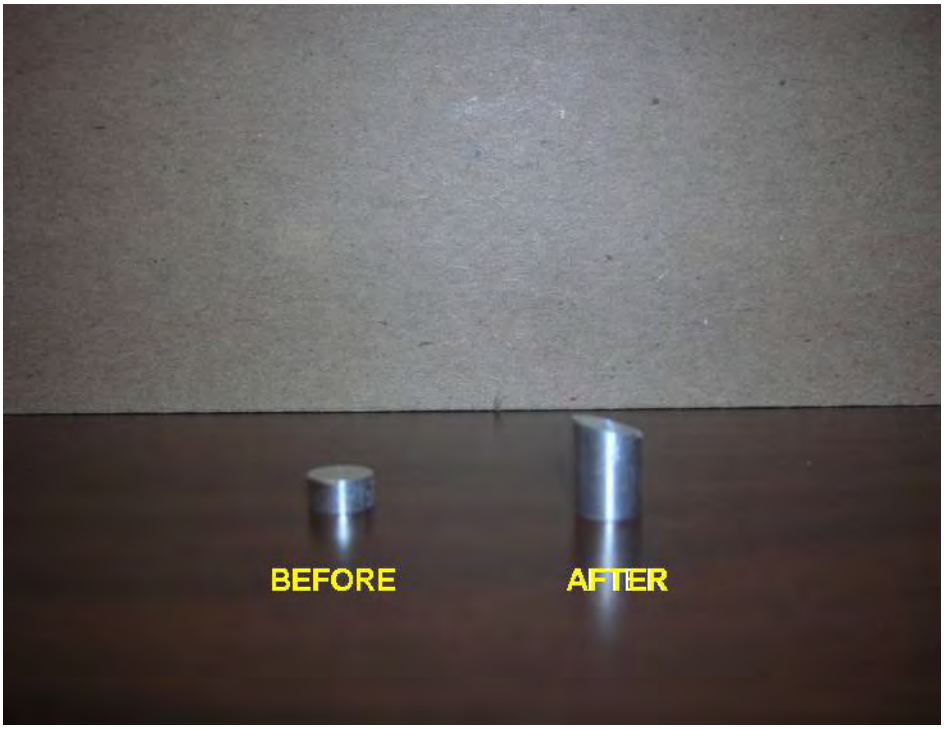

Figure 3-12 Modification of Gage Point for Edge

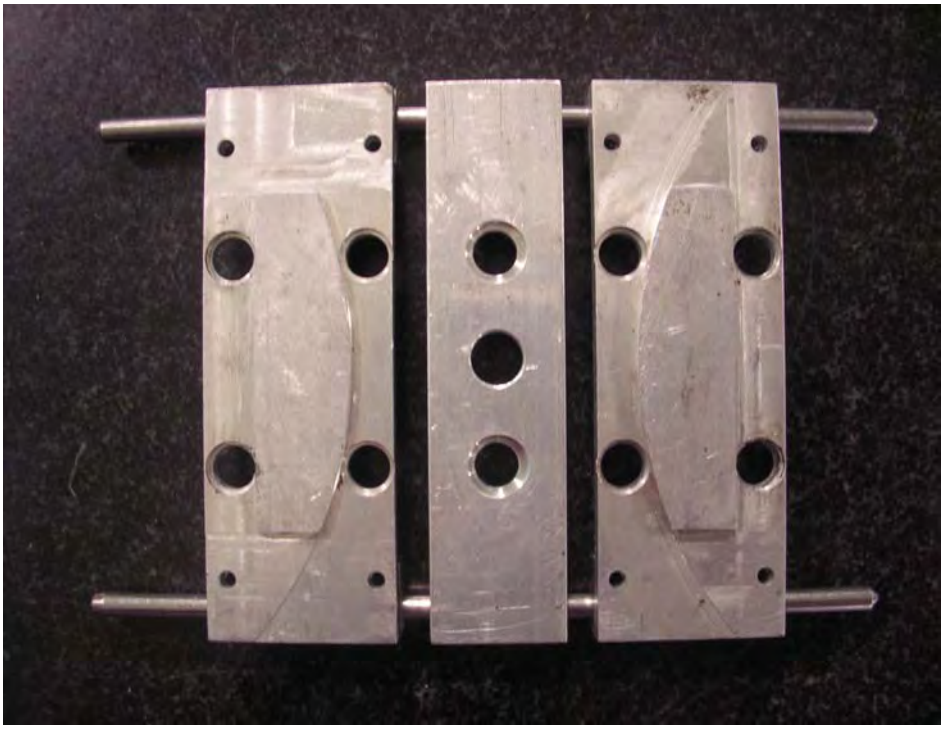
Figure 3-13 Template to Attach Gage Point on Faces

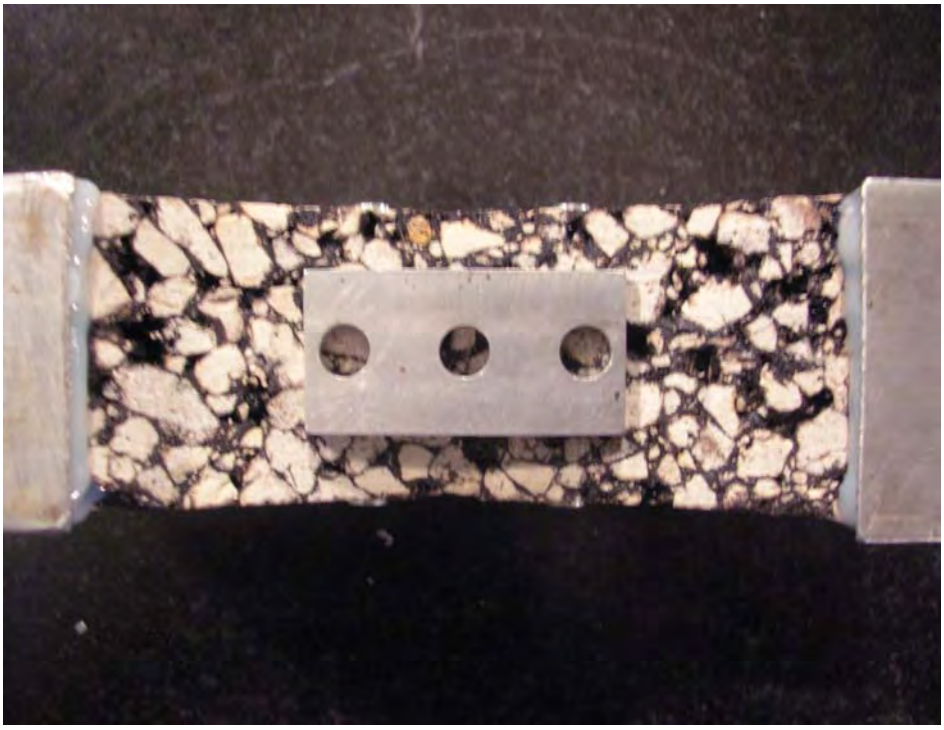

Figure 3-14 Template to Attach Gage Point on Edges

Figure 3-15 Gage Point Attachment

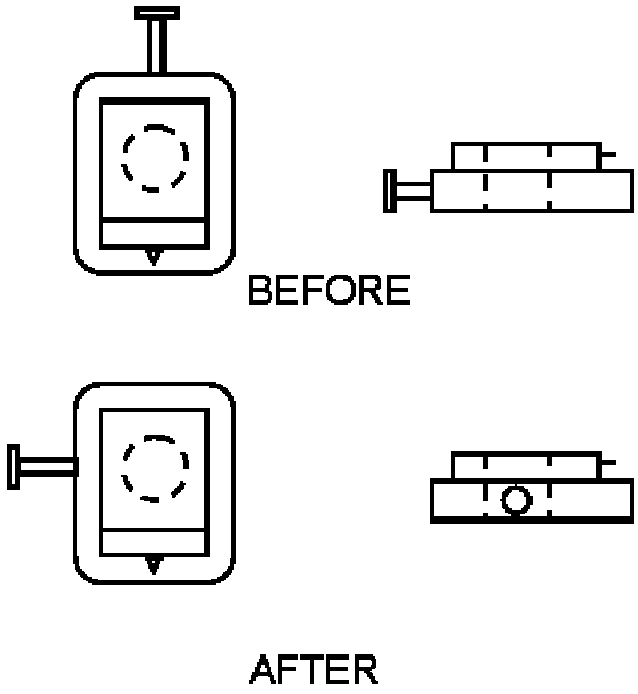

Figure 3-16 Schematic Illustration of Knife Edge Modification

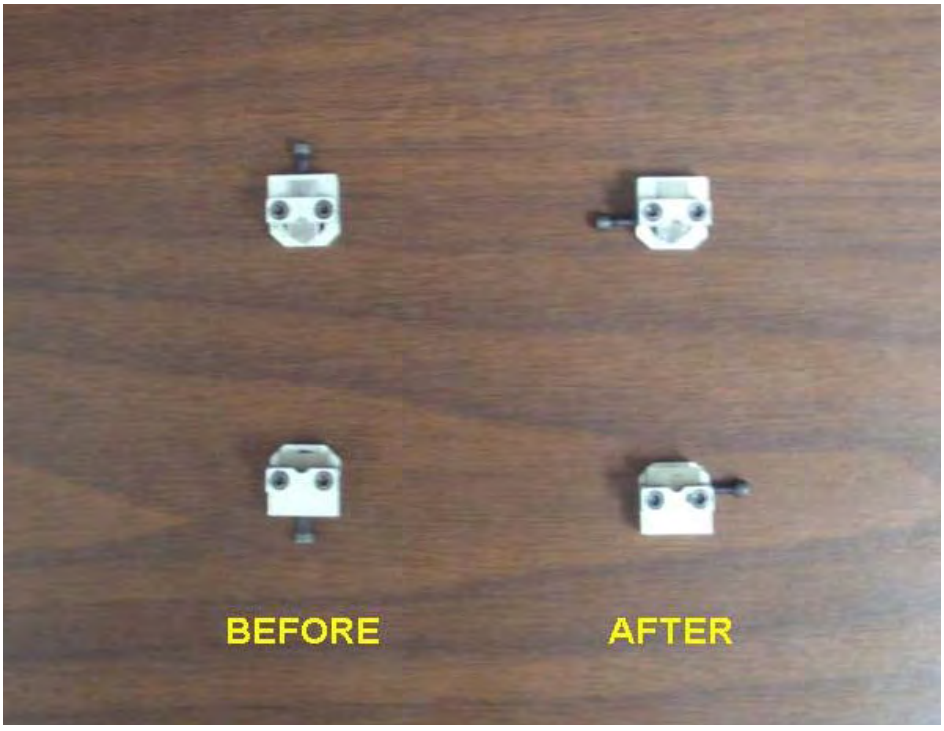

Figure 3-17 Modification of Knife Edge

3.3.4 Load Equalization System

A load equalization system consisting of two interactive hydraulic cylinders was conceived and designed to assure uniform loading across the specimen, that is, to minimize or eliminate eccentric loading that can induce premature failure near the loading heads. This load frame system attaches to the loading heads with two pins to pull on the specimen in a uniform fashion. The upper chambers of both cylinders are filled and plumbed together, and the lower piston chambers are similarly plumbed. Therefore, as one piston goes up, the other piston comes down. In essence, if one side of the specimen starts to fail, the complete load is not transferred to the other side of the specimen. The piston rises moving hydraulic fluid to the other cylinder thereby reducing the load on the non-failing side until the load equalizes and then continues to equalize until failure. This takes place very quickly and extra low friction (ELF) seals were secured and incorporated inside each cylinder to reduce the effects of seal friction on load uniformity. Figure 3-18 shows the actual cylinder loading assembly and Figure 3-19 shows the loading assembly attached to loading rod.

The load frame has a capacity of 22,000 pounds, which far exceeds the needs for most asphalt materials characterization, at even the coldest testing temperatures, and includes an environmental chamber manufactured by ESPEC. The temperature range of the environmental chamber is -20° C to 100° C, with an accuracy of ± 0.2° C, as required by Superpave specifications. Temperature control systems are also available at the University of Florida as shown in Figure 3-20. This type of environmental chamber is useful to maintain the specimen at test temperature during placement of the extensometers through two access holes. Since behavior of asphalt mixtures are highly dependent on temperature, careful control of chamber temperature is necessary to obtain accurate material properties.

Figure 3-18 Dual Cylinder Loading Assembly

Figure 3-19 Dual Cylinder Loading Assembly Attached to Loading Rod

Hydraulic power is provided to the MTS load frame via an MTS SilentFlo hydraulic power supply. This hydraulic power supply provides the actuator, or system, high-pressure hydraulic fluid at 3000 psi, at a flow rate of approximately 5.5 gallons per minute. Heat removal from the hydraulic power supply is accomplished via a portable chiller manufactured by BUDZAR Industries, and is properly sized to the hydraulic power supply. A temperature control chamber is required to be rapid and stable such that a specimen should be quickly stabilized at the testing temperature.

Figure 3-20 Environmental Chamber

3.4 Dog-Bone Direct Tension Test Procedures

Three kinds of tests (i.e., resilient modulus, creep compliance, and strength test) were performed on all mixtures to determine resilient modulus, creep compliance, m-value, tensile strength, failure strain, fracture energy, and dissipated creep strain energy to failure. As mentioned previously, these tests provide the properties needed to define cracking performance using the HMA fracture model developed at the University of Florida (Zhang et al., 2001; Roque et al., 2004a).

3.4.1 Resilient Modulus Test

The resilient modulus is defined as the ratio of the applied stress to the recoverable strain when repeated loads are applied. It is one of the most common methods for measuring the stiffness of the asphalt mixtures. The resilient modulus test was performed in load control mode by applying a repeated haversine waveform load to the specimen for 0.1 second along with a rest period of 0.9 second. The load was selected to keep on-face strain between 100 and 300 micro-strains. A typical load versus time plot is shown in Figure 3-21.

The procedures for resilient modulus test are as follows:

(1) Dog-bone test samples are stored in a humidity chamber at a constant relative humidity of 60 percent for at least 2 days prior to testing to ensure uniform moisture conditions. Specimens are there cooled at the test temperature for at least 6 hours before testing.

(2) Extensometers are mounted and centered on the specimen to the gage points for the measurements of the face and edge deformations.

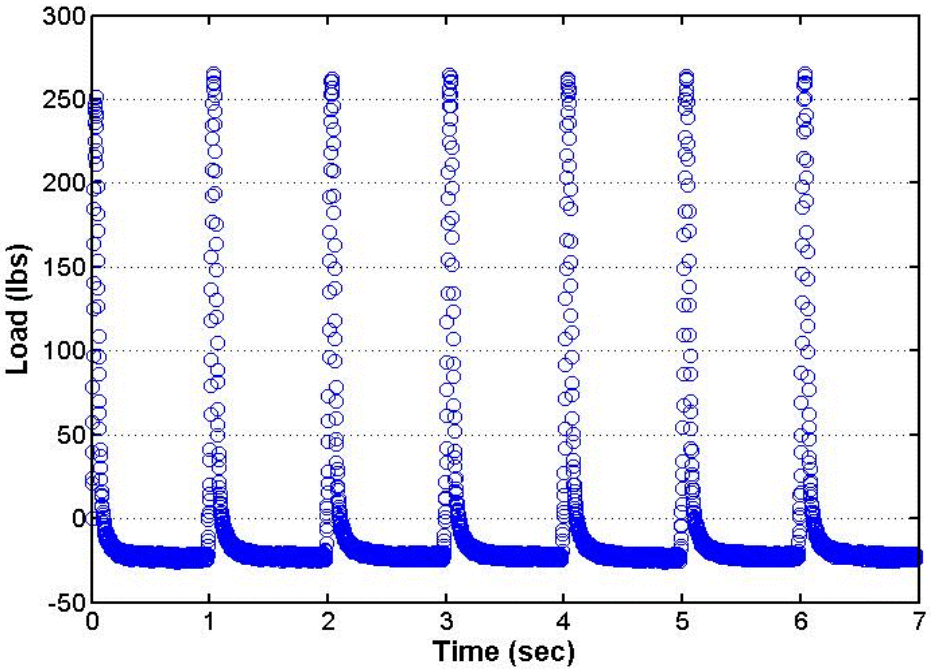

Figure 3-21 An Example of Resilient Load Data

(3) A constant preloading of approximately 5 pounds is applied to the test specimens to ensure proper contact between loading pins and holes in upper loading head through which the load is applied.

(4) The specimen is then tested by applying a repeated haversine waveform load for seven seconds to obtain on-face strain between 100 to 300 micro-strains. If the horizontal strains are higher than 300 micro-strains, the load is immediately removed from the specimen, and the specimen is allowed to recover for a minimum 3 minutes before reloading at a lower load.

(5) When the applied load is determined, the data acquisition program begins recording test data. Data are acquired at a rate of 500 points per second.

(6) The resilient modulus is calculated based on three dimensional finite element analysis described in section 3.5.

3.4.2 Creep Test

Creep compliance is a function of time dependent strain over constant stress. Creep compliance curve is useful not only for predicting thermally induced stress in an asphalt pavement but also for evaluating the rate of damage accumulation of asphalt mixture.

The creep test requires the application of a constant load, applied as a step function, for 1000 seconds. Figure 3-22 shows typical creep load measurements. The magnitude of load is adjusted so that the horizontal deformations meet certain criteria. These criteria are limits set on the horizontal deformations at 100 seconds, and as a not-to-exceed value at the end of the test as mentioned below. These limits can vary with test temperature or with the specimen type, but most importantly, with heavily aged specimens. The load was selected to keep the maximum on-face strain below 750 micro-strain.

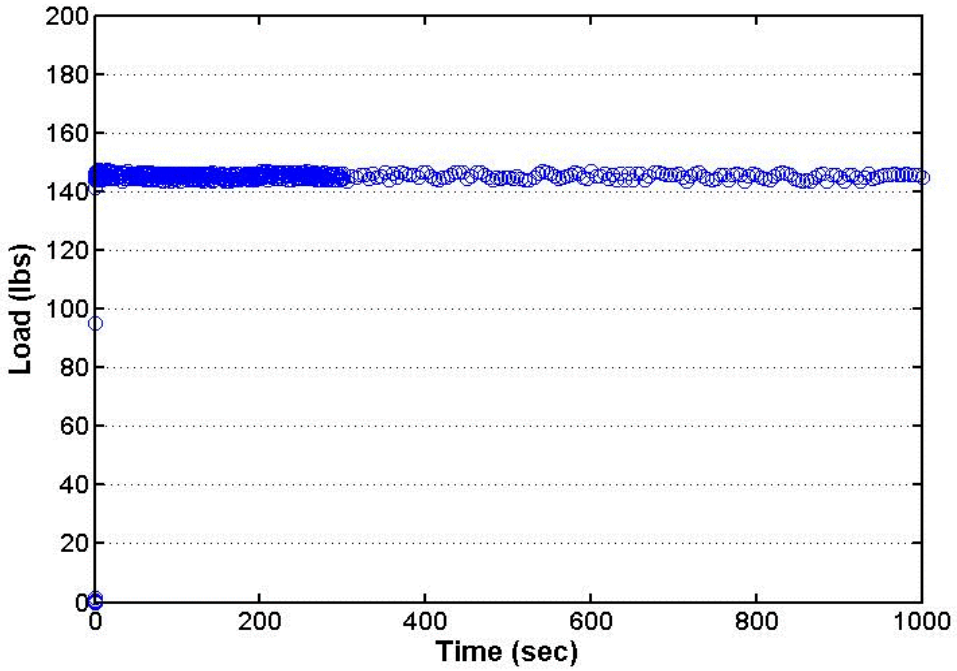

Figure 3-22 An Example of Creep Load Data

The test procedures for creep test with DBDT system consist of the following steps:

(1) The test sample preparation, mounting the extensometers, and preloading procedures are the same as those for resilient modulus test.

(2) The static loading is applying and held for 1000 seconds. If the on-face strains are not between 100 and 180 micro-strains at 100 seconds or are higher that 750 micro-strains at 1000 seconds, the load is immediately removed from the specimen, and specimen is allowed to recover until deformations are relatively constant before reloading at a different level.

(3) When the applied load is determined, the data acquisition program records the loads and deformations at a rate of 10 Hz for the first 10 seconds, 1 Hz for the next 290 seconds, and 0.2 Hz for the remaining 700 seconds of the creep test.

The creep parameters, which are m-value, D_1, creep compliance, and creep rate, are calculated based on three dimensional finite element analysis.

3.4.3 Tensile Strength Test

Failure limits including tensile strength, failure strain, and fracture energy were determined from strength test. These properties are used for estimating the cracking resistance of the asphalt mixtures. The strength test was conducted by applying a constant rate of displacement of loading ram until the specimen failed. After careful observation of displacement rate from two testing modes, displacement rate of DBDT test was determined based on the comparison between horizontal deformation of Superpave IDT and on-face deformation of DBDT test as shown in Figure 3-23. It should be noted that a given rate of ram displacement will result in a strain rate in the Superpave IDT that is approximately twice as high as in the DBDT. Therefore, in order to

achieve approximately the same strain rate in both tests, a deformation rate of 1in/min for dense graded asphalt mixture was used in DBDT test compared to the standard 2in/min used in the Superpave IDT. For open graded asphalt mixture, a deformation rate of 2in/min was used in DBDT test. It should be noted that the non-uniform stress distribution on the DBDT cross-section results in non-uniform strain rates in the cross-section. Therefore, the actual strain rate at the edge of the DBDT specimen will be greater than at its center of face and greater than the Superpave IDT. The on-face and on-edge deformation, and the applied load are recorded.

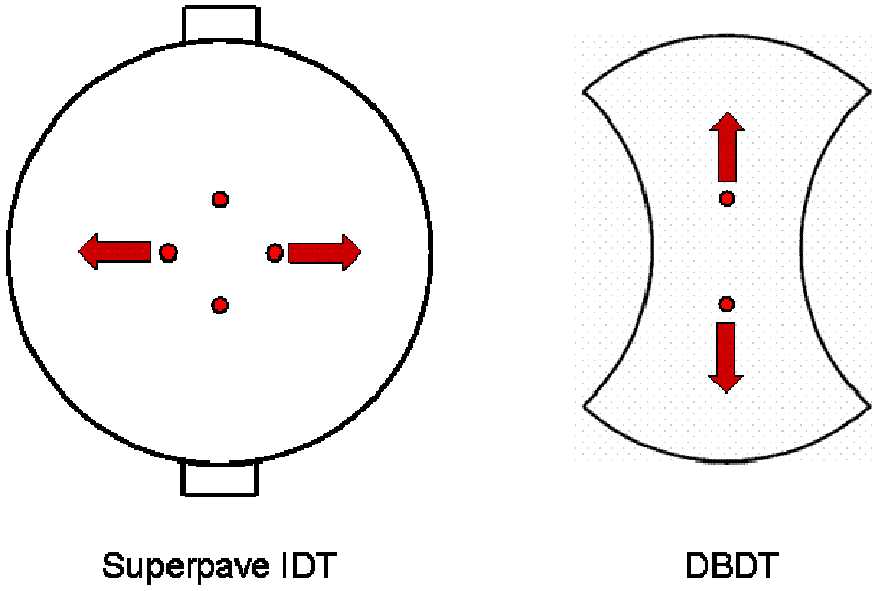

Figure 3-23 Determination of Strain Rate for Strength Test

3.5 Data Interpretation Methods for Dog-Bone Direct Tension Test

The development of appropriate data interpretation methods to accurately determine material properties based on measurements obtained from the DBDT is described in this section. Accurate determination of properties requires accurate prediction of stresses within the specimen, an approach that can accurately identify the instant of fracture from load and

deformation measurements, and procedures to properly determine strain accurately from deformation measurements. Developments in each of these areas are described in the sub-sections below.

3.5.1 Three Dimensional Finite Element Analysis

Three dimensional finite element analysis was conducted to analyze stress and strain of a 6-inch diameter specimen with the proposed system. The commercial computer program ADINA was used for analysis (ADINA, 2005). To simplify analysis and for time savings, symmetry was taken advantage of in all three dimensions. Therefore, only one eighth of the specimen was analyzed without sacrificing any accuracy or information. Roller supports were applied at each node along planes of symmetry. The program ADINA provides proper supports to meet given conditions at the lines and points where the roller supports meet. Full friction was assumed at the interface between steel loading head and the specimen. Figure 3-24 shows the 3-D FEM mesh used to represent the specimen and the coordinate system used. The analysis was conducted assuming an asphalt modulus of 400,000 psi, while varying Poisson's ratio, the center width, and thickness of the specimen.

3.5.1.1 Stress Analysis

Stress at the center of a specimen of uniform cross-section can simply be calculated as applied load divided by cross-sectional area. However, results of the 3-D FEM analyses presented in Figure 3-25 indicate that the stress distribution of the DBDT specimen having a 2-inch thickness and a 2-inch width varies from the center of the face to the center of the edge. The tensile stresses vary along centerline of the specimen (x- and y- axis in Figure 3-26) and reach a maximum at the edge of the specimen.

According to this analysis, tensile failure will initiate at the edge of the specimen. An important finding is that stress distributions are nearly independent of the Poisson's ratio. Based on multiple 3-D finite element analyses performed with a range of variables, stress correction factors were developed to determine the point stress on the face and edge of the proposed DBDT system based on average cross-sectional stress (P/A). The corrected point stresses on the face and edge can be calculated using the following Equations (3-1) to (3.4).

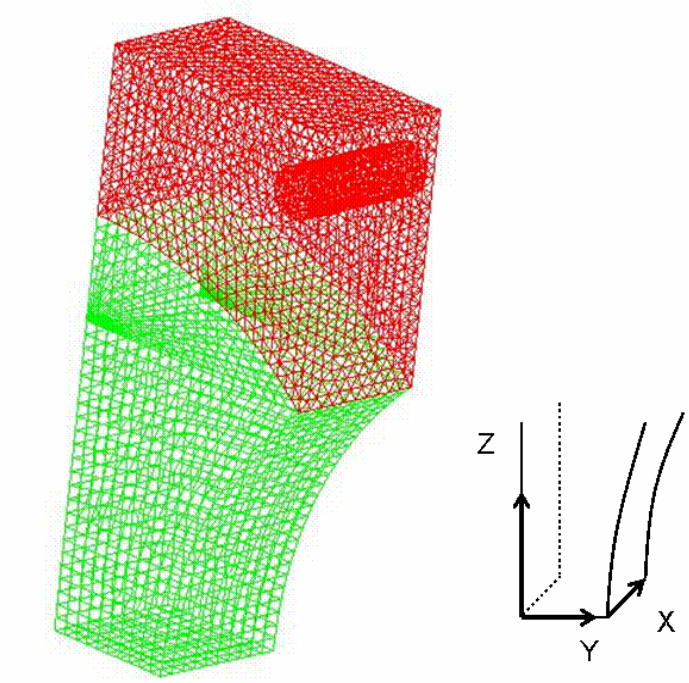

Figure 3-24 3-D FEM Mesh and Coordinates

$$\sigma_{fc} = \frac{P}{A_c} C_{\sigma f} \tag{3-1}$$

$$\sigma_{ec} = \frac{P}{A_c} C_{\sigma e} \tag{3-2}$$

$$C_{\sigma f} = -0.0198t - 0.0158w + 0.9607 \tag{3-3}$$

$$C_{\sigma e} = 0.0177t + 0.0901w + 1.0346 \quad (3\text{-}4)$$

Where, σ_{fc} = stress on face corrected, σ_{ec} = stress on edge corrected, P = applied load (lbs), A_c = area at the center of a specimen (in^2), $C_{\sigma f}$ = stress correction factor on face, $C_{\sigma e}$ = stress correction factor on edge, t = thickness of a specimen (in), w = width at the center of a specimen (in).

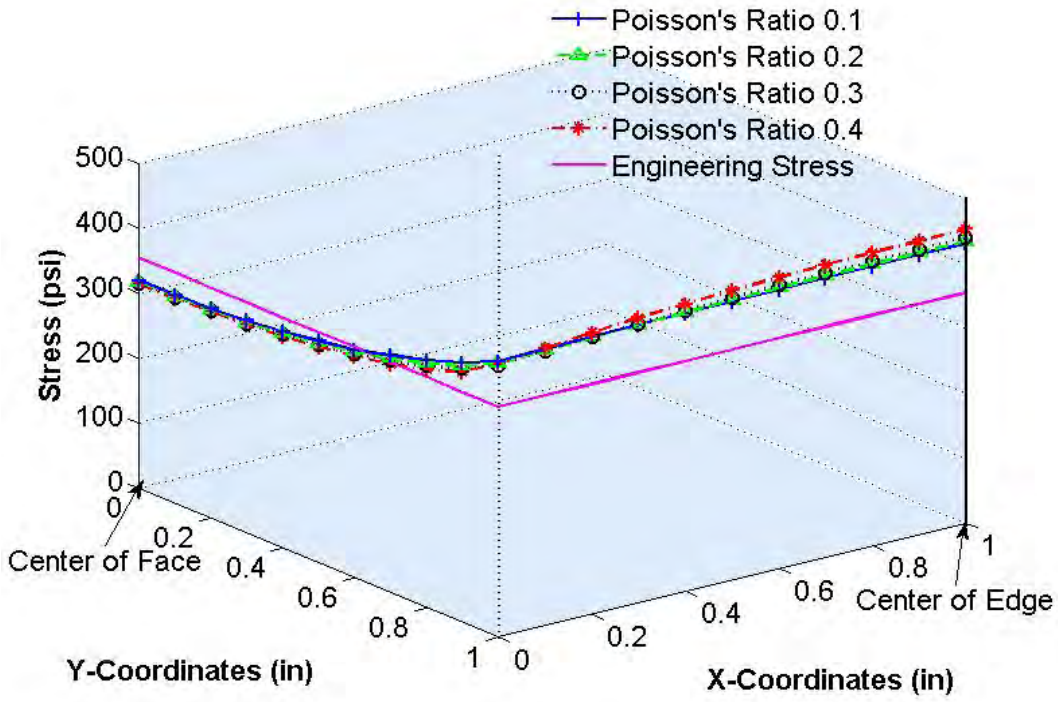

Figure 3-25 Stress Distributions at the Center of DBDT Specimen (2-in thickness specimen with 2-in width)

3.5.1.2 Strain Analysis

The strain values obtained from the DBDT test are based on the point-to-point displacements measured by the finite length extensometers and are better represented by the average of the strain distributions between gage points as expressed by Equations (3-5) and (3-6).

$$\varepsilon_{fa} = \frac{1}{GL}\int_{-GL/2}^{GL/2} f_1(x)dx \quad (3\text{-}5)$$

$$\varepsilon_{ea} = \frac{1}{GL}\int_{-GL/2}^{GL/2} f_2(x)dx \quad (3\text{-}6)$$

Where, ε_{fa} = average strain between two gage points on face, ε_{ea} = average strain between two gage points on edge, GL = gage length (in) = distance over which vertical deformations are obtained.

Since only the average strain can be measured with a finite length gage, strain correction factors were developed to convert the average strain determined from the extensometer to a vertical point strain at the center of a specimen's face and edge. Figures 3-26 and 3-27 present the strain distributions between gage points on the face and edge. It was noted that these values were nearly independent of Poisson's ratio. With respect to strain on the face (Figure 3-26), small differences with Poisson's ratio were observed. However, it was determined that the maximum error in strain resulting from assuming an incorrect value of Poisson's ratio was only 2.6%. The strain is corrected using following Equations (3-7) to (3-10).

$$\varepsilon_{fp} = \varepsilon_{fc} = \varepsilon_{fa} C_{\varepsilon f} \quad (3\text{-}7)$$

$$\varepsilon_{ep} = \varepsilon_{ea} C_{\varepsilon e} \quad (3\text{-}8)$$

$$C_{\varepsilon f} = -0.0028t - 0.0178w + 1.0545 \quad (3\text{-}9)$$

$$C_{\varepsilon e} = 0.0039t - 0.0015t^2 - 0.009w + 1.0770 \quad (3\text{-}10)$$

Where, $\varepsilon_{fp} = \varepsilon_{fc}$ =corrected vertical point strain at the center of a specimen's face, ε_{ep} = corrected vertical point strain at the center of a specimen's edge, $C_{\varepsilon f}$ = strain correction factors on face, $C_{\varepsilon e}$ = strain correction factors on edge, t and w as previously defined.

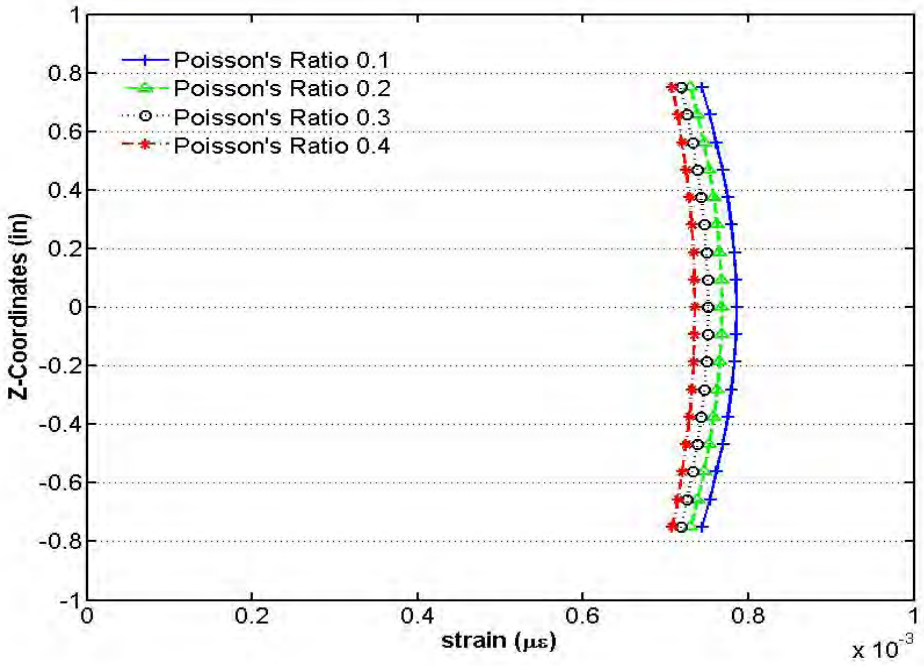

Figure 3-26 Strain Distributions on Faces (2-in thickness specimen with 2-in width)

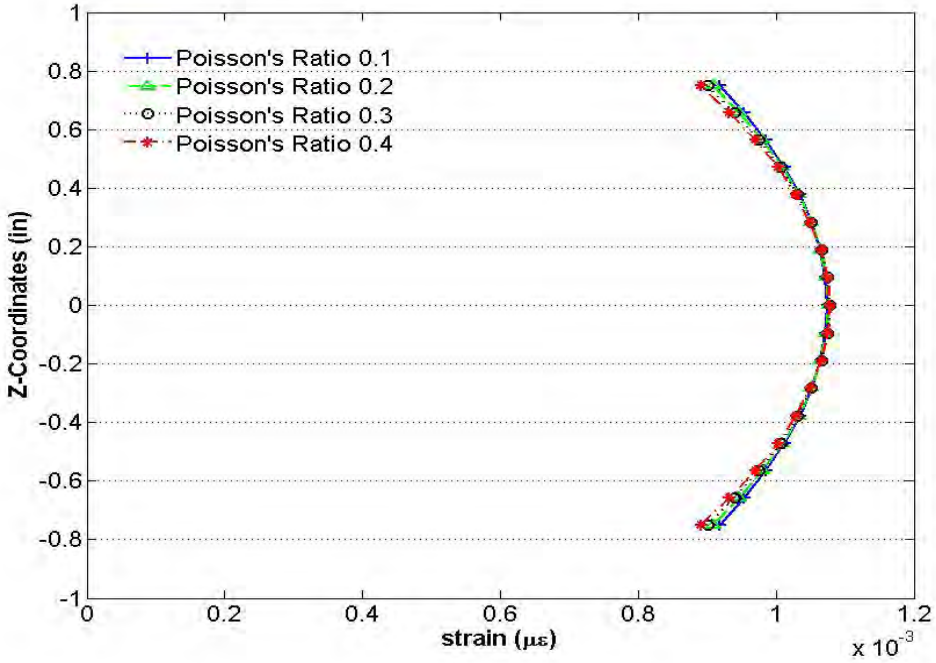

Figure 3-27 Strain Distributions on Edges (2-in thickness specimen with 2-in width)

3.5.1.3 Rotation Effect on Edge Measurements

Figure 3-28 shows how rotational effects of the gage points can influence the deformation measurements at the edges. According to the analysis, it was found that the rotational effects are significant, but not affected by Poisson's ratio, thickness or width of specimen.

Figure 3-29 presents the effect of Poisson's ratio for a 2-inch thick specimen with a 2-inch width. This shows a normalized deformation along axis of the gage point, where the contact surface between specimen and the gage point is given a value of 1. A single correction factor can be applied in all cases as long as gage point length is known. Displacement correction factors can be obtained with knowing that the actual measurement is comprised of the expected measurement plus two times the measurement error as shown in Figure 3-28.

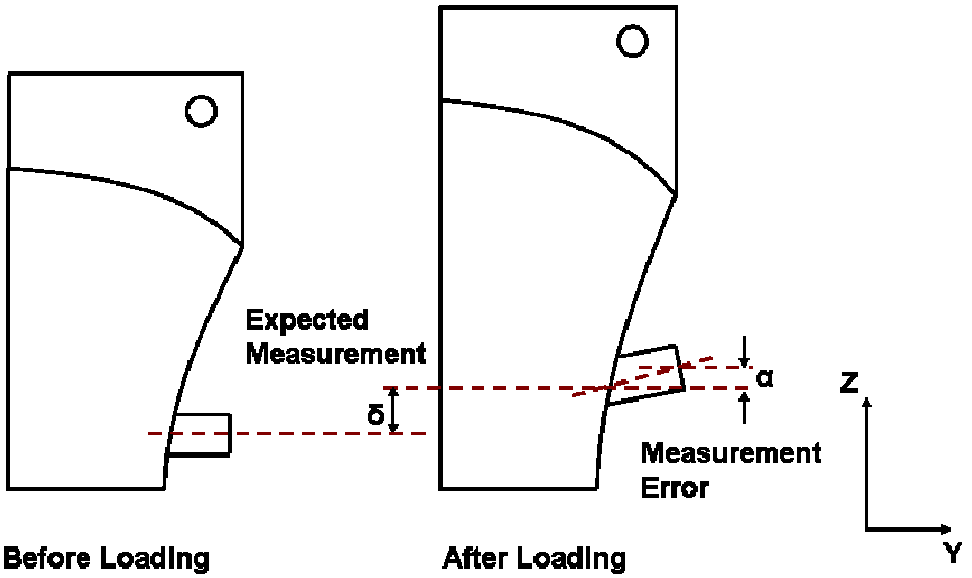

Figure 3-28 Rotational Effect on Edges

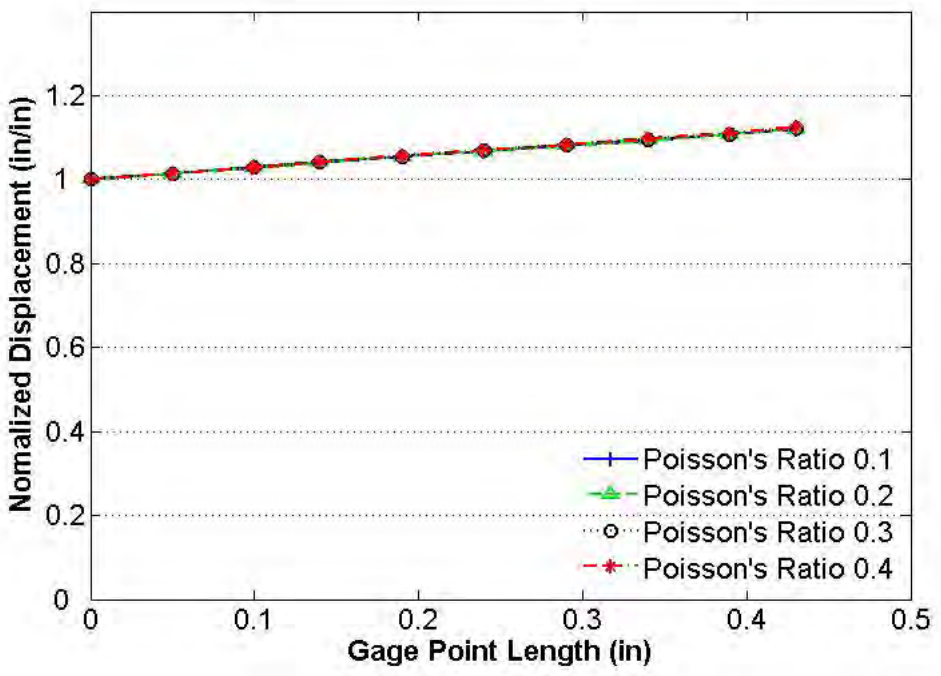

Figure 3-29 Normalized Displacement along Axis of Gage Point on Edge (2-in thickness specimen with 2-in width)

$$\varepsilon_{ed} = \varepsilon_{ea} C_{de} \tag{3-11}$$

Where, ε_{ed} = corrected strain for rotation effect on the edge, C_{de}= displacement correction factors for the edge = 0.81, ε_{ea} as previously defined.

Therefore, a corrected point strain on the edge can be obtained using a combination of Equations (3-8) and (3-11).

$$\varepsilon_{ec} = \varepsilon_{ea} C_{\varepsilon e} C_{de} \tag{3-12}$$

Where, ε_{ec} = corrected strain for rotation effect on the edge, All other variables as previously defined.

3.5.2 Resilient Modulus Test

Resilient modulus has been extensively used in the pavement engineering community to evaluate the relative quality of mixtures and to predict load response of pavements subjected to wheel loads. The resilient modulus test is performed in load control mode by applying a repeated haversine waveform load to the specimen for a period of 0.1 second followed by a rest period of 0.9 seconds. The load for the resilient modulus test was selected to keep the on-surface strains below linear viscoelastic range. Resilient modulus is a function of the load, specimen dimensions, and resilient deformation. For the DBDT specimen, stress and strains required for calculation of resilient modulus can be determined using the correction factor equations which were developed based on 3-D finite element analysis as described above.

The resilient modulus of asphalt mixture was calculated by using the measured face deformation. The instantaneous resilient modulus is calculated by using the recoverable deformation that occurs instantaneously during the unloading portion of each cycle. The total resilient modulus is calculated by using the total recoverable deformation, which includes both the instantaneous recoverable and the time-dependent recoverable deformation during the unloading and rest-period portion of each cycle.

Analysis procedure is summarized as followings:

(1) Determine the beginning of each load cycle.

For each load cycle, the beginning of the load cycle was determined as the first data point in a series that has three sequential load increases (regardless of how small), and for which the total of the three load increases is greater than 10 lbs. Figure 3-30 shows the load start point used for analysis based on measured load data. The noise in the load measurements can be no greater than 10 lbs for this approach to work.

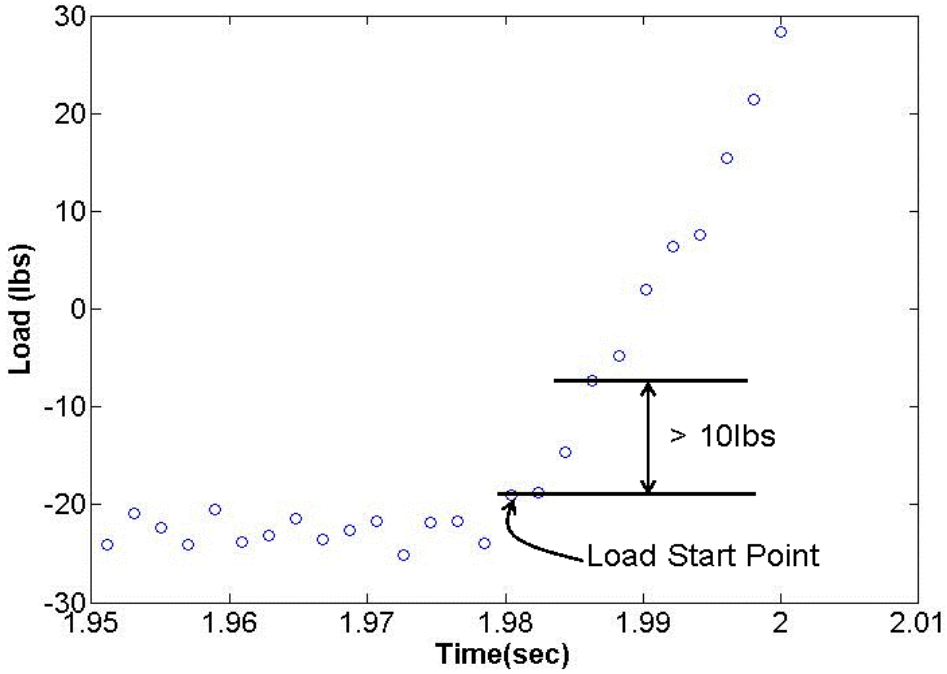

Figure 3-30 Determination of Beginning of Load Cycle

(2) Determine the maximum load for each cycle.

As shown in Figure 3-31, the maximum load is determined as the peak load and the seating load is determined by averaging the 30 loading points recorded immediately prior to the beginning of the load cycle.

(3) Calculate the stress for each cycle.

Load amplitude for each cycle is simply maximum load minus the seating load prior to the cycle:

$$P_i = P_{max\_i} - P_{seat\_(i-1)} \tag{3-13}$$

Stress for each cycle can be simply calculated using following equations with correction factors.

$$\sigma_{fci} = \frac{P_i}{A_c} C_{\sigma f} \tag{3-14}$$

$$\sigma_{eci} = \frac{P_i}{A_c} C_{\sigma e} \tag{3-15}$$

Where, P_i = load amplitude for each cycle, P_{max_i} = maximum load for each cycle, $P_{seat\_(i-1)}$ = seating load prior to each cycle, i = number of cycles (1 ~ 7), σ_{fci} = corrected stress on the specimen face for each cycle, σ_{eci} = corrected stress on the specimen edge for each cycle.

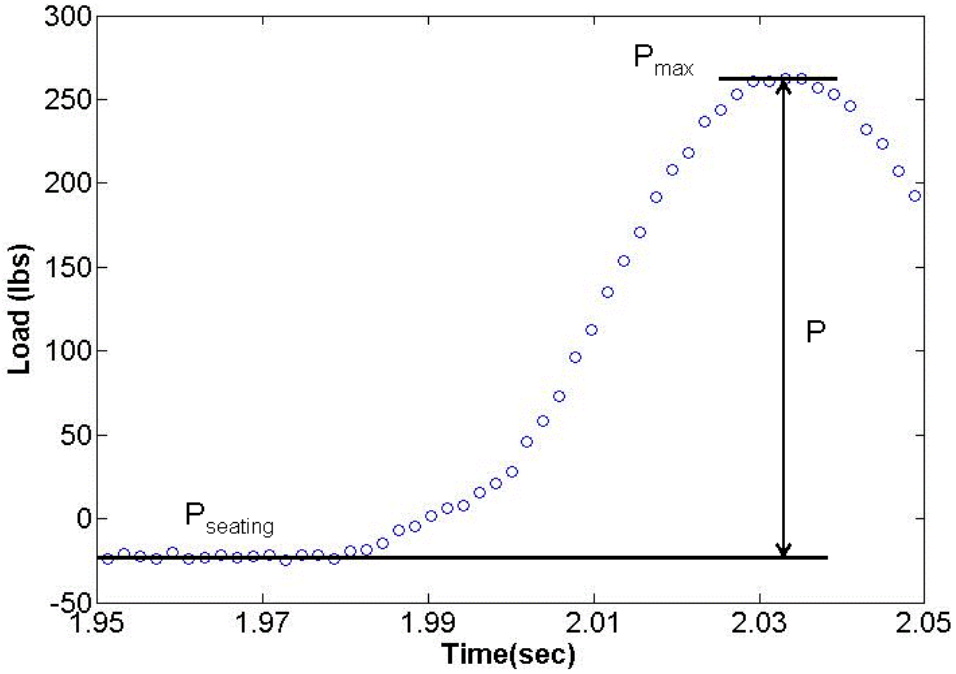

Figure 3-31 Determination of Load Amplitude

(4) Calculate the instantaneous and total recoverable deformation for each cycle

The maximum deformation is determined as the peak deformation for each cycle (see Figure 3-32), and determining the value of the deformation is made by performing the regression analysis of recovery portion of each deformation wave.

The definitions of the instantaneous and total recoverable deformations for resilient modulus test are presented in Figure 3-33. From the maximum deformation point of each cycle, three data points are skipped and the next seven data points are selected to perform the regression on the unloading portion of the wave (regression #1, Figures 3-33). Starting at the end of the loading cycle, the previous 100 data points were used to performe linear regression analysis (regression #2, Figure 3-33).

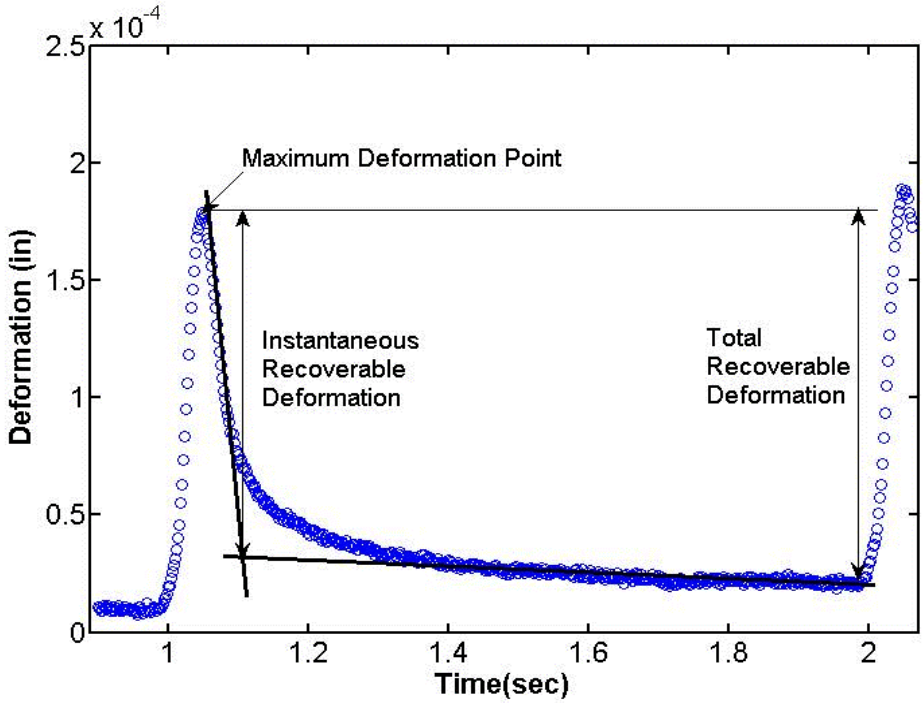

Figure 3-32 Definition of Instantaneous and Total Recoverable Deformation

The intersection of the two best fit lines was used to compute the instantaneous recoverable as shown in Figures 3-33. The total recoverable deformation is based on the deformation at the end of the load cycle where the deformation is defined as the intersection of regression line #2 and the beginning of the following cycle.

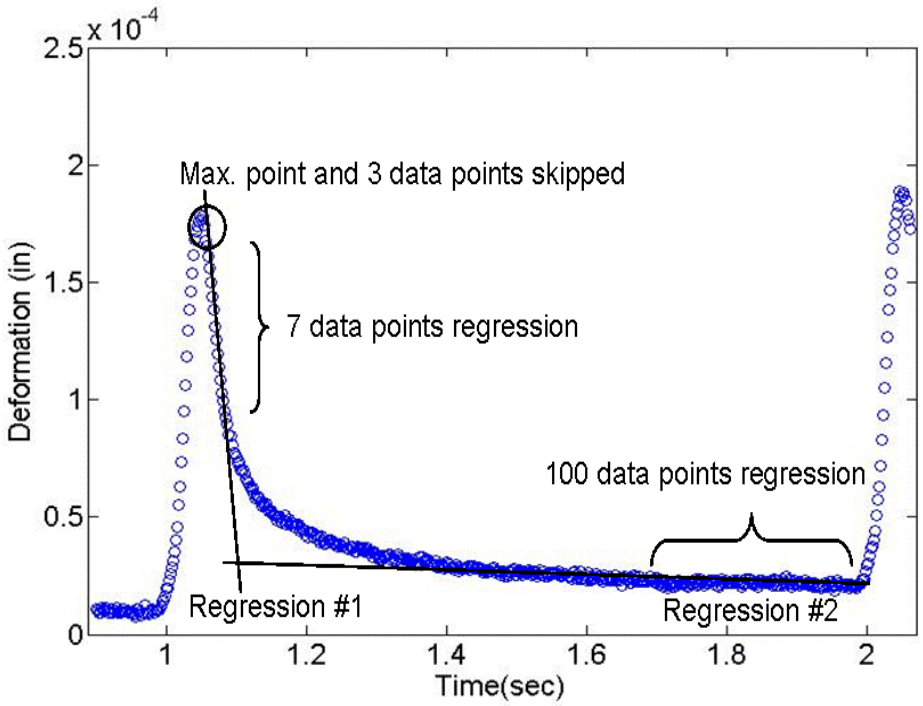

Figure 3-33 Determination of Instantaneous and Total Recoverable Deformation

(5) Calculate the instantaneous and total recoverable strains for each cycle

$$\varepsilon_{fa\_Ii} = \frac{1}{GL}\int_{-GL/2}^{GL/2} f_1(x)dx \tag{3-16}$$

$$\varepsilon_{fa\_Ti} = \frac{1}{GL}\int_{-GL/2}^{GL/2} f_1(x)dx \tag{3-17}$$

$$\varepsilon_{ea\_Ii} = \frac{1}{GL}\int_{-GL/2}^{GL/2} f_2(x)dx \tag{3-18}$$

$$\varepsilon_{ea\_Ti} = \frac{1}{GL}\int_{-GL/2}^{GL/2} f_2(x)dx \tag{3-19}$$

Where, ε_{fa_Ii} = instantaneous average strain between two gage points on face for each cycle, ε_{fa_Ti} = total average strain between two gage points on face for each cycle, $\varepsilon_{ea\_\_Ii}$ = instantaneous average strain between two gage points on edge for each cycle, $\varepsilon_{ea\_\_Ti}$ = total average strain between two gage points on edge for each cycle.

Corrected point strains are determined as follows:

$$\varepsilon_{fc\_Ii} = \varepsilon_{fa\_Ii} C_{\varepsilon f} \tag{3-20}$$

$$\varepsilon_{fc\_Ti} = \varepsilon_{fa\_Ti} C_{\varepsilon f} \tag{3-21}$$

$$\varepsilon_{ec\_Ii} = \varepsilon_{ea\_Ii} C_{\varepsilon e} C_{de} \tag{3-22}$$

$$\varepsilon_{ec\_Ti} = \varepsilon_{ea\_Ti} C_{\varepsilon e} C_{de} \tag{3-23}$$

Where, ε_{fc_Ii} = instantaneous corrected strain at the center of a specimen's face for each cycle, ε_{fc_Ti} = total corrected strain at the center of a specimen's face for each cycle, ε_{ec_Ii} = instantaneous corrected strain at the center of a specimen's edge for each cycle, ε_{ec_Ti} = total corrected strain at the center of a specimen's edge for each cycle.

(6) Obtain trimmed mean modulus for each replicate

Even though seven cycles are recorded, only five are analyzed. It was determined that seven load cycles must be obtained to assure that five complete load cycles are recorded. The seven resilient moduli from the seven cycles are ranked. The highest and lowest values are deleted and the remaining five moduli are averaged to obtain the trimmed mean moduli.

$$M_{RfI\_n} = \left(\sum_{i=1}^{7} \frac{\sigma_{fci}}{\varepsilon_{fc\_Ii}} - Max\left(\frac{\sigma_{fci}}{\varepsilon_{fc\_Ii}} \right) - Min\left(\frac{\sigma_{fci}}{\varepsilon_{fc\_Ii}} \right) \right) \Big/ (i-2) \tag{3-24}$$

$$M_{RfT\_n} = \left(\sum_{i=1}^{7} \frac{\sigma_{fci}}{\varepsilon_{fc\_Ti}} - Max\left(\frac{\sigma_{fci}}{\varepsilon_{fc\_Ti}} \right) - Min\left(\frac{\sigma_{fci}}{\varepsilon_{fc\_Ti}} \right) \right) \Big/ (i-2) \tag{3-25}$$

$$M_{ReI\_n} = \left(\sum_{i=1}^{7} \frac{\sigma_{eci}}{\varepsilon_{ec\_Ii}} - Max\left(\frac{\sigma_{eci}}{\varepsilon_{ec\_Ii}} \right) - Min\left(\frac{\sigma_{eci}}{\varepsilon_{ec\_Ii}} \right) \right) \Big/ (i-2) \tag{3-26}$$

$$M_{ReT\_n} = \left(\sum_{i=1}^{7} \frac{\sigma_{eci}}{\varepsilon_{ec\_Ti}} - Max\left(\frac{\sigma_{eci}}{\varepsilon_{ec\_Ti}} \right) - Min\left(\frac{\sigma_{eci}}{\varepsilon_{ec\_Ti}} \right) \right) \Big/ (i-2) \tag{3-27}$$

Where, M_{RfI} = instantaneous resilient modulus on face, M_{RfT} = total resilient modulus on face, M_{ReI} = instantaneous resilient modulus on edge, M_{ReT} = total resilient modulus on face, n = number of gage on faces or edges from three replicates (3 replicates × 2 faces/edges)

(7) Obtain trimmed mean modulus from three replicates

To more reliably obtain resilient deformation, three replicate specimens were tested and evaluated. Six moduli with on-face measurements and six moduli with on-edge measurements were obtained. The six moduli from each case were ranked. The highest and lowest moduli were deleted and the remaining four moduli were averaged to obtain the trimmed mean modulus.

$$M_{RfI} = \left(\sum_{n=1}^{6} M_{RfI\_n} - Max\left(M_{RfI\_n}\right) - Min\left(M_{RfI\_n}\right) \right) \Big/ \left(n-2\right) \quad (3\text{-}28)$$

$$M_{RfT} = \left(\sum_{n=1}^{6} M_{RfT\_n} - Max\left(M_{RfT\_n}\right) - Min\left(M_{RfT\_n}\right) \right) \Big/ \left(n-2\right) \quad (3\text{-}29)$$

$$M_{ReI} = \left(\sum_{n=1}^{6} M_{ReI\_n} - Max\left(M_{ReI\_n}\right) - Min\left(M_{efI\_n}\right) \right) \Big/ \left(n-2\right) \quad (3\text{-}30)$$

$$M_{ReT} = \left(\sum_{n=1}^{6} M_{ReT\_n} - Max\left(M_{ReT\_n}\right) - Min\left(M_{efT\_n}\right) \right) \Big/ \left(n-2\right) \quad (3\text{-}31)$$

According to Roque et al. (1997), however, the method used to determine the instantaneous recoverable deformation should be reviewed. This method may not be suitable for mixtures that exhibit significant delayed elastic recovery, where the recovery portion of the unloading deformation curve is highly nonlinear since this fits a straight line though the last 100 points of each loading cycle regardless of mixture stiffness. At this present time, thus, the used of total resilient modulus is recommended because it is less affected by this effect.

3.5.3 Creep Test

Creep compliance is a function of time-dependent strain over stress. Creep compliance can be used to predict thermally induced stress in asphalt pavement, as well as to evaluate the rate of damage accumulation of asphalt mixture. D_0, D_1, and m-value are mixture parameters obtained from creep compliance tests. D_1 and m-value have been used to determine the rate of damage accumulation in asphalt mixture.

Analysis procedure is summarized as follows:

(1) Calculate stresses and strains with correction factors

The stresses and strains for face and edge were corrected with correction factor equations.

$$\sigma_{fc} = \sigma_{f0} = \frac{P_0}{A_c} C_{\sigma f} \quad (3\text{-}32)$$

$$\sigma_{ec} = \sigma_{e0} = \frac{p_0}{A_c} C_{\sigma e} \quad (3\text{-}33)$$

$$\varepsilon(t)_{fc} = \varepsilon(t)_{fa} C_{\varepsilon f} \quad (3\text{-}34)$$

$$\varepsilon(t)_{ec} = \varepsilon(t)_{ea} C_{\varepsilon e} \quad (3\text{-}35)$$

Where, $\sigma_{fc} = \sigma_{f0}$ = constant stress with time on face, $\sigma_{ec} = \sigma_{e0}$ = constant stress with time on face, $\varepsilon(t)_{fc}$ =corrected strain at the center of a specimen's face with time, $\varepsilon(t)_{ec}$ =corrected strain at the center of a specimen's edge with time.

(2) Calculate creep compliance

For uniaxial stress conditions, creep compliance is defined as time-dependent over constant stress (Equations 3-36, 37). Six creep compliances on faces from three replicates can be fitted with the generalized power. Similarly, six compliances are obtained on edges.

$$D(t)_{f\_n} = \frac{\varepsilon(t)_{fc\_n}}{\sigma_{fc\_n}} \quad (3\text{-}36)$$

$$D(t)_{e\_n} = \frac{\varepsilon(t)_{ec\_n}}{\sigma_{ec\_n}} \quad (3\text{-}37)$$

Where, $D(t)_f$ = creep compliance with time on face, $D(t)_e$ = creep compliance with time on edge, n = number of gage on faces or edges from three replicates (3 replicates × 2 faces/edge)

(3) Obtain trimmed mean creep compliance

The trimmed mean of creep compliance was obtained by plotting creep compliance (Figure 3-34) and ranking each of the face and edge compliance. The data in the middle of test were used for ranking. That is, ranking was performed using sum of compliance between 450 seconds and 550 seconds (Equation 3-38). These sums of the face and edge compliance were ranked numerically to identify the middle four face and middle four edge compliances. The upper and lower values from the three replicates were discarded (trimmed) and not included in the calculation. Results from the Superpave IDT introduced by Buttlar and Roque (1994) showed that more reliable estimates of creep compliance were obtained using the trimmed mean approach.

$$\sum D(t)_{middle\,of\,test} = \int_{450}^{550} D(t)dt \quad (3\text{-}38)$$

Where, $\sum D(t)_{middle\ of\ test}$ = sum of creep compliance in the middle of test

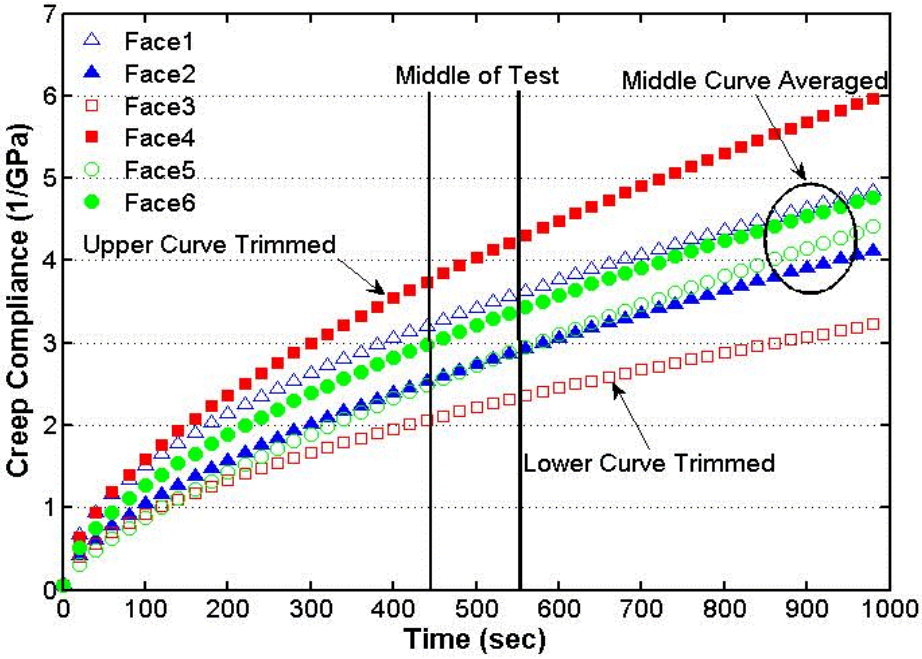

Figure 3-34 Trimmed Mean Method for Obtaining the Creep Compliance

After trimming the upper and lower values, the remaining four compliances were averaged to create representative creep parameters for face and edge.

$$D(t)_{f\_trimmed} = \frac{\varepsilon(t)_{fc\_trimmed}}{\sigma_{fc\_trimmed}} = D_{0f} + D_{1f}{}^{m_f} \tag{3-39}$$

$$D(t)_{e\_trimmed} = \frac{\varepsilon(t)_{ec\_trimmed}}{\sigma_{ec\_trimmed}} = D_{0e} + D_{1e}{}^{m_e} \tag{3-40}$$

Where, $D(t)_{f\_trimmed}$, D_{0f}, D_{1f}, m_f = representative creep parameters on face at certain condition, $D(t)_{e\_trimmed}$, D_{0e}, D_{1e}, m_e = representative creep parameters on edge at certain condition.

3.5.4 Tensile Strength Test

Failure limits of asphalt mixtures provide insight into their resistance to fracture. In addition, failure limits are required to determine whether load and temperature induced stresses and strains will cause failure of asphalt pavement. Also, since stress-strain information can be obtained from the strength test, it is possible to determine a measure of the mixture's stiffness by computing its tangent modulus from stress-strain results.

The true tensile strength of an asphalt mixture can be determined by determining the stress level at the edge of the specimen at the instant of failure. To accomplish this experimentally, a measurement system must be able to detect the instant when fracture occurs at the edge of the specimen. According to 3-D finite element analysis, fracture should occur on either edge first or on both edges simultaneously in the DBDT testing system, since tensile stress is highest at the edges.

Analysis procedure for strength test is summarized as follows:

(1) Determine the beginning of the loading

The start of the load is determined as the first data point in a series that has three sequential load increases, and the total load increase is greater than 30 lbs as shown in Figure 3-35. This guarantees that the subsequent data points are part of the loading cycle and not just initial load fluctuation or noise.

(2) Determine the end of the loading

It was determined that the instant of failure can be detected by examining the difference between the average face deformations and each edge deformation, since failure first occurs at the location where the rate of deformation increases as shown in Figure 3-36.

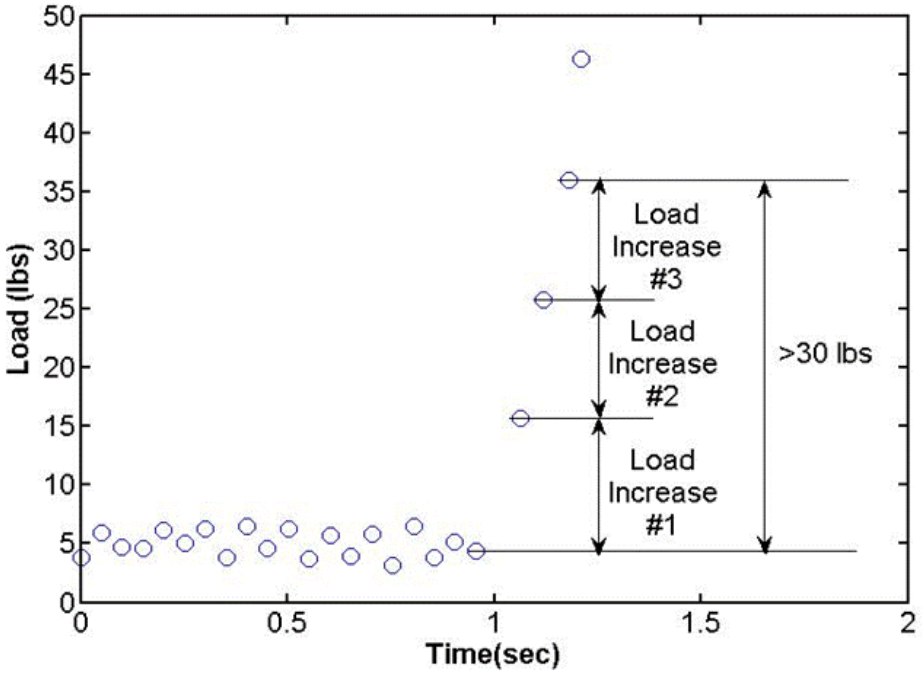

Figure 3-35 Determination of the Beginning of Loading

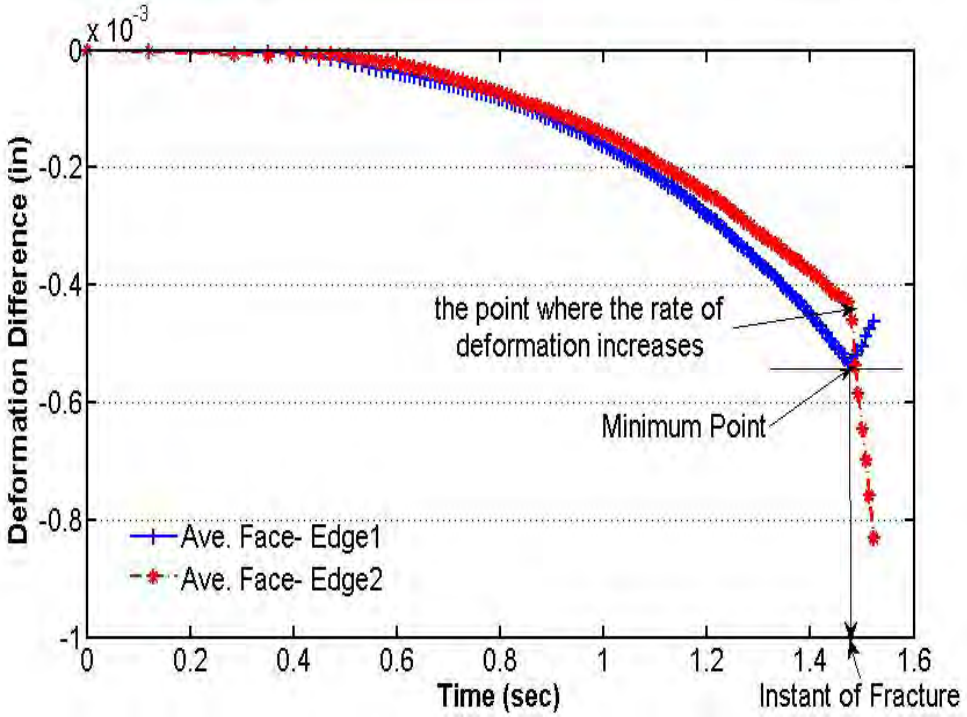

Figure 3-36 Instant of Fracture for DBDT System

(3) Calculate the strength of each specimen

Tensile strength of each specimen is calculated as follows:

$$S_t = \frac{P_{fracture}}{A_c} C_{\sigma e} \tag{3-41}$$

Where, S_t = tensile strength, $P_{fracture}$ = applied load at the instant of fracture, A_c = initial cross section area of the specimen.

(4) Calculate stress and strain at loading cycle time

Stresses and strains are calculated from the start of the load to the instant of specimen failure. When calculating stress, the initial seating load is subtracted from the applied loads to simulate a zero stress state at the beginning of the loading cycle. Failure strain was determined strain on edge at failure.

$$\sigma(t) = \frac{P(t) - P_{seating}}{A_c} C_{\sigma e} \tag{3-42}$$

$$\varepsilon_{ec}(t) = \varepsilon_{ea}(t) C_{\varepsilon e} C_{de} \tag{3-43}$$

Where, $\sigma(t)$ = corrected stress during loading time (t), P(t) = tensile load during loading time (t), $P_{seating}$ = initial seating load applied to specimen, ε_{ec} (t) = corrected strain effect on the edge during loading time (t).

(5) Calculate fracture energy and tangent modulus

To obtain fracture energy and tangent modulus, the stress-strain curve was fitted with a polynomial function. The three order polynomial function that forces the fitted curve through the origin.

$$\sigma(t) = a_1 \varepsilon(t) + a_2 \varepsilon(t)^2 + a_3 \varepsilon(t)^3 \quad (3\text{-}44)$$

It was noticed that when the function was not forced through the origin, the fit of the curve through the initial stress-strain points was strongly influenced by the data at the end of the test. Since the response at the end of the test is probably not purely elastic, it was decided to reduce the influence that this data has on the initial tangent modulus. By applying this constraint, the basic law that strain equals zero when stress equals zero is satisfied. By taking the derivative of the function, a tangent modulus can be computed at any strain level. Also, the function can be integrated to obtain the area under the curve, which presents the fracture energy as shown in Figure 3-37.

The fitted curve was obtained from stress-strain data that does not have the seating stress included. As mentioned earlier, this simulates a zero stress state at time equal to zero. However, when calculating fracture energy, the initial seating load must be included.

$$FE = \left(\int_{\varepsilon @ t=0}^{\varepsilon @ t=fail} a_1 \varepsilon(t) + a_2 \varepsilon(t)^2 + a_3 \varepsilon(t)^3 \right) + \left(P_{seating} \cdot \varepsilon_{@t=fail} \right) \quad (3\text{-}45)$$

Where, $\varepsilon_{@t=fail}$ = failure strain.

(6) Obtain trimmed mean values from three replicates

Like resilient modulus and creep compliance tests, three replicate specimens were tested and evaluated to reliably obtain the tensile properties from strength test. Trimmed mean method which eliminates the highest and lowest values was also used for analyzing the data. Tensile strength (S_t), failure strain ($\varepsilon_{failure}$), fracture energy (FE), and tangent modulus (M_T) were obtained from strength test.

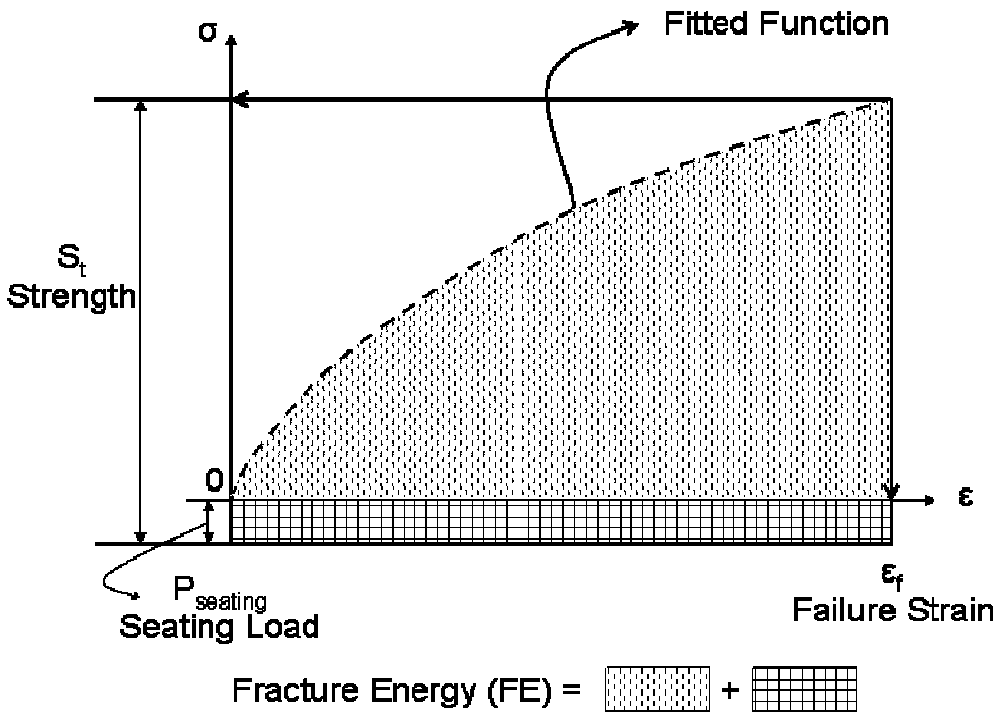

Figure 3-37 Determination of Fracture Energy

$$S_t = \left(\sum_{n=1}^{6} S_{t\_n} - Max(S_{t\_n}) - Min(S_{t\_n}) \right) \Big/ (n-2) \tag{3-46}$$

$$\varepsilon_{failure} = \left(\sum_{n=1}^{6} \varepsilon_{failure\_n} - Max(\varepsilon_{failure\_n}) - Min(\varepsilon_{failure\_n}) \right) \Big/ (n-2) \tag{3-47}$$

$$FE = \left(\sum_{n=1}^{6} FE_{\_n} - Max(FE_{\_n}) - Min(FE_{\_n}) \right) \Big/ (n-2) \tag{3-48}$$

$$M_T = \left(\sum_{n=1}^{6} M_{T\_n} - Max(M_{T\_n}) - (M_{T\_n}) \right) \Big/ (n-2) \tag{3-49}$$

All the variables were previously defined.

3.6 Preliminary Test Results

Preliminary tests were performed using the proposed DBDT prototype to investigate the feasibility and accuracy of this system for determining the tensile properties of asphalt mixtures and to validate the correction factors identified. In addition, preliminary tests are to evaluate all the sub-systems of the testing unit and determine whether there were any needs for modification. The sub-systems to be tested include: the on-specimen measuring system, the loading system, the data acquisition and control systems. Modifications to the subsystems were made as necessary, until the entire unit was functioning properly. Preliminary testing of the prototype system was performed on material of known mechanical and physical properties, Delrin. The system noise and data quality were also evaluated at this time.

3.6.1 Calibration Sample (Delrin Specimen)

Delrin plastic specimen was fabricated for calibration purposes. It has the same dimension as asphalt mixture tested in the prototype of DBDT test system. Only difference is that calibration specimen is one single unit as shown in Figure 3-38, not separated with loading heads. Published material specifications for Delrin report a modulus of 3.1 Gpa (450 ksi). A resilient modulus test was performed on the Delrin DBDT specimen to determine the material modulus.

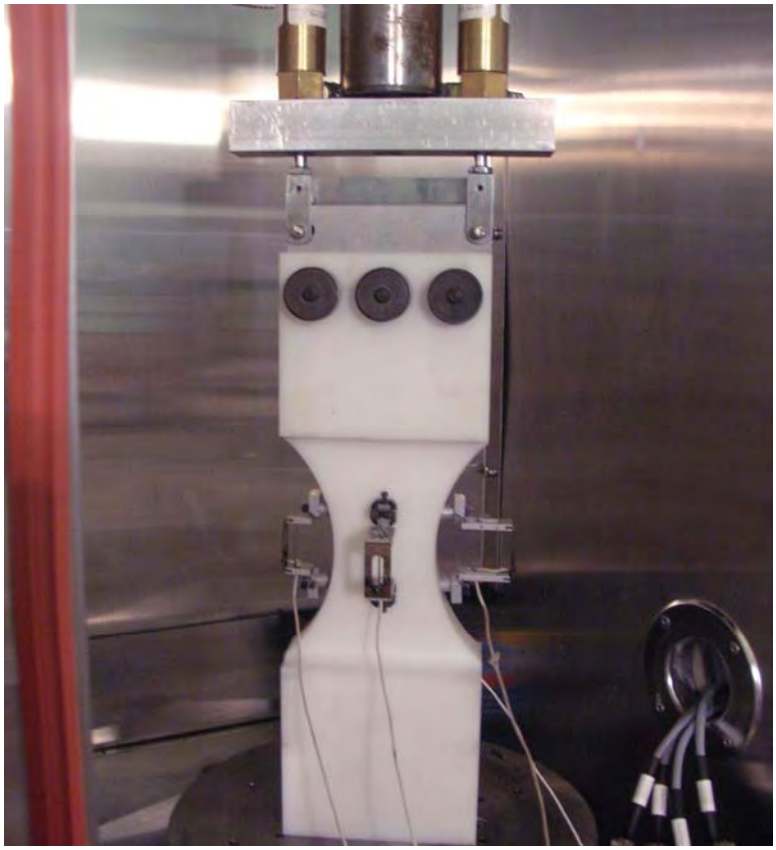

Figure 3-38 Test Set-up on Delrin Calibration Sample

The specimen was loaded using a repeated haversine waveform lasting 0.1 seconds, followed by a 0.9 second rest period. Figure 3-39 shows resilient deformation results on face and on edge. Results from the test presented in Figure 3-40 clearly show that before applying the correction factors, moduli on the edges and on the faces are significantly different and do not agree with the modulus reported by the manufacturer. However, after stress, strain and rotation correction factors are applied, modulus values as calculated from the edge and face deformations approach or equal the manufacturer reported value of 3.1 GPa. This result appears to indicate that these correction factors allow stress and strain to be accurately determined from the proposed DBDT system. The verification of correction factors with asphalt mixtures is also shown in section 4.4.2.

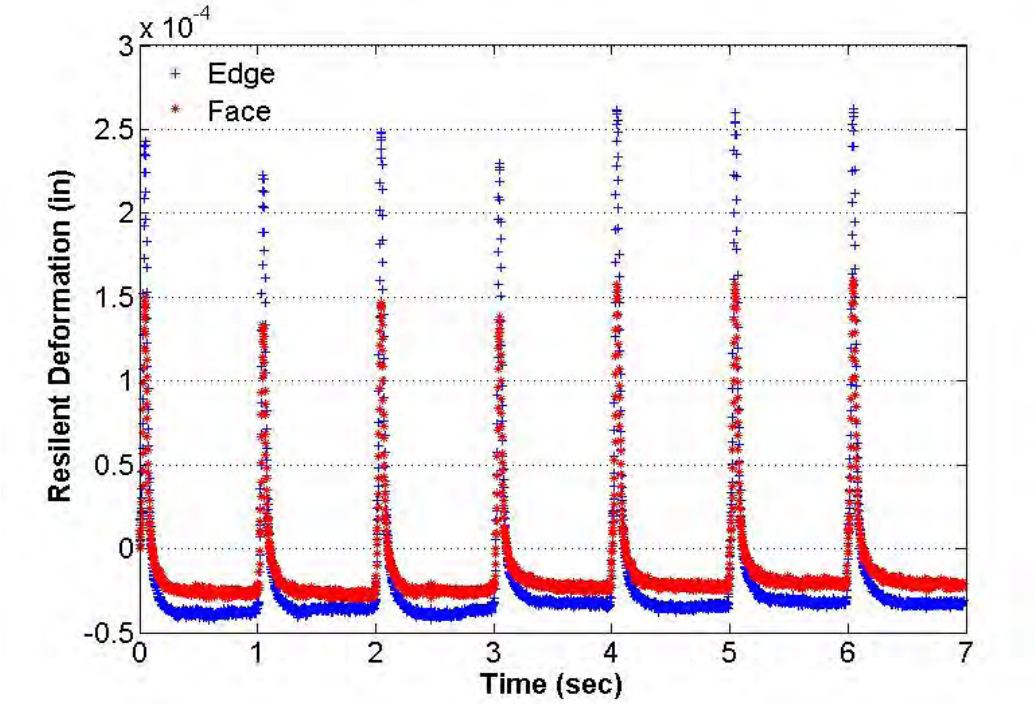

Figure 3-39 Resilient Deformation on Delrin Calibration Sample

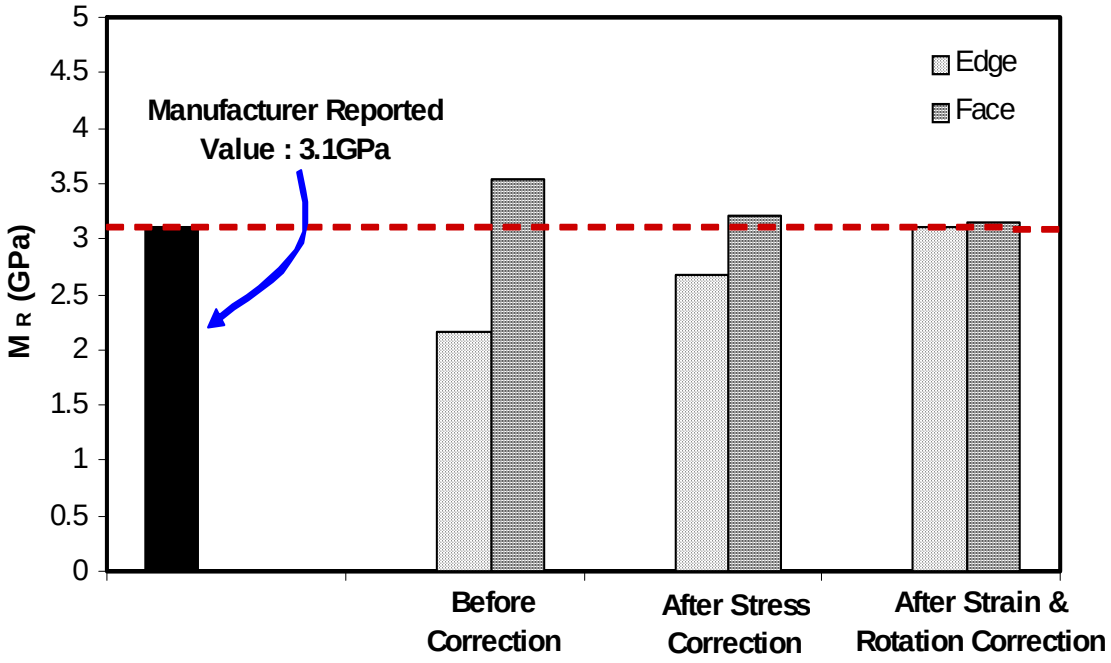

Figure 3-40 Resilient Modulus on Delrin Calibration Sample

CHAPTER 4
IMPLEMENTATION OF SUPERPAVE IDT AND DOG-BONE DIRECT TENSION TESTS

The need for asphalt mixtures tests that satisfactorily provide tensile fracture properties of mixture is well recognized since it was observed that the asphalt mixture properties cannot be reliably determined through the current empirical binder-to-mixture relationships (Roque et al., 1997). Superpave IDT and a newly developed tension test, DBDT, were conducted to evaluate tensile properties of dense graded and open graded asphalt mixtures. Three types of mixture tests were performed: resilient modulus test, creep compliance test, and tensile strength test. Figure 4-1 shows test plan with Superpave IDT and DBDT test for this study.

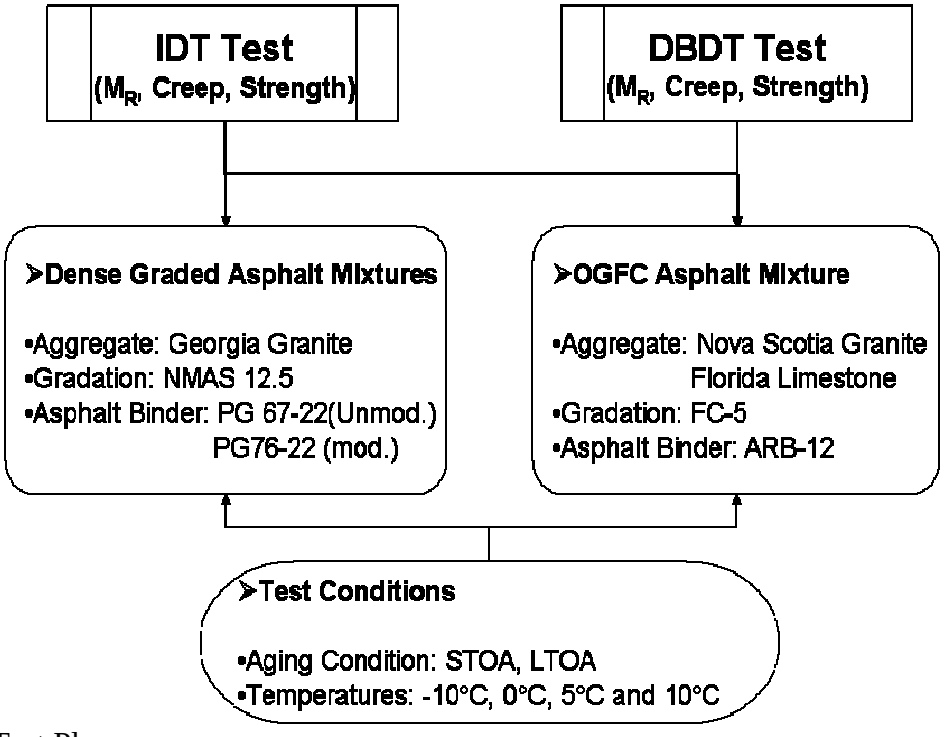

Figure 4-1 Test Plan

4.1 Materials

This section provides information regarding the materials used for production of asphalt mixture specimens in the laboratory for this study. Two gradations of asphalt mixtures were used: one dense graded asphalt mixture and one open graded asphalt mixture. Usually, dense graded asphalt mixture is used for surface structural layer while open graded asphalt mixture is used as wearing course.

4.1.1 Dense Graded Asphalt Mixtures

Georgia granite was used for dense graded asphalt mixtures in this study with both unmodified asphalt binder (PG 67-22) and modified asphalt binder (PG 76-22).

Aggregate sources for dense graded asphalt mixtures are shown in Table 4-1. All mixtures were 12.5 mm nominal maximum aggregate size gradations according to Superpave system. Figure 4-2 shows the gradation chart of the dense graded asphalt mixture including the restricted zone and control points. Detailed gradation information and blend proportions are available in Appendix A.

Two binders were uesd in this study: a control binder and an SBS modified asphalt binder. The control asphalt binder graded as a PG 67-22 or AC 30, while the modified asphalt binder graded as a PG 76-22. SBS polymer (3%) was blended with the control asphalt in the process to produce the SBS modified asphalt. Both of asphalt binders were provided by CITGO Asphalt Refining Company. It is of particular interest to compare an SBS modified (PG 76-22) mixture an unmodified mixture (PG 67-22), with all other mixture characteristics being the same. Previous research by Roque et al. (2004b) has shown that SBS modification results in slower rate of fracture damage in mixtures, as compared to unmodified mixtures.

Table 4-1 Aggregate Source for Dense Graded Asphalt Mixture

Type of Material	FDOT Code	Producer	Pit No.
# 78 Stone	43	Junction City Mining	GA-553
# 89 Stone	51	Junction City Mining	GA-553
W-10 Screenings	20	Junction City Mining	GA-553
Local Sand	-	V. E. Whitehurst & Sons	Starvation Hill

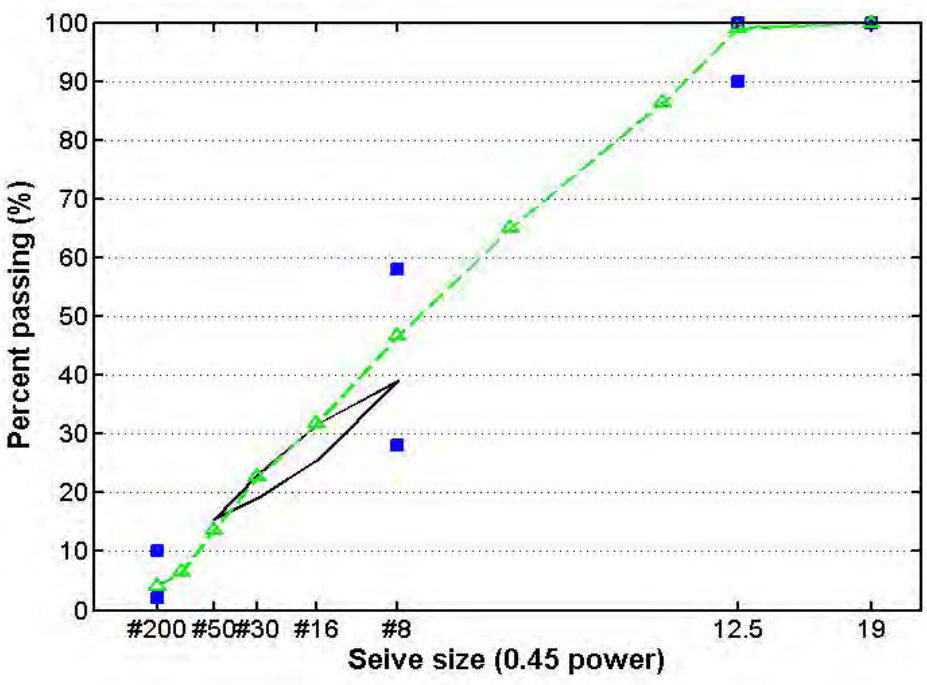

Figure 4-2 Dense Graded Asphalt Mixture Gradation

4.1.2 Open Graded Asphalt Mixtures

Two aggregates were used for open graded asphalt mixtures: Florida oolitic limestone and Nova Scotia granite. Both were used to produce mixtures conforming to FDOT's specifications for FC-5 mixture

FC-5 is one kind of open graded friction course gradation designated in specifications of Florida Department of Transportation (FDOT, 2007). Table 4-2 shows aggregate sources and Figure 4-3 shows the gradation chart for the open graded asphalt mixtures. In this particular case, gradations follow that used in the test sections on U. S. Highway 27 Highlands County test project (Varadhan, 2004; Thai, 2005). These are aggregates extensively used in the state of Florida and are approved by the FDOT for road construction and rehabilitation projects.

Table 4-2 Aggregate Source for Open Graded Asphalt Mixture

Type of Material		FDOT Code	Producer	Pit No.
Florida Limestone	S1A Stone	41	White Rock Quarries	87-339
	S1B Stone	53	White Rock Quarries	87-339
	Screenings	22	White Rock Quarries	87-339
	Filler	-	-	-
Nova Scotia Granite	# 7 Stone	44	Martine Marietta Aggregates	TM-322 NS-315
	# 789 Stone	51	Martine Marietta Aggregates	TM-322 NS-315
	Screenings	22	Martine Marietta Aggregates	TM-322 NS-315
	Hydrated Lime	-	-	-

Asphalt rubber binder (ARB-12) was used, along with 1 percent lime pretreatment for the granite mixture. Base binder for ARB-12 is unmodified binder, which is PG 67-22 or AC-30 which is the same unmodified binder used for dense graded asphalt mixtures. Asphalt rubber binder (ARB-12) containing 12% ground tire rubber was blended prior to use. Based on multi-year research project on state road 16 in Florida, this pre-blended asphalt rubber binder (wet process) improved the cracking resistance of open graded asphalt mixture compared to the dry

mix process (Choubane et al., 1998). They also suggested that the amount of rubber used for FC-5 be within 10 to 15%.

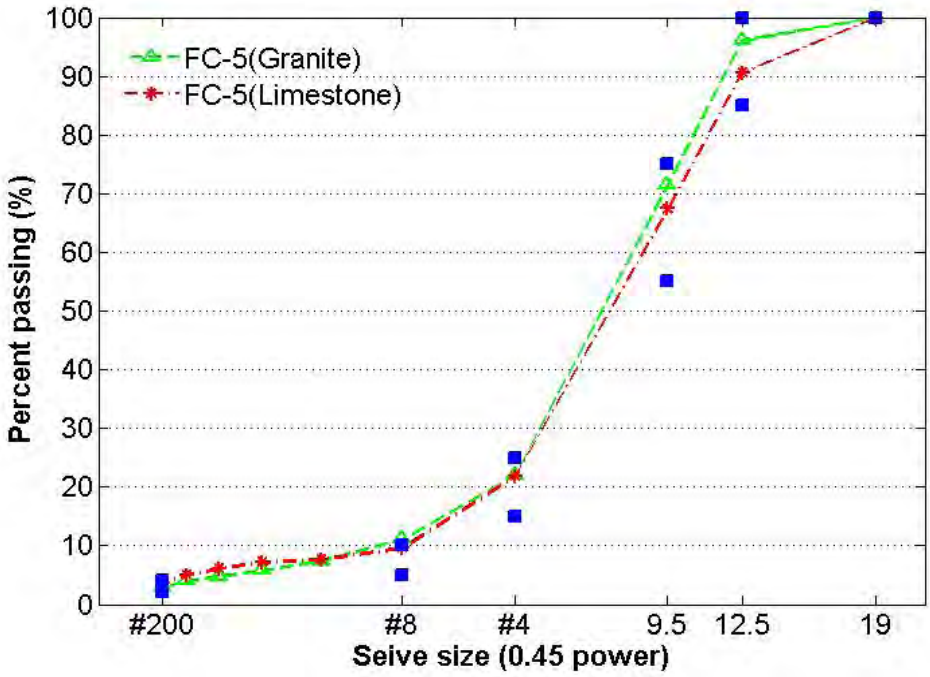

Figure 4-3 Open Graded Asphalt Mixture Gradation

4.2 Asphalt Mixture Design

4.2.1 Dense Graded Asphalt Mixtures

The dense graded asphalt mixtures produced for testing and evaluation were designed with the Superpave volumetric mix design procedure, which bases its selection for design asphalt content on a set of criteria on the volumetric properties of the mixture (VMA, VFA, density) at 4% air voids. Also, the aggregates need to meet criteria for the consensus and source properties that aim to prevent the use of substandard aggregates in producing asphalt mixture.

4.2.1.1 Selection of Traffic Level

The Superpave design method for compacted asphalt mixtures specifies the number of gyrations to which a sample must be compacted with the Superpave gyratory compactor. The number of gyrations for these traffic levels as specified by the Florida Department of Transportation is presented in Table 4-3. Per FDOT's request, dense graded asphalt mixtures were designed for traffic level C, which is more than 3 million and less than 10 million ESALs.

Table 4-3 Traffic Levels and Gyratory Compaction Efforts

Traffic Level (Millions of ESALs)	N_{ini}	N_{des}	N_{max}
A (<0.3)	6	50	75
B (0.3-3)	7	75	115
C (3-10)	7	75	115
D(10-30)	8	100	160
E (≥ 30)	8	100	160

4.2.1.2 Batching and Mixing

Aggregate batching sheets, attached in Appendix A, were prepared for 4500g samples based on the JMF for the aggregates. The batched 4500g samples were heated in oven at the mixing temperature for approximately 3 hours. The mixing tools and asphalt used were also heated at the mixing temperature. The mixing temperature of the unmodified mixture and modified mixture are 300-315°F and 320-335°F, respectively. The aggregates were then removed from the oven and mixed until the aggregates were well coated (approximately 3-5 minutes) with asphalt binder. Figure 4-4 shows a picture of laboratory mixer used. The mixed samples were spread out in pans and heated in an oven for 2 hours at the same temperature as

mixing for short-term oven aging. Each of the mixtures was stirred after 1 hour to obtain a uniformly aged sample.

Figure 4-4 Mixing

4.2.1.3 Compaction

After short-term oven aging, the 4500g samples were then removed and quickly compacted using the Superpave Gyratory Compactor. Figure 4-5 shows the Superpave Gyratory Compactor used. The samples were compacted with a ram pressure of 600kPa at a gyratory angle of 1.25°. The compaction data of the samples were used in determining the design asphalt content. That is, volumetric properties from the mixture such as air voids (AV), voids in mineral aggregates (VMA), and voids filled with asphalt (VFA) were calculated at these asphalt contents and then each was plotted as a function of asphalt content at N_{des}. The design asphalt content was obtained by interpolating the air void versus asphalt content curve to obtain asphalt content at 4% air voids.

Figure 4-5 Superpave Servopac Gyratory Compactor

The other volumetric properties were then obtained at this design asphalt content as presented in Table 4-4. Design asphalt content was determined to be 4.8 % for dense graded asphalt mixtures.

Table 4-4 Volumetric Information for Dense Graded Asphalt Mixtures

AC (%)	Gmm	Gsb	VMA (%)	VFA (%)
4.8	2.579	2.770	14.9	73.1

4.2.1.4 Long Term Oven Aging (LTOA)

Laboratory aging is one of the most influential factors that affect asphalt mixture properties and predicted performance. Aging effects were evaluated by comparing long term oven aging

tension test results to short term oven aging tension test results. The mixes were subjected to long term aging according to AASHTO PP2 (2001). A new procedure was developed by Varadhan (2004) to contain the open graded compacted specimens from falling apart during aging.

A wire mesh with openings of 1/8” and steel hose clamps were used. The mesh size was chosen to ensure good circulation of air within the sample for oxidation and at the same time, to prevent the smaller aggregate particles from falling through the mesh. The samples were placed on porous plates in an oven at 185°F for 5 days. The specimen was turned over twice during long term oven aging. The test samples with the wired mesh and porous plate for LTOA are shown in Figure 4-6.

Figure 4-6 Long Term Oven Aging (LTOA) Conditioning Set-up

4.2.2 Open Graded Asphalt Mixtures

Asphalt content for open graded asphalt mixture was determined to produce a minimum voids in the mineral aggregate (VMA) at a sufficient effective asphalt film thickness to ensure adequate durability of the mixture. The processes of batching and mixing are the same as those of dense graded asphalt mixtures. Mixing temperature was kept around 320-335°F to obtain proper workability. A Superpave Gyratory Compaction (SGC) set to 50 gyrations was used for the open graded mixture compaction as suggested by prior research (Mallick et al., 2000; Varadhan, 2004) to meet specified air void content.

The sample was allowed to cool down for about 2 hours after compaction before ejecting from the mold. This was done to prevent collapse of these high air void content mixtures. Once the specimen was ejected from the mold, it was allowed to cool for 5 minutes before removing from the ejector. All compacted specimens were then allowed to cool at room temperature for at least 24 hours before further handling. The optimum asphalt content was selected as the asphalt content resulting in the lowest VMA. Optimum asphalt contents were determined as 6.4% for Florida limestone and 6.0% for Nova Scotia Granite. Open graded asphalt mixtures were also subjected to LTOA. Since these mixtures are very coarse and open, special care must be taken to prevent specimen damage during aging process.

4.2.2.1 Measuring Air Void for Open Graded Asphalt Mixtures

For many years, bulk specific gravity for asphalt mixture have been measured by weighing compacted specimens in air and water, commonly referred to as water displacement. Test procedures for this method are provided in AASHTO T 166 (AASHTO, 2001) or ASTM D 2726 (ASTM, 2002). However, it has been found that this method results in erroneous air void contents when testing coarser gradations such as open graded mixture and stone matrix asphalt

(SMA) (Buchanan, 1999; Cooley et al., 2002). Therefore, determination of G_{mb} with the Corelok device has been recommended for coarse graded asphalt mixtures. Crouch et al. (2002) stated that the Corelok device performed well with a variety of sample types and was the most widely applicable method of G_{mb} determination. Figure 4-7 shows the Corelok equipment and Figure 4-8 shows the vacuum sealing process for asphalt mixture. This method is specified in ASTM D 6752 (2002) as a vacuum sealing method. Bulk specific gravity (G_{mb}) was calculated using following equation (InstroTek, 2003):

$$G_{mb} = \frac{W_{d1}}{W_b + W_{d2} - W_s - \frac{W_b}{F_c}} \quad (4\text{-}1)$$

Where, W_{d1} = dry sample weight before sealing (g), W_{d2} = dry sample weight after water submersion (g), W_b = bag weight (g), W_s = sealed sample weight in water (g), F_c = bag volume correction factor provided by manufacturer.

Dimensional analysis for measuring bulk specific gravity specified in AASHTO T 269 (2001) was also performed on open graded asphalt mixture. Alvarez et al. (2008) recommended utilizing dimensional analysis for determining G_{mb} of porous friction course mixtures rather than the vacuum sealing method. They also stated that this method is relatively simpler, fast, and less expensive and additional testing supplies are not needed.

Figure 4-7 Corelok Equipment to Measure Air Void

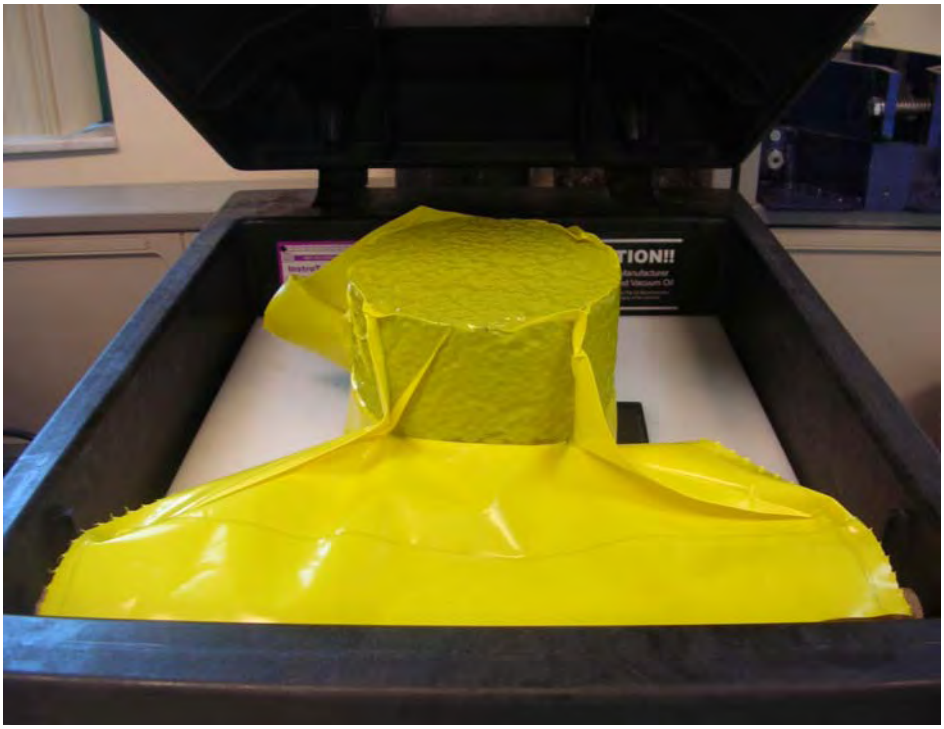
Figure 4-8 Vacuum Sealing in Corelok

The dimensional analysis method directly calculates volume assuming that the specimen is a regular cylinder with smooth faces. The dimensional G_{mb} was calculated as:

$$G_{mb} = \frac{W_m / V_m}{\rho_w} \quad (4\text{-}2)$$

Where, W_m = total dry weight of asphalt mixture (g), V_m = total volume of asphalt mixture (cm^3), ρ_w = density of water (g/cm^3)

Table 4-5 and Figure 4-9 show the air void contents from both Corelok and dimensional method. These results imply that the air voids determined from dimensional analysis are higher than those obtained from the vacuum method. This discrepancy between two methods resulted from the surface air voids. Dimensional analysis includes all surface voids, whereas the vacuum method partially includes them because the bag partially follows the surface voids with depth once the vacuum sealing process is applied.

Table 4-5 Air Void Contents for Open Graded Asphalt Mixture

Type of Aggregate	Test	G_{mm}	Dimensional Method		Corelok Method	
			G_{mb}	Air Void (%)	G_{mb}	Air Void (%)
Florida Limestone	IDT	2.309	1.918	16.9	1.963	15.0
	DBDT		1.927	16.6	1.973	14.5
	Ave.		1.922	16.7	1.968	14.8
Nova Scotia Granite	IDT	2.441	1.948	20.2	1.982	18.8
	DBDT		1.953	20.0	1.997	18.2
	Ave.		1.950	20.1	1.990	18.5

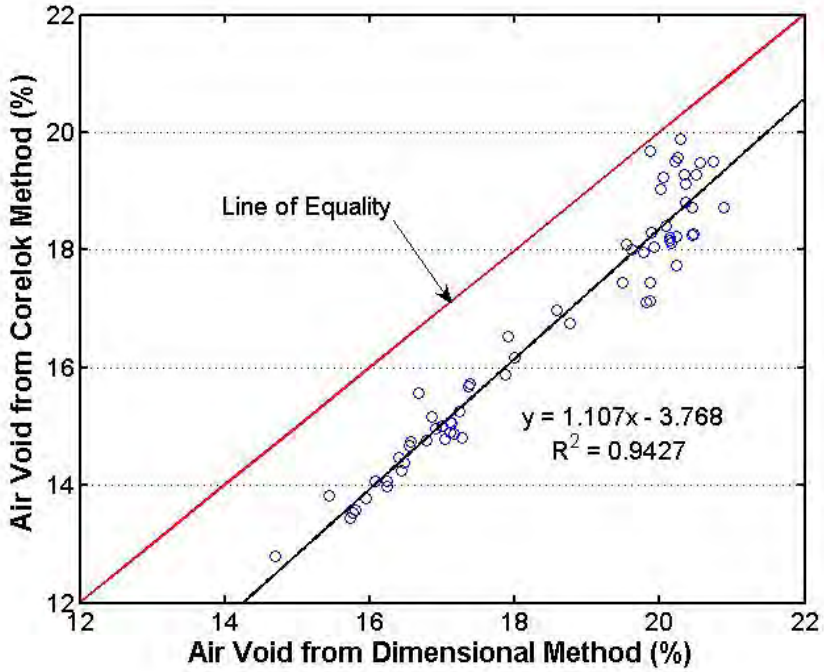

Figure 4-9 Air Voids of Open Graded Asphalt Mixture

The specimens were then measured for thickness at four equally spaced locations approximately 90° apart, and an average thickness was calculated. These specimens were laboratory produced and compacted in a Superpave Gyratory Compactor (SGC), therefore, their diameter was fixed at 150 mm.

4.3 Test Specimen Preparation

4.3.1 Dog-Bone Direct Tension Test Specimen

Dog-Bone Direct Tension Test (DBDT) specimens were prepared with the materials for dense and open graded asphalt mixtures mentioned section 4.1. 150mm diameter specimens were compacted by the Superpave gyratory compactor. After waiting for the specimen to fully cool down, for dense graded asphalt mixture, the bulk specific gravity of each compacted specimen

was measured, and the air void content was determined. The target air voids of the gyratory pill was 7.5%, because the air void of the sliced specimen taken from the middle of the pill is generally 0.5% less than that of the compacted specimen. The compacted specimens were sliced with a masonry cutting saw with a special attachment to hold the pills (Figure 4-10) to obtain the desired thickness of specimen for each gradation (1.5 inch thickness for dense graded asphalt mixtures 2 inch for open graded asphalt mixtures). Based on prior research done by Varadhan (2004), this thickness was determined to minimize end effect during testing. Also, this thickness provides for representative sample of OGFC. Figure 4-11 shows that after cutting, each side of the test specimens was cored to produce the dog-bone shape specimen using a specially designed coring fixture. As stated in section 3.3.1, coring fixture was designed to core each opposing side using round shape steel block as shown in Figure 4-12. Figure 4-13 shows the specimen after coring each side. Because the coring saw uses water to keep the blade wet, the specimens were dried one day at room temperature prior to further testing. The bulk specific gravity was taken to obtain air void contents for each dense graded specimen. Specimens had to be in the range of $7 \pm 0.5\%$ air voids to be considered for testing. Specimens were placed in the humidity chamber for at least two days to negate moisture effects. To increase the effectiveness of the bonding interface, the top and bottom of the test specimens were coarsely sanded to remove the asphalt film as shown in Figure 4-14. The test samples were then bonded to the loading heads using simple alignment bars. Figure 4-15 shows a specimen being bonded to the loading heads. All bonding was performed on a machinist granite block to provide a flat reference surface. After bonding, the specimens were allowed to cure for one day at room temperature. This ensures the bonding agent has revealed full strength. Gage points were attached onto the face and edge of specimens using a simple steel template, adhesive, and activator for rapid cure. Figures 4-16 and

4-17 illustrate the attachment of gage points. Four pairs of gage points were placed at distance of 1.5 in for each pair: two on the faces and two on the edge along the vertical axes on the center of the specimen. Figure 4-18 shows how knife edges are placed over the gage points. Prior to testing, the prepared DBDT specimen was kept in the environmental chamber at the desired test temperature for at least six hors to ensure uniform temperature within the specimen. Mounting of extensometers is completed in the environmental chamber through access holes.

Figure 4-10 Slicing Asphalt Mixture

Figure 4-11 Coring Asphalt Mixture Sliced

Figure 4-12 Coring the Other Side of Asphalt Mixture Sliced

Figure 4-13 Specimen after Coring

Figure 4-14 Sanding Asphalt Mixture to Eliminate Asphalt Film

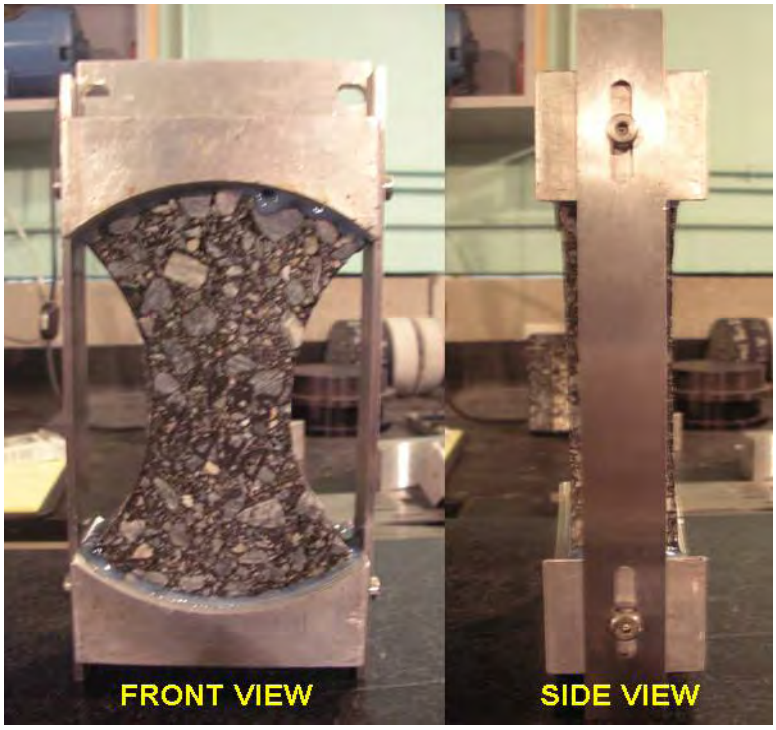

Figure 4-15 Bonding between a Specimen and Loading Heads

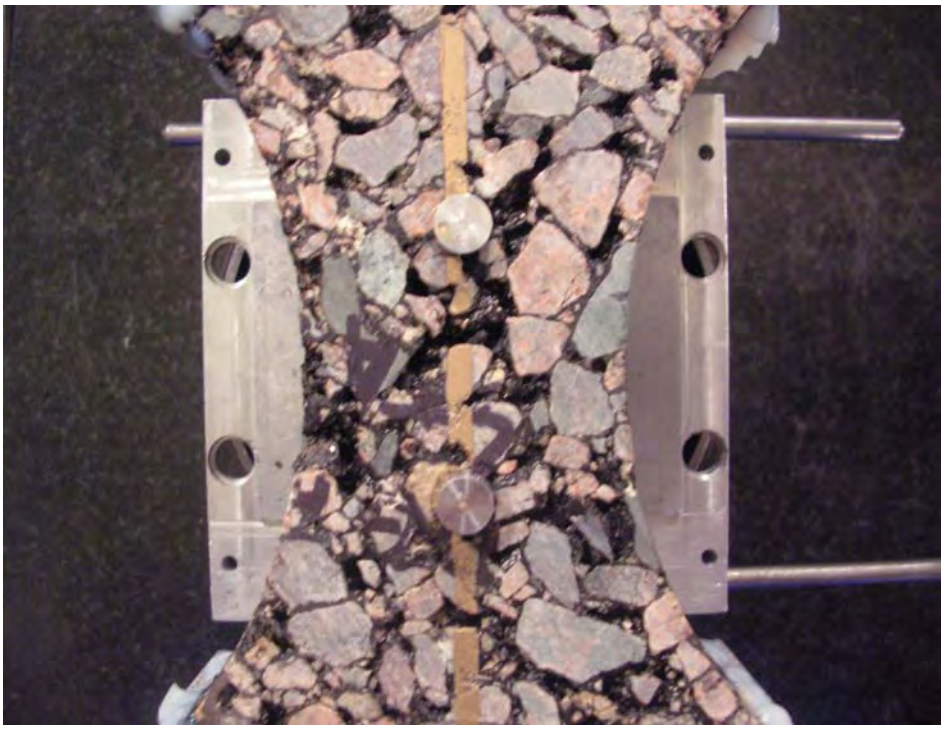
Figure 4-16 Gage Points Attachment on Faces

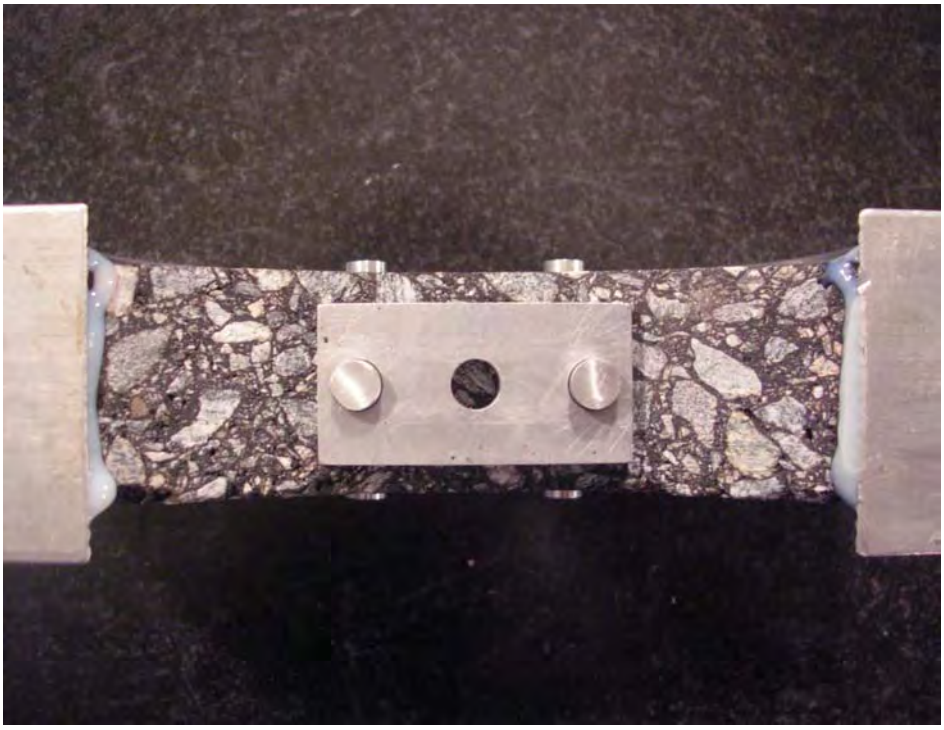

Figure 4-17 Gage Points Attachment on Edges

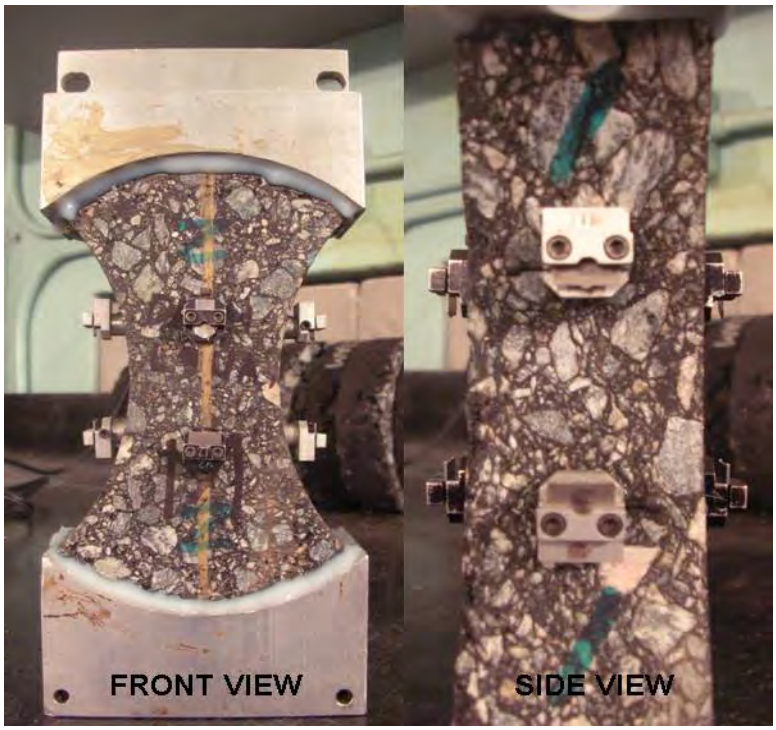

Figure 4-18 Set-up of Knife Edge on Gage Points

4.4 Mixture Performance Evaluation

4.4.1 Introduction

A mixture tension test is necessary to evaluate and control cracking performance of the asphalt mixtures for use in the pavements. Both Superpave IDT and a newly developed DBDT test were performed on all mixtures at various conditions. The use of both tests might enhance reliability of the asphalt mixture properties. But, routine use of a direct tension test may not be feasible due to the multiple complications involved with this test such as specimen preparation and test interpretation. Therefore, it would be advantageous to adopt the Superpave IDT to the testing of open graded asphalt mixtures. Also, there is a concern that the open graded nature of these mixtures may require a modified IDT testing protocol from that used for dense graded asphalt mixtures. A study is essential to optimize the test conditions needed to obtain consistent fracture properties of open graded asphalt mixtures with the Superpave IDT. In particular, the effects of temperature need to be evaluated. Thus, experiments were performed with asphalt mixtures at four temperatures to evaluate the precision and accuracy of the new DBDT testing system. At the same time, cracking performance of the asphalt mixture was evaluated with three different loading modes.

4.4.2 Use of Non-Uniform Stress States of Tests for Tensile Failure Limits

Superpave IDT and DBDT share a common advantage. Both tests result in non-uniform tensile stress states within a mixture, which allows for identification of the failure plane a priori.

Cracking (fatigue, thermal, and top-down) in flexible pavement is one of the most common and crucial distresses that clearly affects the service quality and life of flexible pavement. Therefore, cracking is an important structural and functional deficiency that should be addressed

in pavement design and maintenance planning. In order to evaluate and predict asphalt pavement performance and develop appropriate models with respect to cracking resistance, it is necessary to measure the tensile failure limits of asphalt mixtures such as tensile strength, failure strain, and fracture energy. For many years, various testing methods have been used for evaluating tensile failure limits of asphalt mixture that are related to cracking performance in the field. However, if the properties are not fundamental, the results may be dependent on the testing systems employed.

Fracture energy is believed to be one of the most important failure limits for describing and modeling the fracture behavior of asphalt mixtures. It is defined as the energy required to initiate fracture in a mixture. Previous studies have determined that fracture energy is a reliable indicator of the crack resistance of a mixture when other conditions such as pavement structure and traffic are similar (Sedwick, 1998). Research conducted by Wen and Kim (2002) confirms that fracture energy is an excellent indicator of the resistance of mixture to fatigue cracking through the use of the indirect tension test. In the HMA fracture mechanics model developed at the University of Florida, fracture energy is one of the key properties governing a mixture's resistance to fracture (Zhang, 2000; Zhang et al., 2001). Tensile strength and failure strain have also been commonly used for evaluating cracking performance of the flexible pavement. However, these properties are rate-dependent, so they are not fundamental (i.e., independent of geometry and mode of loading).

It is noted that once fracture occurs in asphalt mixture, post behavior has no meaning in terms of cracking performance and is not easily interpretable because of localizing effects of the crack. Thus, for an accurate determination of the tensile failure limits, the testing system should capture the exact instant of fracture. According to Roque et al. (1997), first fracture in the

indirect tension test sample occurs prior to the peak load. They developed an approach to identify the instant of first fracture in the Superpave IDT sample using vertical and horizontal measurements. Tensile strength, failure strain, and fracture energy were obtained using load and deformation measurements corresponding to the instant of first fracture. The same phenomenon was observed in the dog-bone direct tension test in this study. First fracture occurs either at the center of one edge or the center of both edges at the same time where tensile stress is the highest.

4.4.2.1 Uniform Stress State of Uniaxial Direct Tension Test

For many years, it has been assumed that uniform normal stresses distributeover a cross-section of a cylindrical specimen, providing satisfactory results unless sudden changes in cross-section along the specimen were involved. The stress and strain can be simply calculated with following equations (4-3) and (4-4).

$$\sigma = \frac{P_{applied}}{A} \tag{4-3}$$

$$\varepsilon_G = \frac{\Delta}{L} \tag{4-4}$$

Where, σ = stress over the cross-section, $P_{applied}$ = applied load, A = cross-section area, ε_G = global strain, Δ = global deformation, L = height of a specimen.

However, it has also been recognized that uniform stress distribution changes once non-uniform (non-homogeneous) damage and/or the first fracture occurs within the specimen, most frequently near the loading platens. Consequently, the stress and/or strain distribution cannot be predicted or determined after non-homogeneous damage or first fracture since one does not know the exact location and geometry of damage zones and cracks, as shown in Figure 4-19.

Therefore, failure limits including fracture energy calculated from global stress-strain measurements from uniform specimens may not be accurate or reliable. Measurements obtained from direct tension tests can only provide an average failure strain and energy. It must be acknowledged that microcrack and localized damage occur throughout the loading within a whole specimen. The key assumption that must be made in calculating and/or determining fracture energy from a non-uniformly loaded specimen is the surface area of the first crack area over which the fairly uniform maximum tensile stress was acting.

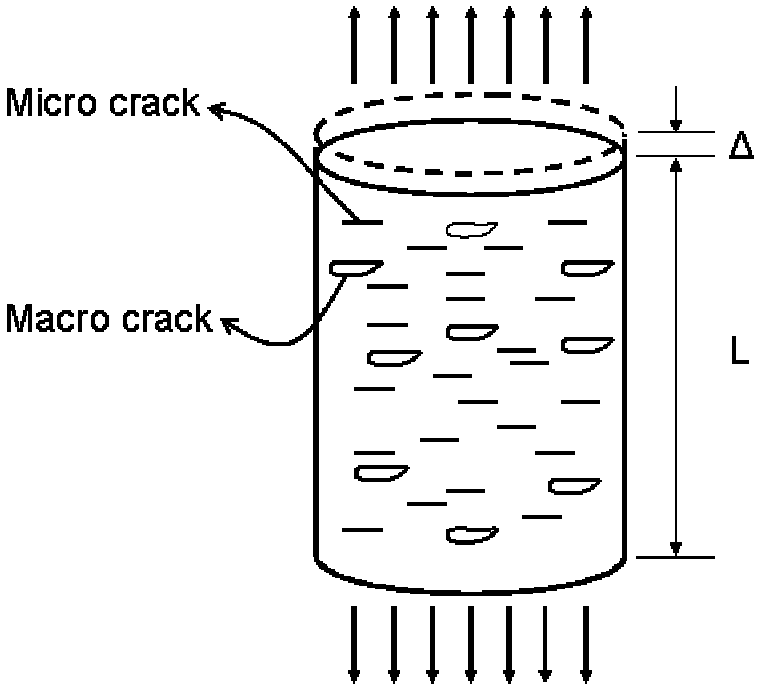

Figure 4-19 Uniform Stress Condition under Direct Tension

Using a non-uniform stress state test is one possible solution (Figure 4-20). Non-uniform stress state or a stress concentration would induce the first fracture at a known location, indicating that most microdamage also occurs there. If the measurement systems could be well positioned in that region, predicted stress and measured strain through first fracture would be

more accurate. Strains, which can be measured at the location of first fracture, will be less affected by microdamage that occurs throughout the rest of the specimen, whereas global strains are affected by all damage throughout the specimen. The local strains can be calculated with the same equation (4-5), substituting global deformation and height of specimen with local deformation and gage length, respectively.

$$\varepsilon_l = \frac{\delta}{l} \tag{4-5}$$

Where, ε_l = local strain, δ = local deformation, l = gage length.

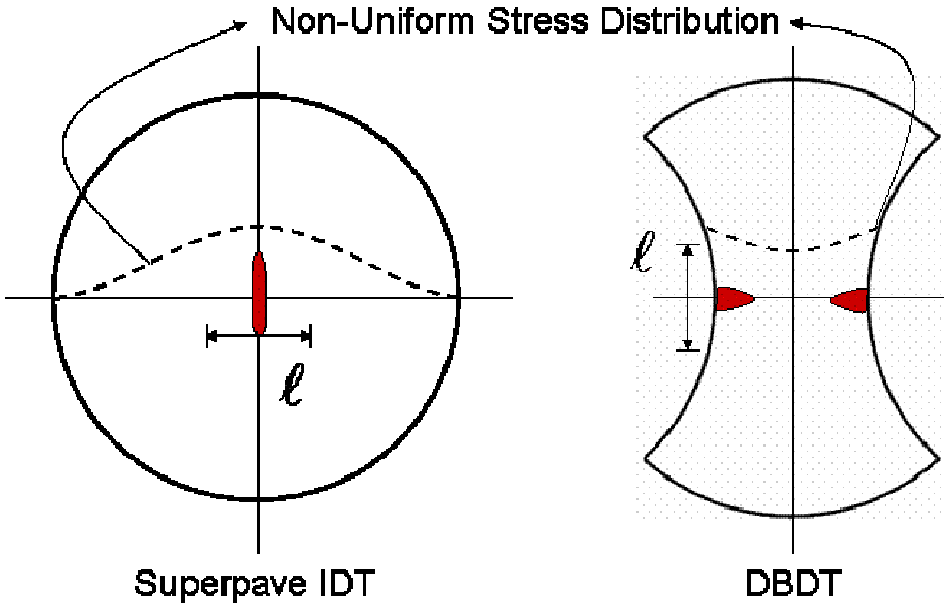

Figure 4-20 Non-Uniform Stress State of Superpave IDT and DBDT

4.4.2.2 Non-Uniform Stress State of Superpave IDT

As mentioned previously, fracture in asphalt mixture usually occurs at a lower load than that required to break the whole specimen. In other words, the load to initiate fracture is always less than the maximum load measured in the system ($P_{fail} < P_{measured} = P_{max}$). Thus, it is necessary

to measure the load at the instant of fracture ($P_{fail} = P_{measured} < P_{max}$) to accurately determine failure limits. Therefore, identification of first fracture is very important. Furthermore, it is of considerable interest that comparative analysis of failure limits at first fracture obtained from indirect and direct loading conditions would be made to verify their independence of loading conditions.

Superpave IDT has been extensively used to characterize the tensile properties of asphalt mixtures among pavement engineers and researchers since it was introduced to the asphalt community. This test was developed and improved during the Strategic Highway Research Program (Roque and Buttlar, 1992; Buttlar and Roque, 1994). Roque and Buttlar (1992) showed that the Superpave IDT overcame many of the problems that have been typically associated with the existing indirect tensile test. One of the major improvements they made was the introduction of on-face measurements at the center of the specimen, where maximum compressive and tensile stresses take place. Figure 4-21 represents the tensile stress distribution on the horizontal axis, which indicates that first fracture will develop on the vertical axis at the center of the specimen. Therefore, measurements can be obtained on the failure plane, which allows accurate determination of failure limits. That is, more accurate measurements can be obtained on the failure plane by placing a horizontal sensor at the center of the specimen. The on-face measurement system also eliminates effects of specimen rotation. Roque et al. (1997) also developed a method for identifying first fracture using the vertical and horizontal measurements on the center area of the indirect tension specimen. This idea was initiated with the fact that the failure occurred first at the location where the rate of horizontal deformation increased. According to Romeo (2008), this method to detect fracture initiation matches very well with the observation using Digital Image Correlation (DIC) system. Test procedure and analysis methods

for Superpave IDT were well documented in the references (Roque and Buttlar, 1992; Buttlar and Roque, 1994; Roque et al, 1997). For convenience, the method developed to consistently identify the instant of fracture from deformation from Superpave IDT is described below.

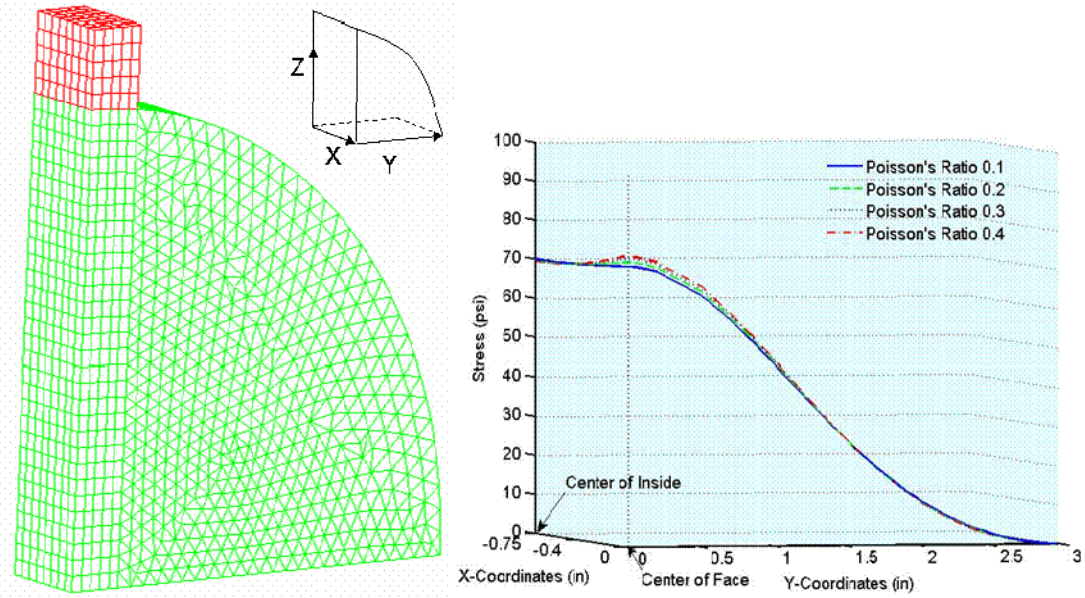

Figure 4-21 Non-Uniform Stress State of Superpave IDT from 3D FEM Analysis

In the Superpave IDT system, the extensometers measure deformations in the immediate vicinity of maximum tensile stress, and were found to be suitable in identifying the instant when fracture develops at the face of the specimen. At the instant when cracking initiates at the faces of the specimen, an increase in the rate of horizontal deformation in the vicinity of the crack can be seen due to the weakening of the specimen near the crack. If this is the case, the instant of specimen fracture can be identified by analyzing the rate of deformation of the horizontal strain gage during strength test. Figure 4-22 presents the method to detect the instant of fracture from deformation measurements. The change in horizontal response can be identified by plotting the difference between vertical and horizontal measurements. When first fracture occurs, the rate of

horizontal deformation will increase relative to the rate of vertical deformations. This will cause the difference between horizontal and vertical deformations to reach a maximum. The instant of fracture is identified as the time when the difference between the vertical and horizontal deformations reaches a peak. If both sets of vertical and horizontal gages reach a peak, the instant of fracture is taken as the time when the first peak is reached.

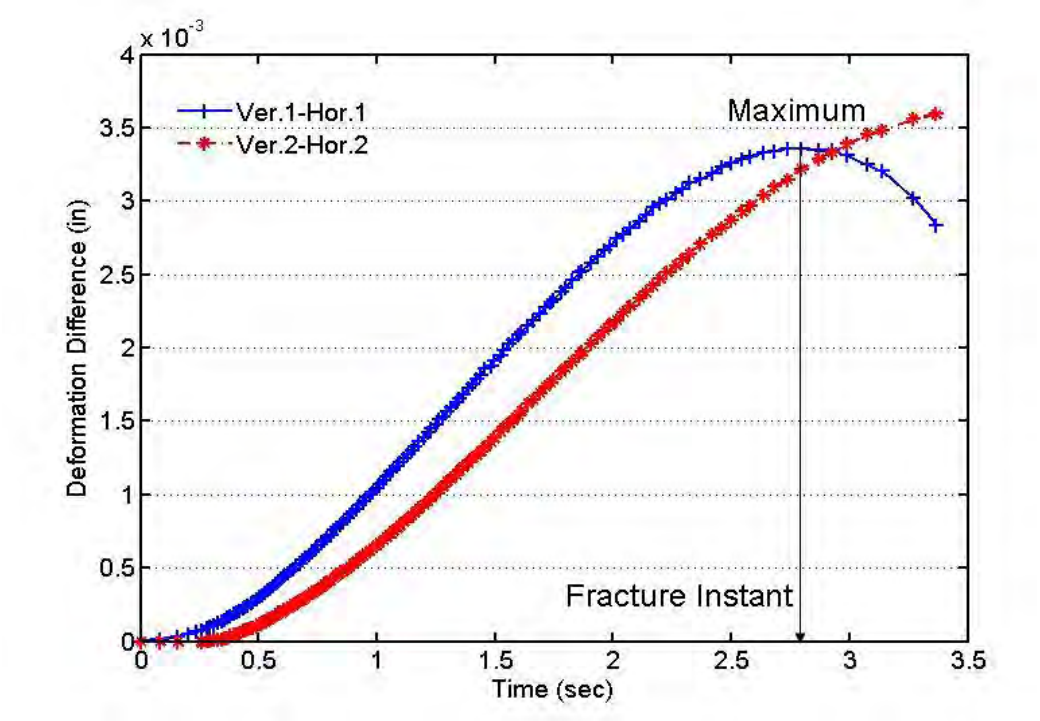

Figure 4-22 Detection of the Fracture Instant of Superpave IDT

4.4.3 Verification of DBDT Correction Factors with Asphalt Mixtures

It is imperative to validate correction factors based on three dimensional finite element analysis for asphalt mixtures even though they were verified with a Delrin plastic specimen as described in section 3.6. The results from on-face and on-edge measurements in two testing modes, resilient modulus and creep compliance, were evaluated for this purpose. Figure 4-23

shows that resilient modulus results from face and edge measurements were in excellent agreement, regardless of mixture type, once correction factors were applied. This indicates correction factors work well for short loading times or small strain tests.

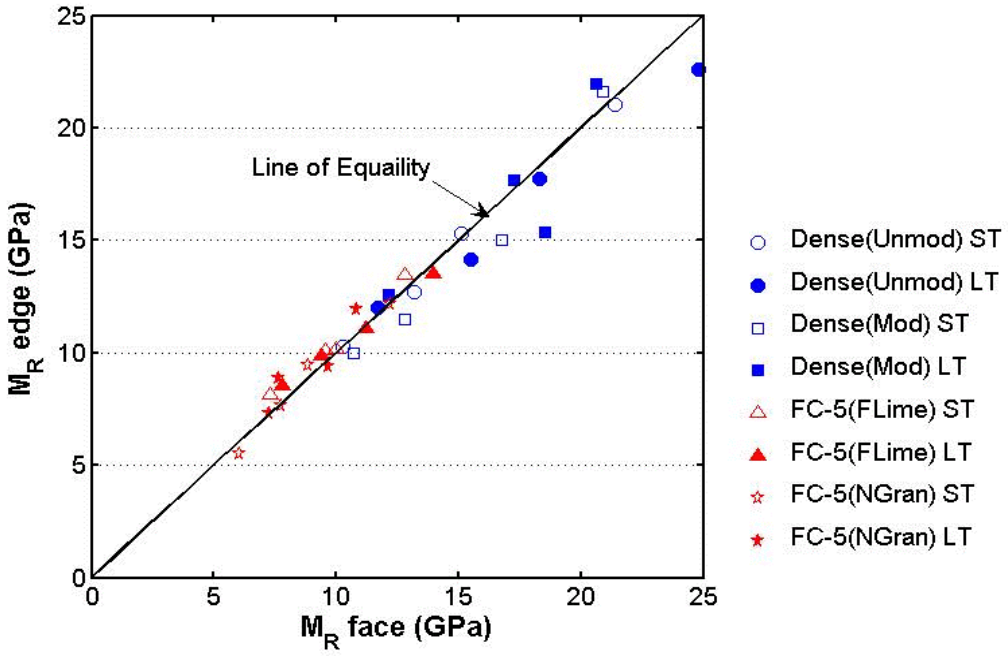

Figure 4-23 Resilient Modulus Results on Face and Edge

Examination of creep compliance test results which involve longer loading times (1000 seconds) yielded similar results. Creep compliance results of unmodified short term oven aged dense graded asphalt mixture at multiple temperatures are presented in Figure 4-24. As can be seen in this Figure, creep compliance curves from both face and edge measurements were in excellent agreement. This was also observed for open graded asphalt mixture as shown in Figure 4-25, which shows creep compliance curves for long term oven aged Florida limestone OGFC.

To corroborate this further, creep compliance values for all the mixtures evaluated were compared in Figure 4-26. Again, values from both measurement positions were in excellent

agreement. Based on these comparisons, it appears that correction factors developed result in accurate predictions of stresses and strains in asphalt mixtures subjected to tension using the dog-bone direct tension test system proposed. In addition, correction factors were found to be independent of loading time.

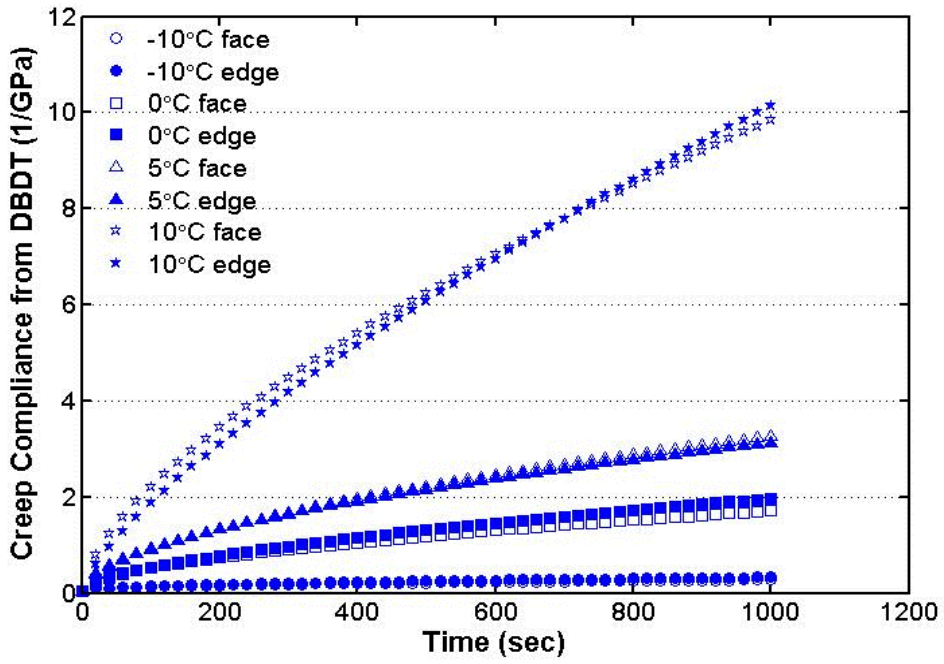

Figure 4-24 Creep Compliance of Dense (Unmod) STOA Mixtures on Face and Edge

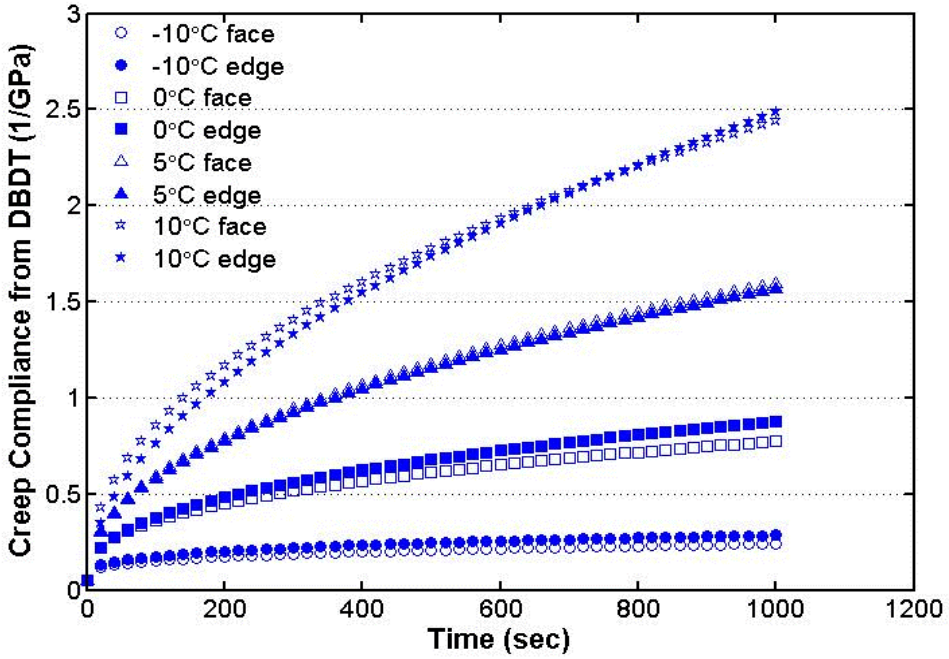

Figure 4-25 Creep Compliance of FC-5 (FLime) LTOA Mixtures on Face and Edge

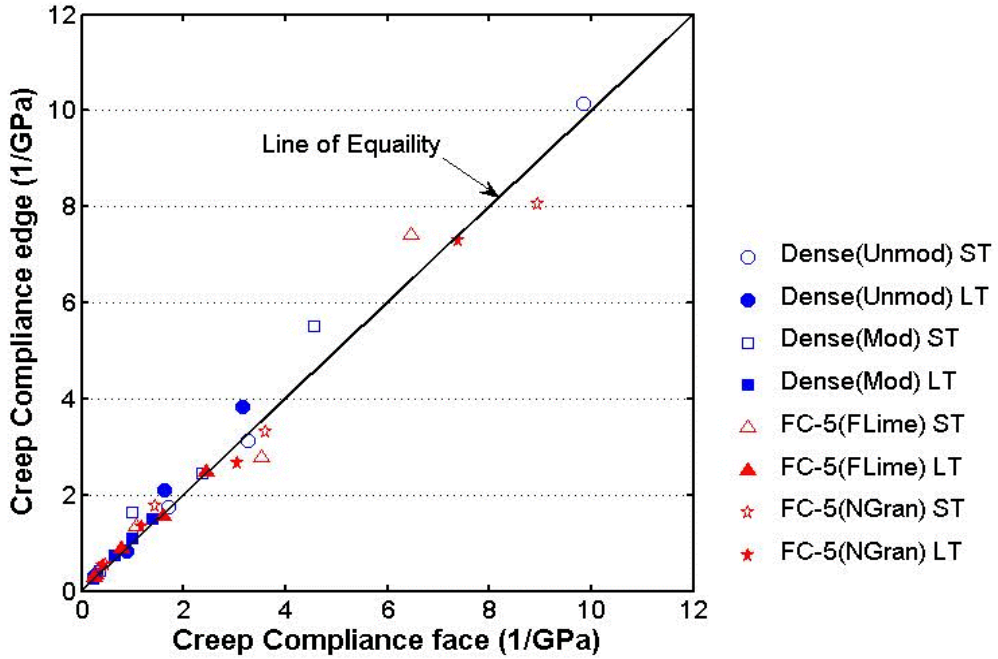

Figure 4-26 Creep Compliance Results on Face and Edge

4.4.4 Superpave IDT Test Results

The test results obtained from Superpave IDT were analyzed with the ITLT program developed at the University of Florida. Detailed analysis and interpretation methods for IDT test results were presented by Roque, Buttlar and their associates (1992; 1994; 1997).

Superpave IDT results presented in Appendix B, appear to follow the expected trend with respect to temperature, aging condition, and binder modification. For example, as test temperature increased, resilient modulus and strength exhibited lower values while the absolute value and rate of creep compliance and failure strain showed higher values. Also, results indicated that aging conditioning made an asphalt specimen stiffer. With respect to binder modification, SBS decreased creep response and increased fracture energy. However, SBS did not affect resilient modulus or strength.

The resilient modulus (M_R) is a measure of a material's elastic stiffness. Resilient modulus results are shown in Figure 4-27. As expected, the dense graded asphalt mixture had greater resilient modulus than open graded asphalt mixture. This clearly indicates that mixture structure affects resilient response.

Creep compliance is related to the ability of a mixture to relax stresses. Generally speaking, mixtures with higher creep compliances can relax stresses faster than mixtures with low creep compliance, which is primarily of significance for thermal stress evaluation. As shown in Figures 4-28 and 4-29, open graded asphalt mixture and unmodified dense graded asphalt mixture shows higher creep response than modified dense graded asphalt mixture.

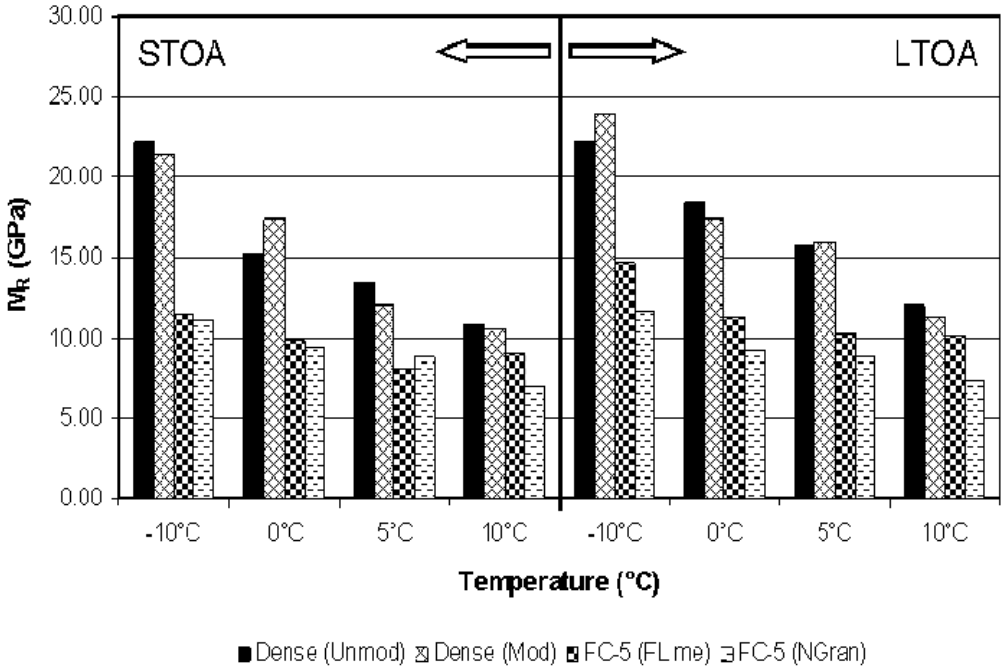

Figure 4-27 Resilient Modulus from IDT Test

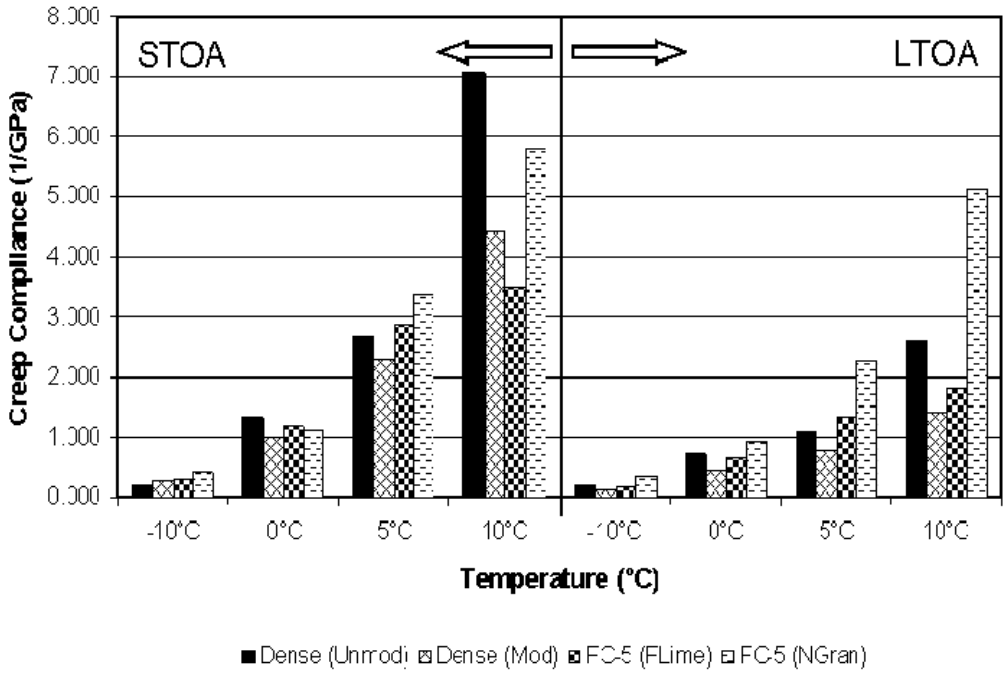

Figure 4-28 Creep Compliance from IDT Test

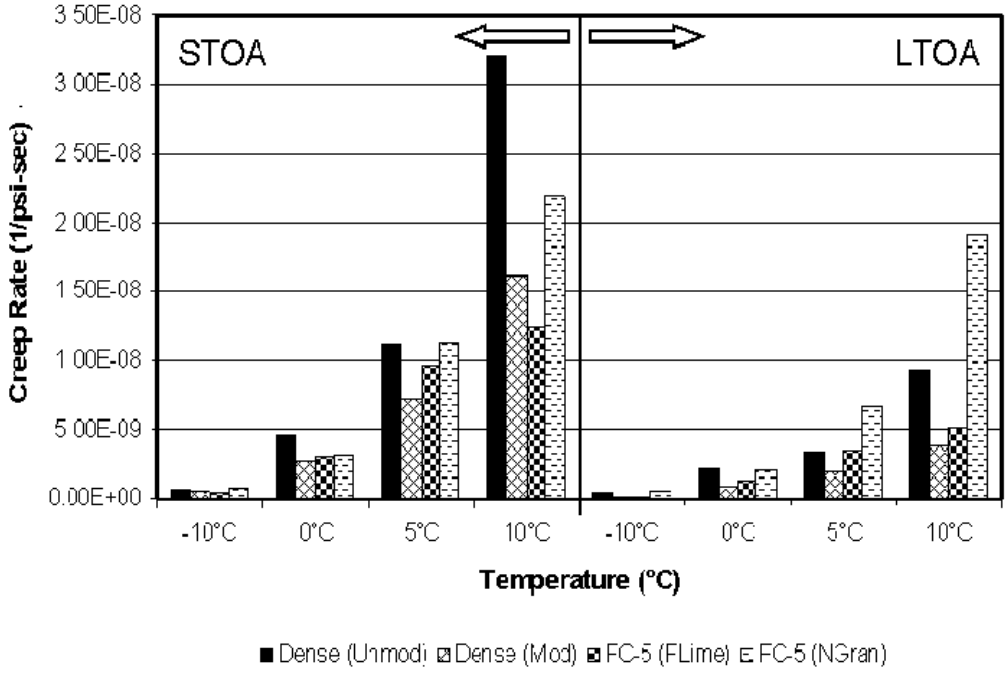

Figure 4-29 Creep Rate from IDT Test

The SBS polymer appears to have much greater influence on the time-dependent response of dense graded asphalt mixture than on the short loading time response. As shown in Figures 4-28 and 4-29, it was also noted that reduction in absolute value and rate of creep compliance of unmodified dense graded mixture with aging is remarkable compared to modified dense graded asphalt mixture. This implies that modified binder reduces the rate of oxidative aging.

Tensile strength is the maximum tensile stress the mixture can tolerate before fracture. As shown in Figure 4-30, results of tensile strength had a similar trend as that of resilient modulus. Dense graded asphalt mixtures have higher tensile strength than open graded asphalt mixtures.

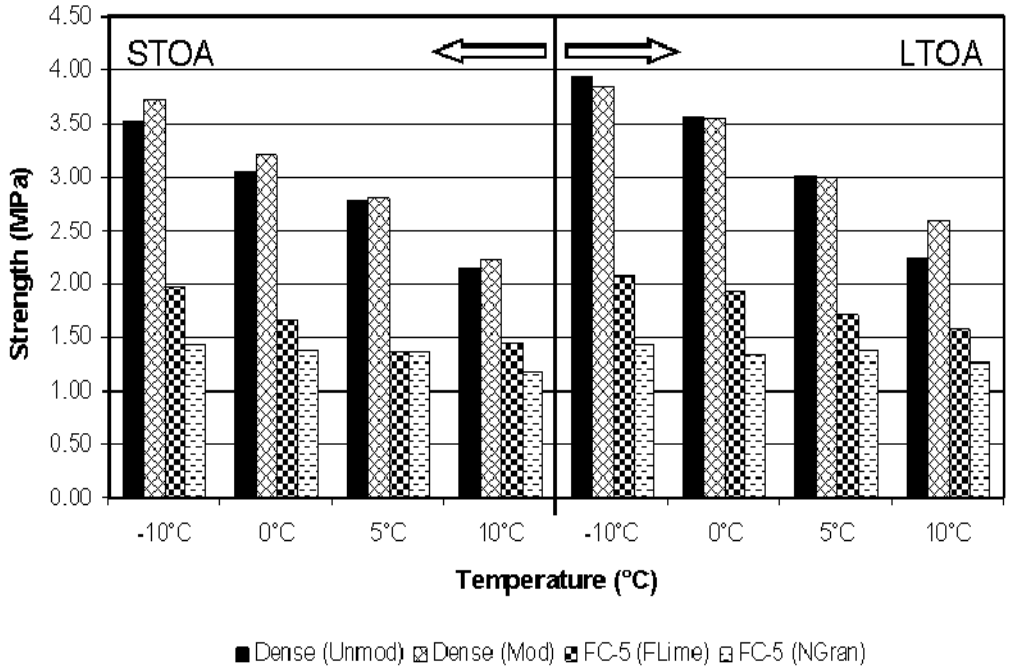

Figure 4-30 Strength from IDT Test

Failure strain, which characterizes the brittleness of a mixture, was higher for dense graded asphalt mixtures than for open graded asphalt mixtures at both aging conditions as presented in Figure 4-31. With respect to open graded asphalt mixture, age conditioning did not have significant influence on the failure strain for either aggregate type. This might be due to binder contents. The binder contents of open graded asphalt mixtures are higher than that of dense graded asphalt mixture and it might take open graded asphalt mixtures more time to be aged enough to influence failure strain. Similar values of fracture energy and dissipated creep strain energy were observed regardless of age conditioning for open graded asphalt mixtures.

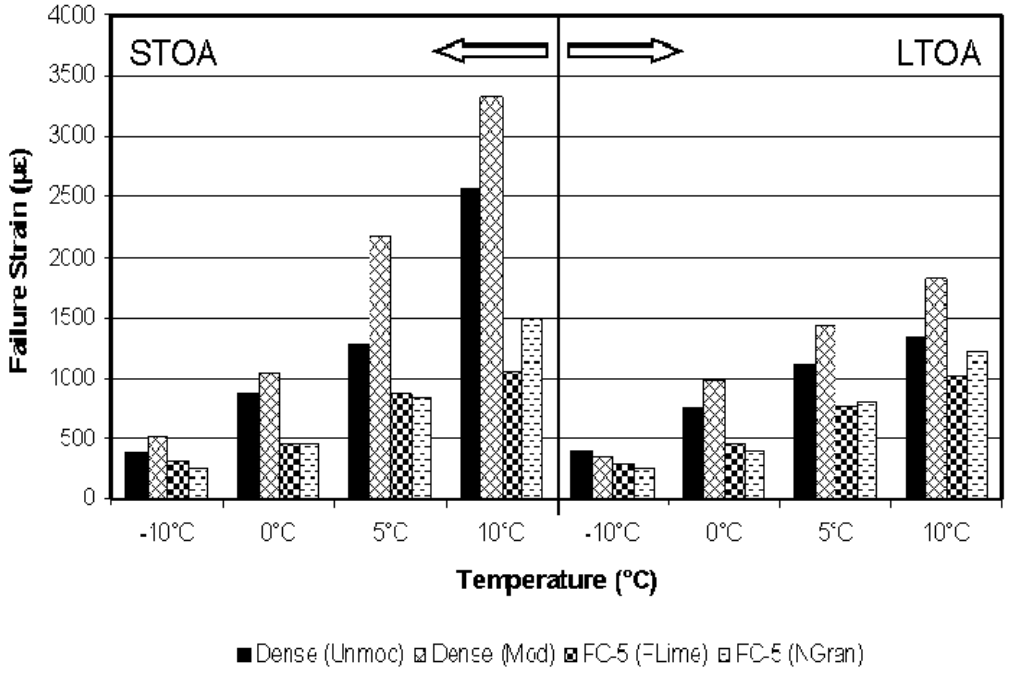

Figure 4-31 Failure Strain from IDT Test

Fracture energy (FE) results are shown in Figure 4-32. Fracture energy is calculated from the indirect tensile strength test by computing the area under the stress-strain curve up to the point of first fracture. The fracture energy of dense graded asphalt mixture is much higher than that of open graded asphalt mixture at all test temperatures and aging conditions. As mentioned above, there is no significant difference in fracture energy between two aging conditions for open grade asphalt mixture. Also, no considerable difference was observed between the two aggregate types.

The dissipated creep strain energy at failure ($DCSE_f$) is defined as the fracture energy minus the elastic energy (Zhang, 2000). Since $DCSE_f$ is a function of the fracture energy, it generally followed a similar trend as fracture energy (Figure 4-33).

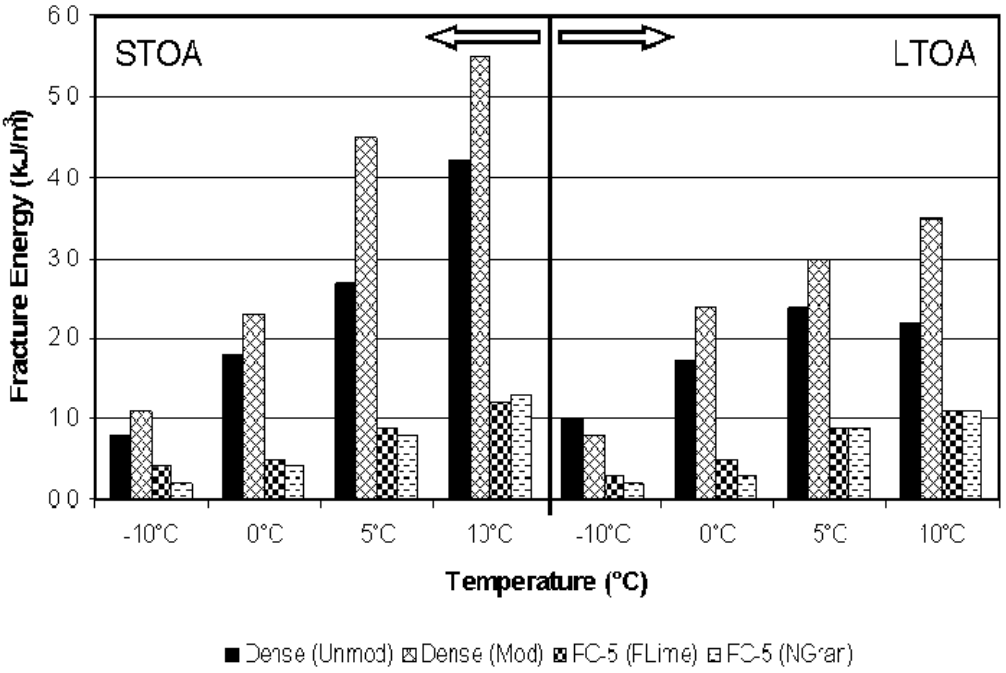

Figure 4-32 Fracture Energy from IDT Test

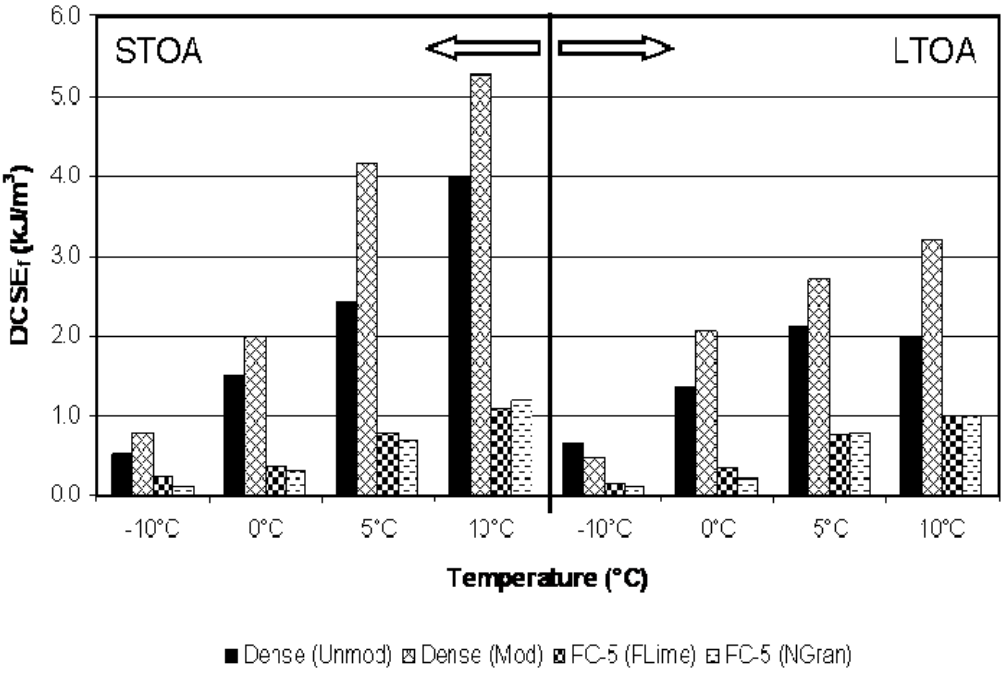

Figure 4-33 Dissipated Creep Strain Energy from IDT Test

The energy ratio (ER) was developed by Roque et al. (2004a) to represent the cracking resistance of asphalt mixtures. Energy ratios at 10°C with STOA conditioned asphalt mixture are shown in Figure 4-34. This parameter allows the evaluation of cracking performance for different pavement structures by incorporating the effects of mixture properties and pavement structural characteristics. Energy ratio can be considered as a criterion for fatigue cracking. Higher ER values typically result for mixture with higher $DCSE_f$ and lower creep rate. The results indicate the significantly higher energy ratio of the dense graded asphalt mixtures compared to open graded asphalt mixtures. Even though the energy ratio was developed for dense graded mixtures and it has not been truly calibrated for friction course mixtures, it may at least provide a relative evaluation for cracking performance, which indicates that open graded asphalt mixtures would exhibit worse cracking performance than dense graded asphalt mixture.

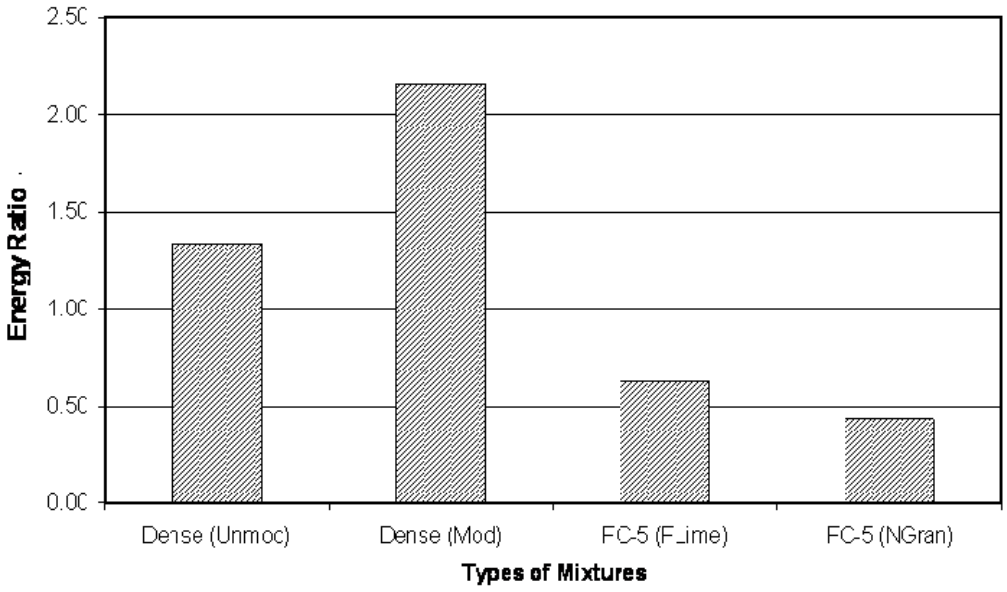

Figure 4-34 Energy Ratio from IDT Test

4.4.5 Dog-Bone Direct Tension Test Results

The newly developed dog-bone direct tension test (DBDT) was also performed with the same three loading modes as for Superpave IDT (i.e., resilient modulus, creep compliance, and strength test). Test procedure and data analysis were already discussed in the sections 3.4 and 3.5. All DBDT test results are presented in Appendix C. Generally, the DBDT test results shown in Figures 4-35 through 4-42 followed the similar trend as results from Superpave IDT.

Resilient modulus results are presented in Figure 4-35. Dense graded asphalt mixture showed higher resilient modulus than open graded asphalt mixture, and the resilient modulus of limestone open graded asphalt mixture was higher than granite open graded asphalt mixture. These observations clearly indicate that elastic response of asphalt mixture is dependent on characteristics of aggregate gradation and aggregate type.

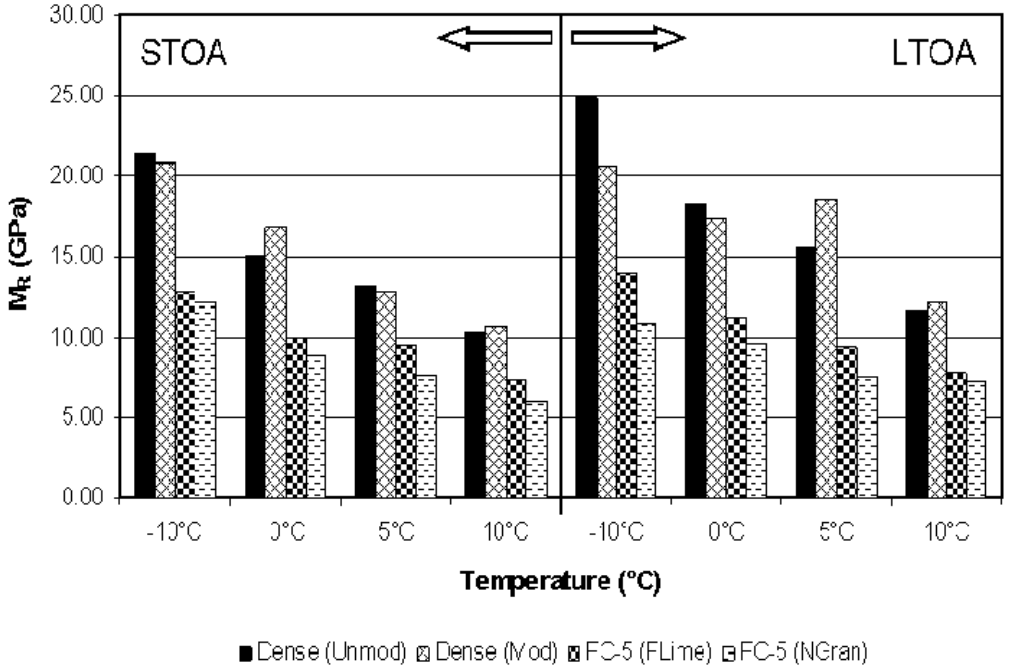

Figure 4-35 Resilient Modulus from DBDT Test

Absolute value and rate of creep compliance are shown in Figures 4-36 and 4-37. Clearly, modified dense graded asphalt mixture exhibited lower creep compliance at 1000 seconds and lower creep rate than open graded asphalt mixture. It is well known that creep behavior of asphalt mixture is strongly related to both aggregate and binder characteristics. Thus, the combination of dense gradation and binder modification plays a beneficial role in reducing the absolute value and rate of creep compliance.

Strength results shown in Figure 4-38 are very intriguing. As expected, dense graded asphalt mixture showed much higher strength than open graded asphalt mixture. However, no significant difference with temperature or aging condition was observed. This was unexpected and different from Superpave IDT test results. Potential explanations for these observations will be presented later in this chapter.

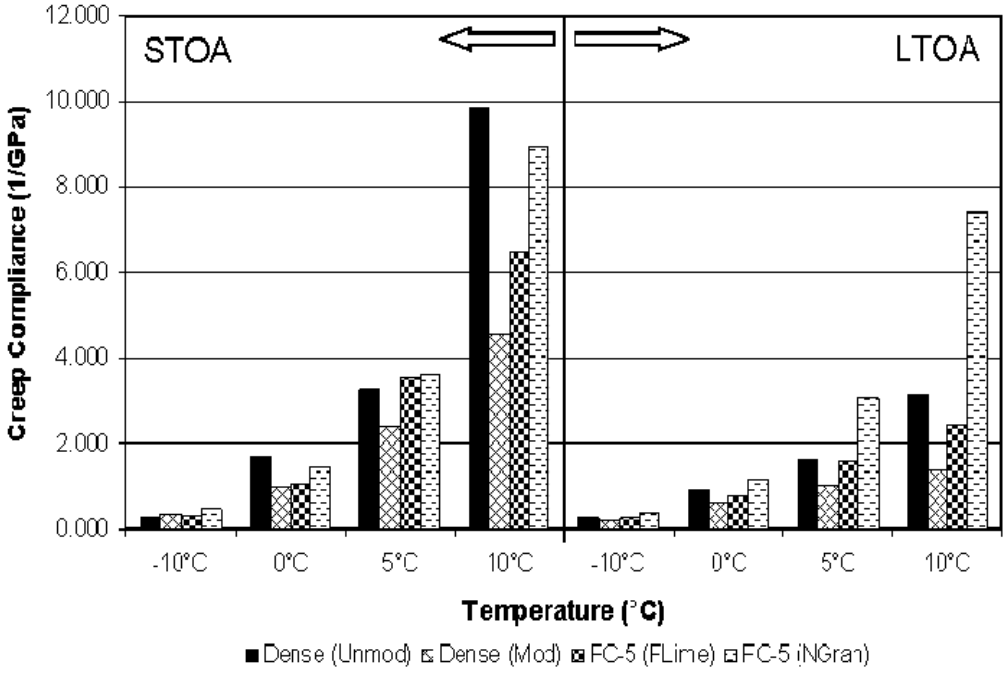

Figure 4-36 Creep Compliance from DBDT Test

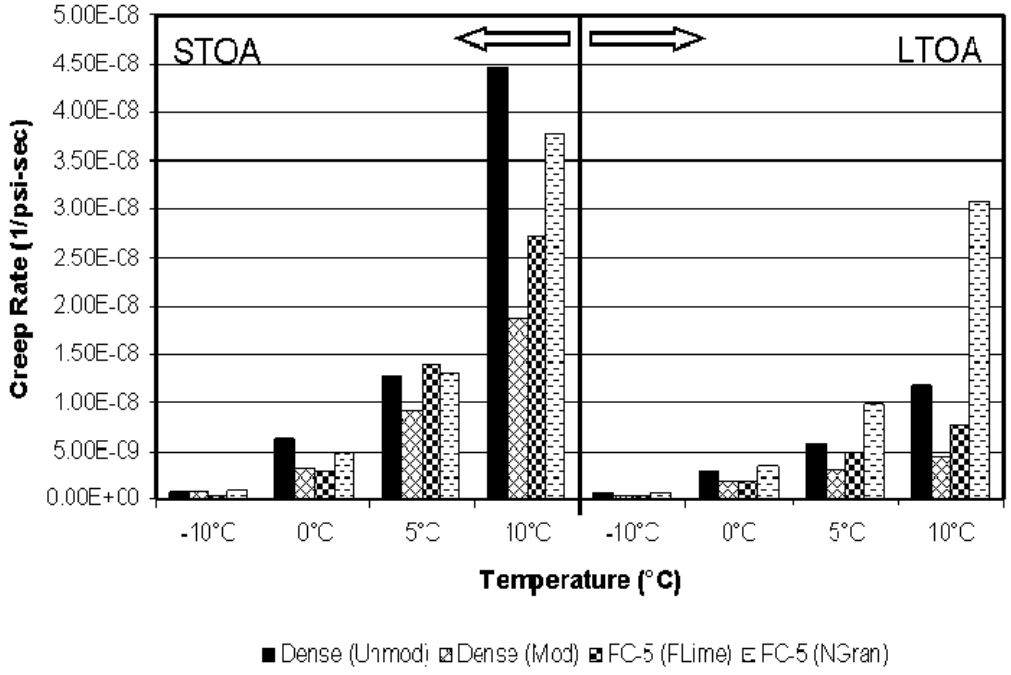

Figure 4-37 Creep Rate from DBDT Test

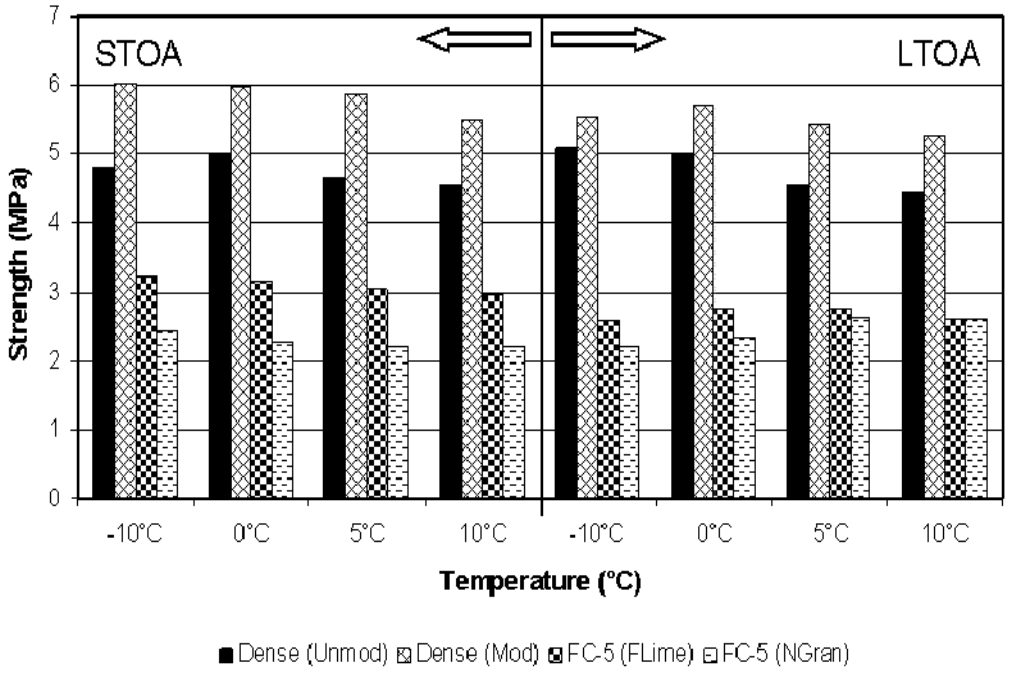

Figure 4-38 Strength from DBDT Test

Figure 4-39 shows the failure strain from DBDT. Failure strain seems to be strongly related to mixture gradation. Dense graded asphalt mixture showed higher values of failure strain. This can be observed more clearly for the short term oven aging condition. As for the Superpave IDT results, the change of failure strain due to aging was relatively small for open graded asphalt mixture. As mentioned previously, this might be due to higher binder contents in open graded asphalt mixture.

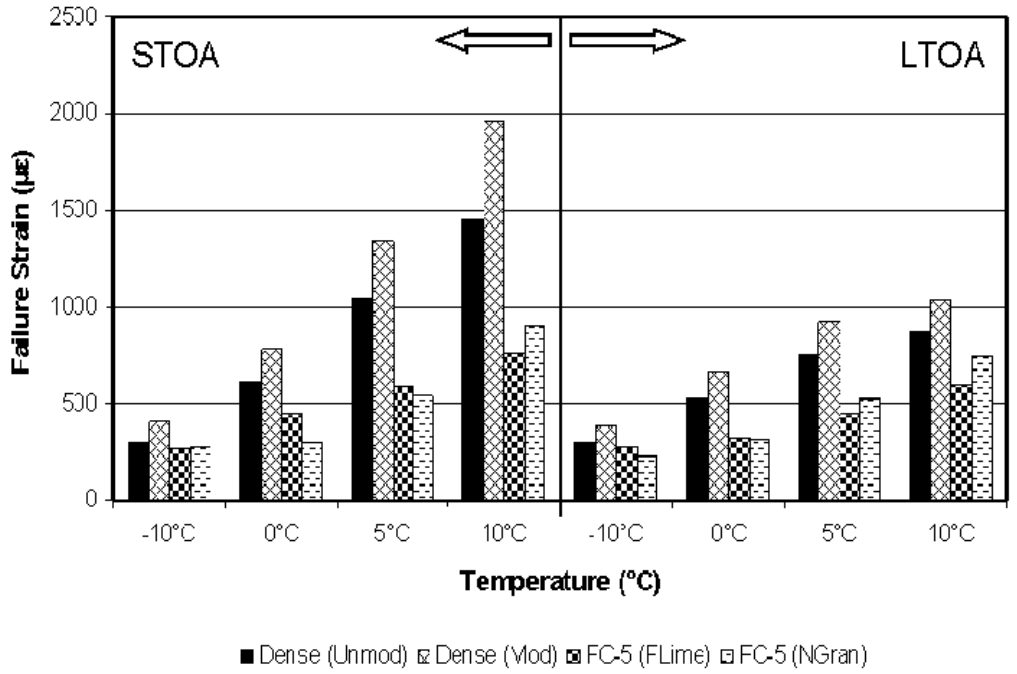

Figure 4-39 Failure Strain from DBDT Test

Fracture energy of dense graded asphalt mixture was also higher than that of open graded asphalt mixture as shown in Figure 4-40 because of higher strength and strain. Figure 4-41 presents dissipated creep strain energy at failure ($DCSE_f$). Higher $DCSE_f$ of dense graded asphalt mixture is attributed to higher fracture energy. Figure 4-42 shows a specimen after strength test, which clearly shows fracture occurred at the center of the specimen, as expected. As indicated

previously, it is one of advantages of DBDT test system that failure limits can be measured directly on the failure plane because failure plane is known a priori.

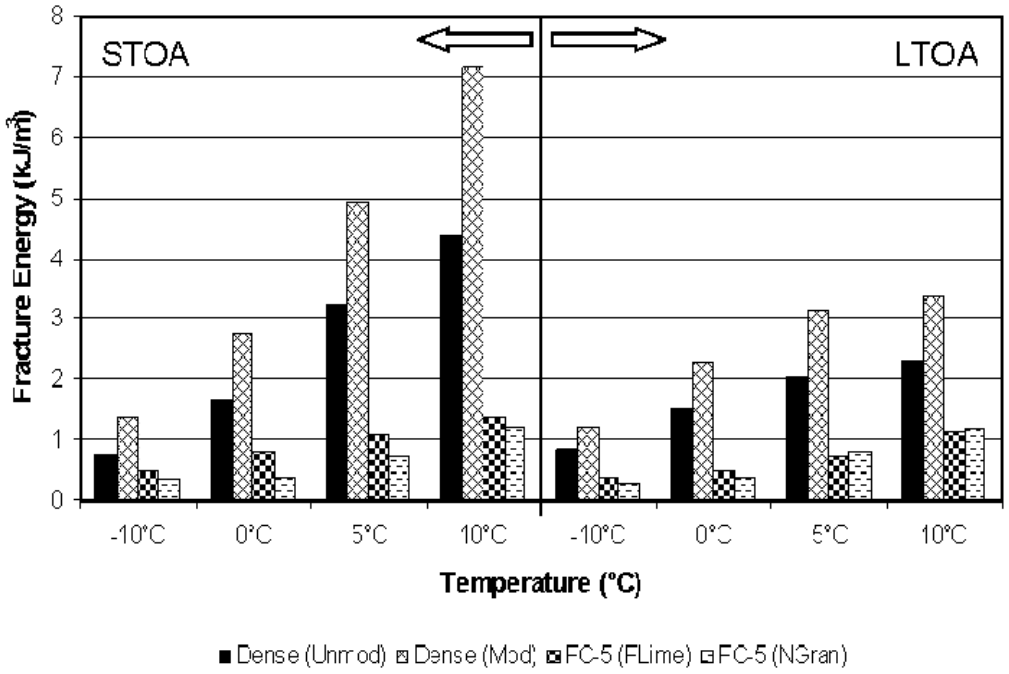

Figure 4-40 Fracture Energy from DBDT Test

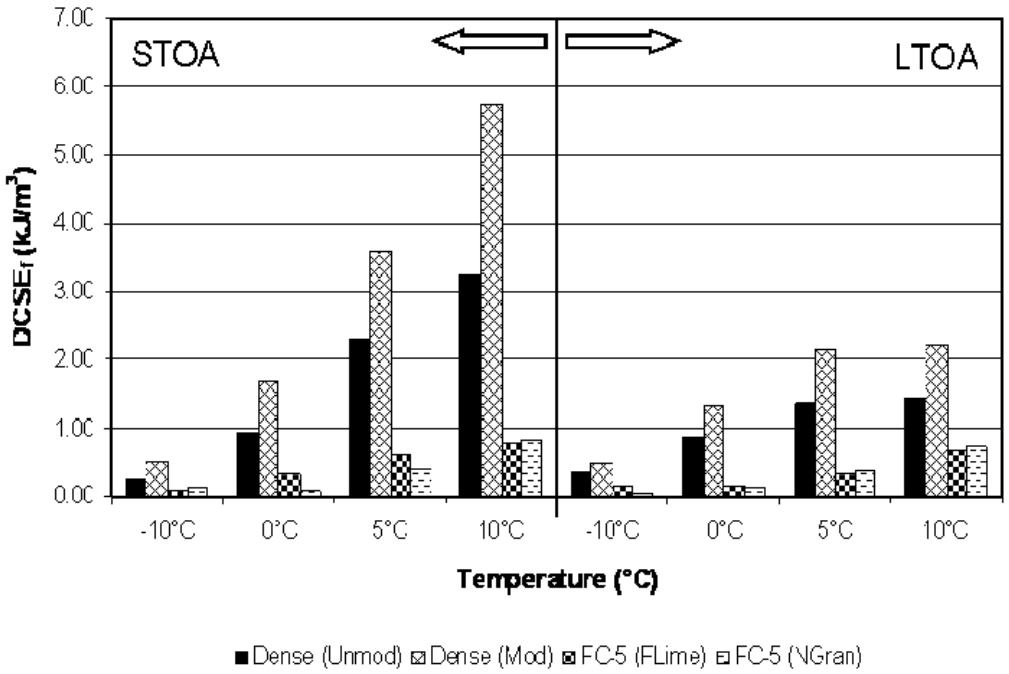

Figure 4-41 Dissipated Creep Strain Energy from DBDT Test

Figure 4-42 Specimen after Strength Test

Because energy ratio has not been fully calibrated for DBDT, it is not certain whether energy ratio determined from DBDT provides reliable information for evaluating top-down cracking performance. Therefore, the HMA fracture mechanics model which is based on more fundamental prediction of crack initiation and growth was used to assess DBDT data. HMA fracture mechanics model developed at the University of Florida (Zhang et al., 2001) was used to evaluate top-down cracking performance by calculating the number of load cycles needed to create a certain length of crack. STOA conditioned asphalt mixtures at 10°C were used for this analysis. Figure 4-43 shows crack depth as a function of load cycles and Figure 4-44 illustrates the number of load cycles needed to create a 1 inch crack. Results clearly indicate that modified

dense graded asphalt mixture exhibits the best performance while two types of open graded asphalt mixtures show the poorest cracking performance.

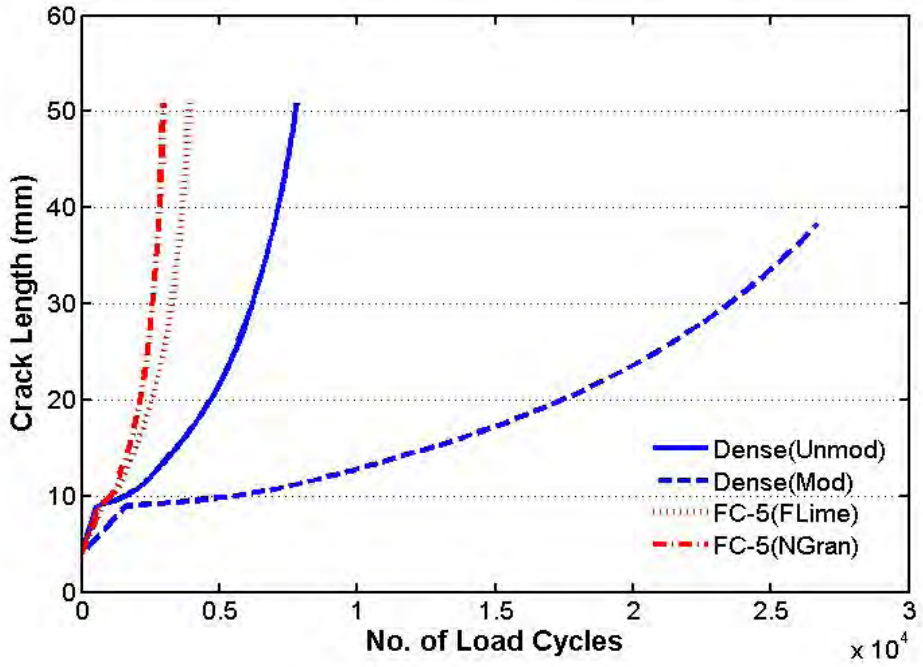

Figure 4-43 Crack Length with Load Cycles

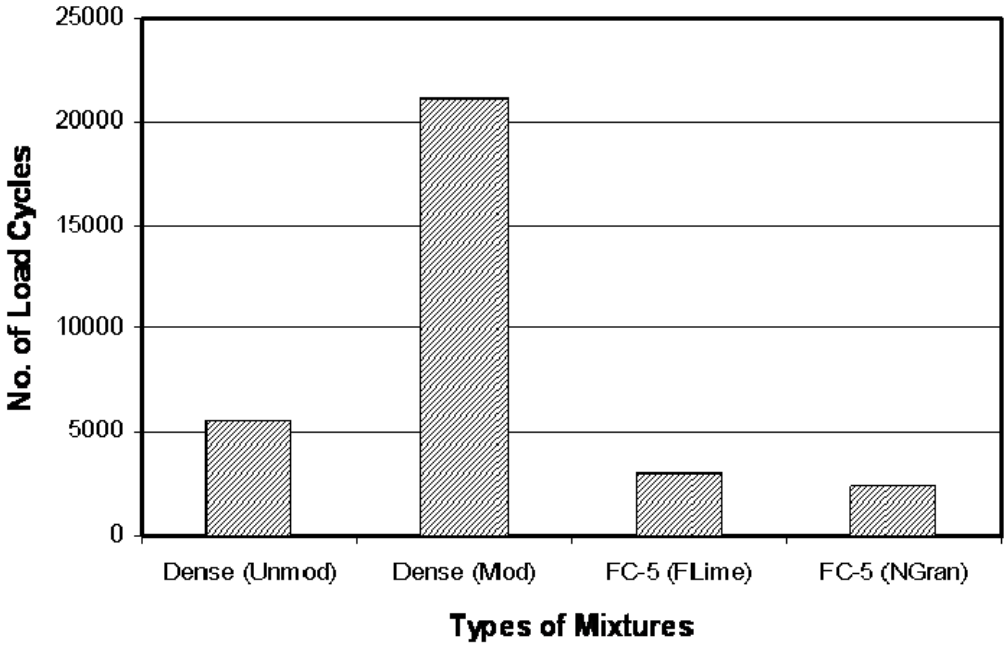

Figure 4-44 No. of Load Cycles at 1 inch Crack Length

4.4.6 Comparison between Superpave IDT and DBDT Test Results

This section provides comparisons of results from Superpave IDT and DBDT tests. It is generally thought that Superpave IDT test is the most convenient test to evaluate tensile properties of asphalt mixture while direct tension mode is more of a research tool for the asphalt testing community. Therefore, comparative analysis of two tests might be of great interest.

Figure 4-45 presents resilient modulus comparison for all tests performed. The comparison clearly shows that resilient modulus from the two tests were in excellent agreement, which indicates that elastic response due to rapid and repeated loading could be reliably obtained regardless of testing mode, i.e. indirect and direct mode.

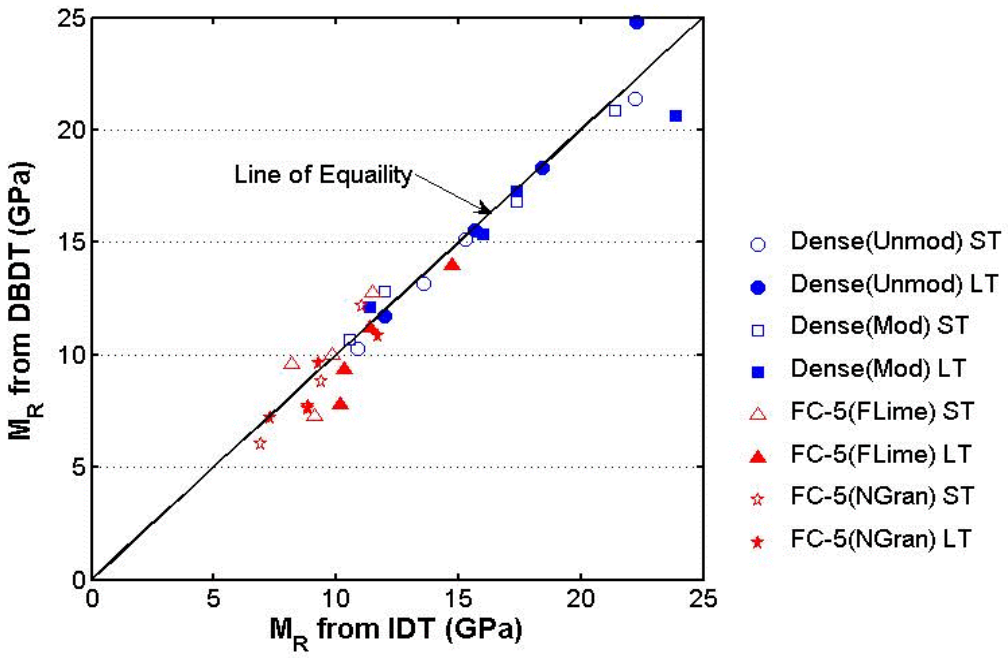

Figure 4-45 Resilient Modulus from IDT and DBDT Tests

Absolute value and rate of creep compliance are shown in Figures 4-46 and 4-47, respectively. These two properties show almost the same tendency between the two tests.

Absolute value and rate of creep compliance from DBDT at 1000 seconds are higher than those from Superpave IDT. Cristensen and Bonaquist (2004) observed a similar trend when they studied Superpave IDT and uniaxial tension test. They showed significant discrepancy between two tests, having higher compliance in uniaxial tension test. They reported that this might result from the anisotropy and differences in air void, air void distribution, or both.

However, there may be another potential reason. That is related to the fundamental behavior of asphalt mixture. Superpave IDT induces tension stresses in the presence of significant confinement induced by vertical compressive stresses. Lanaro et al. (2009) stated that compressive confinement is induced perpendicularly to the direction of the tensile stress in IDT test system. Behavior of particulate materials, such as granular soils and asphalt concrete at high and intermediate temperatures, is known to be strongly influenced by confinement. Greater confinement results in higher stiffness or lower compliance, which is the effect reflected in the data: for a given level of stress, Superpave IDT results in lower compliance.

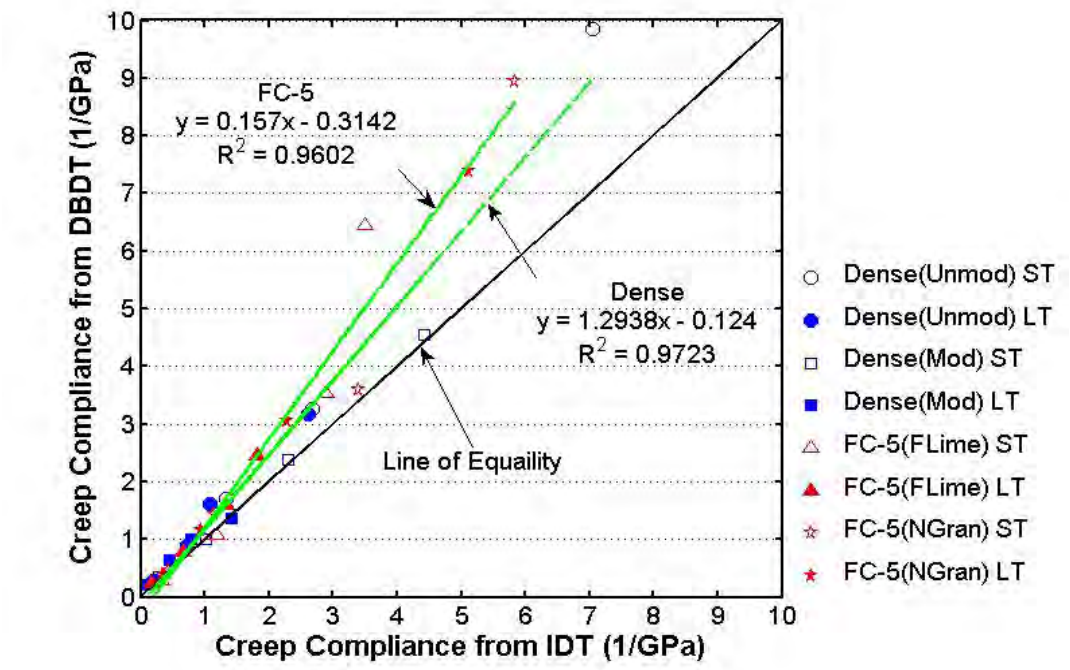

Figure 4-46 Creep Compliance from IDT and DBDT Tests

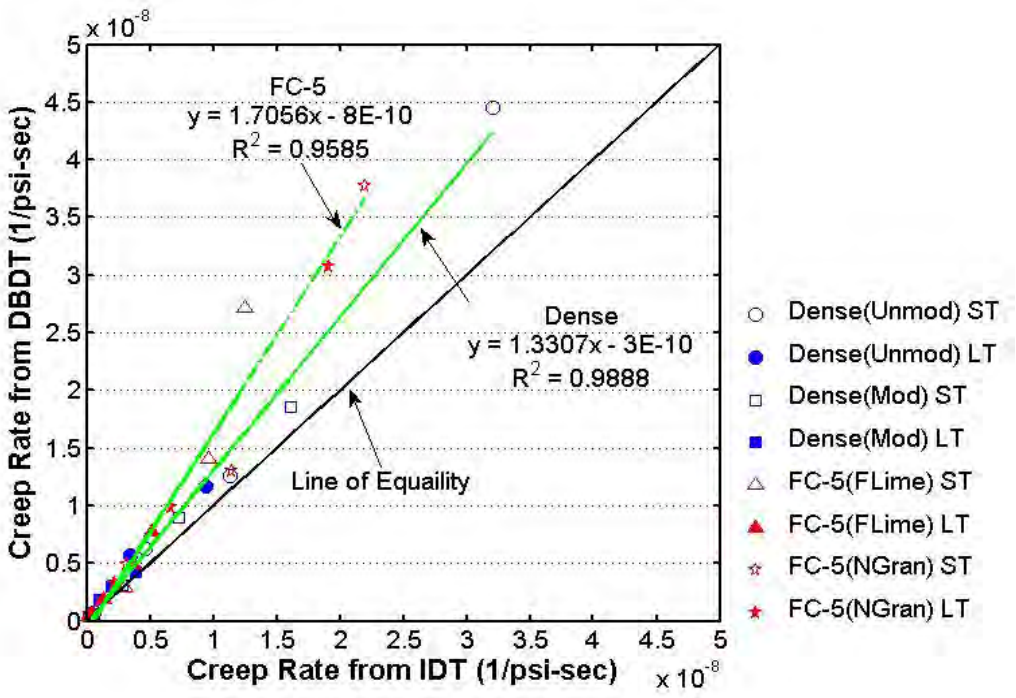

Figure 4-47 Creep Rate from IDT and DBDT Tests

It indicates that uniaxial stresses in the surface course (no confinement) accelerate tension-induced damage accumulation relative to uniaxial stress at the bottom of the structural layer (with confinement). These results also indicate that open graded asphalt mixture exhibited greater confining effect than dense graded asphalt mixture. Open graded asphalt mixture that has a relatively larger dominant aggregate size, which has a higher friction angle that results in a greater confinement effect in the IDT system.

Figure 4-48 presents strength comparisons between the two tests. As can be seen, strength results from DBDT are higher than those from Superpave IDT. It was determined that this was due to the difference in strain rate between Superpave IDT and DBDT. Because of stress concentrations at the specimen's edge, the DBDT tension test results in higher strain rates than

Superpave IDT, even when the same rate of displacement is used for both tests. This effect was also observed in differences in initial tangent modulus presented in Figure 4-49.

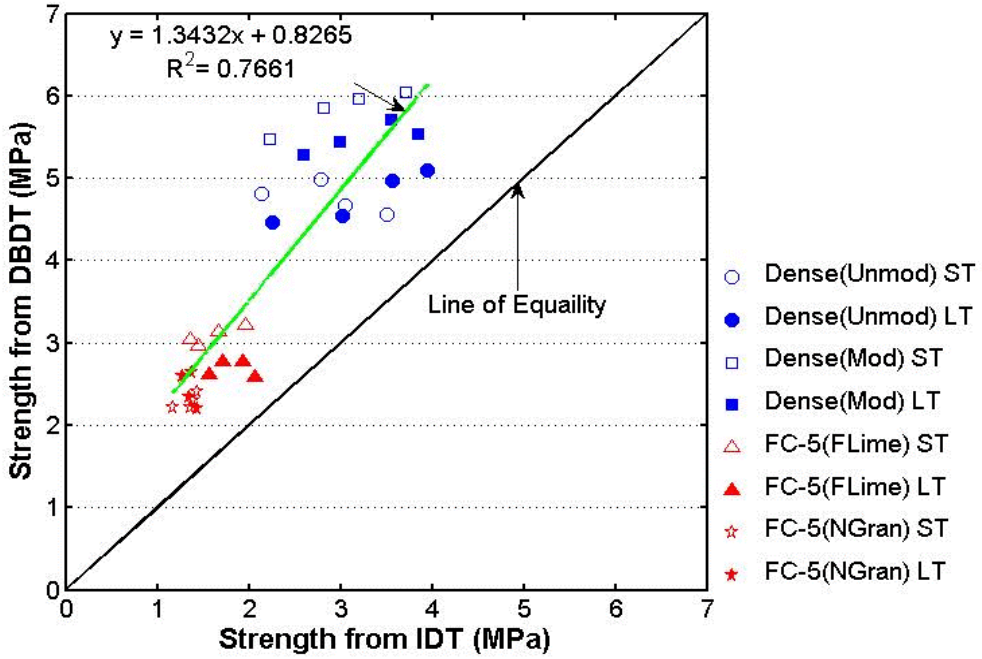

Figure 4-48 Strength from IDT and DBDT Tests

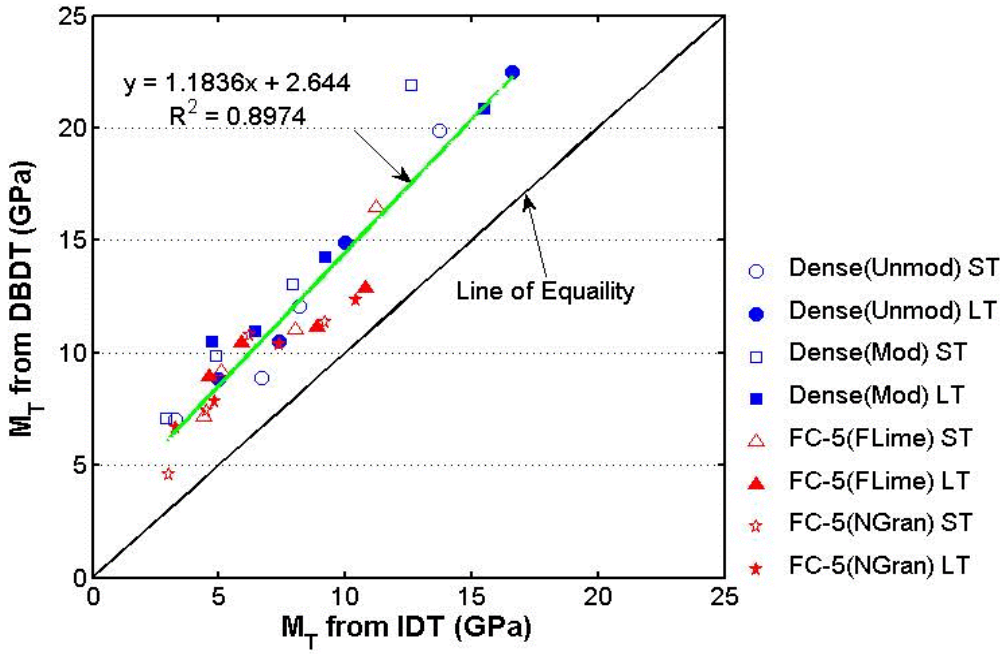

Figure 4-49 Initial Tangent Modulus from IDT and DBDT Tests

As shown in Figure 4-50, failure strain obtained from DBDT is generally less than that from Superpave IDT. This is also explained by the difference in strain rate between the two tests. It is well known that higher strain rate results in lower failure strain and higher strength. The higher failure strain, the greater the difference in failure strain between the two tests. Figure 4-51 shows that the difference between the tests is negligible for very brittle mixtures. This makes sense, since more brittle materials also exhibit more elastic, less strain-rate dependent behavior.

One of the more interesting observations from this study is that fracture energy was almost exactly the same for the two tests (Figure 4-51), even though the tensile strength and failure strain between Superpave IDT and DBDT were different.

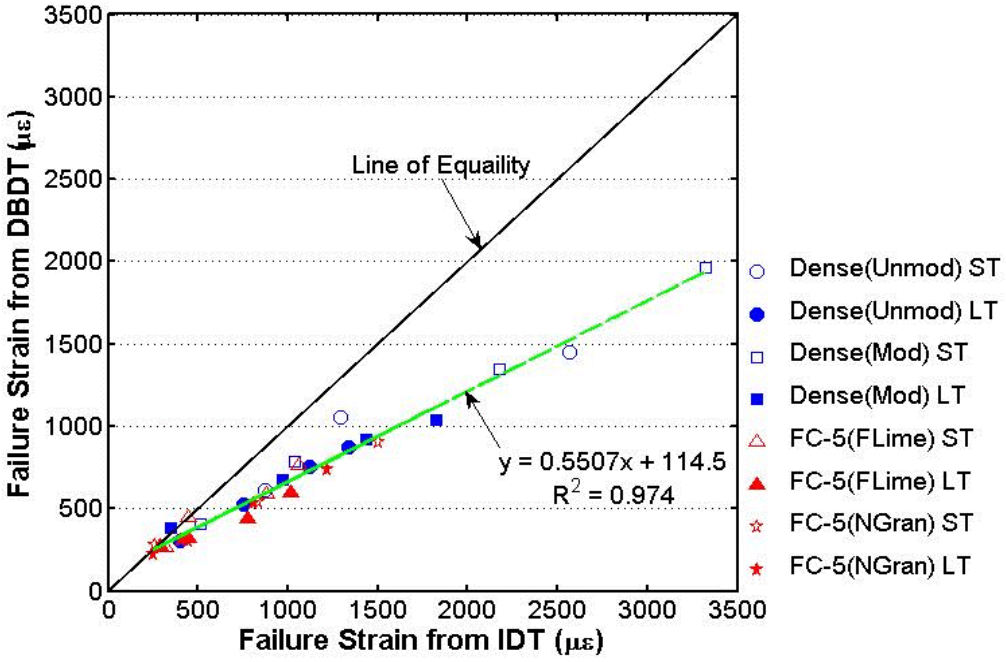

Figure 4-50 Failure Strain from IDT and DBDT Tests

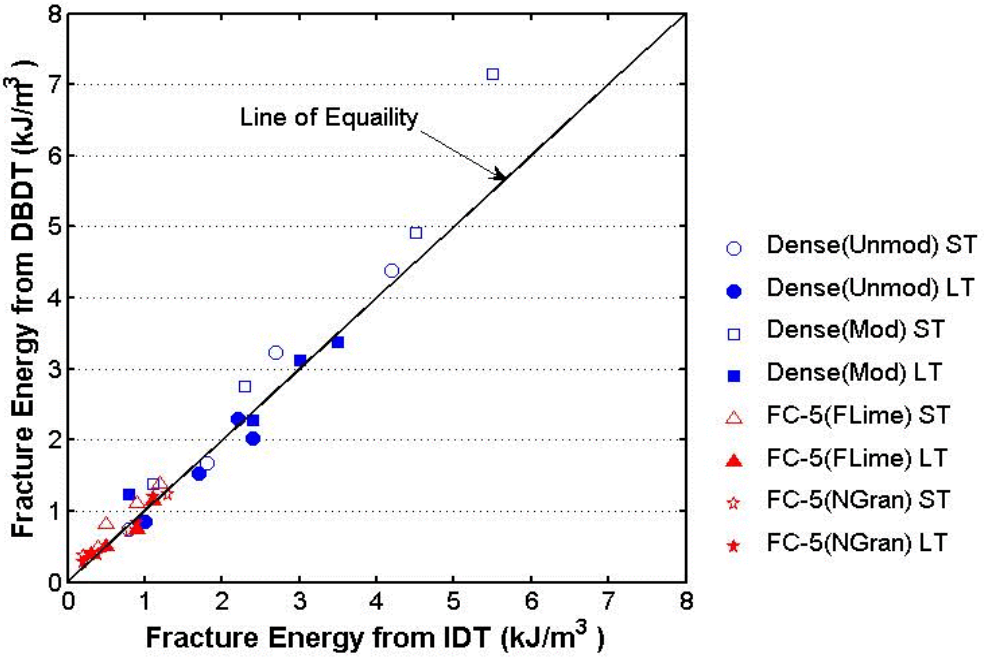

Figure 4-51 Fracture Energy from IDT and DBDT Tests

This provides further support that fracture energy is in fact a fundamental property that is independent of stress state and loading conditions, and is thus the most appropriate and necessary property to evaluate mixture fracture potential. Significantly different stress and strain states are induced in DBDT than in Superpave IDT and both strength and failure strain are known to be stress-state and load-rate dependent. However, fracture energy, which accounts for both stress and strain, was found not to be dependent on these factors. This result is in itself a very important validation involving the used of fracture energy as the basis for the HMA fracture mechanics models.

Dissipated creep strain energy at failure ($DCSE_f$) was also compared as presented Figure 4-52. This was calculated based on fracture energy and resilient modulus. $DCSE_f$ from the DBDT was slightly lower than that from Superpave IDT. This might result from slight differences in the

stress-strain curves from the strength tests. For illustrative purpose, Figure 4-53 shows schematic relationship of strength, failure strain, fracture energy, and $DCSE_f$ from two tests. DCSE is inherently dependent on loading rate. This makes sense since the faster loading rate, the more elastic response, while the slower loading rate, the less elastic response.

Since the stress-strain relationship is different for each test while both fracture energy and resilient modulus are almost the same between two tests, $DCSE_f$ from DBDT shows slightly lower values. This was corrected by using the tangent modulus to compute $DCSE_f$, since elastic energy is dependent on loading rate.

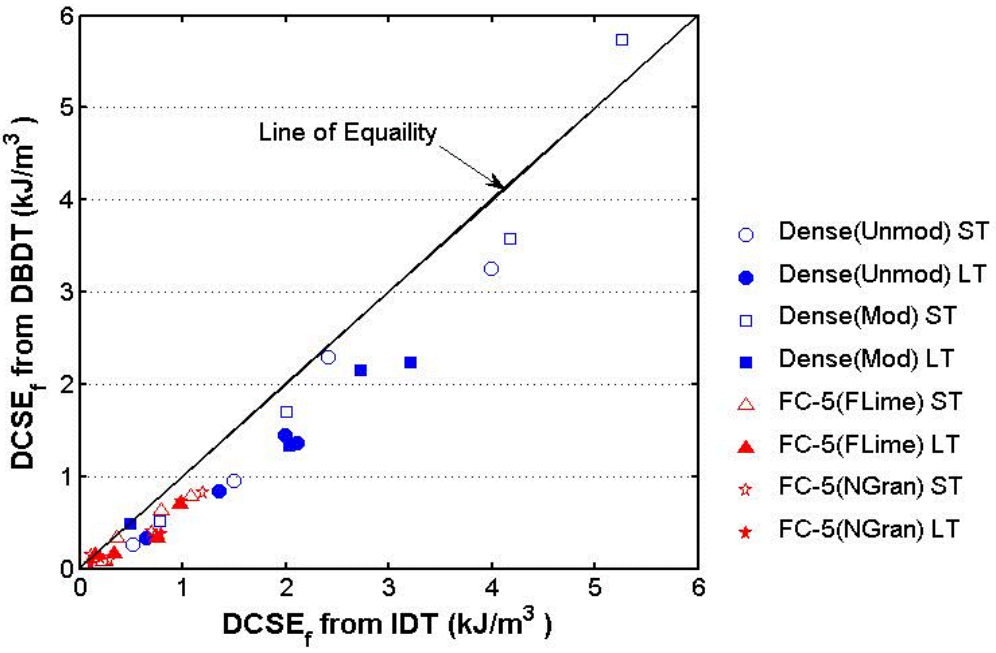

Figure 4-52 Dissipated Creep Strain Energy from IDT and DBDT Tests

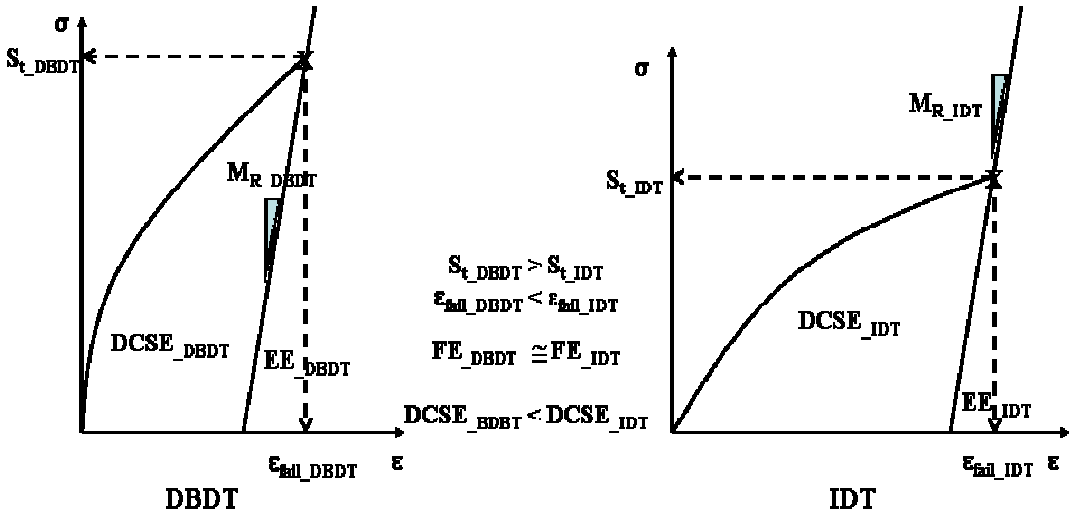

Figure 4-53 Schematic Illustration of Stress-Strain Relation between DBDT and Superpave IDT

Equation 4-6 shows rate correction to the M_R from DBDT test, which is illustrated in Figure 4-54. This equation does not mean that tangent modulus should be used for distinguishing EE from FE. Resilient modulus is still recommended since it is more consistent and repeatable than tangent modulus. However, it was thought that the simplest and easiest way to incorporate the effect of loading rate was to use the ratio of tangent modulus between two loading rates. i.e., this was done for comparative purposes only.

$$M_{R\_DBDT\_corrected} = M_{R\_DBDT} \times \frac{M_{T\_DBDT}}{M_{T\_IDT}} \qquad (4\text{-}6)$$

Where, $M_{R\_DBDT\_corrected}$ = corrected resilient modulus from DBDT used in obtaining energy ratio, M_{R_DBDT} = resilient modulus from DBDT, M_{T_DBDT} = initial tangent modulus from DBDT, M_{T_IDT} = initial tangent modulus from Superpave IDT.

Corrected $DCSE_f$ was re-plotted as shown in Figure 4-55. As can be seen, $DCSE_f$ from both tests were in excellent agreement.

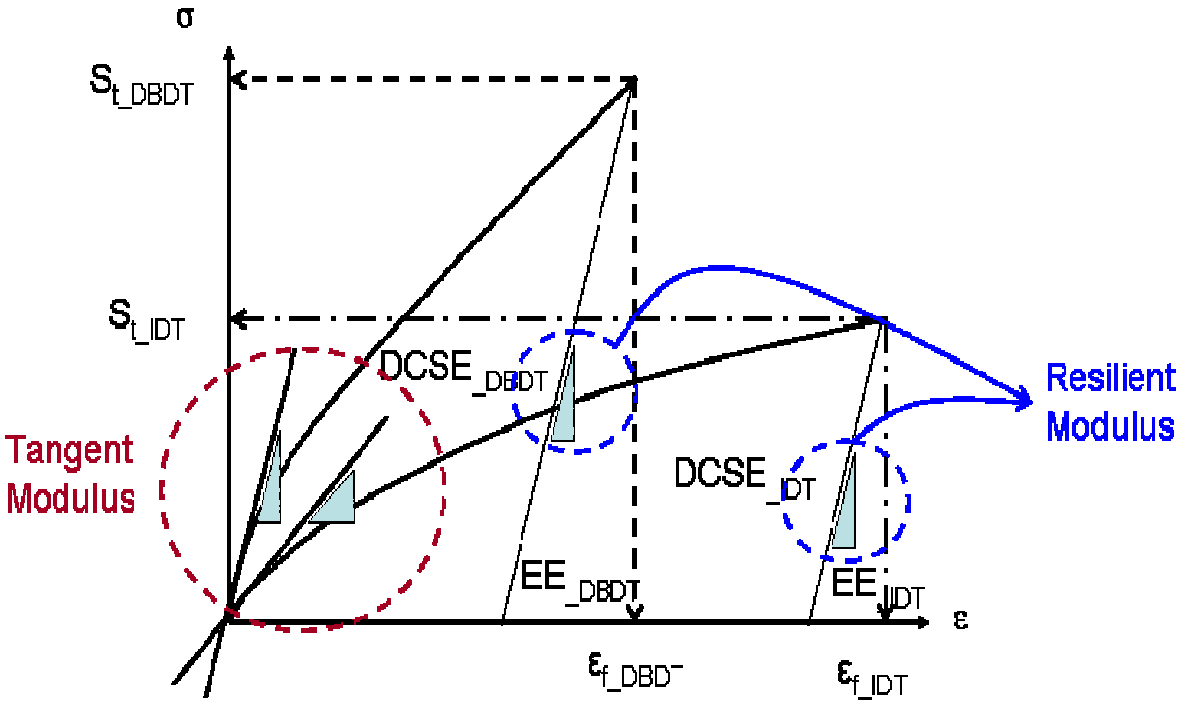

Figure 4-54 Loading Rate Correction with Tangent Modulus

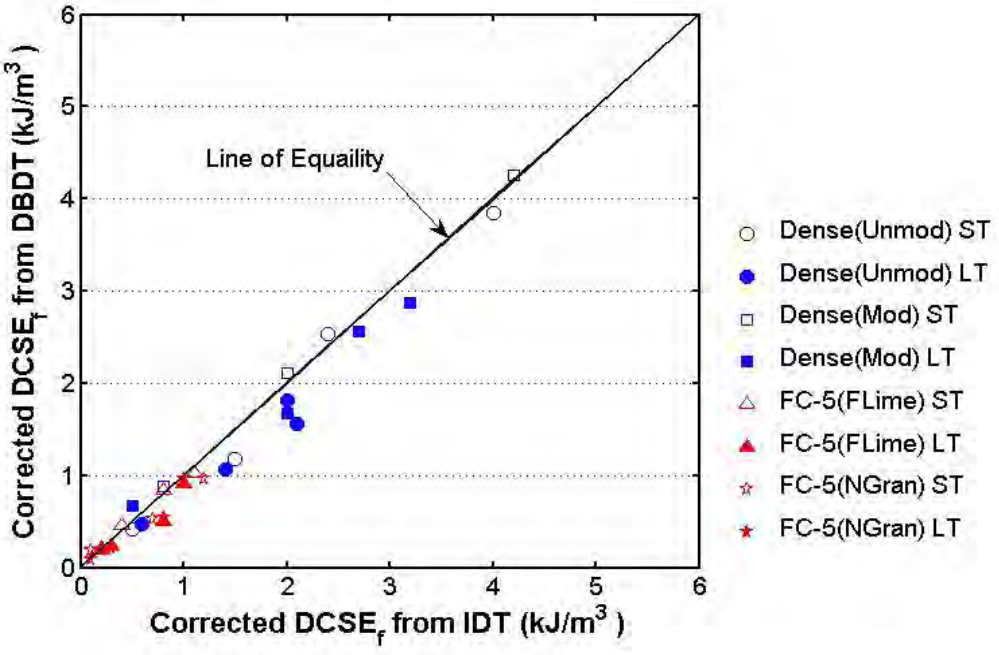

Figure 4-55 Corrected Dissipated Creep Strain Energy from IDT and DBDT Tests

CHAPTER 5
DEVELOPMENT OF COMPOSITE SPECIMEN DIRECT TENSION TEST

5.1 Background

Top-down cracking has been widely reported on pavements with open-graded friction course in Florida. In an effort to find the cause behind this, one possible way is to perform direct tension on composite specimen consisting of open-graded mixture and dense-graded mixture. Although the dog-bone configuration is ideal for uniform specimens composed of a single mixture, i.e. dense-graded or open-graded mixtures, it was determined not to be suitable in its current form for testing composite specimens. The dog-bone specimen results in excessively non-uniform and complex stress states once composite specimens composed of two different mixtures are introduced. Also dog-bone specimen is suitable for evaluation of cracks propagating inwards to the specimen center but not suitable for evaluation of cracks propagating downwards from OGFC to dense-graded mixture. Therefore, it was decided that modified specimen geometry and loading configuration was needed to properly test and evaluate composite specimen behavior.

5.2 Objective

The objective of this part of the work was to develop a composite specimen direct tension test and testing protocols, including specimen preparation, testing protocols, data acquisition and interpretation methods.

5.3 Scope

Superpave IDT tests were performed to evaluate the possible damage to the dense-graded HMA induced during the OGFC compaction process. In addition, constant stroke rate strength tests at 3 different loading rates were performed on asymmetrical composite specimens, and repeated loading tests were performed on asymmetrical and symmetrical composite specimens.

5.4 Evaluation of the Effect of OGFC Compaction on the Integrity of the Dense-Graded Mixture

Composite specimen can be prepared by compacting open-graded mixture on top of the pre-compacted dense-graded mixture using Superpave Gyratory Compactor (SGC). The compacted dense-graded Gyratory specimen was sliced into two halves; each half was placed back in the gyratory mold and open-graded mixture placed on top of it and compacted to the desired air voids using SGC. Either a conventional tack coat or Novabond tack was applied to the base material surface before placing the open-graded mixture.

5.4.1 Materials and Testing Methods

The dense-graded mixture that is commonly used by the FDOT and identified as Dense-GA-Granite was selected for this evaluation. Its aggregate was made up of four components: coarse aggregate, fine aggregate, screenings, and sand. Its gradation is shown in Table 5-1. This mixture was designed according to the Superpave volumetric mix design method. Design asphalt contents for the mixture was determined such that each mixture had 4 percent air voids at N_{design}= 75gyrations. PG 67-22 asphalt was used for the mixture. A total of 9 dense-graded Gyratory specimens were prepared. Table 5-2 shows the bulk specific gravity of the prepared specimen. In order to save time, 2000 grams of Superpave mixture available in the lab was used instead of open-graded mixture for purposes of evaluation of additional compaction on the

integrity of underlying dense mixture. Better uniformity is expected with dense-graded mixture on top instead of open-graded mixture, and additionally compacted mixture is sliced off prior to testing, therefore the choice of additional materials has little effect on the evaluation of additional compaction on the integrity of underlying dense mixture.

Table 5-1 Dense-Graded Mixture Aggregate Gradation

		Percent Passing				
Blend		33%	7%	50%	10%	100%
Number		1	2	3	4	JMF
Sieve Size	3/4"	100	100	100	100	100
	1/2"	97	100	100	100	99
	3/8"	59	100	100	100	86
	# 4	9	30	100	100	65
	# 8	4	4	70	100	47
	# 16	2	2	42	100	32
	# 30	2	1	25	94	23
	# 50	1	1	16	53	14
	# 100	1	1	10	11	7
	# 200	1.0	1.0	7.0	3.0	4.2

Table 5-2 Bulk Specific Gravity

Number	1	2	3	4	5	6	7	8	9
Bulk Specific Gravity	2.446	2.459	2.454	2.454	2.448	2.445	2.447	2.451	2.449

The following tests and analyses were performed:

- Dense-graded mixtures were designed according to the Superpave™ volumetric mix design method. 4500 grams of aggregate were prepared for each mixture. Asphalt content was 4.8%. A total of nine samples were prepared.
- Compacted dense graded mixtures were cut into two halves. Nine of them were used for Superpave IDT control test, while the other nine were used for recompaction evaluation.

- Tack coat was applied onto the cut side of dense-graded mixture pills. The reason that the cut side was selected was that the mixture was more uniformly compacted than that of the uncut side; the ends of gyratory compacted specimens have lower density. The tack coat was applied in form of pure asphalt (AC-20) to save time on emulsified asphalt setting. The reason that AC-20 was used was that the viscosity of the residual asphalt of the emulsion corresponded to AC-20. The calculation of amount of AC-20 applied on each cut side is presented in Appendix E.
- 2000 grams of Superpave mixture available in the lab were placed on top of each of the nine half cut dense-graded specimens. Three were compacted to 50 gyrations, three to 100 gyrations and three to 150 gyrations. The ring holding the rotating base was taken off the gyratory compaction mold so the prepared dense-graded specimen could be more easily put back into the mold from the bottom.
- Three groups of Superpave IDT tests were performed on no re-compaction and re-compacted specimens, respectively. Each group had three specimens. A total of 18 IDT tests were performed. All tests were performed at 10°C.

5.4.2 Analysis of Test Result

Superpave IDT test results are summarized in Appendix F. The results show that additional compaction actually improved the specimen strength. Student's t-tests show that by conventional criteria, the differences between no re-compaction and re-compaction for m-value, D_1, S_t, M_R, FE, DCSE, ER, and damage rate were not statistically significant; in other words, no damage was induced by the additional compaction process.

Damage rate was defined as creep rate, which is one of the most critical parameters affecting mixture performance evaluation; the creep rates presented in Appendix F was calculated using equation 5-1.

$$\frac{dD(t)}{d(t)} = \dot{\varepsilon}_{cr} = mD^{1}t^{m-1} \quad \text{where, t} = 1000 \tag{5-1}$$

The creep rates calculated from equation (5.1) show that there is some improvement in damage resistance. This improvement might be normal material variation, like one or several specimen sides of the six specimen sides in each group. Careful examination of the results indicated that some measurements were clearly unreliable and appeared to be affected by problems with the gages. Only measurements that were clearly reliable were included in the analysis and presented in Figures 5-1 through 5-5.

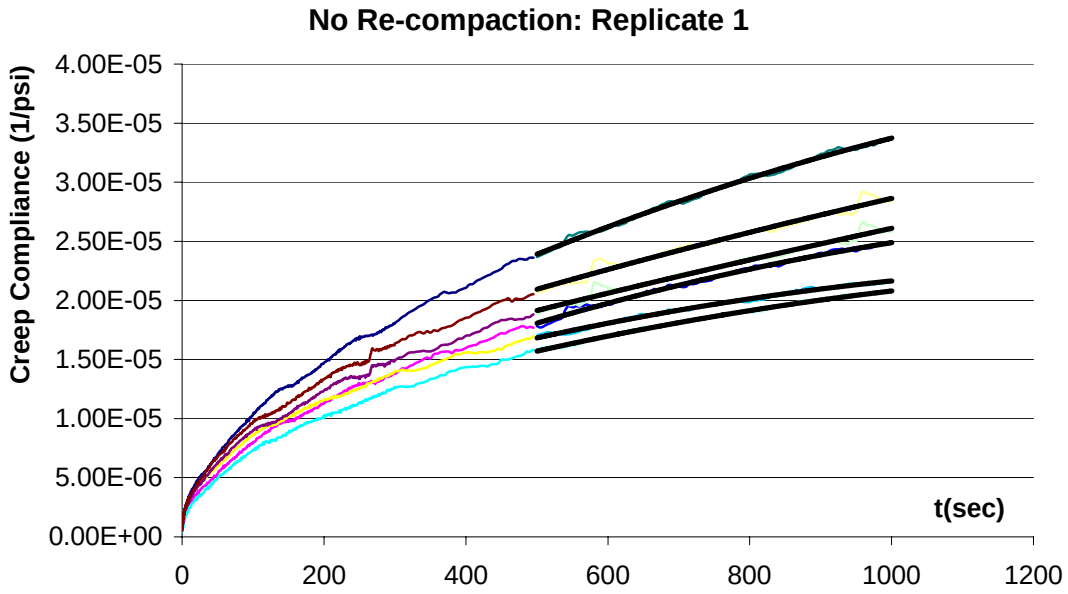

Figure 5-1 Creep Compliance versus Time for No Re-compaction Replicate 1

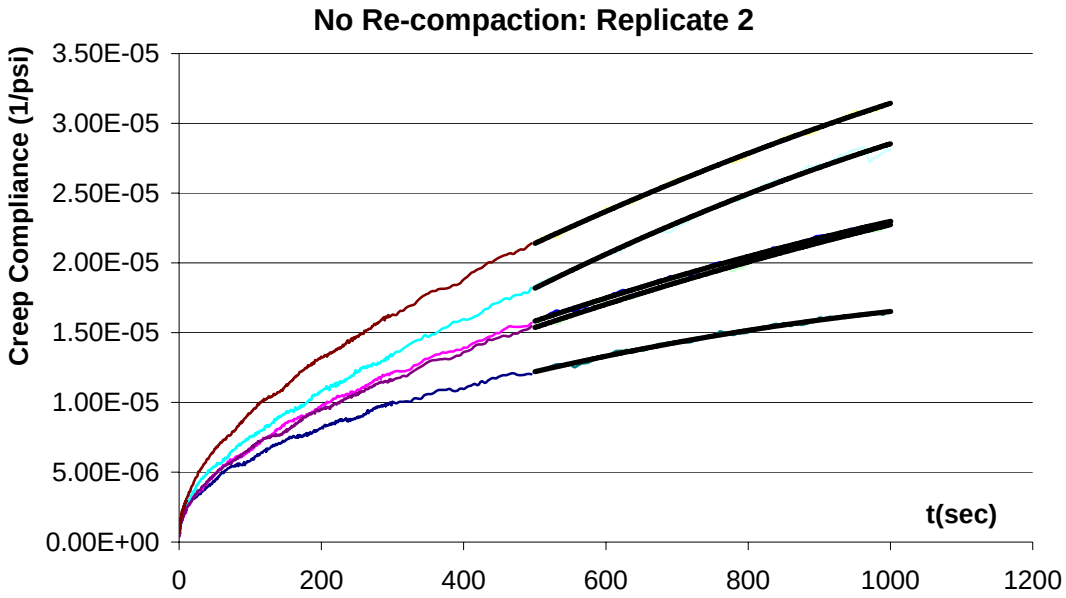

Figure 5-2 Creep Compliance versus Time for No Re-compaction Replicate 2

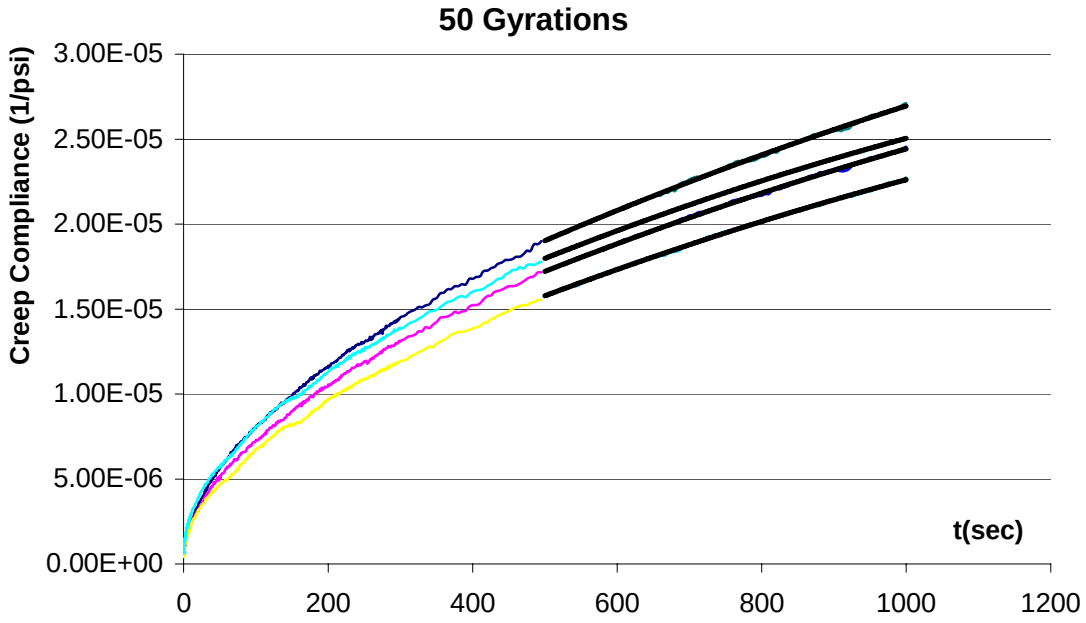

Figure 5-3 Creep Compliance versus Time for 50 Additional Gyrations

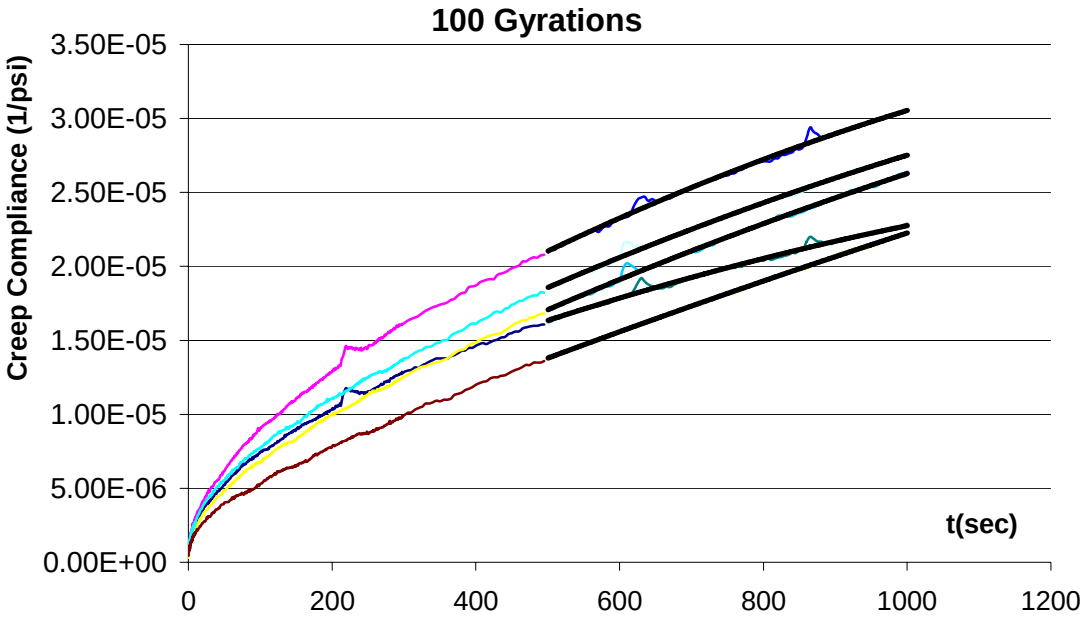

Figure 5-4 Creep Compliance versus Time for 100 Additional Gyrations

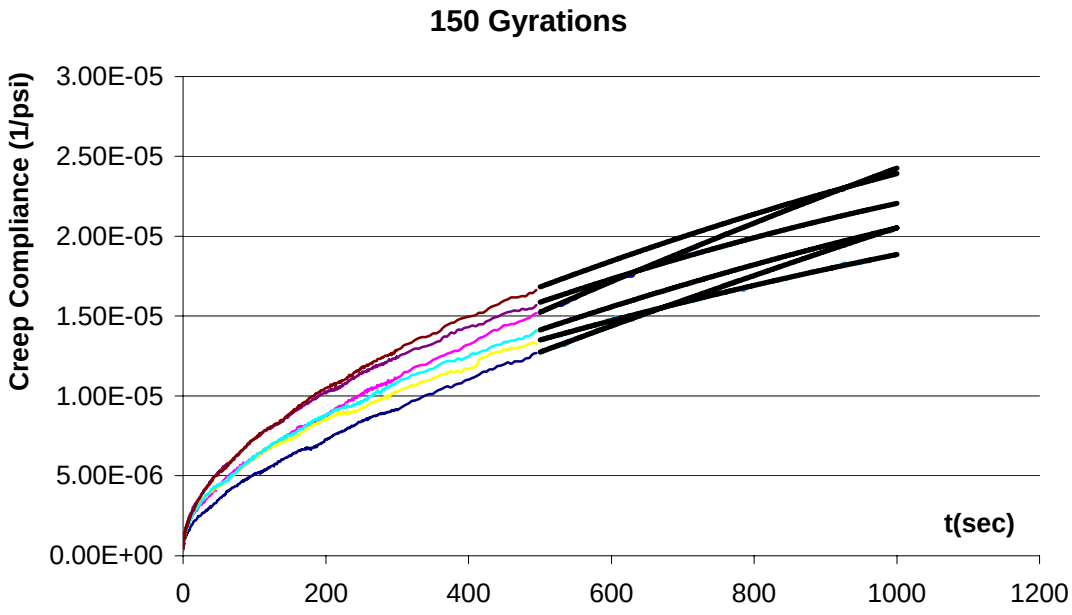

Figure 5-5 Creep Compliance versus Time for 150 Additional Gyrations

The creep rates were recalculated with only reliable measurements and presented in Table 5-3 and figure 5-6.

Table 5-3 Creep Rate Recalculation

Project Name	Creep Rate (1/psi-sec)	Average
No Re-compaction: Replicate 1	1.27E-08	1.36E-08
No Re-compaction: Replicate 2	1.45E-08	
50 gyrations	1.25E-08	1.34E-08
100 gyrations	1.45E-08	
150 gyrations	1.32E-08	

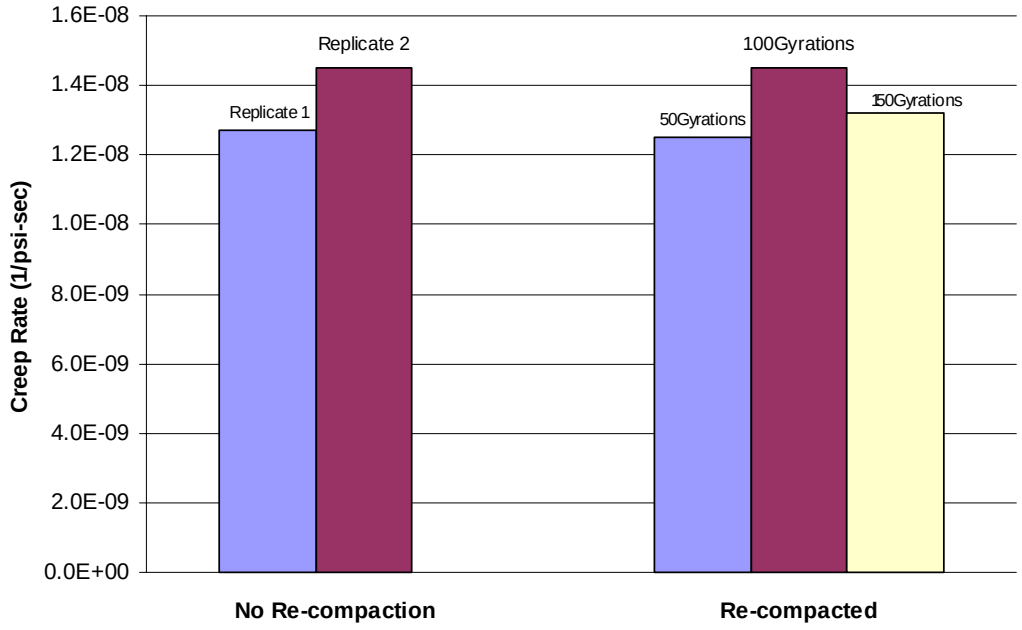

Figure 5-6 Re-calculated Creep Rates for No Re-compaction and Re-compacted specimens

The data in Table 5-3 and Figure 5-6 show that additional compaction had no effect on the integrity of the dense-graded mixture. If anything, there appeared to be a slight improvement in damage resistance.

5.5 Composite Specimen Preparation

As indicated in section 5.4, composite specimens can be prepared in the lab using SGC. Conventional tack coat or Novabond tack may be applied to the base material before compacting open-graded material on the top of it. After compaction, compacted specimens were sliced to the desired thickness; cut to the desired geometry; a semi-circular groove will be introduced to induce sufficient stress concentration along the surface (OGFC side); composite specimen edge surfaces will be sanded and then glued with the load heads.

5.5.1 Compaction and Application of Conventional Tack Coat or Novabond Tack

The following procedures were followed:

- Compact dense-graded mixture using SGC to desired air voids. Dense-graded mixture was designed according to Superpave^{TM} volumetric mix design method.
- Slice compacted dense-graded mixture specimen into two halves or slice appropriate thickness off on one side based on the desired dense-graded mixture thickness to be used in the composite specimen.
- Apply conventional tack coat or Novabond tack to the cut side of the dense-graded mixture. The amount of binder or emulsion should correspond to the anticipated field application rate. As example with conventional tack (at 0.045 gal/yd^2) apply 1.98 grams to 150mm diameter specimen. For Novabond tack (at 0.30 gal/yd^2, this upper bound application rate was applied to maximize the ability to see effects of Novabond at this developmental stage. Additional work is needed to evaluate the effect at appropriate Novabond application rate.) apply 15.2 grams to a 150 mm diameter specimen (Appendix E). For a hot binder tack material, preheat the silicone rubber mold in a 135°C (275°F) oven for 7±2 minutes. Pour the hot binder

into the appropriate size silicone rubber mold (Figure 5-7) based on the specimen size to be prepared; here 150mm diameter silicone rubber mold was used in this study. Place the silicone rubber mold on a level shelf in the 135°C (275°F) oven for 10±2 minutes to allow the binder to self level. Remove the mold from the oven, place on a level surface and allow the mold to cool to room temperature. For an emulsion tack material, pour the emulsion into the appropriate size room temperature silicone rubber mold. Place the mold on a level shelf in a 60°C (140°F) oven and allow the emulsion to cure to a constant weight. Remove the mold from the oven, place on a level surface and allow the mold to cool to room temperature.

Figure 5-7 Silicone Rubber Mold on Level Shelf

- With the silicone rubber mold sitting on a level surface, place compacted dense-graded mixture in the silicone rubber mold. Allow the weight of the specimen to remain on the silicone rubber mold for at least 5 minutes. Transfer the compacted

specimen with the silicone rubber mold to a freezer. Remove the compacted specimen with the attached mold after at least 15 minutes in the freezer. Invert the specimen to where the silicone rubber mold is on top the specimen. Slowly remove the mold from the dense-graded mixture surface. Allow the specimen to warm to room temperature while sitting undisturbed. The dense-graded base materials with applied tack coat and novabond are shown in Figure 5-8.

- Heat SGC compaction mold and top mold plate in the oven at the required compaction temperature for at least 30 minutes prior to compaction.
- Push the SGC compaction mold along the edge surface of the compacted room temperature specimen sitting on a level surface after removing the ring holding rotating base from falling off the compaction mold. Place a room temperature base plate and a paper disk underneath the compacted dense-graded mixture in the compaction mold.
- Place desired weight of open-graded mixture into the compaction mold on top of the base material. A paper disk was placed on top of the mixture followed by the top mold plate. Compaction mold was loaded and the compaction was initiated. The amount of open-graded mixture was calculated based on the relationship among mixture maximum specific gravity, air void content, and desired height of open-graded mixture in the composite specimen after compaction. This calculation is illustrated in Appendix G.
- After compaction, remove the mold from the gyratory compactor. Extrude the compacted composite specimen from the mold after an appropriate cooling period. Compacted specimen is shown in Figure 5-9.

Figure 5-8 Dense-graded Specimens with Applied Tack Coat (left) and Novabond (right)

Figure 5-9 Newly Compacted Composite Specimen

5.5.2 Slicing, Straight Cutting and Grooving of Composite Specimen

The following procedures were followed:

- Slice the top and bottom of the compacted composite specimen to obtain the desired thickness for both open-graded and dense-graded mixtures. The diamond saw used for slicing is shown in Figure 5-10. The sliced composite specimen is shown in Figure 5.11. The option of slicing on OGFC side depends on testing purposes.

Figure 5-10 Diamond Saw Used for Specimen Slicing

Figure 5-11 Sliced Composite Specimen

- Cut the sliced specimen to desired width (3.5”). The diamond saw used for straight cutting is shown in Figure 5-12. The straight cut composite specimen is shown in Figure 5-13.
- Two straight cut specimens were held together by a clamp to core through both OGFC surfaces and obtain one semicircular groove on each specimen. The coring setup is shown in Figure 5-14. The composite specimen with groove is shown in Figure 5-15.

Figure 5-12 Diamond Saw Used for Composite Specimen Straight Cutting

Figure 5-13 Straight Cut Composite Specimen

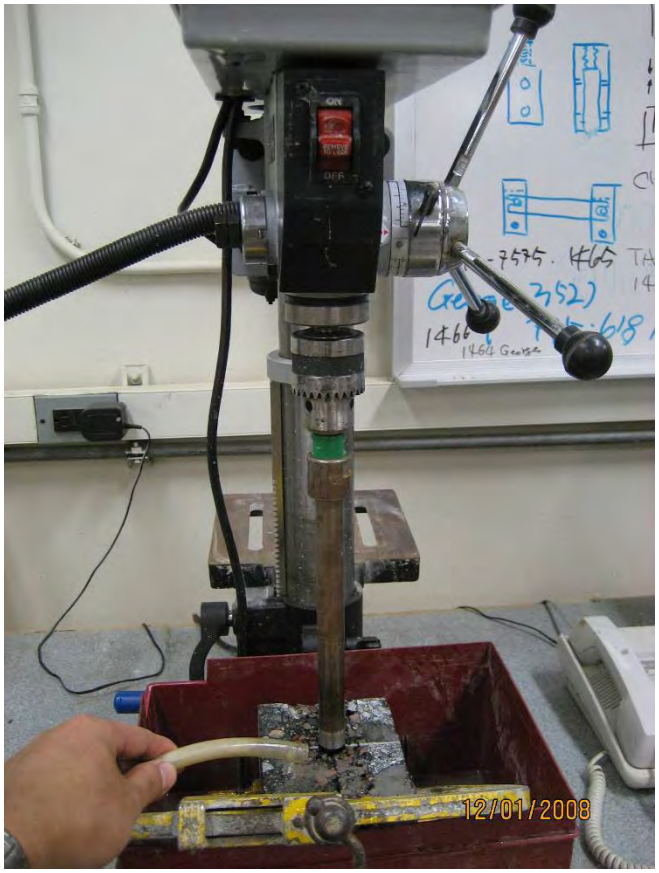

Figure 5-14 Composite Specimen Stress Concentrator Drilling Setup

Figure 5-15 Grooved Composite Specimen

5.5.3 Sanding, Gluing, and Gage Points Attachment of Composite Specimen

The following procedure was followed:

- In order to make sure the loading head and specimen edge surface have solid contact, loose material (i.e. mastic) has to be sanded off until aggregates are fully exposed. The spindle sander and sanded specimen are shown in Figure 5-16.

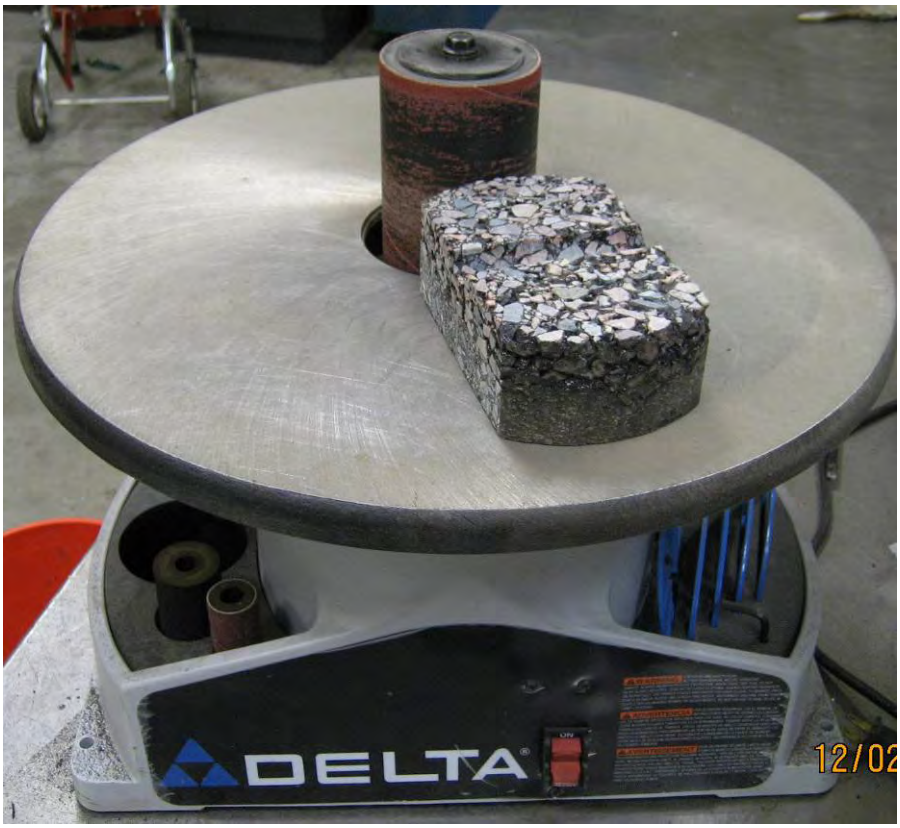

Figure 5-16 Spindle Sander and Sanded Specimen

- Four brass gage points (5/16-inch diameter by 1/8-inch thick) were affixed with epoxy to each side of the specimen. The locations of the gage points are shown in Figure 5-17.

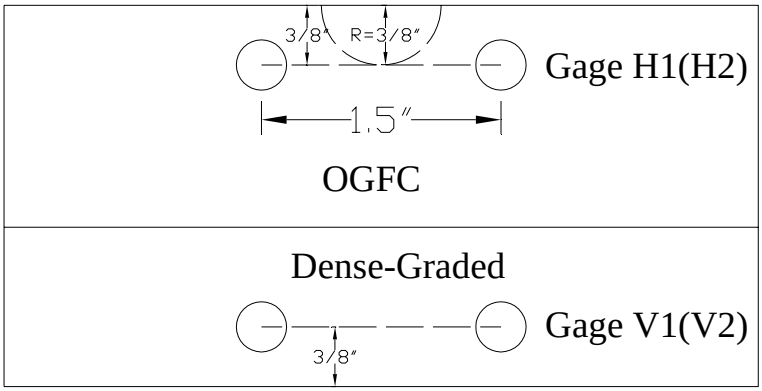

Figure 5-17 Strain Gage Distributions on the Specimen

- Both the loading head inner surfaces and specimen end surfaces need to be uniformly coated with epoxy and the voids on the end surfaces need to be filled with epoxy before joining them together. The epoxy used was LOCTITE® Hysol® Product E-20HP epoxy. It takes about 6 hours for this epoxy to get about 90% of its full strength on aluminum at 25°C. The loading heads and epoxy used are shown in Figure 5-18.

Figure 5-18 Loading Head and Epoxy Used

5.6 Constant Stroke Rate Strength Tests on Asymmetrical Composite Specimens

Since constant stroke rate strength test was used to determine strength and fracture energy in single mixture specimens, the loading rate applied in DBDT for single dense-graded mixture, 25mm/minute, and 2.5mm/minute and 0.25 mm/minute, were selected for testing. Composite specimen is sketched in Figure 5-19.

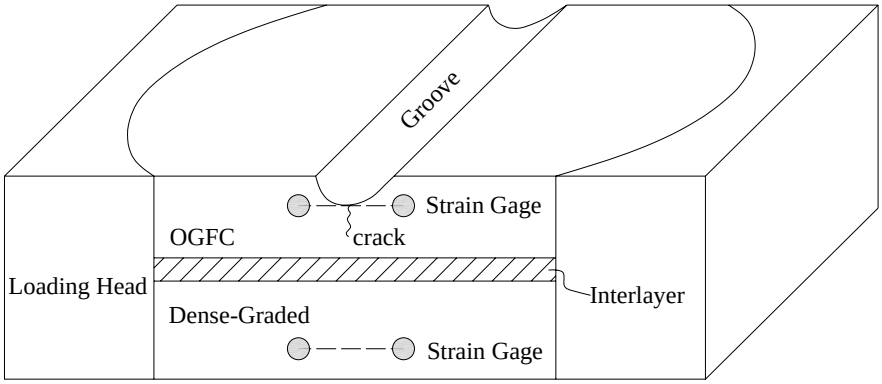

Figure 5-19 Composite Specimen Sketch

5.6.1 Materials

The dense-graded mixture used for composite specimen is the same as that used for evaluation of the effect of OGFC compaction on the integrity of the dense-graded mixture in section 5.4.1. Oolitic limestone FC-5 (open-graded friction courses) was used for top layer of the composite specimen. Its aggregate gradation is shown in Table 5-4. The asphalt binder used for oolitic limestone FC-5 is ARB-12; namely, PG67-22 with 12% ground tire rubber and 0.4% mineral fiber by weight of the mixture.

Table 5-4 Oolitic Limestone FC-5 Mixture Aggregate Gradation

		Percent Passing				
Blend		44.7%	49.4%	3.2%	2.7%	100%
Number		1	2	3	4	JMF
Sieve Size	3/4"	100	100	100	100	100
	1/2"	79	100	100	100	91
	3/8"	36	92	100	100	67
	# 4	7	26	100	100	22
	# 8	3	7	68	100	10
	# 16	3	3	67	100	8
	# 30	3	3	55	100	7
	# 50	3	2	35	100	6
	# 100	2	2	14	100	5
	# 200	1	1	3	100	4

The compacted composite specimen consisted of 1” dense-graded mixture and 1 3/8” open-graded mixture with 15% air voids. The open-graded mixture has natural compacted surfaces without slicing. The amount of each component of open-graded mixture needed was 78.4grams of ARB-12 and 1147.0grams of aggregate with 6.4% binder content. For initial testing to evaluate the effectiveness of this specimen geometry, neither conventional tack coat nor Novabond tack was introduced to the interface between open-graded mixture and dense-graded mixture.

5.6.2 Constant Stroke Rate Strength Test at 25mm/minute

While the ¾ inch diameter diamond-tip coring bit was being made, an attempt was made to cut a groove using a diamond saw as shown in Figure 5-20. Five cuts were made to form the groove. The resulting specimen is shown in Figure 5-21 and the test setup is shown in Figure 5-22.

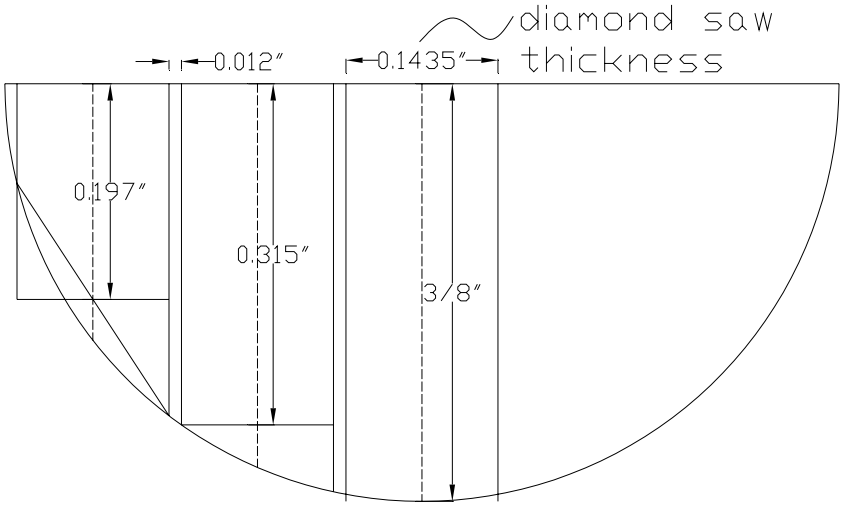

Figure 5-20 Geometry of the Five Cuts to Form the Groove

Figure 5-21 Prepared Composite Specimen with Diamond Saw Cut Groove

Figure 5-22 Test Prototype for Specimen with Diamond Saw Cut Groove

Test results of 3 composite specimens prepared as described above showed that the newly introduced groove successfully concentrated the stress in middle of the specimen on the OGFC side. This indicated that the diamond-tip saw approach can be used to form an effective groove when a diamond-tip coring bit is not available. The cracks in the specimen are shown in Figure 5-23.

Typical displacements at a loading rate of 25mm/minute are shown in Figures 5-24 and 5.25.

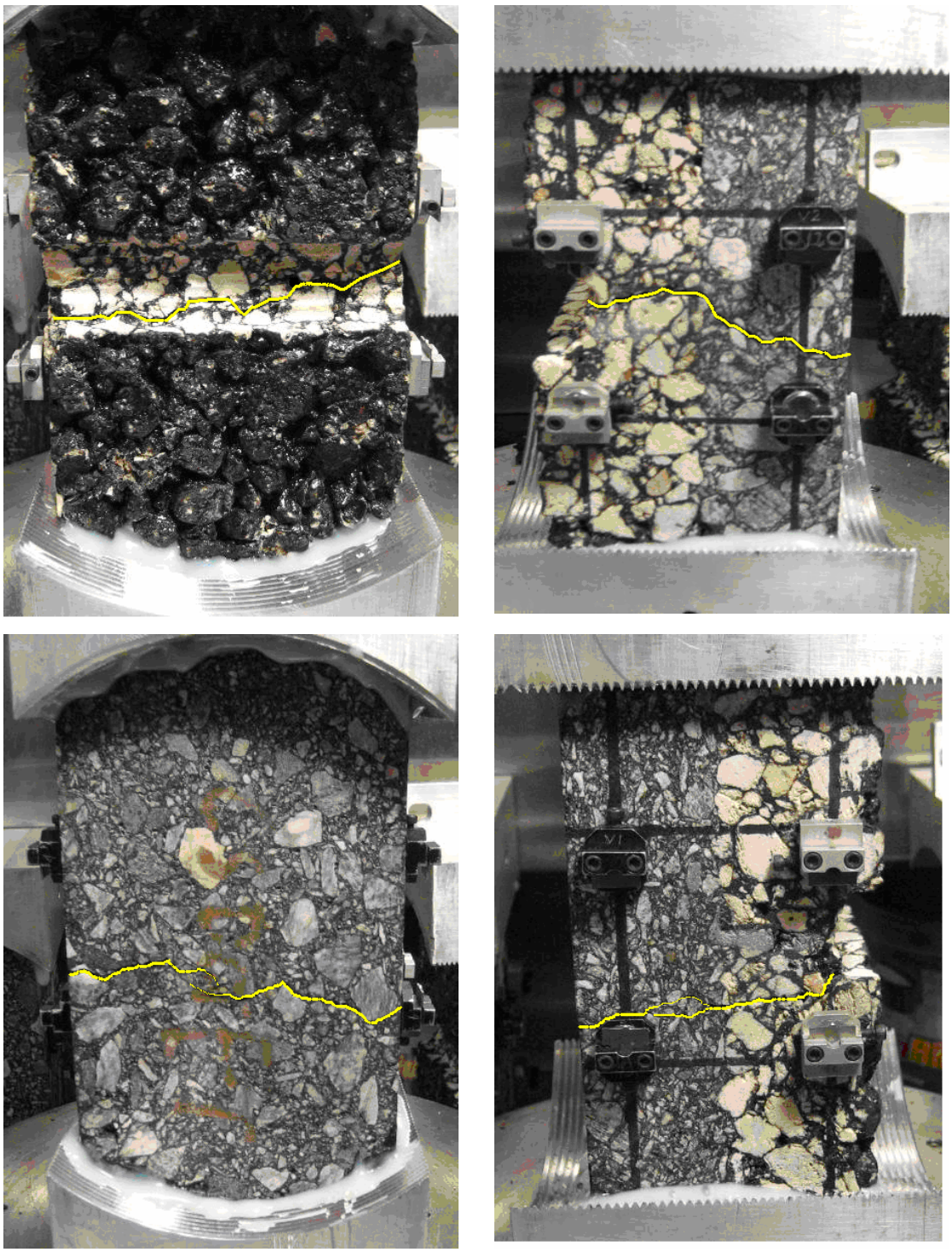

Figure 5-23 Cracks in the Specimen at Loading Rate of 25mm/minute

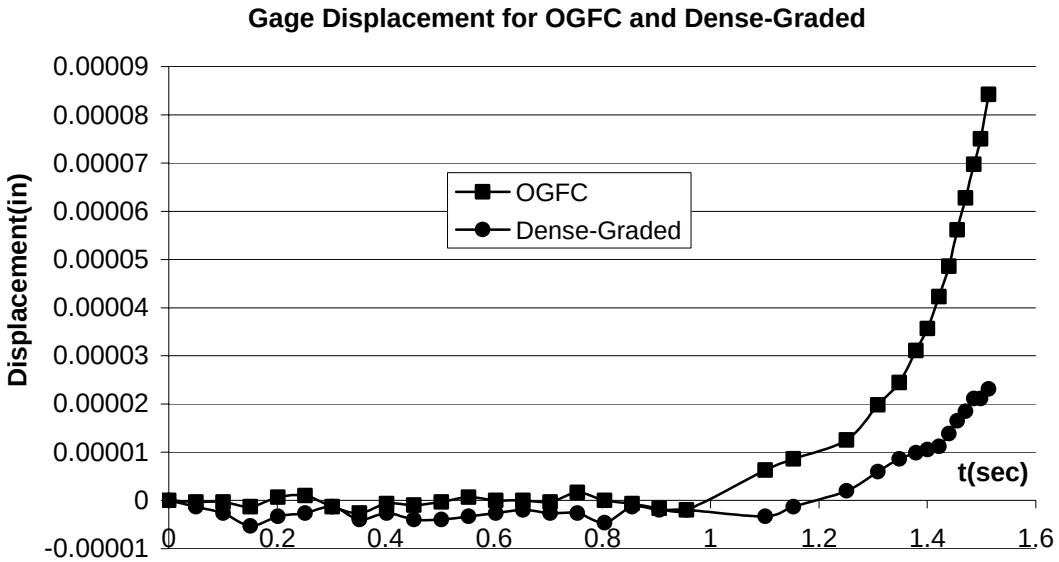

Figure 5-24 Strain Gages Displacement at Loading Rate of 25mm/minute

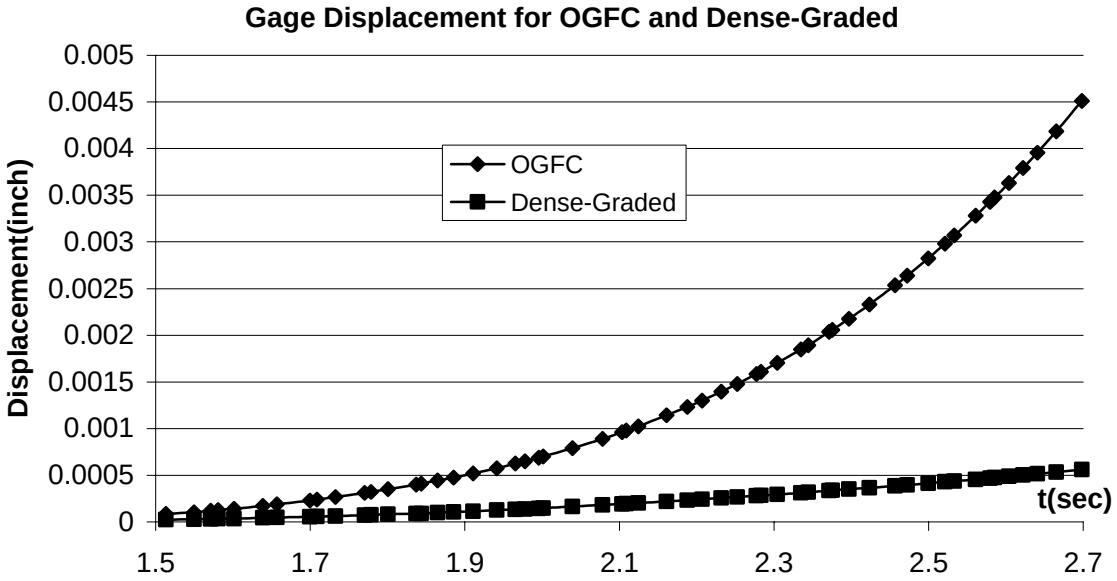

Figure 5-25 Strain Gages Displacement at Loading Rate of 25mm/minute

The strain gage displacement Figures did show that specimens start to crack from the open-graded mixture side and propagate all the way through to the dense-graded side. All tests

were completed in 4 seconds. Unfortunately, these results indicated that it is almost impossible to identify the instant of crack initiation. This constant stroke rate 25mm/minute was determined to be too fast for testing.

5.6.3 Constant Stroke Rate Strength Test at 2.5mm/minute and 0.25mm/minute

Since loading rate at 25mm/minutes was determined to be too fast, and diamond-tip coring bit was successfully secured, loading rates were reduced to 2.5mm/minute and 0.25mm/minute on specimens with ¾" diameter semi-circular groove. Tests performed on three specimens at a loading rate of 2.5mm/min showed that all composite specimens broke from the open-graded mixture side; but 2 of them broke near the ends, and one of them broke at the center. The cracks in composite specimen are shown in Figure 5-26.

Typical displacements at loading rate of 2.5mm/minute are shown in Figures 5-27 and 5-28.

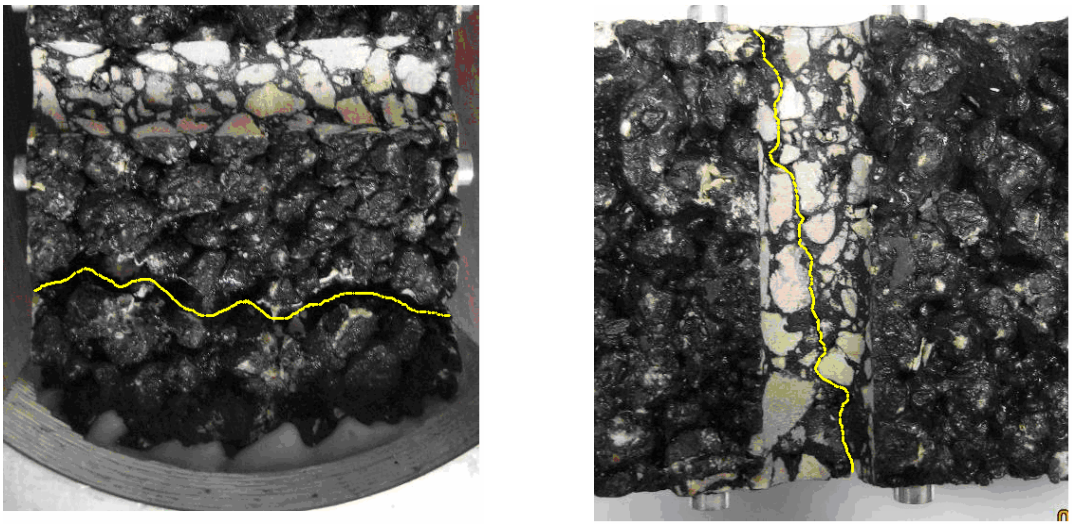

Cracks near the End Cracks at the Center

Figure 5-26 Cracks in the Specimen at Loading Rate of 2.5mm/minute

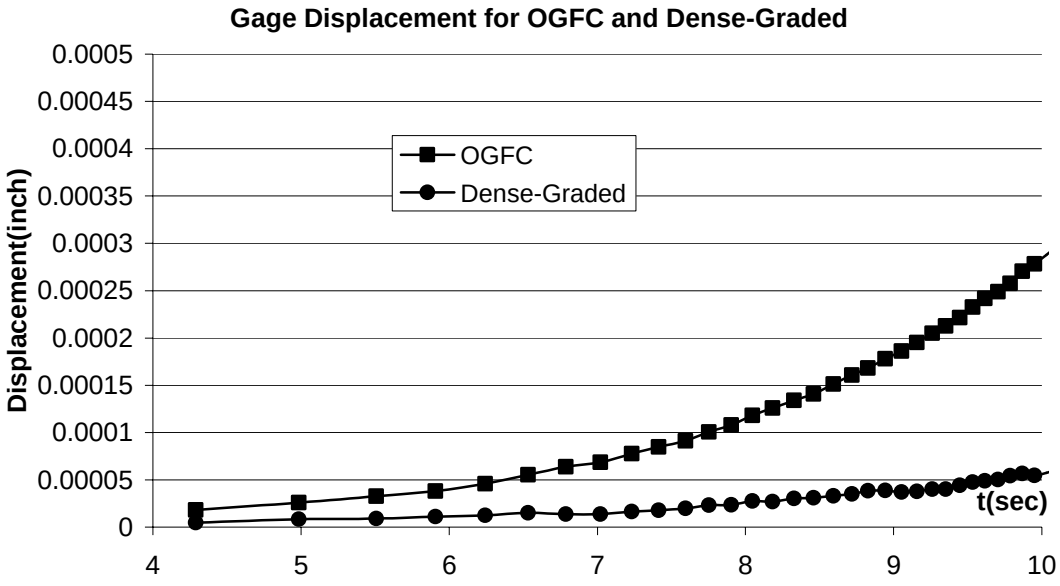

Figure 5-27 Strain Gages Displacement at loading rate 2.5mm/minute-broke near the end

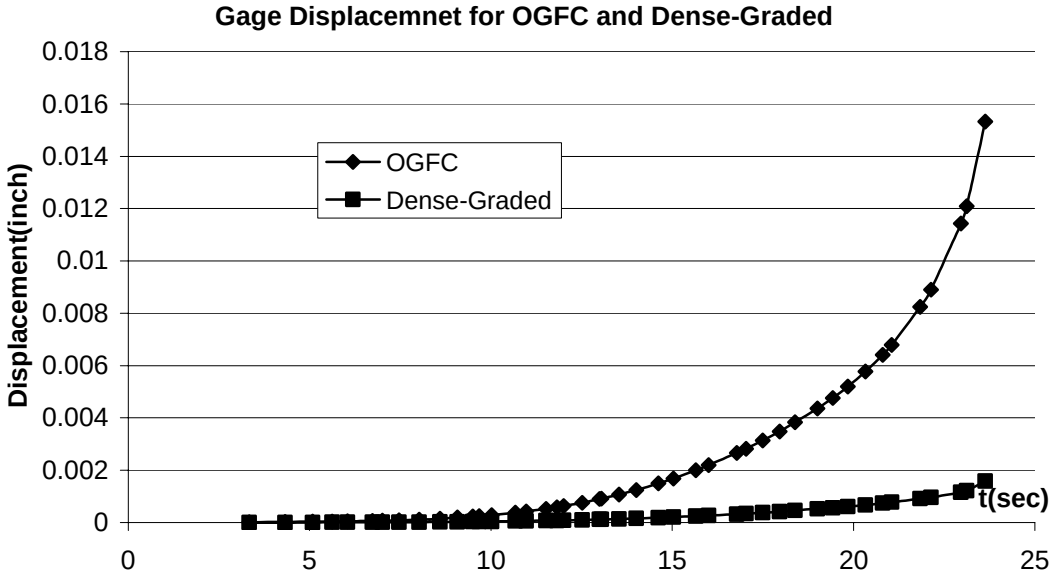

Figure 5-28 Strain Gages Displacement at loading rate 2.5mm/minute-broke at the center

These two Figures clearly indicated that composite specimens broke from the open-graded mixture side. The reason that it took around 2 times longer for the specimen that broke at the center to fail than the specimen that broke near the ends to fail is that the rough surface of open-graded mixture forms natural stress concentrators; these natural stress concentrators work much more effectively than the cored groove stress concentrators.

Loading rates were further reduced to 0.25mm/minute on specimens with cored groove. Test results showed that all composite specimens broke from the dense-graded mixture side. The cracks in composite specimen are shown in Figure 5-29. Typical displacements at loading rate 0.25mm/minute are shown in Figure 5-30.

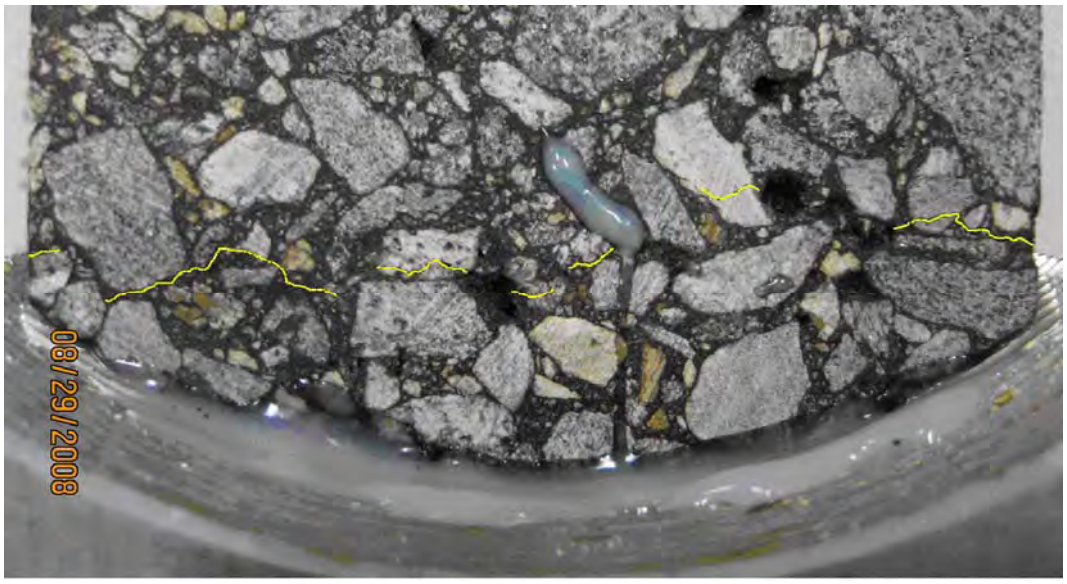

Figure 5-29 Cracks in the specimen at Loading Rate of 0.25mm/minute

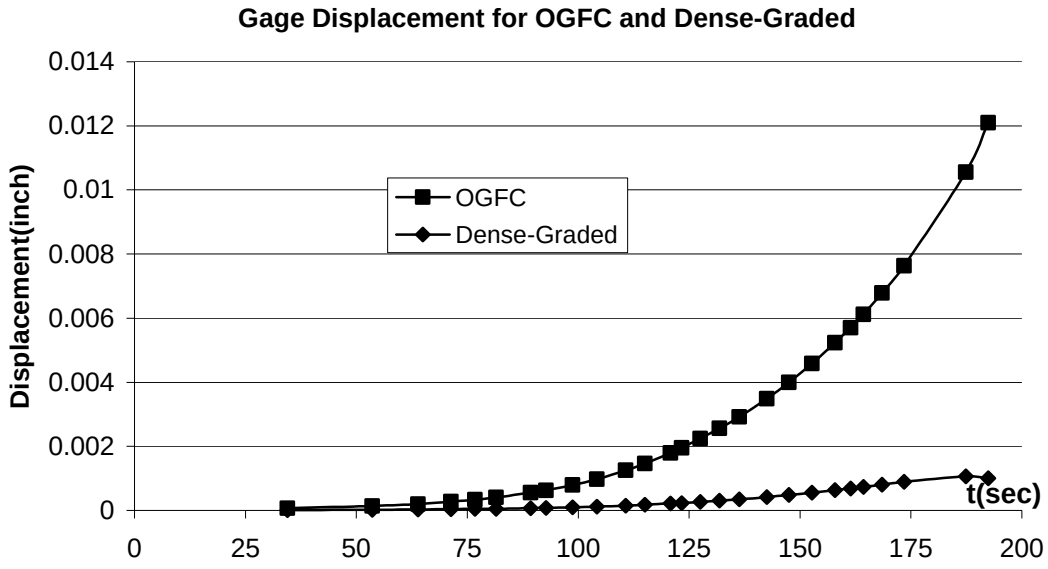

Figure 5-30 Strain Gages Displacement at Loading Rate of 0.25mm/minute

The reason that the specimens broke at the dense-graded side instead of the open-graded side is that at this slow loading rate, the stiffer, lower compliance dense-graded mixtures attract more stress and relax less stress during testing, while the lower stiffness and higher strain tolerance of open-graded mixtures have higher capacity to release part of the input energy used to damage the material. Also, the open-graded structure has higher strain resistance and at this low loading rate, the composite specimens are failed when the strain limit of dense-graded mixture is reached.

5.6.4 Conclusion for Asymmetric Constant Rate of Displacement Tests

Tests performed on composite specimens at the loading rate of 25mm/min, 2.5mm/min, and 0.25mm/min show that this constant stroke rate strength test is not a good choice for interface evaluation because either the testing time is too short to identify the crack initiation point or composite specimen broke from the dense-graded mixture side even though stress concentrators are introduced on open-graded mixture side.

5.7 Repeated Loading Test on Asymmetrical Composite Specimens

Based on the results presented above, it seems clear that a simple constant stroke rate strength test, which is appropriate to determine strength and fracture energy in single mixture specimens, is not suitable for composite specimens. Therefore, repeated loading tests on asymmetrical composite specimen were performed.

5.7.1 Repeated Loading Test on Asymmetrical Composite Specimen with 1" Dense-graded Mixture Layer

5.7.1.1 Materials

The dense-graded mixture used for composite specimen is the same as that used for evaluation of the effect of OGFC compaction on the integrity of the dense-graded mixture in section 5.4.1. The open-graded mixture used for the top layer was the same as that used in section 5.6.1. The composite specimen configuration is the same as that in section 5.6.1 except that a ¾" diameter semi-circular groove was used instead of diamond saw cut groove. Neither conventional tack coat nor Novabond tack was introduced to the interface between open-graded mixture and dense-graded mixture.

5.7.1.2 Analysis of Results

Repeated loading approach, a constant repeated haversine load of one-tenth of a second and then resting for nine-tenth of a second, was attempted using a 1200·lb peak load. Initial trials showed the composite specimen broke near the loading head instead of through the groove (Figure 5-31). The failure occurred near the loading head partly because of end effects, and partly because of less compaction density than at the center and a lot of small holes (air voids) on

the rough open-graded mixture surface forming natural stress concentrators. It appears that these natural stress concentrators may be more effective than the drilled groove to initiate cracks. Figures 5-32 and 5-33 show the comparison between newly compacted open-graded mixture surfaces and cut surfaces.

Since composite specimens tend to fail near the loading head because the higher air voids on open-graded mixture surface form natural stress concentrators, which might concentrate more stress than the groove, slicing off the natural surface to have a more uniform surface like in Figure 5-33 was attempted. Tests on composite specimen with top 3/8-inch sliced off show that specimens broke through the bottom of the groove right at the center. Failed specimen is shown in Figure 5-34.

Figure 5-31 Composite Specimen Broke Near the End

Figure 5-32 Compacted Open-Graded Mixture Surface Without Slicing

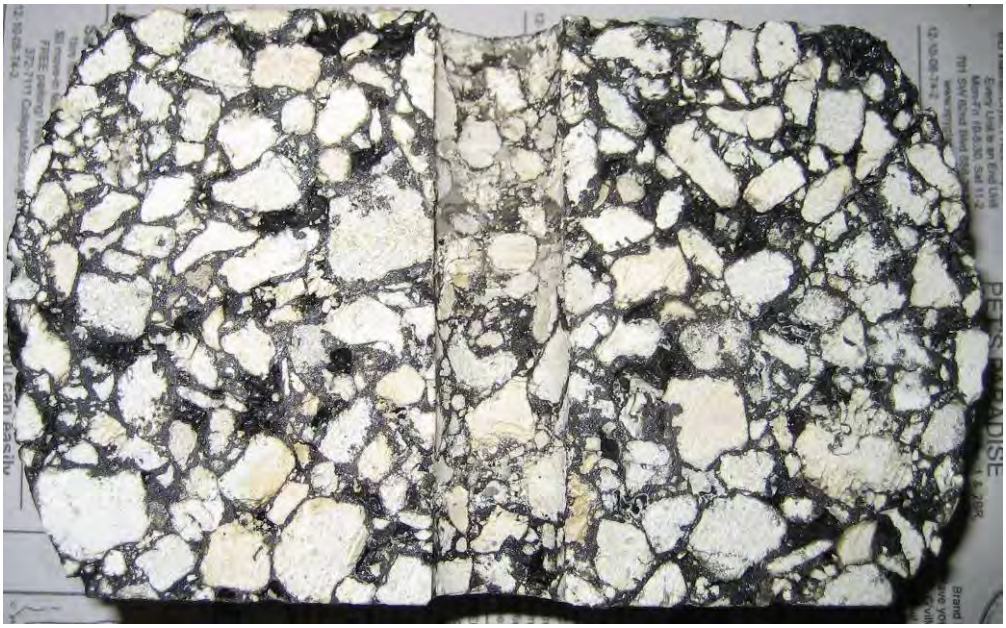
Figure 5-33 Compacted Open-Graded Mixture Surface After Slicing

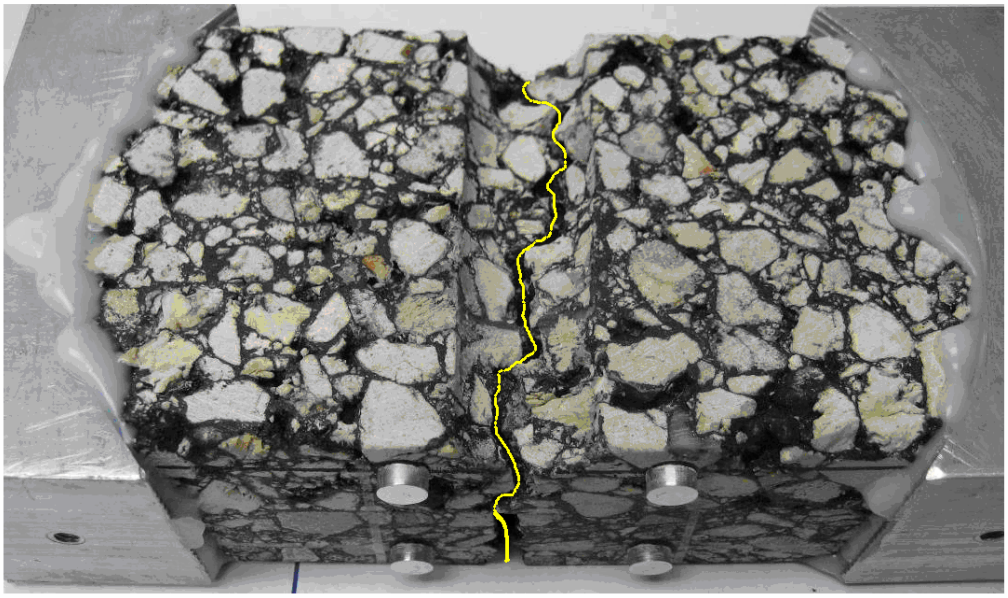

Figure 5-34 Composite Specimen with Top 3/8 inch Surface Sliced off

Typical total recoverable deformations for OGFC and Dense-Graded mixture are shown in Figure 5-35; total or instantaneous recoverable deformation from repeated loading test is a measure of resilient modulus and increase in recoverable deformation is a measure of damage induced in the specimen.

During this repeated loading process, damage started to accumulate in open-graded mixture right after loading; but little or no damage was induced in dense-graded mixture until cracks prorogated into it. This damage feature can be used to evaluate the effect of different types of interface materials, like tack coat and novabond. For specimens with same geometry and external load but with different interface materials, differences in the number of loading cycles to failure are a direct indication of the effectiveness of the interface conditions to resist crack propagation.

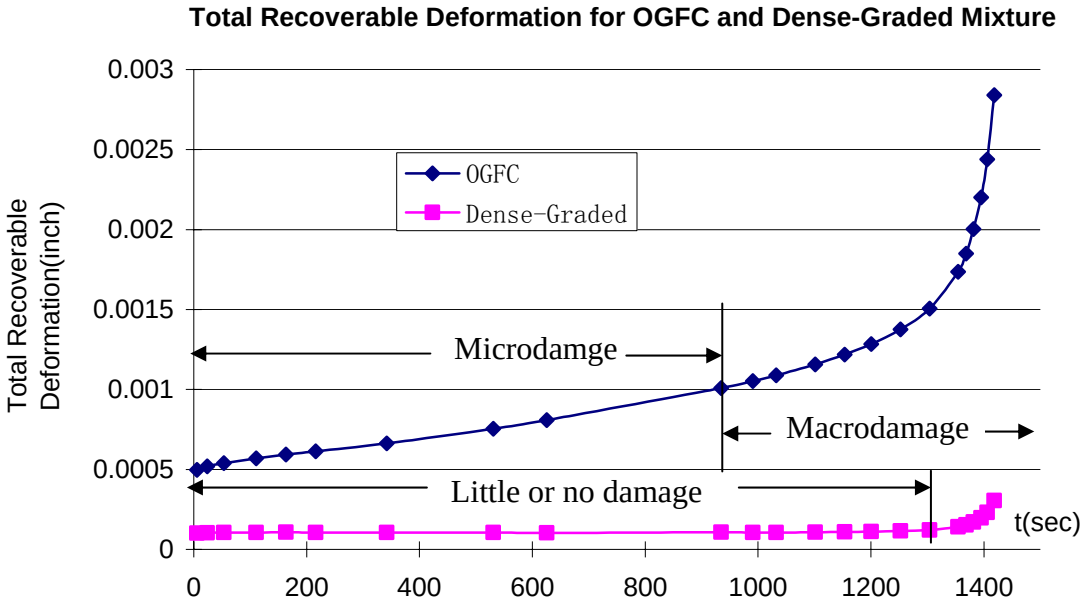

Figure 5-35 Total Recoverable Deformation for OGFC and Dense-Graded Mixture

5.7.2 Repeated Loading Test on Asymmetrical Composite Specimen with 3" Dense-graded Mixture Layer

The success of composite specimen with ¾ inch diameter semi-circular groove introduced on OGFC surface under repeated loading make it possible to evaluate the effect of interface layer on stress redistribution in OGFC and dense-graded layer along the interface and on cracking retardation from OGFC layer into dense-graded layer. Considering the fracture process involves crack initiation, stable crack propagation and unstable crack propagation, dense-graded mixture thickness in composite specimen was increased to 3 inches from the original 1 inch to make sure that the cracking is still in stable crack propagation period in order to evaluate the effect of interlayer; otherwise the effect of interlayer may be masked by the unstable crack propagation period. In order to identify the crack tip once the crack propagates from the OGFC through the

interlayer to the dense-graded mixture, strain gages in dense-graded mixture were moved to near the interface as shown in Figure 5-36.

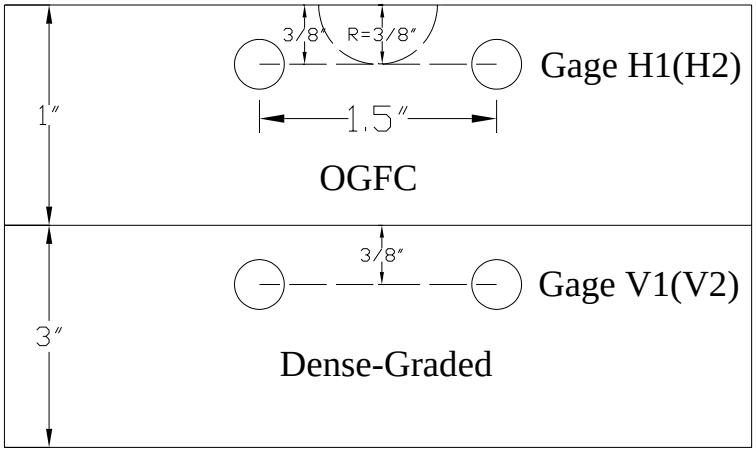

Figure 5-36 Strain Gage Distributions on Specimen with 3” Dense-Graded Mixture Layer

5.7.2.1 Materials

The dense-graded mixture used for composite specimen was the same as that used for evaluation of the effect of OGFC compaction on the integrity of the dense-graded mixture in section 5.4.1. The open-graded mixture used for the top layer was the same as that used in section 5.6.1. The composite specimen configuration was the same as that in section 5.7.1 except that dense-graded mixture thickness was increased to 3”. Conventional tack coat and Novabond tack were applied on dense-graded specimen surface at an application rate of 0.045gal/yd^2 and 0.3gal/yd^2, respectively (Appendix E). These two application rates were selected as two extreme cases to evaluate the effect of this interlayer.

5.7.2.2 Analysis of Results

Since the composite specimen thickness was increased up to 4 inches, external load was increased up to 2850lbs (from 1200lbs for 2 inches thick specimen) to reduce the number of

loading cycles to fail the specimens. Typical total recoverable deformations for OGFC and Dense-Graded mixture are shown in Figure 5-37 and 5-38 for conventional tack coat and Novabond tack interlayer, respectively.

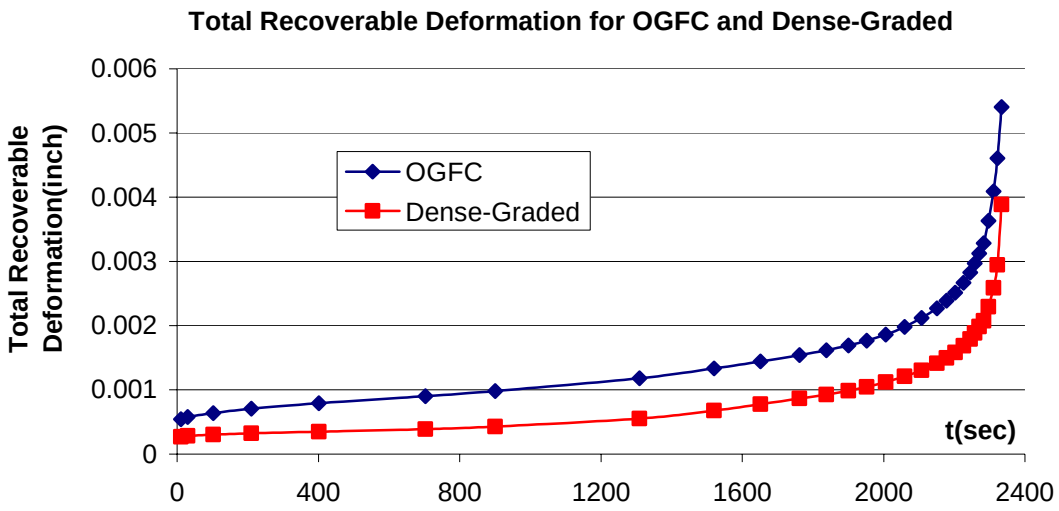

Figure 5-37 Total Recoverable Deformation for OGFC and Dense-Graded Mixture with Conventional Tack Coat Interlayer (3" dense-graded mixture layer)

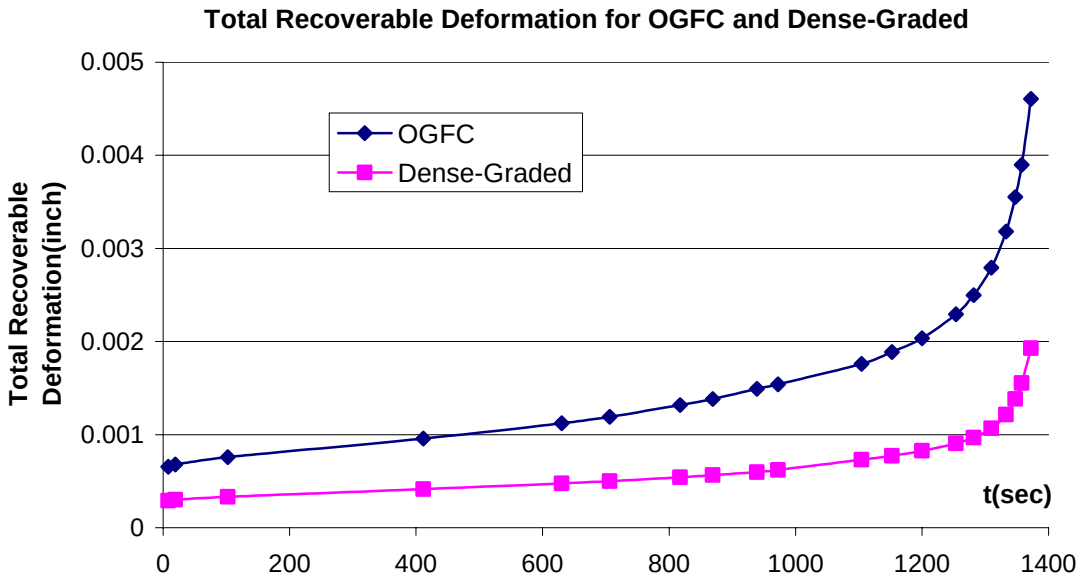

Figure 5-38 Total Recoverable Deformation for OGFC and Dense-Graded Mixture with Novabond Tack Interlayer (3" dense-graded mixture layer)

Both figures 5-37 and 5-38 indicate that damage was accumulating in dense-graded mixture even though the damage rate is lower than that in OGFC for thick specimens; the reason is that 3 inches thick dense-graded mixture is carrying a larger portion of the external load than the 1 inch thick dense-graded mixture composite specimen. It took more loading cycles for specimen with the conventional tack coat interlayer than specimen with Novabond tack interlayer to fail; actually, specimens with Novabond tack interlayer were expected to fail after much more loading cycles than specimens with the conventional tack coat interlayer. The idea of increasing dense-graded mixture thickness to keep interlayer in stable crack propagation region was proved to be inappropriate because OGFC and dense-graded are accumulating damage at the same time; thus, premature failure in the underlying HMA layer can be addressed by introducing a more effective stress concentrator, like a rectangular groove, to concentrate higher stress in OGFC so that dense-graded damage is caused by crack propagation rather than external load during the loading process.

5.7.3 Repeated Loading Test on Asymmetrical Composite Specimen with Rectangular Groove

Rectangular groove was introduced on OGFC surface in composite specimen with dense-graded mixture thickness reduced back to 1 inch, Figure 5-39. The groove is 3/8 inch deep and 5 diamond saw cuts wide along the external load pulling direction.

5.7.3.1 Materials

The dense-graded mix used for composite specimen was the same as that used for evaluation of the effect of OGFC compaction on the integrity of the dense-graded mixture in section 5.4.1. Nova Scotia-granite FC-5 (open-graded friction courses) instead of oolitic

limestone FC-5 was used for top layer of the composite specimen. Its aggregate gradation is shown in Table 5-5.

Figure 5-39 Composite Specimen with Rectangular Groove

Table 5-5 Nova Scotia-granite FC-5 Mixture Aggregate Gradation

		Percent Passing				
Blend		77%	12%	10%	1%	100%
Number		1	2	3	4	JMF
Sieve Size	3/4"	100	100	100	100	100.0
	1/2"	95	100	100	100	96.2
	3/8"	64	92	100	100	75.0
	# 4	11	20	97	100	21.6
	# 8	3	5	68	100	10.7
	# 16	2	3	43	100	7.2
	# 30	2	3	28	100	5.7
	# 50	2	3	18	100	5.0
	# 100	2	3	11	100	4.0
	# 200	1.1	2.5	8.0	100	3.1

The asphalt binder used in the FC-5 is ARB-12. The compacted composite specimen consisted of 1” dense-graded mixture and 1 3/8” open-graded mixture with 20% air voids. The top 3/8” OGFC was sliced off. The amount of each component of open-graded mixture needed was 83.8grams of ARB-12 and 1313.2grams of aggregate with 6.0% binder content. Conventional tack coat and Novabond tack were applied on dense-graded specimen surface at an

application rate of 0.045gal/yd^2 and 0.3gal/yd^2, respectively (Appendix E). These two application rates were selected as two extreme cases to evaluate the effect of interlayer.

5.7.3.2 Analysis of Results

Tests on 4 samples of composite specimen with the conventional tack coat interlayer and 3 samples of composite specimen with Novabond tack interlayer were performed. Because of the rectangular groove was used, external load was reduced to 720lbs. Tests results are shown in Figures 5-40 through 5-43. Samples are denoted as: CST1, CST2, CST3, CST4, CSN1, CSN2, CSN3, with letters CS denoting composite specimen, the letter T denoting conventional tack coat interlayer, and N denoting Novabond tack interlayer.

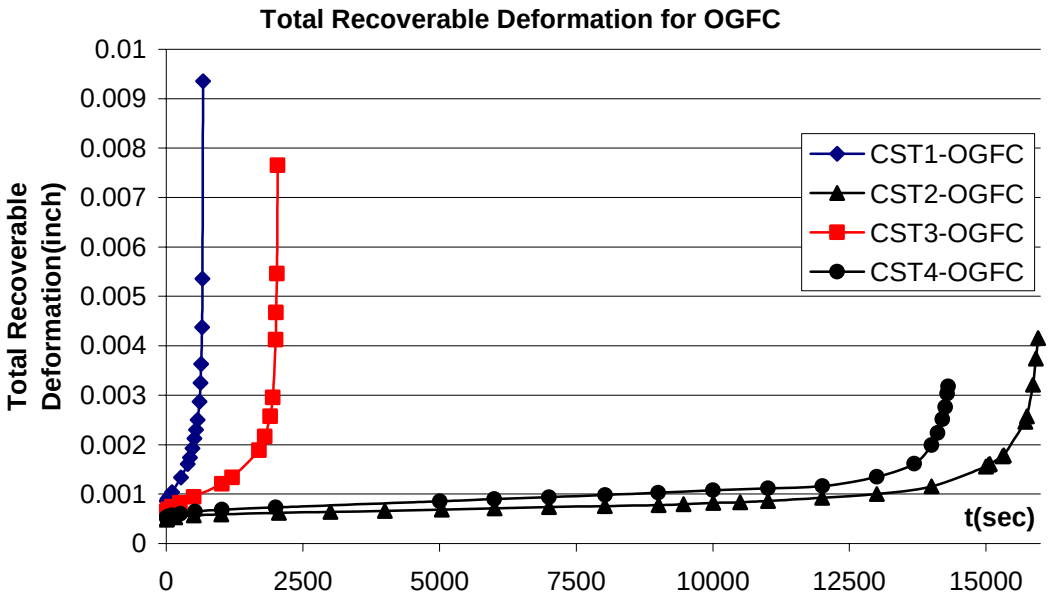

Figure 5-40 Total Recoverable Deformation for OGFC with Conventional Tack Coat Interlayer (Rectangular Groove)

Figures 5-40 to 5-43 indicate huge variation from sample to sample for both composite specimens with conventional tack coat interlayer and Novabond tack interlayer. Specimen CST1

and CST3 failed shortly after loading; but specimen CST2 and CST4 failed by slowly accumulated damage.

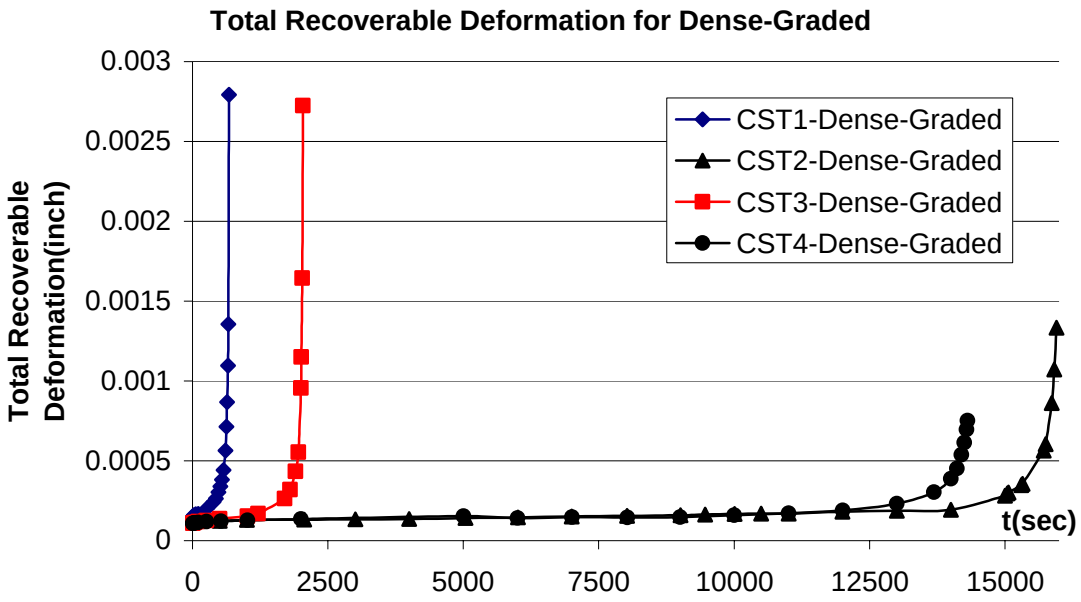

Figure 5-41 Total Recoverable Deformation for Dense-Graded with Conventional Tack Coat Interlayer (Rectangular Groove)

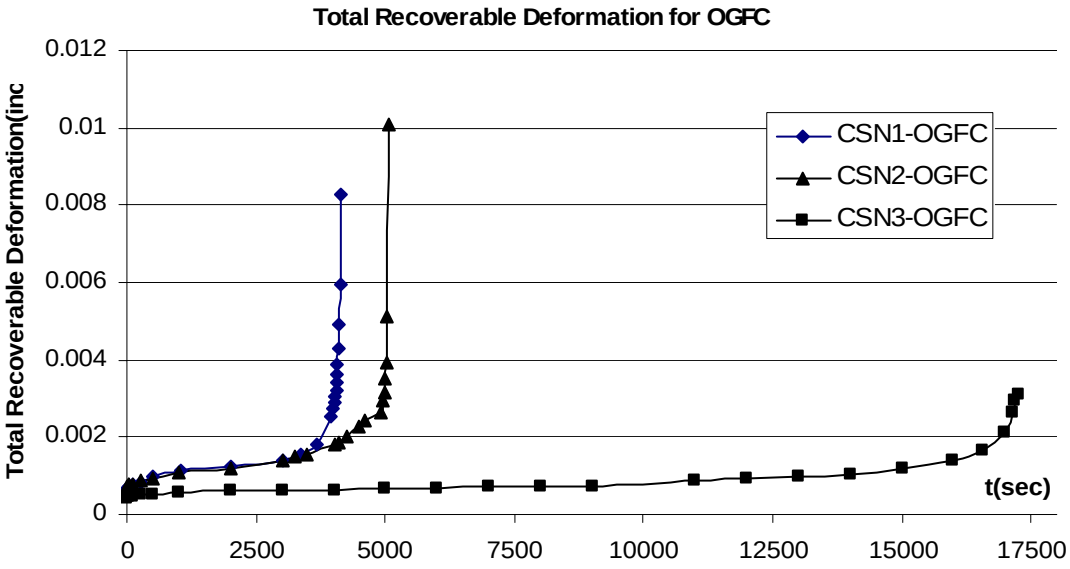

Figure 5-42 Total Recoverable Deformation for OGFC with Novabond Tack Interlayer (Rectangular Groove)

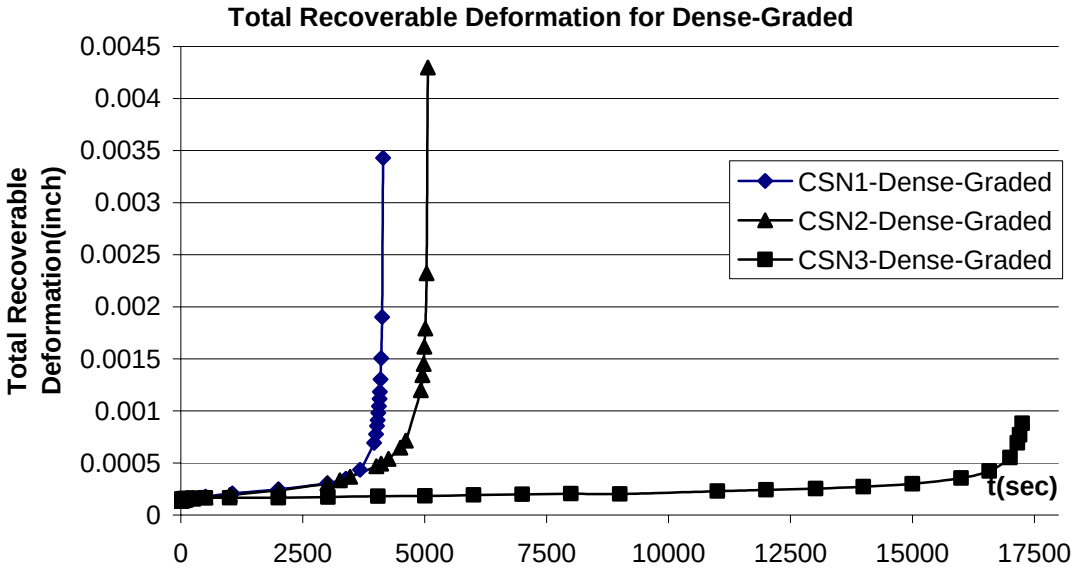

Figure 5-43 Total Recoverable Deformation for Dense-Graded with Novabond Tack Interlayer (Rectangular Groove)

It took relatively the same time for CST2, and CST4 and CN3 to fail; this indicates that the effect of Novabond interlayer was cancelled somehow. This huge variation was determined to be caused by the bending of composite specimen. Accordingly, it was found that it is impossible to pull on an asymmetric composite specimen without at the same time bending and or twisting the composite specimen (Jones, 1980).

5.8 Repeated Loading Test on Symmetrical Composite Specimen

Since large variation from specimen to specimen was determined to be caused by the bending of single asymmetrical composite specimen, a symmetrical composite specimen configuration was adopted to minimize the bending induced during the pulling of single asymmetrical composite specimen .

5.8.1 Materials and Testing Method

The dense-graded used for composite specimen was the same as that used for evaluation of the effect of OGFC compaction on the integrity of the dense-graded mixture in section 5.4.1. Nova Scotia-granite FC-5 (open-graded friction courses) was used for top layer of the composite specimen. The asphalt binder used in the FC-5 is ARB-12. The compacted composite specimen consisted of 1" dense-graded mixture and 1" open-graded mixture with 23% air voids. The natural voids on compacted OGFC surface were used as stress concentrators to initiate crack. The amount of each component of open-graded mixture needed was 50.6grams of ARB-12 and 792.3grams of aggregate with 6.0% binder content. Conventional tack coat and Novabond tack were applied on dense-graded specimen surface at an application rate of 0.045gal/yd^2 and 0.3gal/yd^2, respectively (Appendix E).

In order to mitigate bending induced during pulling on single composite specimen, two single composite specimens were bonded together with one spacer throughout the whole interface except 1 inch wide at the center as in Figure 5-44. Both sides of the spacers were fully bonded to the OGFC surfaces.

Figure 5-44 Symmetrical Composite Specimen

This 1 inch open space will create a gap between two single composite specimens and functions as a stress concentrator. The horizontal strain gage is mounted on each interface center; the vertical strain gage is mounted on each dense-graded mixture surface center.

Fiber glass and cardboard were both tried as spacers. The cracking surfaces are presented in Figure 5-45.

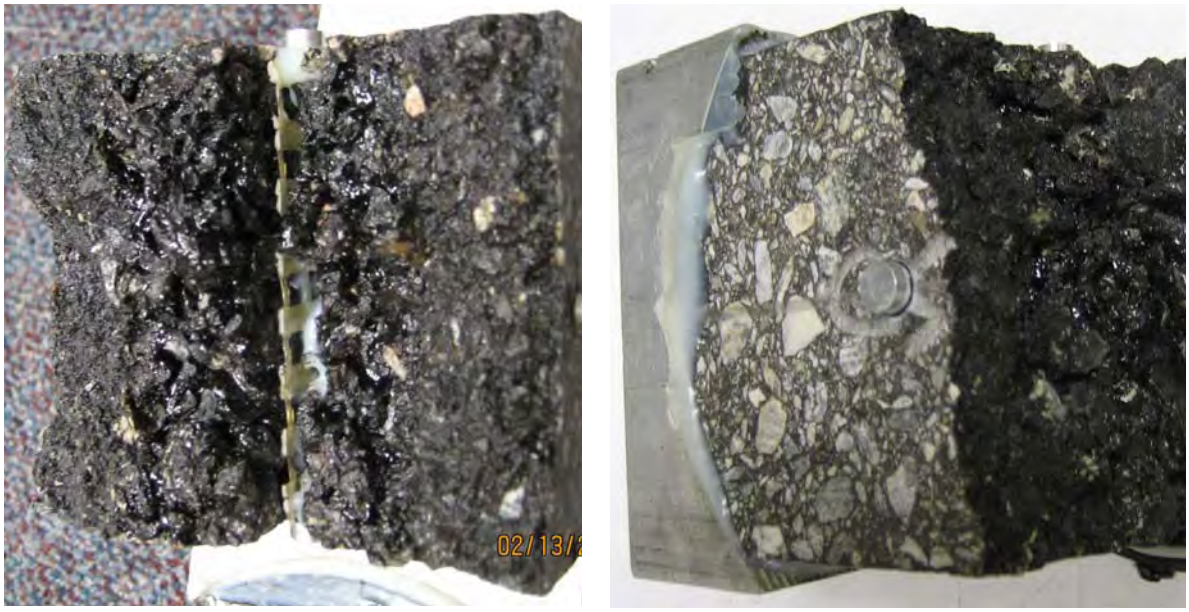

Figure 5-45 Cracking Surfaces for Fiber Glass (left) and Cardboard (right) Interface

Because of the brittleness of the fiber glass, the composite specimen broke right along the edge of the fiber glass; while the composite specimen with cardboard spacer broke along the natural weak path. Thus cardboard was selected as the spacer material.

5.8.2 New Alignment System for Composite Specimen Preparation

One of the issues encountered in composite specimen preparation was the alignment of the composite specimen and loading heads. Poor alignment not only makes the testing setup difficult but also introduces bending in the specimen because the specimen is not pulled straight. Two

pieces of steel angles were mounted on two diagonal corners of the loading heads to assure good alignment. Loading heads assembled with two steel angles are shown in Figure 5-46.

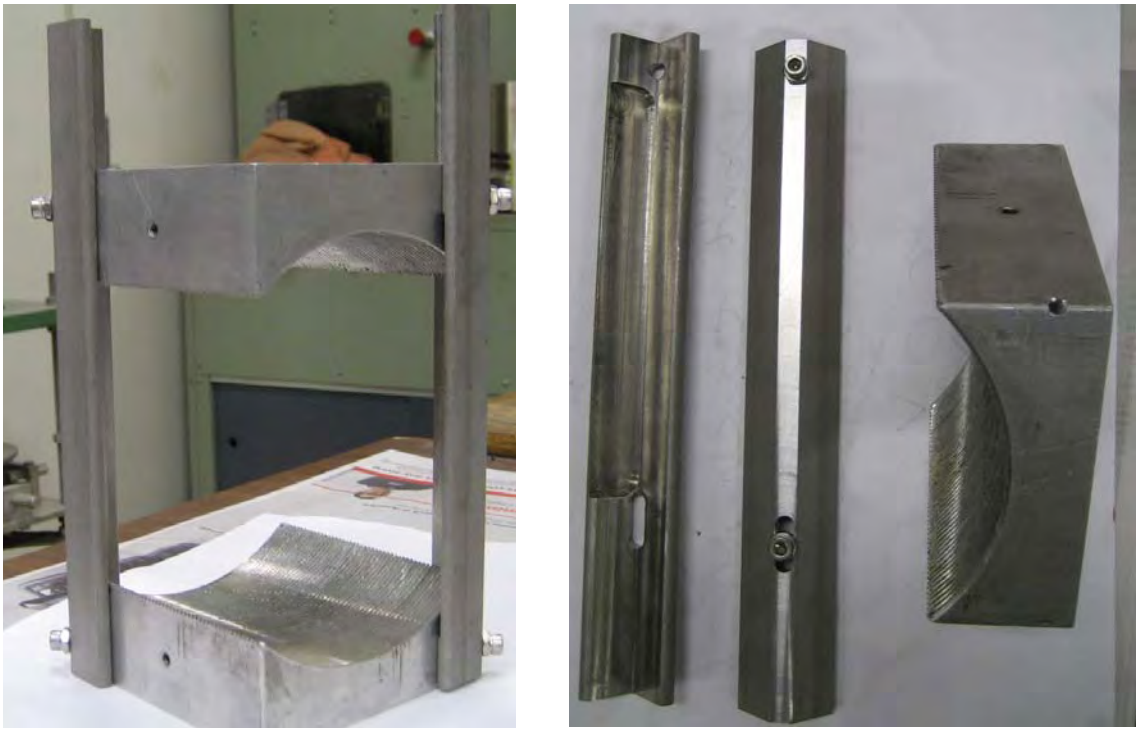

Figure 5-46 Loading Heads with Two Steel Angles

5.9 Results of Repeated Loading Test on Symmetrical Composite Specimen

5.9.1 Results of Symmetrical Composite Specimen W/ and W/O Alignment System

Two symmetrical composite specimens for conventional tack coat and Novabond tack interface each were tested and the results are shown in Figure 5-47. Samples are denoted as: CSST1, CSST2, CSSN1, and CSSN2 with letters CSS denoting composite specimen with symmetrical configuration, the letter T denoting conventional tack coat interlayer, and N denoting Novabond tack interlayer. Four extensometers were positioned at the center of each of the symmetrical composite specimen's four surfaces with gage H1 and H2 mounted on the

interface and gage V1 and V2 mounted on dense-graded mixture surface. The results shown in Figure 5-47 are the average results of gage H1 and H2, and gage V1 and V2. Repeated load with 0.1 second loading and 0.9 rests was applied and the peak load was 2500 lbs.

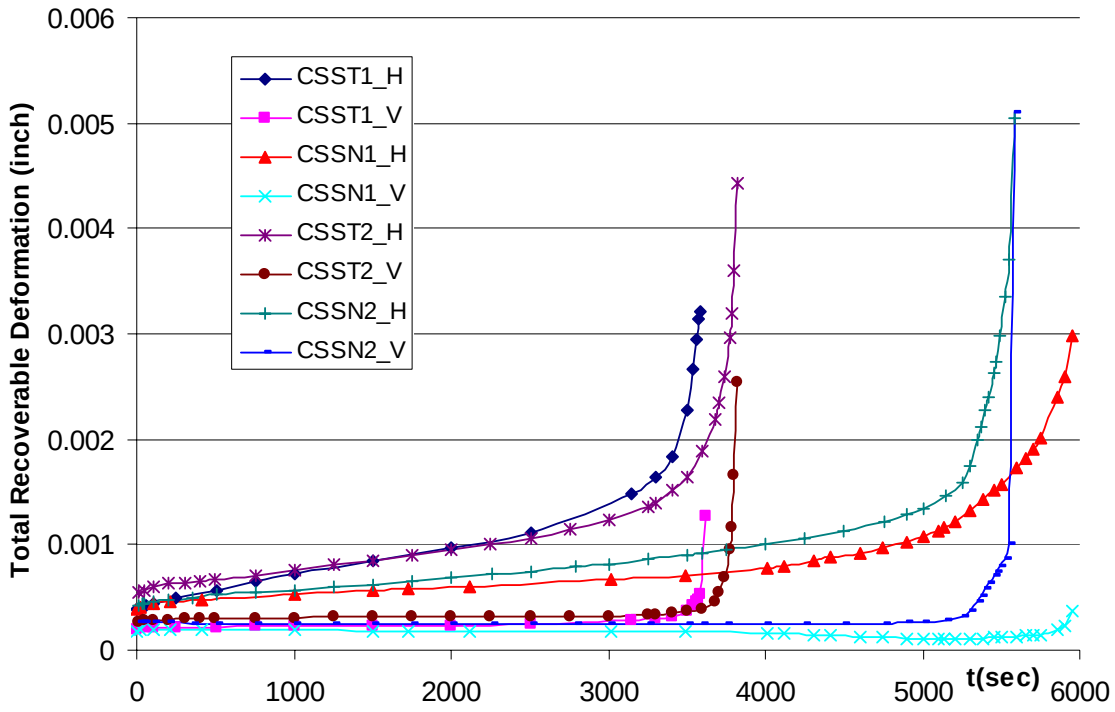

Figure 5-47 Total Recoverable Deformation for Symmetrical Composite Specimens

The results show that Novabond Tack interface extended the crack initiation time from around 2500 seconds for conventional tack coat interface to around 4000 seconds, which is approximately 60% increase. The total failure life also increased approximately 60% from around 3600 seconds to around 5750 seconds for composite specimen with Novabond tack interface with respect to composite specimen with conventional tack coat interface.

Test results from symmetrical composite specimens prepared with the new alignment system are shown in Figure 5-48.

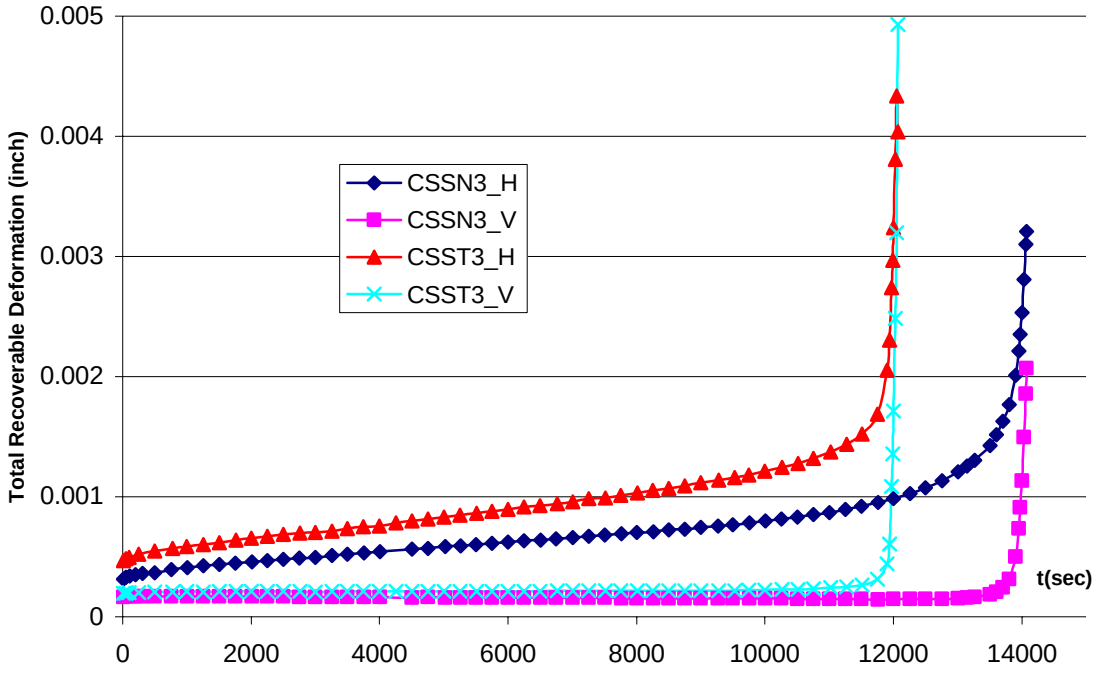

Figure 5-48 Total Recoverable Deformation for Symmetrical Composite Specimens with New Alignment System

The results clearly show that identification of crack initiation and total failure life are both enhanced with the removal of bending under this new alignment system. Novabond tack interface extended the crack initiation time from around 9000 seconds for conventional tack coat interface to around 10500 seconds, which is approximately 17% increase. The total failure life also increased approximately 17% from around 12000 seconds to around 14000 seconds for composite specimen with Novabond tack interface with respect to composite specimen with conventional tack coat interface.

5.9.2 Conclusion

With the mitigation of bending from asymmetrical composite specimen, test results on symmetrical composite specimen show 17%~ 60% improvements in both crack initiation time and total failure life. This test approach can be used to evaluate the effect of interface on the

crack initiation and propagation but needs further improvement to remove the sample to sample variation.

5.10 Summary and Recommendation

5.10.1 Summary

In this chapter, composite specimen preparation method was developed using Superpave gyratory compactor in the lab; various specimen geometries and loading modes were tried to develop composite specimens for direct tension testing method in order to evaluate the effect of interlayer materials on stress release between OGFC and dense-graded layers.

Constant stroke rate strength tests were conducted on composite specimen with semi-circular groove on OGFC surface at three loading rates, 25mm/minute, 2.5mm/minute and 0.25mm/minute. Test results indicate that constant stroke rate strength tests were either too fast to identify the crack initiation point or too slow such that cracks initiate from the dense-graded side.

Repeated loading approach with a constant repeated haversine load of one-tenth of a second and then resting for nine-tenth of a second was adopted; in part of the stress in dense-graded mixture can be released during rest period. Rough surface of newly compacted OGFC had to be sliced off to have a more uniform surface and avoid the natural stress concentrators. Tests on composite specimens without interlayer show that damage starts to accumulate in the OGFC right after loading but little or no damage is induced in dense-graded mixture until cracks propagate to it. This damage feature can be used to evaluate the effect of interlayer.

In order to keep the interlayer in stable crack propagation range, dense-graded mixture was increased to 3 inches thick from the original 1inch thick. Test results with this configuration

show that damage was accumulating in dense-graded mixture even though the damage rate was lower than that in OGFC.

A rectangular groove was introduced in OGFC surface to concentrate high enough stress to reduce the damage induced in dense-graded mixture during loading process before cracks propagated into it. Tests were conducted on composite specimens with rectangular groove and conventional tack coat and Novabond tack interlayer applied. Test results show that there were huge variations from sample to sample for both composite specimens with conventional tack coat interlayer and Novabond tack interlayer. This variation was determined to be caused by composite specimen bending towards OGFC side because of the asymmetric composite structure.

Symmetrical composite specimen configuration was successfully used to remove the bending induced in the single composite specimen during pulling. Test results show 17%~ 60% improvements in both crack initiation time and total failure life. For the Novabond tack versus conventional tack interlayer, it appears that this test approach can be used to evaluate the effect of interface on the crack initiation and propagation but needs further improvement to remove the sample to sample variation.

5.10.2 Recommendations

Benefits of Novabond tack interface were shown using symmetrical composite specimen test. However, OGFC mixture surface macrotexture leads to big variations in terms of Novabond tack interface improvement in crack initiation time and total failure life with respect to conventional tack coat interface. Further tests on composite specimens with sliced OGFC surface or cored specimen from the field are needed to assess this issue.

Modest benefit of Novabond tack interface compared with conventional tack coat interface on crack resistance has been shown on newly compacted composite specimens. However, it should be noted that the greatest benefit of Novabond tack may come from enhanced durability, like potential to reduce age-hardening, moisture damage and healing potential.

Further assessments are strongly recommended as follows,

- Tests on composite specimens with sliced OGFC surface or cored specimen from the field.
- Conditioning (age-hardening and moisture conditioning) procedures need to be developed for composite specimen.
- Evaluation methods to quantify benefits of age-hardening.
- Sample to sample variability of OGFC needs to be reduced.

CHAPTER 6
CONTINUUM AND MULTI-SCALE ANALYSIS OF OGFC STRUCTURE COMPOSITES

In conventional macro-mechanical analysis, asphalt mixture is generally assumed to exhibit homogeneous properties and a continuum model can be used to describe the behavior of composite systems. The constitutive model can include elastic, viscoelastic and other common behavior. Model parameters are generally obtained through laboratory testing of materials. Asphalt mixture stiffness, usually described as resilient, dynamic or relaxation modulus, is generally used to evaluate mixtures and to predict stress, strain and deformation response of mixtures and pavements. However, hot mix asphalt (HMA) is a complex conglomerate of asphalt binder, aggregate particles and air voids. The relative proportions, distribution, and characteristics of these individual components determine the macroscopic behavior of the HMA. Considering the internal structure using micro-mechanical analysis is essential to capture the stress and strain conditions within HMA.

Unfortunately, micro-mechanical analysis increases computer run time exponentially relative to continuum analysis, and it is impractical to model an entire pavement layer using this approach.

One solution to this dilemma is to employ a multi-scale analysis approach, where the majority of the pavements layers are modeled using a continuum approach, and only specific zones of particular interest are modeled using micromechanics. This would result in manageable computer run time, while providing the level of detailed modeling necessary to predict important micro-scale behaviors needed to capture important local effects that likely govern performance

of mixtures and interfaces. Therefore, a multi-scale approach is ideally suited to evaluate behavior of OGFC, particularly as it relates to crack resistance and transfer of stress at the interface between OGFC and the underlying HMA layer.

Both continuum and multi-scale approaches are used in this study to evaluate the effects of OGFC and interface condition on top-down cracking performance. Results of both analyses were combined with the fundamental HMA crack growth law developed at the University of Florida to evaluate effects of different factors on OGFC performance.

6.1 Continuum Analysis of OGFC Performance

The objective of the continuum analysis is to evaluate the contribution of OGFC and the bond between the OGFC and underlying layer to the resistance of top-down cracking model. In the continuum analysis of the pavement structure, a FEM model was created to capture the stress and strain distribution in the structure. Then the Florida HMA fracture mechanics was implemented to calculate the load cycles needed to create the different size cracks, which was used to evaluate the crack resistance of the structure.

6.1.1 FEM Model of Different composite systems

Four composite systems, as shown in Figure 6-1 to 6-4, were considered:

Case 1: Dense graded asphalt mixture (i.e. No OGFC);

Case 2: Dense graded asphalt mixture with 1 inch OGFC (conventional tack coat condition);

Case 3: Dense graded asphalt mixture with 1 inch OGFC saturated with Novabond tack;

Case 4: Dense graded asphalt mixture with 1 inch, where the bottom 0.4 inch of OGFC was saturated with Novabond tack.

Case 4 represents the bonded friction course condition, since the thick bond will permeate about 0.4 inch into the OGFC. Case 3 was used to evaluate effect of using additional Novabond, in this case saturated through the entire OGFC thickness. Semi-circular hole was introduced to create a stress concentration at the top of each pavement system to increase top-down cracking.

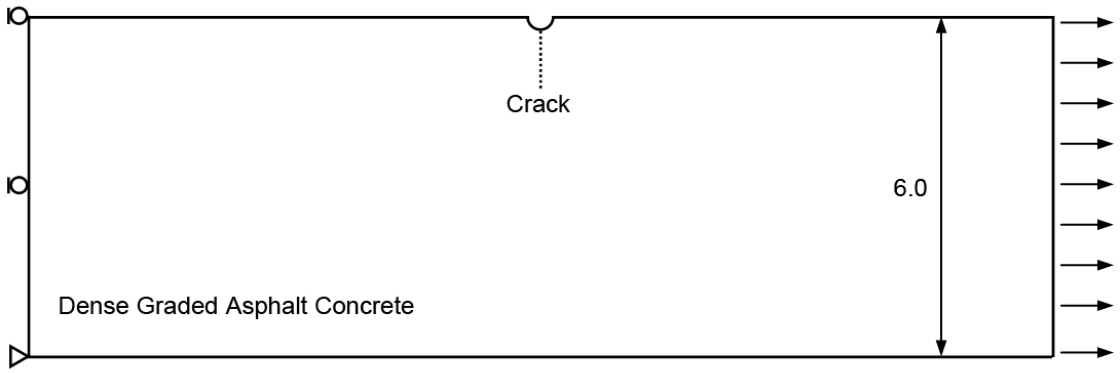

Figure 6-1 Case 1: Dense Graded Asphalt Mixture (No OGFC)

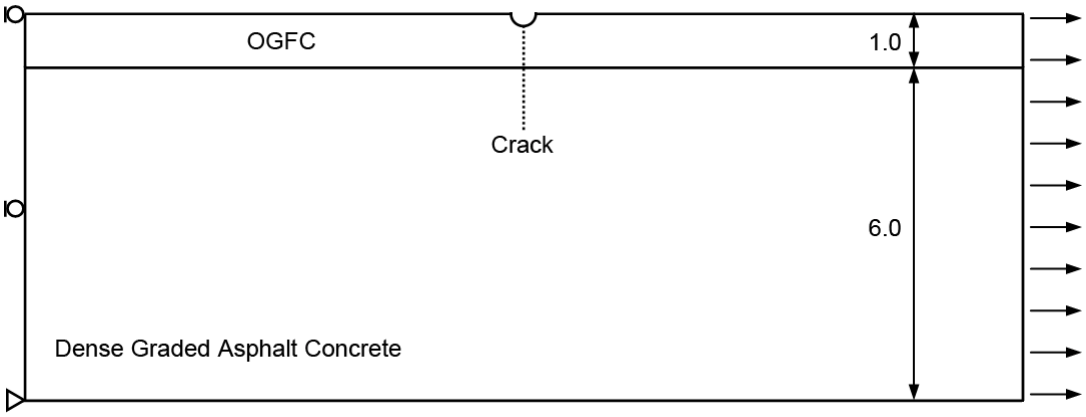

Figure 6-2 Case 2: Dense graded Asphalt Mixture with 1 inch OGFC (conventional tack coat condition)

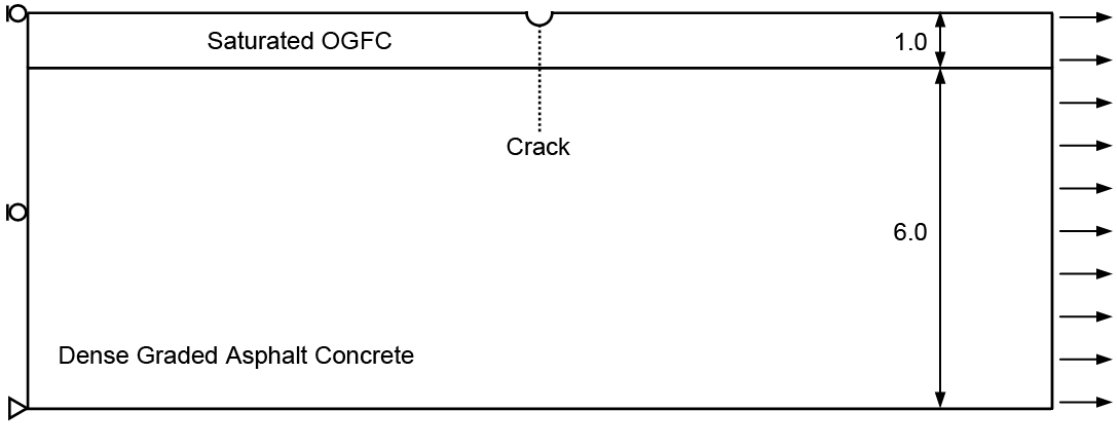

Figure 6-3 Case 3: Dense Graded Asphalt Mixture with 1 inch OGFC Saturated (1.0) with Novabond Tack

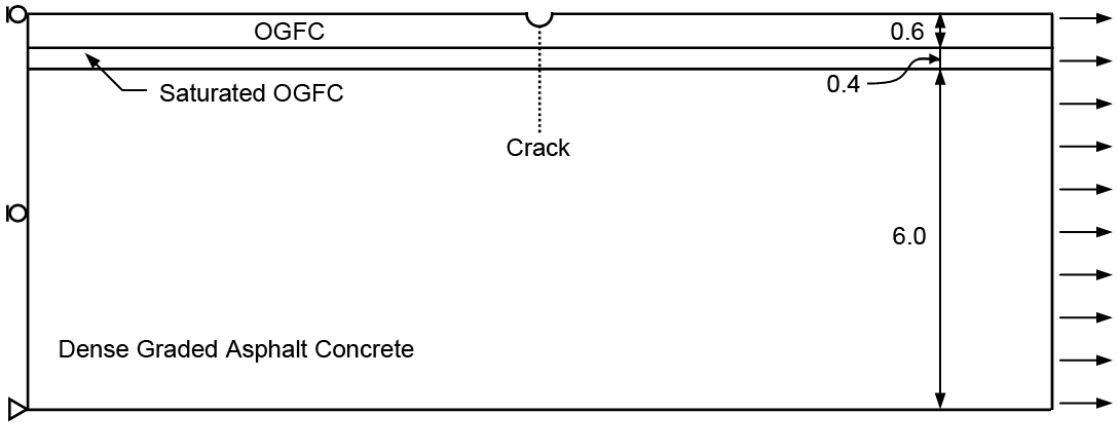

Figure 6-4 Case 4: Dense Graded Asphalt Mixture with 1 inch OGFC Partially Saturated (0.4) with Novabond Tack

In the model, the asphalt mixture layers were assumed homogenous and isotropic. The layers were fully bonded with each other. A global tensile stress of 100psi was applied. The

thickness of dense graded asphalt concrete in the model is 6 inches. The dimension of the model in the tensile direction is 18 inches. Plain stress 8-node elements were used in the analysis.

The tensile stress distribution below the semi-circular stress concentrator was calculated using the finite element method (FEM). Crack initiation and propagation were calculated based on the Florida HMA cracking model. Each crack zone was set at 5mm. these predictions required that a different FEM model be created to calculate the stress distribution for each crack length evaluated. The stress was adjusted to satisfy the condition that the material strength could not be exceeded.

The material properties for the OGFC and dense graded asphalt mixture presented in Table 6-1 were obtained from Superpave IDT and dog-bone-direct tension (DBDT) tests presented earlier in this report. Properties of saturated OGFC were also obtained from the IDT tests.

6.1.2 Results of Continuum Modeling

Figure 6-5 and 6-6 present predictions of crack initiation and growth for the four composite systems evaluated.

These results clearly indicate that introduction of conventional OGFC with conventional tack coat only, actually causes cracking to develop faster that if no OGFC were used. Figure 6-5 shows that roughly 25% fewer load cycles were required to produce a 2-inch crack in the OGFC with conventional tack only systems (Case 2) than in the system with no OGFC (Case 1). This is due to the significantly lower fracture resistance which results in early crack initiation and associated stress intensities.

The results in Figure 6-5 also indicate that introduction of the Novabond tack significantly improves the cracking performance of OGFC. In fact, the number of cycles to produce a 2-inch crack was equivalent to the system with no OGFC. Introduction of the Novabond increased the

fracture energy and damage resistance of the OGFC (see Table 6-1). It was interesting to note that the performance of the partially saturated OGFC was similar to the fully saturated OGFC. This implies that full saturation is not necessary to achieve significant improvements in cracking performance. Partial Saturation is representative of what is achieved in the Novachip/bonded friction course process

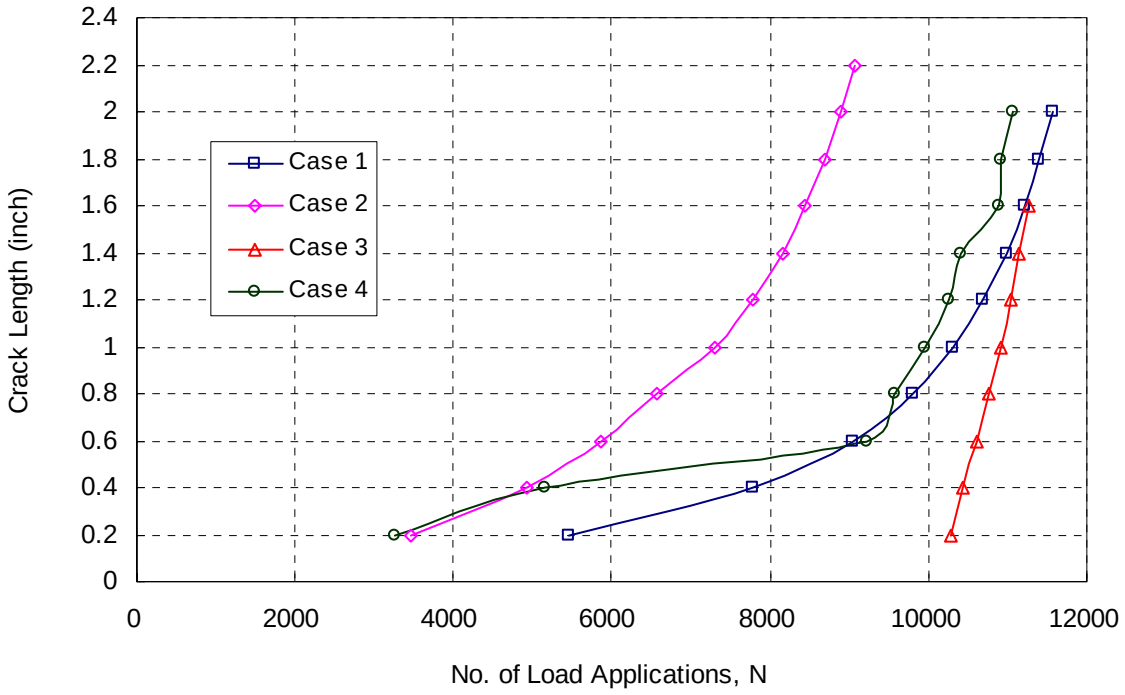

Figure 6-5 Load Cycles with Crack Length of the Whole Structure

Table 6-1 Material Properties Used in FEM Calculation

	m	D_1	S_t Mpa	M_R Gpa	FE kJ/m^3	$DCSE_{HMA}$ kJ/m^3	$DCSE_{MIN}$ kJ/m	ER
OGFC (NSG)	0.557	8.38E-07	1.17	6.93	1.3	1.2	2.740	0.44
Dense Unmodified	0.668	4.77E-07	2.14	10.85	4.2	4.0	2.971	1.34
Saturated OGFC (FC-5 G)	0.64	7.08E-7	1.4	5.31	4.4	4.21	2.11	2.0

Figure 6-6 illustrates the same points by directly comparing the number of load cycles needed to create a 1-inch crack in the dense-graded mixture for each of the four cases. Clearly, the OGFC with conventional tack only performs more poorly than the system with no OGFC, while OGFC either partially or fully saturated with Novabond tack results in a slight improvement in performance over the system with no OGFC.

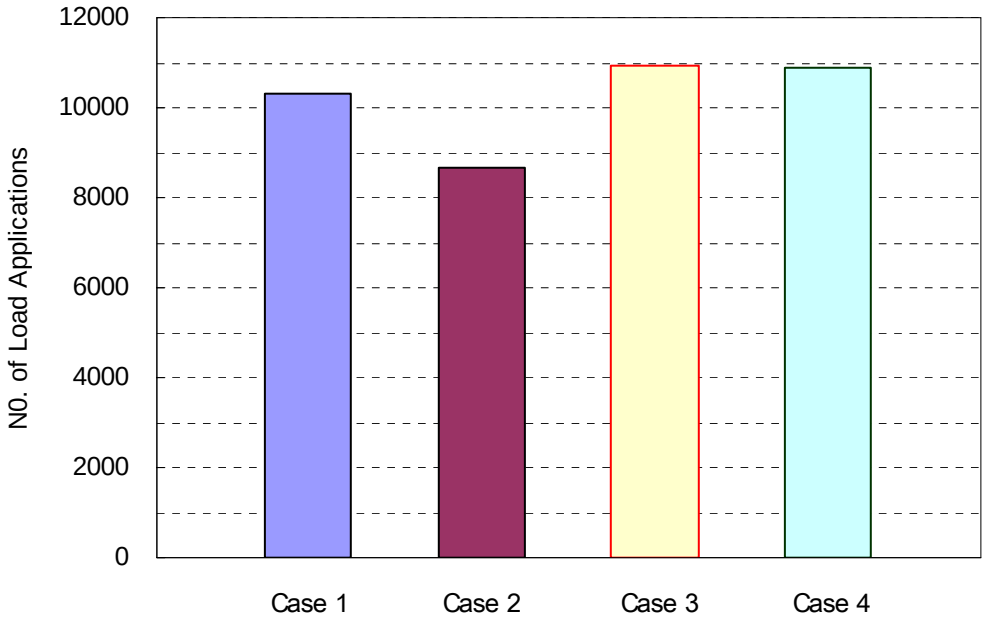

Figure 6-6 The Cycles Needed to Create 1 inch Crack in the Dense Graded Asphalt Concrete

Figures 6-7 to 6-10 indicate how the crack initiates and propagates for each of the 4 cases. For the Case 1 dense graded asphalt concrete and Case 2 OGFC on dense graded asphalt concrete, the crack initiates at the surface and propagates downward (Figures 6-7 and 6-8). For the fully saturated OGFC on dense graded asphalt concrete, the crack initiates on the top of the dense graded asphalt concrete and continues to propagate downward; it actually never breaks through the OGFC. After many load cycles the saturated OGFC experienced crack initiation. For the partially saturated OGFC with bond on dense graded asphalt concrete, the crack initiates first

in the OGFC, and then a second crack initiates on top of the dense graded asphalt concrete once the crack in the OGFC propagates to the surface of the saturated OGFC. The crack continues to propagate in the dense-graded mixture and the top crack eventually propagates into the saturated zone.

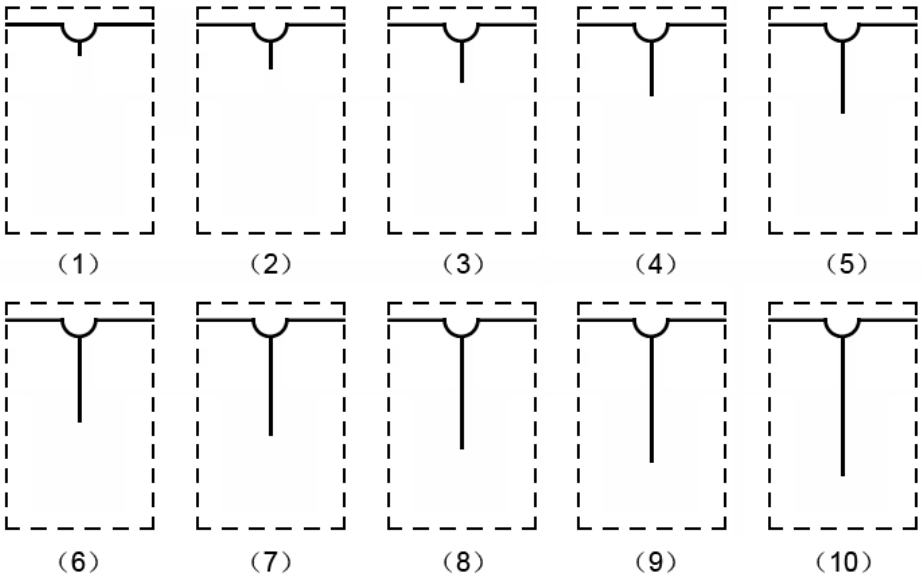

Figure 6-7 The Propagation of the Crack of Case 1: Dense Graded Asphalt Concrete

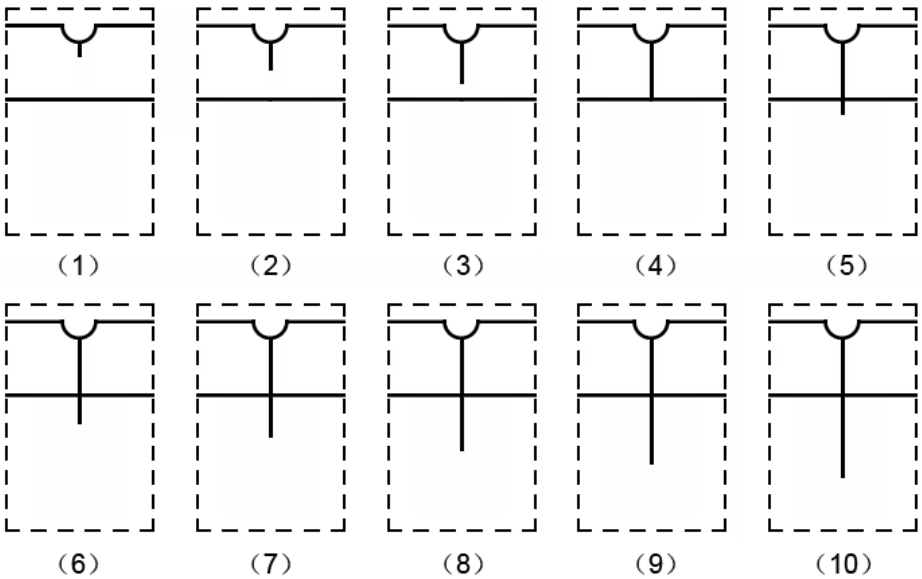

Figure 6-8 The Propagation of the Crack of Case 2: OGFC on Dense Graded Asphalt Concrete

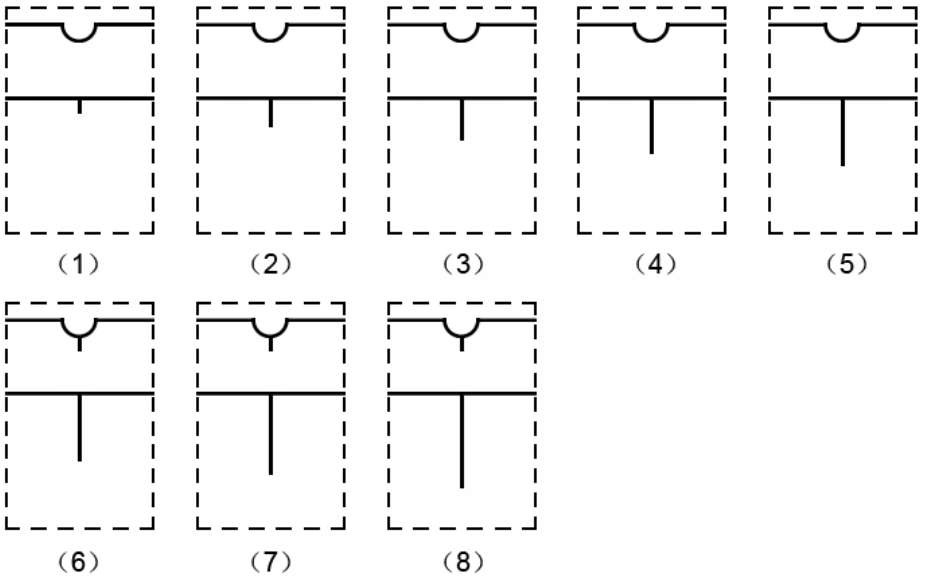

Figure 6-9 The Propagation of the Crack of Case 3: Saturated OGFC on Dense Graded Asphalt Concrete

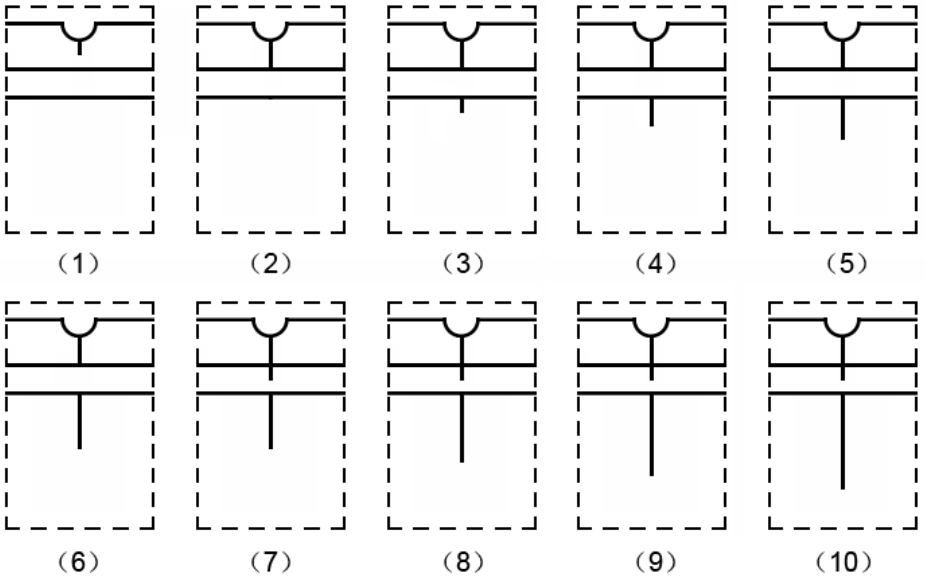

Figure 6-10 The Propagation of the Crack of Case 4: OGFC with Bond on Dense Graded Asphalt Concrete

6.1.3 Summary of Continuum Analysis

The continuum analysis of the four case mixture structures was done using FEM and Florida HMA fracture mechanics. The key points of the analysis are summarized as follows:

- OGFC with conventional tack only does not help to increase the resistance of the structure to top-down cracking, instead, it will accelerate the initiation and propagation of the crack.
- The bonded OGFC will increase the load cycles needed to crack the same size crack in the structure about 25% to 41%, relative to conventional OGFC.

6.2 Multi-Scale Analysis of OGFC Performance

6.2.1 Introduction

As presented above, the properties of OGFC with conventional tack coat only and OGFC saturated at the interface with Novabond tack are totally different (Table 6-1). For the continuum model, the higher predicted fracture resistance of partially and fully bonded OGFC was primarily due to the introduction of a layer or sublayer of OGFC having higher fracture energy. However, the continuum approach did not allow for evaluation of other effects such as interface conditions (less than 100% stress transfer) and potential stress relief induced by micro-structural effects, including OGFC Particle contact condition, potential stress relief with in the OGFC itself, and properties of the mastic in the OGFC. Multi-scale models are used to capture the effects of each of these factors on top-down cracking performance.

6.2.2 Objective of Multi-scale Analysis

The objective of this multi-scale analysis was to evaluate the effects of microstructure characteristics on stress distribution and top-down cracking performance. The stresses within the microstructure were captured and the Florida HMA fracture mechanics was implemented to predict crack length as a function of load cycles.

6.2.3 Multi-scale FEM Model

A finite element model was used to predict the global pavement response, which defined the boundary conditions for the micro-mechanical model used to predict the local response of the OGFC and the interface. For the local response of the micro-mechanical model, different contact conditions between the aggregate particles and the underlying layer were evaluated. These conditions included the gap between the aggregate particles and the contact condition between the particles and the AC layer. The aggregate particles are not perfect sphere and have different size faces, so the contact between the particles and the underlying asphalt concrete layer may be different. The conditions evaluated also include the thickness of the layer that bonds the aggregate particles and the underlying layer together. For the interface without bond, the contact between particles and underlying layer is more like penetration or direct contact with the AC layer, which will cause much higher friction between these two. In contrast, the highly polymer-modified Novabond tack may create a relatively thin, but highly effective layer that allows the aggregate to move independently of the HMA surface, thereby reducing the stresses on top of the HMA layer.

The model was created based on the structure of the pavement with OGFC on top, as shown in Figure 6-11. Figure 6-12 shows the two dimension multi-scale model. The size of the model is based on the direct tension test for the OGFC composites (Chapter 5). In Figure 6-12 (a)

is the global model where the OGFC and the underlying layer were taken as homogenous materials with 6-inch length and 2-inch thickness, consisting of 1-inch OGFC and 1-inch underlying asphalt concrete. Figure 6-12 (b) is part of the global model, in which the OGFC is taken as non-homogenous material composed of aggregate particles and mastic, which includes the fine aggregates, asphalt and air voids. The aggregate particles are simplified as sphere of different diameters. Figure 6-12 (c) is the local model composed of the two half same size aggregate particles, mastic and the underlying AC layer. The local model is a portion of the global model with 0.4 inch height and 0.2 to 0.25 inch width, depending on the gap between the two particles. A particle diameter of 0.2 inch was used. The global model and the local model were meshed using different elements. For the global model, quadrangle elements were used. For the local model, the aggregate particles and the underlying AC layer were also meshed using quadrangle elements; while the mastic was meshed using triangle elements to better represent the angular shapes involved. Figure 6-13 is the mesh of the local model.

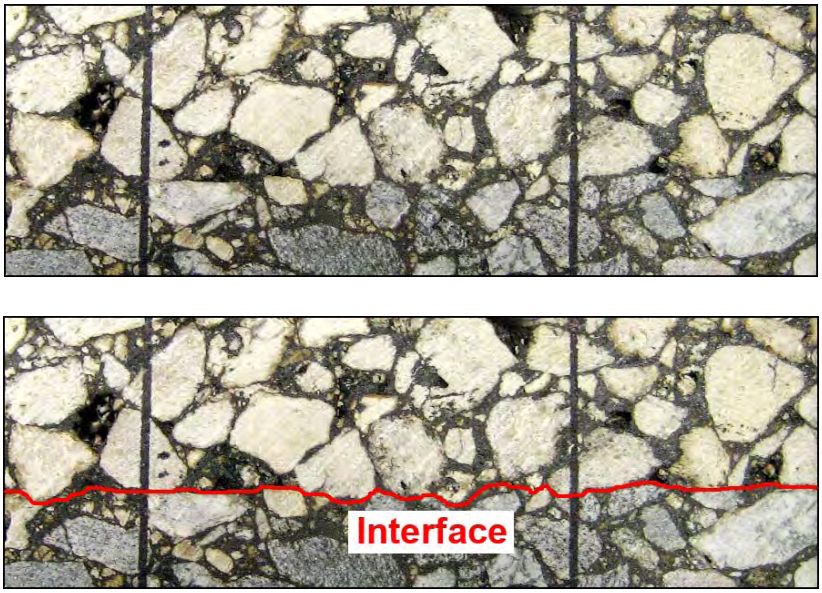

Figure 6-11 Structure of OGFC

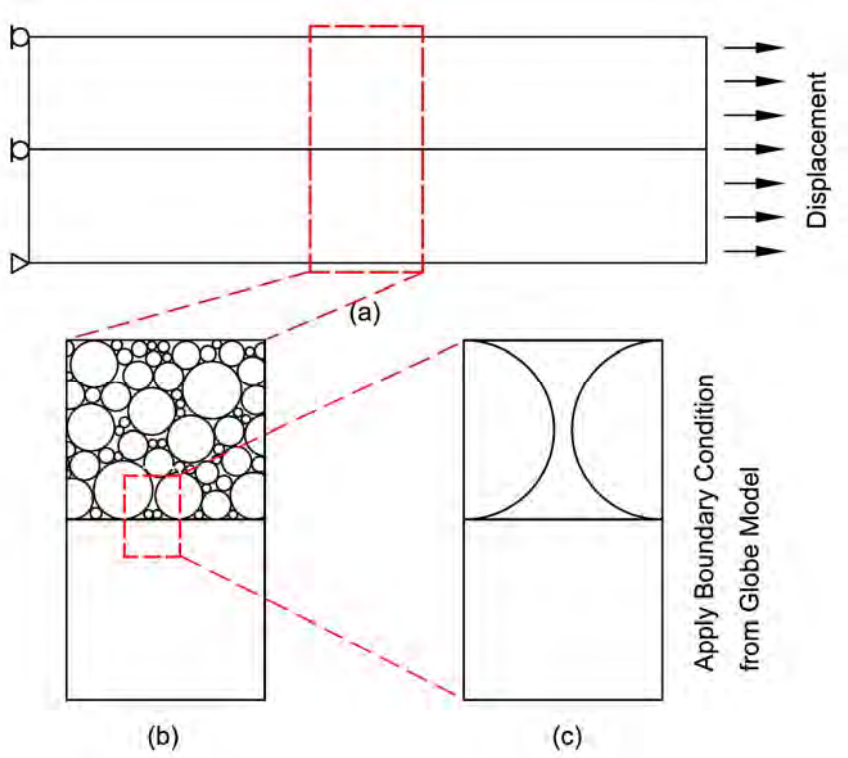

Figure 6-12 The Multi-Scale Model

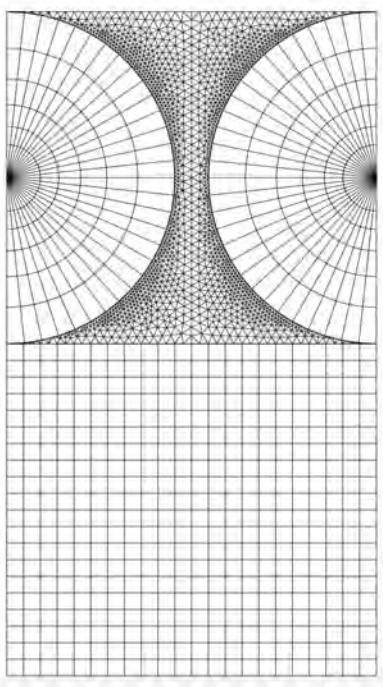

Figure 6-13 Mesh of the Local Model

Elastic materials were used for both global and local models. Model parameters are shown in Table 6-2. The parameters used were based on the laboratory tests by calibration (or back-calculation). The primary propose of the modeling effort was to evaluate the contribution of different OGFC characteristics to the fracture resistance of the pavement system, so exact parameters value were not required.

Table 6-2 Material Properties used in the Multi-Scale Analysis

	E (psi)	Poisson's Ratio
Underlying AC	500000	0.4
Aggregate Particles	7000000	0.2
Bond	10000	0.45
Mastic	50000	0.4
OGFC	250000	0.4

A global displacement of 0.0019 inch was applied to the global model. The resulting local stress, strain and displacement within the systems were calculated. The boundary displacements of the local model were taken from the global model calculation results, and applied to the local model. The stress distribution of the local model was then calculated.

Figure 6-14 shows that the horizontal tensile stress distribution along the vertical center line in the local model and corresponding line in the global model are totally different. The horizontal stress distribution in global model is very uniform, while in local model, due to the micro structure effects, there are stress concentrations where the gap between the two half particles is smallest. This difference shows the value of micromechanics to more accurately capture actual stresses within pavement system and the mixtures in particular.

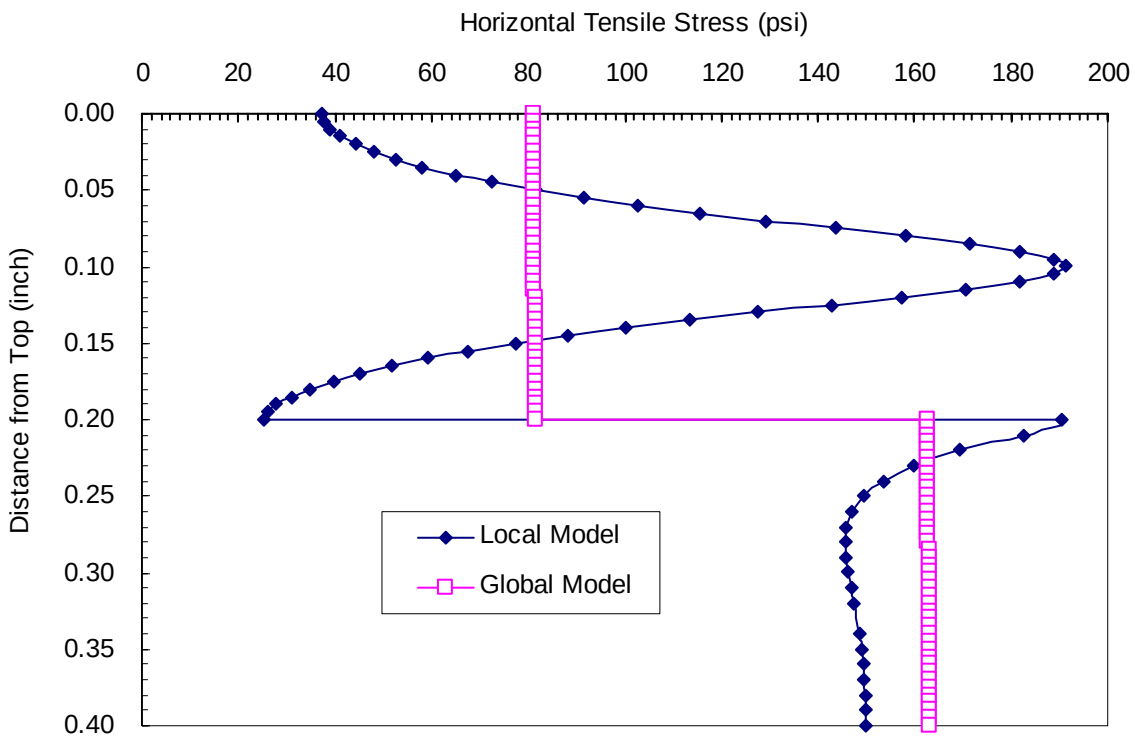

Figure 6-14 The Difference of Global Model and Local Model

6.2.4 Microstructure Characteristics Effects

The model is run for different conditions to obtain stress distributions in the OGFC and underlying asphalt concrete. For the gap between the two half particles, the 0.002, 0.01, 0.02, 0.05, 0.1 inch were used to check the gap effect. Different bond thicknesses, including no bond, 0.01, and 0.002 inches, were used to check the bond thickness effects between aggregates and underlying layer. Since aggregate particles may have different size faces, the contact area between the particle and the underlying asphalt concrete were varied. Contact sizes of 0, 0.01, 0.02, 0.05, 0.1 inch were used in the model. In addition, different mastic modulus values were used to check their effect on stress distribution.

(1) The effect of the particle gap

Gap sizes of 0.002, 0.01, 0.02, 0.05 and 0.1 inch were modeled. The contact size used was 0, which mean just one point contact with underlying HMA layer. Figure 6-15 is the stress distribution on top of the underlying AC layer. The results clearly show that non-uniform stress distributions result when local effects are considered. A higher maximum tensile stress was predicted with the micromechanics model than with the continuum model. However, the width of the gap between particles had a minimal effect on maximum tensile stress (Figure 6-16).

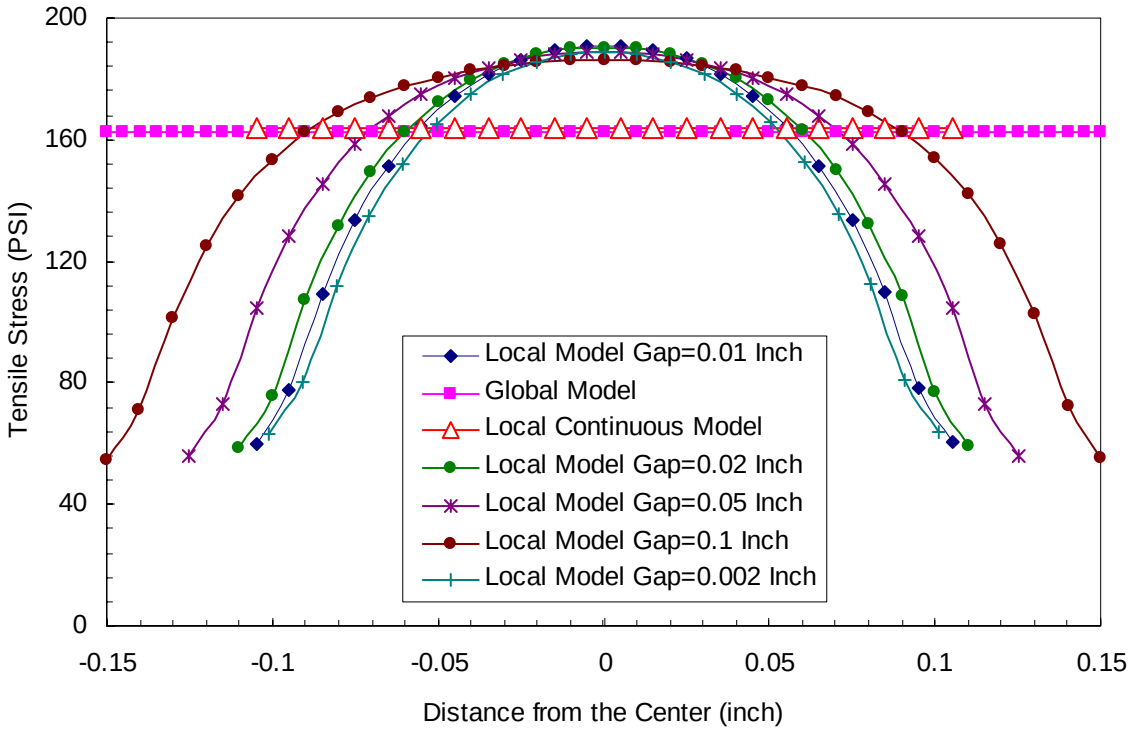

Figure 6-15 Stress Distribution on the top of the underlying AC Layer

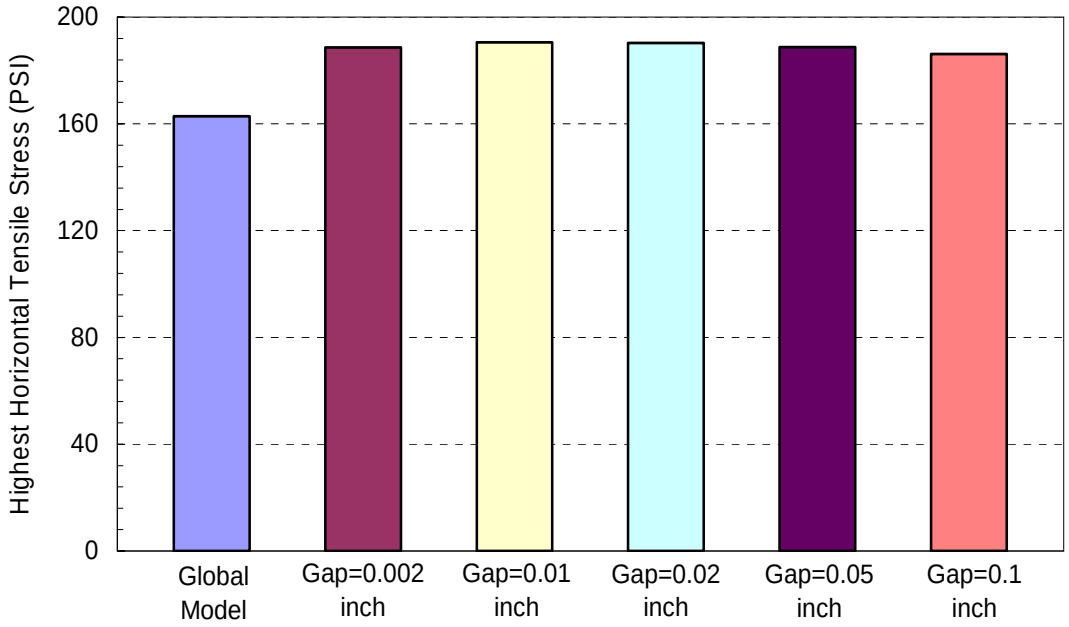

Figure 6-16 Highest Horizontal Tensile Stress Change For Different Gap Conditions

(2) The effect of the bond thickness

Different bond conditions between OGFC and the underlying AC layer may be described as shown in Figure 6-17. Figure 6-17 (a) shows a conditional bond layer between the OGFC and the underlying layer, where the contact is more like a penetration or direct contact with the underlying layer, which results in a higher contact friction. Figure 6-17 (b) shows the two layers bonded by a thin layer that might offer a high reduction of the stress transfer between the top and the underlying AC layer by allowing movement of the OGFC particles relative to the underlying layer. This figure was a bit exaggerated to illustrate that in actuality, the potential effect of the thick Novabond type tack coat, which may serve to provide a thin stress relief layer between the OGFC aggregate and the underlying asphalt concrete. However, it is also possible that the OGFC aggregate may penetrate the Novabond and contact the underlying dense mix. Both analyses were performed and this effect appeared to result in a minor difference in stress transfer.

Different bond thicknesses, 0, 0.002, 0.01 inches were inserted into the global and local models to check the effect of different bond conditions. A constant gap of 0.02 inch between aggregate particles was used as shown in Figure 6-18.

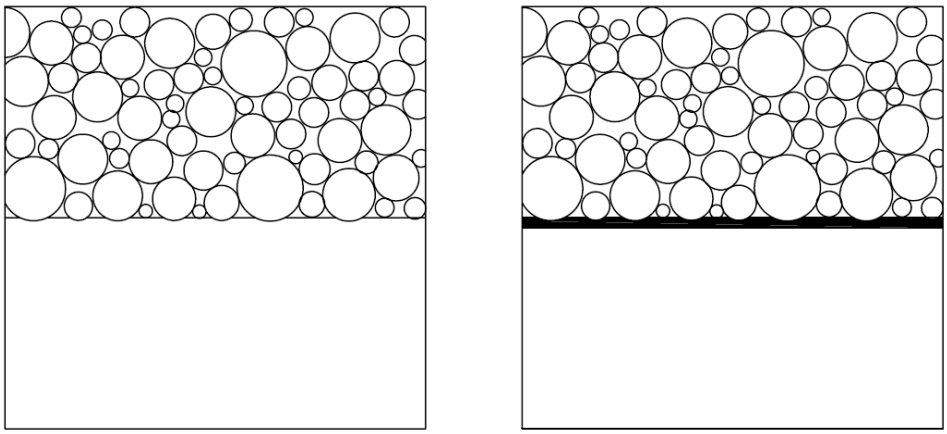

(a) (b)

Figure 6-17 The Different Bond Conditions

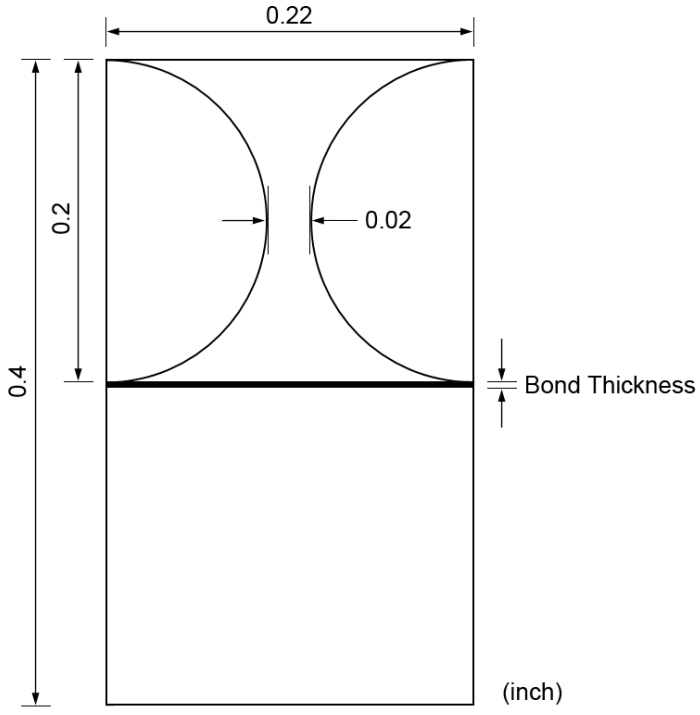

Figure 6-18 The Model Used to Calculate the Stress for Different Bond Thickness

The calculation results of stress distribution on top of the underlying AC layer for different bond conditions are shown in Figure 6-19 and Figure 6-20. For no thickness, the results clearly show that the presence of the bond reduces the maximum tensile stress, and the thicker the bond, the greater the reduction. Figure 6-20 shows that a bond thickness of 0.01 inch completely negates the stress concentration effects induced by local stresses between individual particles.

The effect is more clearly illustrated in Figure 6-21, which shows the horizontal stress distribution along the center vertical line in global and local model for different bond conditions. As shown in the figure, as the bond thickness increase, the highest stress on top of the underlying asphalt concrete layer decreases dramatically. When the bond thickness is equal to 0.01 inch, the highest stress on top of the underlying asphalt concrete layer is almost near the stress of the global model.

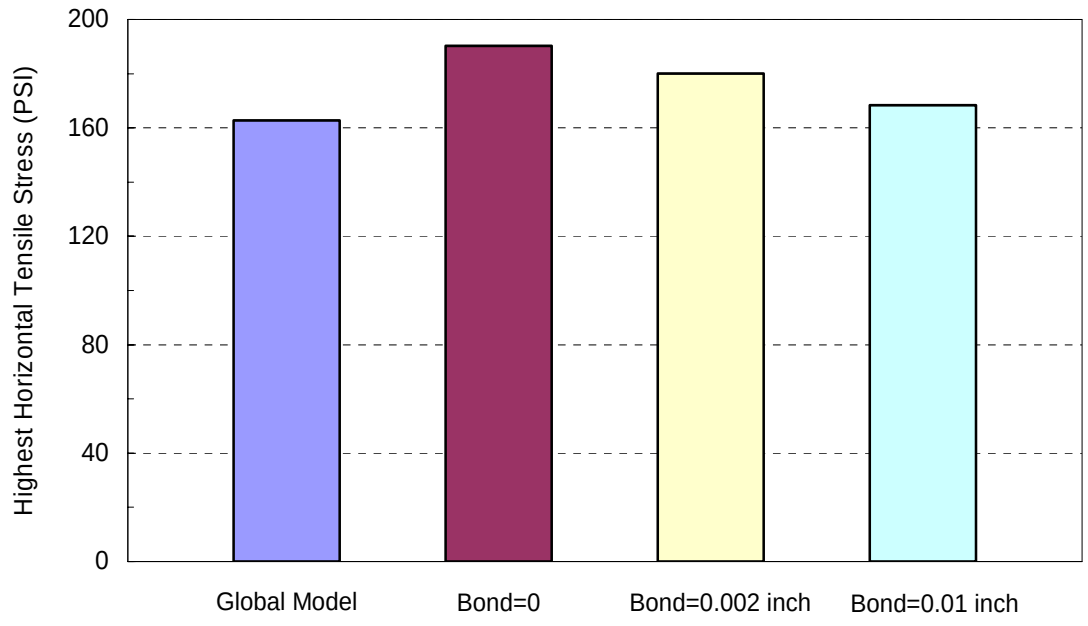

Figure 6-19 Highest Horizontal Tensile Stress Change of Different Bond Thickness

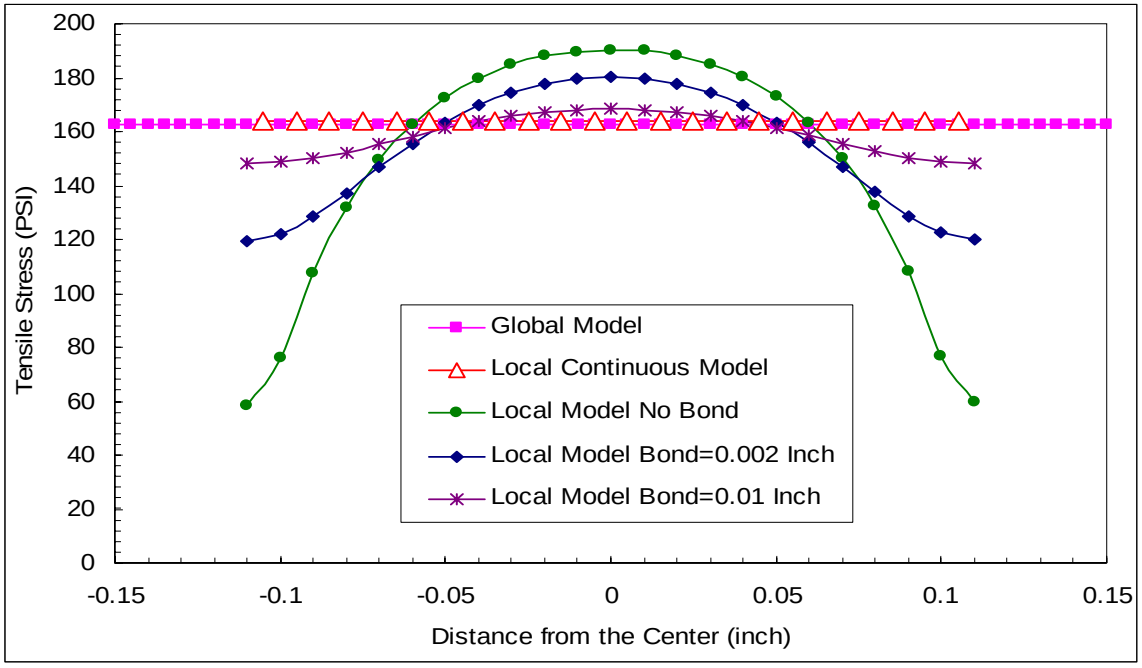

Figure 6-20 The Stress Distribution on Top of the Underlying AC Layer

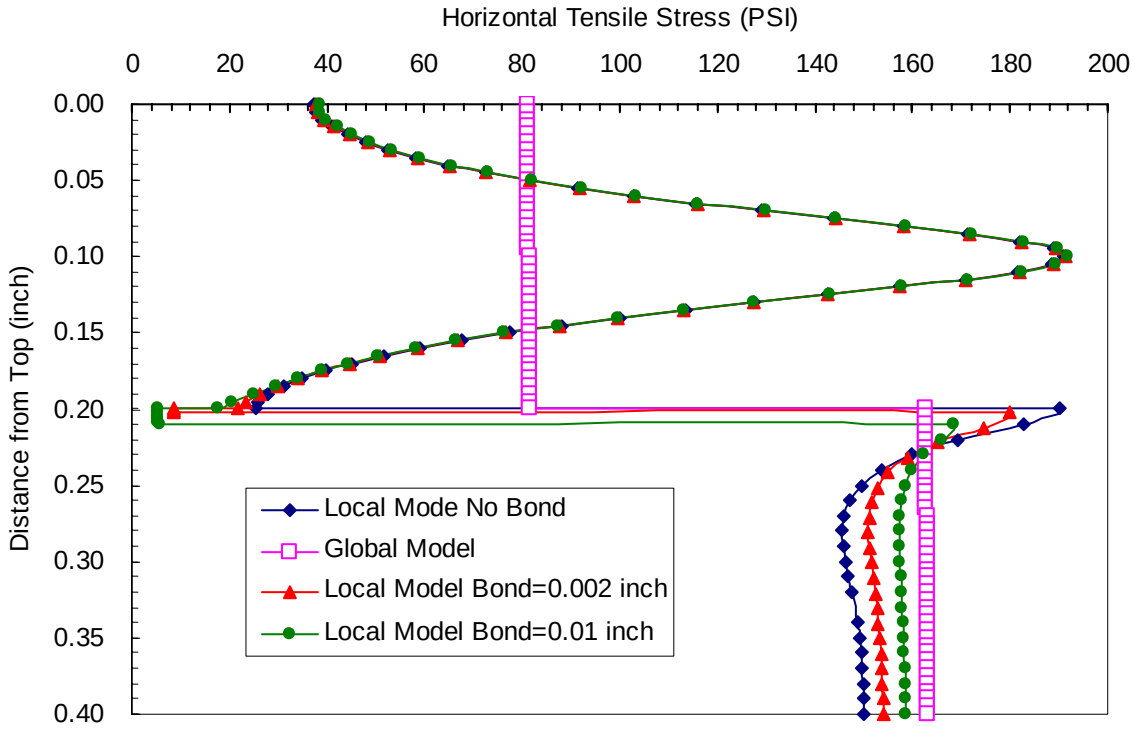

Figure 6-21 The Horizontal Stress Distribution along the Center Vertical Line

(3) Effect of contact size

Different contact conditions were modeled using different contact sizes in the local model as shown in Figure 6-22. Contact sizes of 0, 0.01, 0.02, 0.05 and 0.1 inches were modeled in the local model. Figure 6-23 shows the mesh for different contact conditions in the local model.

Figure 6-24 shows the results of the calculation for the horizontal stress distribution on top of the underlying asphalt concrete. As shown in the figure, as contact size increases, the highest horizontal stress on top of the underlying asphalt concrete layer increases. The maximum stress increased dramatically once the contact size was 0.1 inch. These results clearly indicate that contact size may strongly influence performance.

Figure 6-25 and Figure 6-26 shows how horizontal tensile stress distribution on top of the underlying asphalt concrete and along the vertical center within local model for different contact conditions.

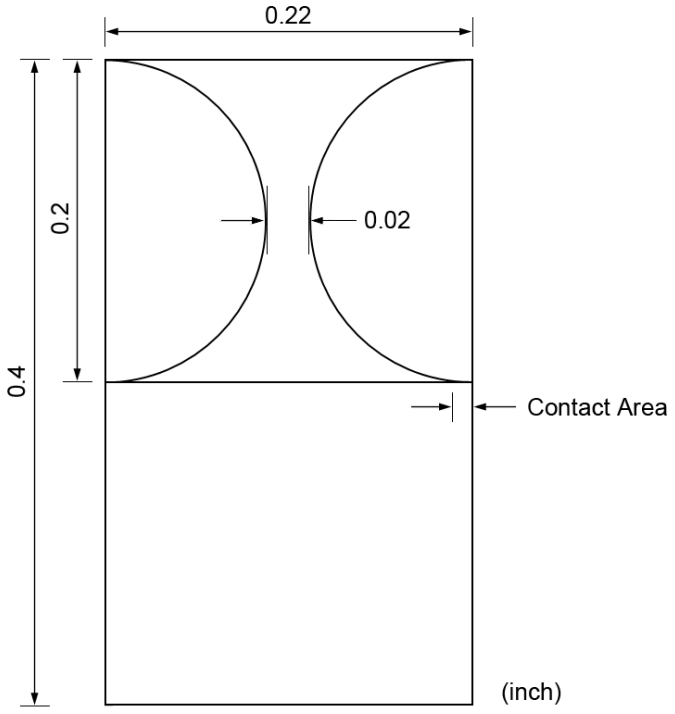

Figure 6-22 The Model Used to Calculate the Stress for Different Contact Conditions

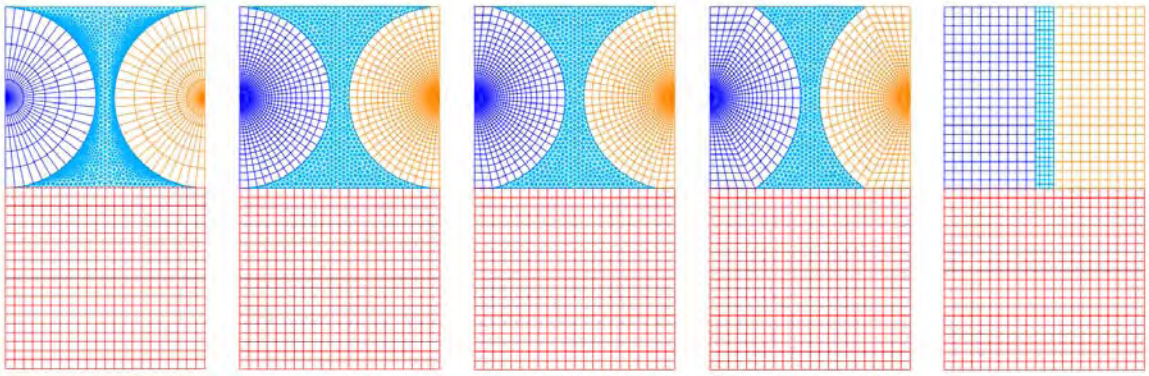

Figure 6-23 Mesh of the Different Contact Conditions

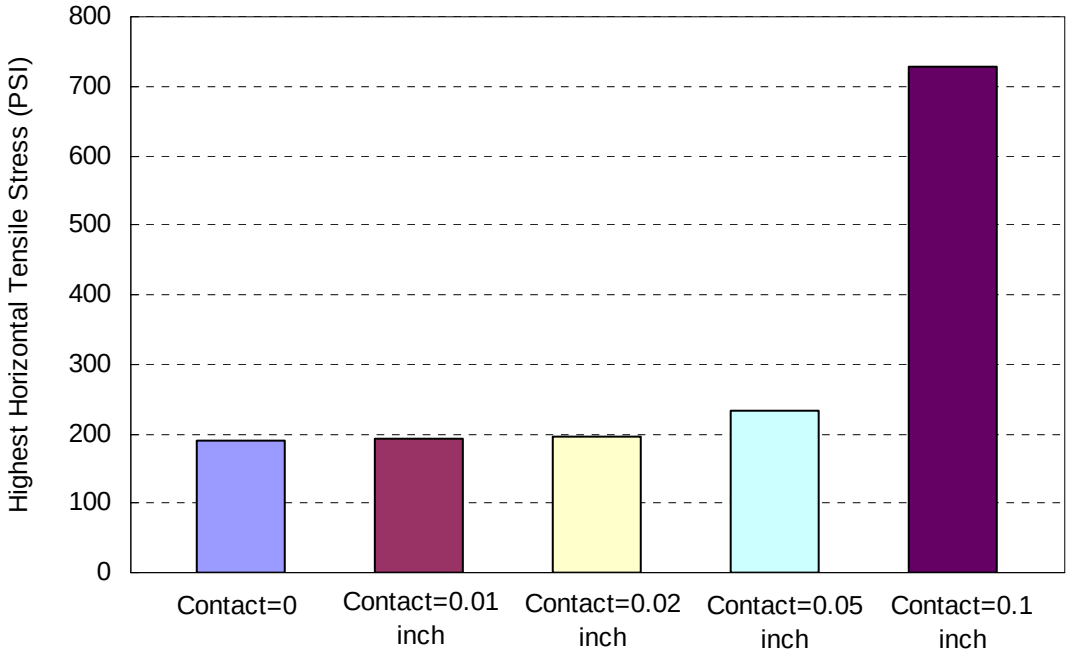

Figure 6-24 Highest Horizontal Tensile Stress Distribution

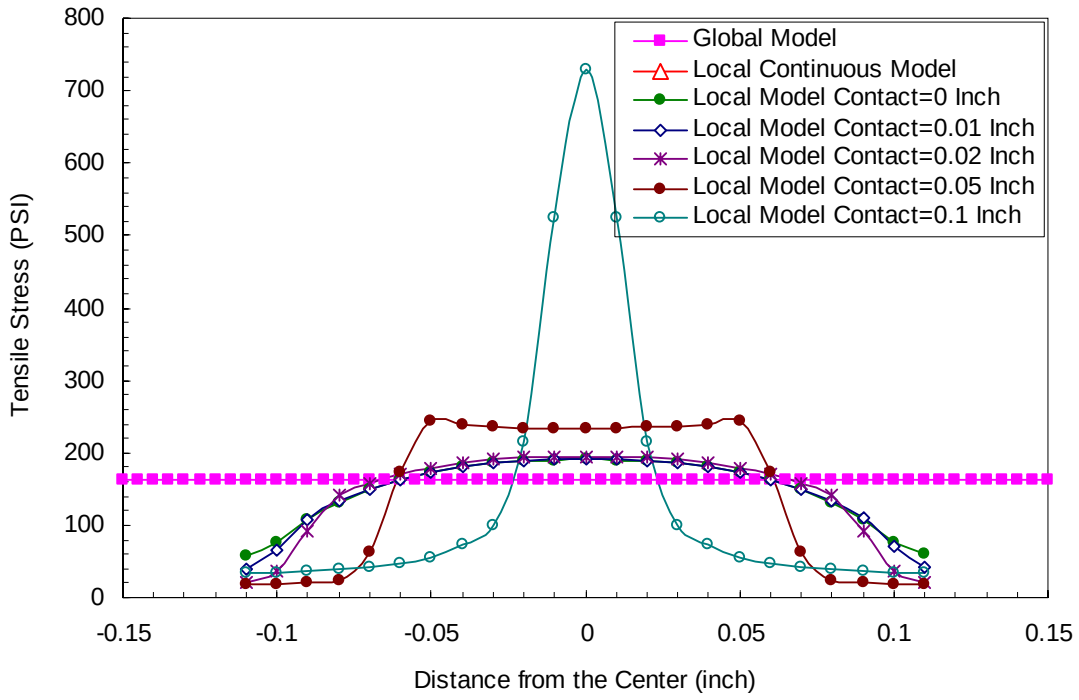

Figure 6-25 Horizontal Tensile Stress Distribution on Top of the Underlying AC

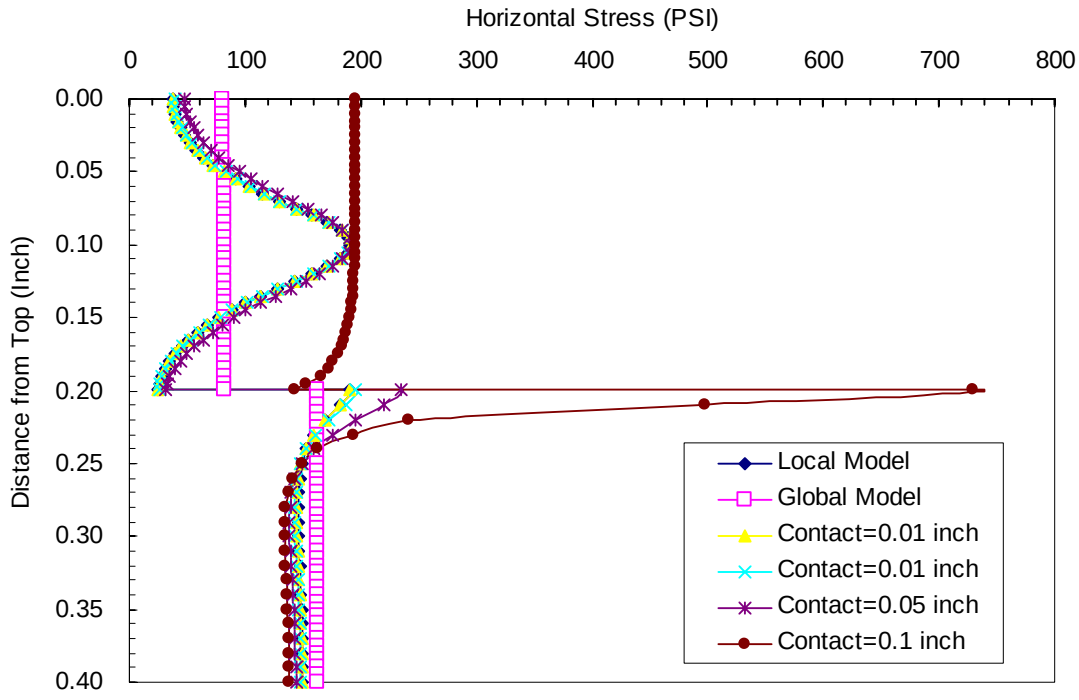

Figure 6-26 Horizontal Tensile Stress Distribution along the Vertical Center Line

(4) Effect of the mastic properties

Modulus values of 5000, 10000, 20000 and 50000 psi were used to model the mastic, which may include Novabond, asphalt rubber, or polymer modified binder. The results are shown in the Figure 6-27 and 6-28. The local model was calculated for two contact sizes, 0 and 0.02 inches. As shown in the Figure 6-27 and Figure 6-28, the highest horizontal tensile stress on top of the underlying asphalt concrete does not change much with the increase of the mastic modulus for the two contact conditions.

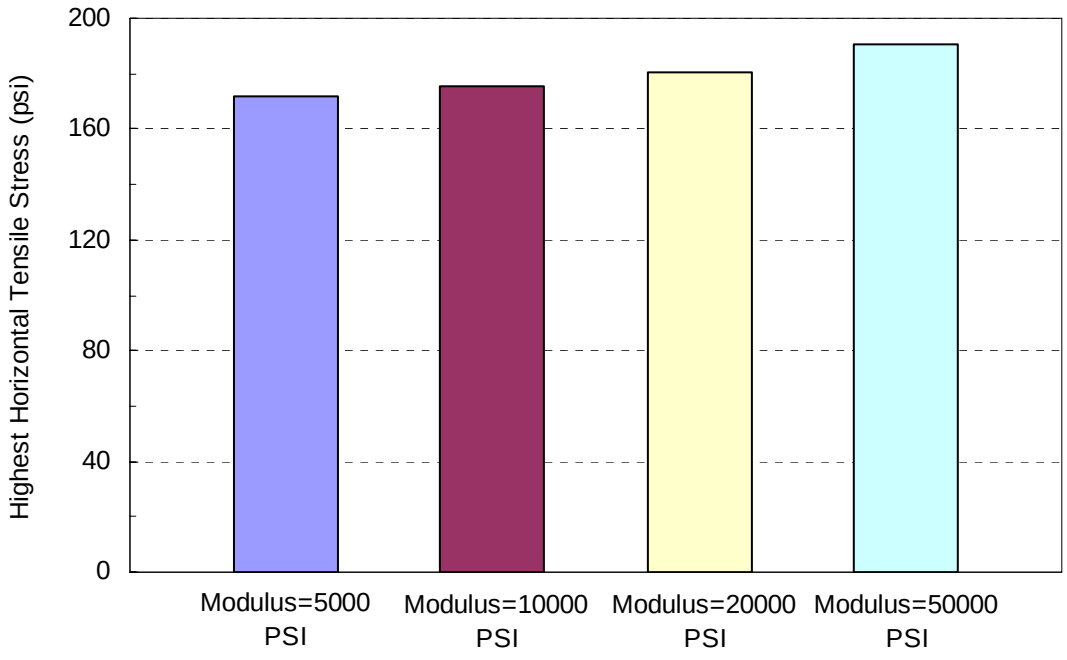

Figure 6-27 Highest Horizontal Tensile Stress Change for Different Mastic Modulus (Contact=0)

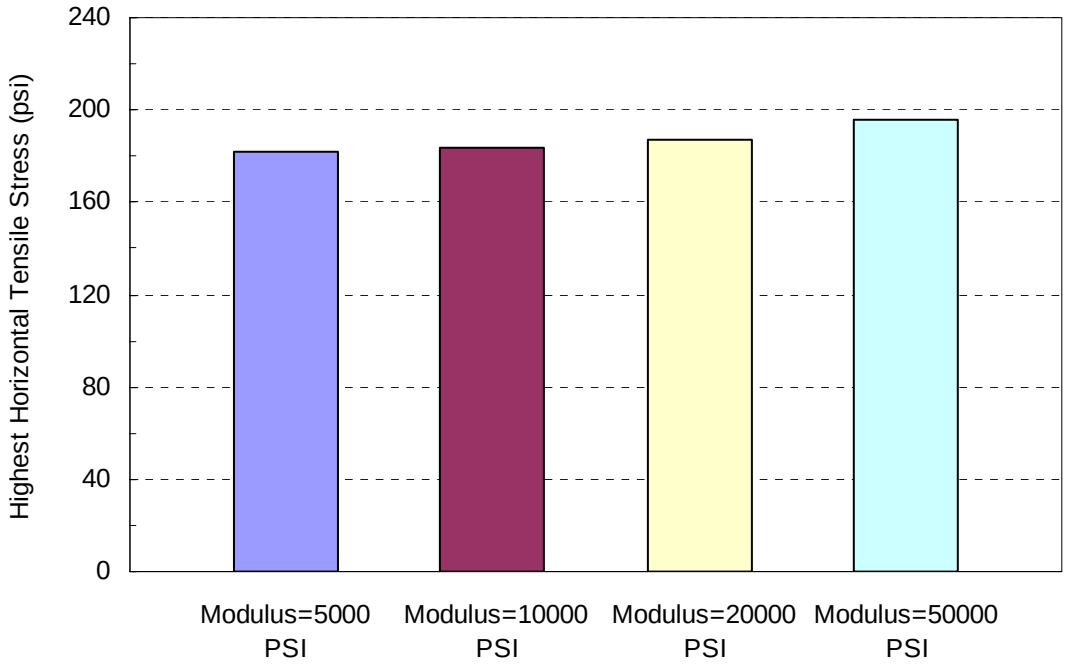

Figure 6-28 Highest Horizontal Tensile Stress Change for Different Mastic Modulus (Contact=0.02 inch)

6.2.5 Crack Growth for Different Bonding Condition

Three cases, as shown in Figure 6-29 and Figure 6-30, were considered:

Case 1: OGFC on the dense graded asphalt concrete.

Case 2: OGFC with bond on the dense graded asphalt concrete.

Case 3: OGFC with bond and film on dense graded asphalt concrete.

The film in Case 3 was 0.01 inch thick. Since the thick bond will permeate into the OGFC and partially saturate the OGFC, the 0.2 inch saturated OGFC layer was used in Case 2 and Case 3. A 0.8 inch crack was introduced in the OGFC. A displacement of 0.0019 inch, which resulted in about 136psi average stress, was applied to the global model. The stress distribution in the structure was calculated using FEM. The boundary conditions from the global model were

applied to the local model. The stress distributions in the local model were calculated using FEM. The material properties are the same as in section 6.1.

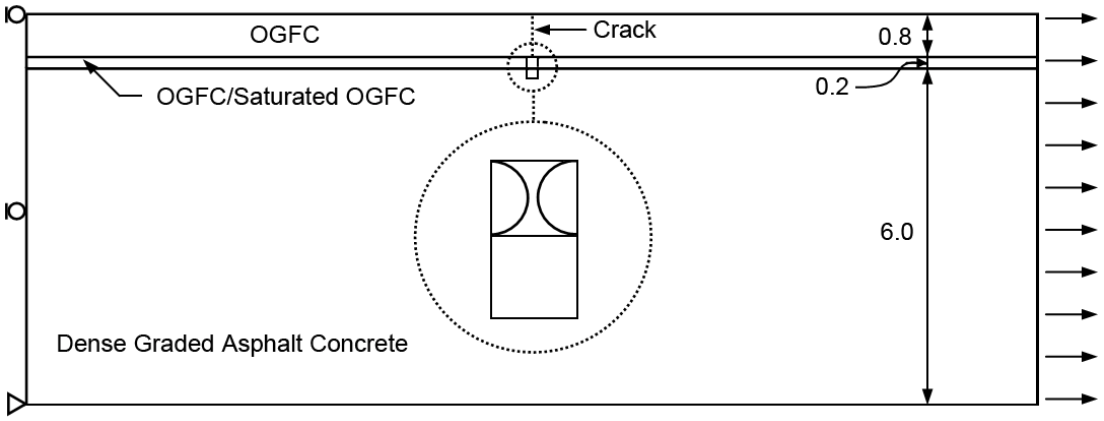

Figure 6-29 Structure Used to Calculate the Loading Cycles for Different Bonding

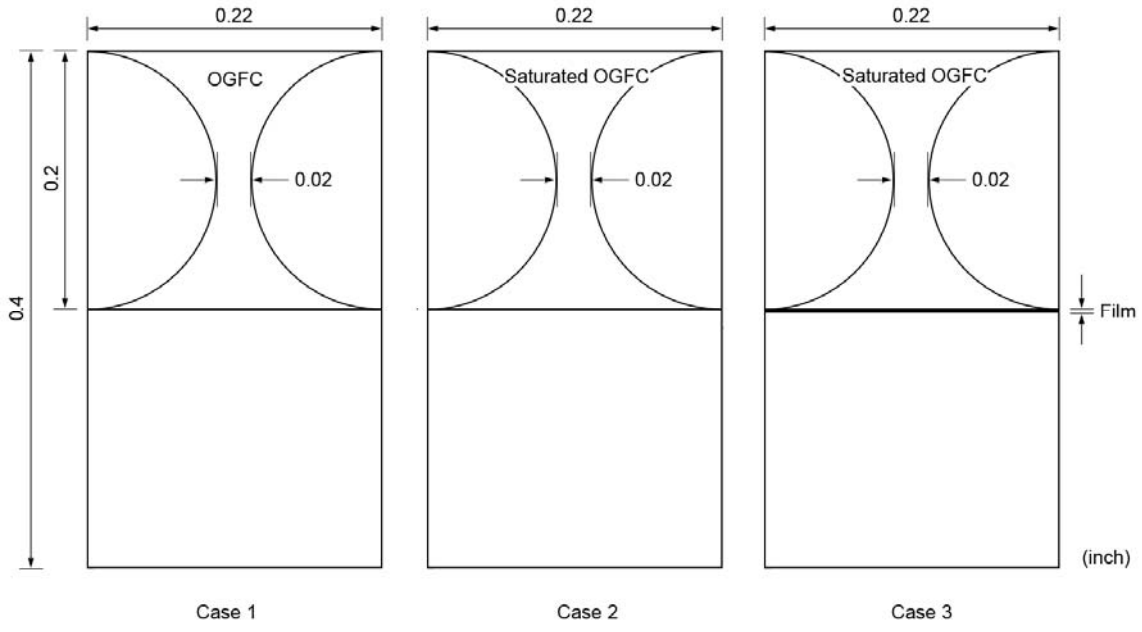

Figure 6-30 Three Local Models

The load cycles needed to create the structure in the local model were calculated using the Florida HMA cracking model. Since the size of this model was small compared to the structure discussed in 6.2, the cracking zone size was set as 0.04 inch in the local model. For each crack length, the boundary conditions of the local model were calculated from the global model with the same size crack length. The stress distribution in front of the crack tip was then calculated using FEM. The stress distribution was used to calculate the load cycles needed to crack the next zone.

Figure 6-31, Figure 6-32 and Figure 6-33 show the calculation results for three structures. As shown in Figure 6-31, OGFC with bond on dense graded asphalt concrete (Case 2) required more load cycles to create the same length crack. Figure 6-31 shows that OGFC on dense graded asphalt concrete (Case 1), only 3321 load cycles was required for first zone crack, while for Case 2 (OGFC with bond on dense graded asphalt concrete) and Case 3 (OGFC with bond and film on dense graded asphalt concrete), 5714 load cycles were required (i.e. a 72% improvement relative to traditional OGFC).

Similar trends were observed for crack propagation, where 8340 load cycles were required to advance the crack by 0.2 inch for Case 1 (OGFC on dense graded asphalt concrete) (Figure 6-32). 12375 cycles were required for Case 2 (OGFC with bond on dense graded asphalt concrete) and 13011 cycles were required for Case 3 (OGFC with bond and film on dense graded asphalt concrete). This represents an improvement of 53% for the bonded system and 56% for bond plus film.

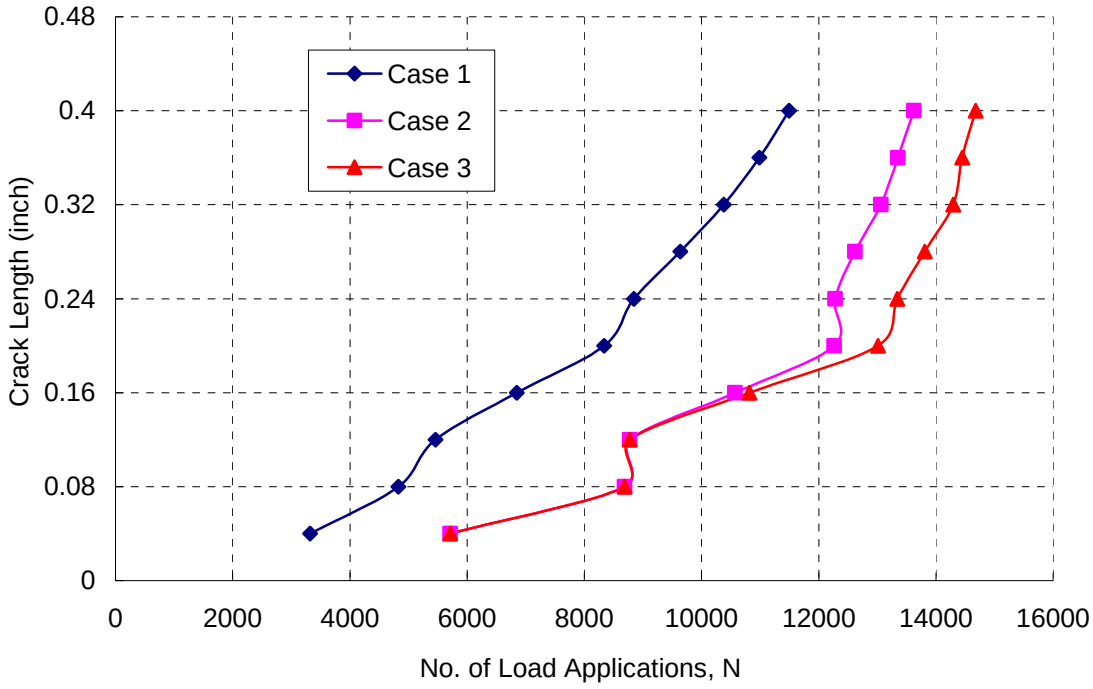

Figure 6-31 Loading Cycles with Crack Length

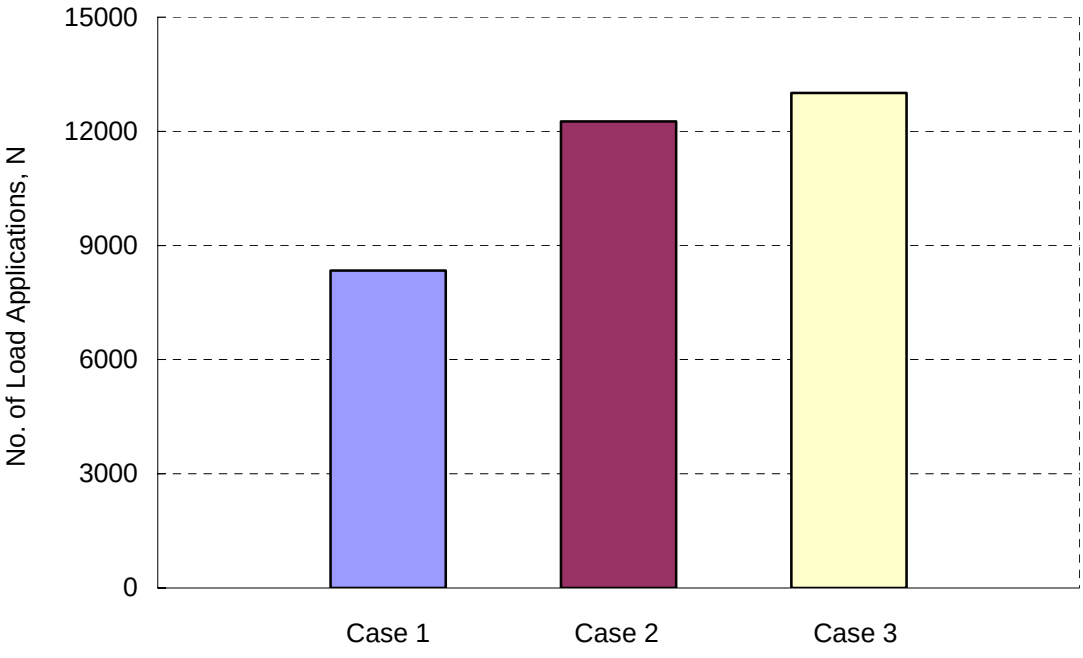

Figure 6-32 Loading Cycles to create 0.2 inch crack in the Local Model

As shown in figure 6-33 the effect is less pronounced as the crack continues to grow. This is because as crack length increases, resistance is primarily driven by the properties of the underlying HMA layer, which is the same for all cases.

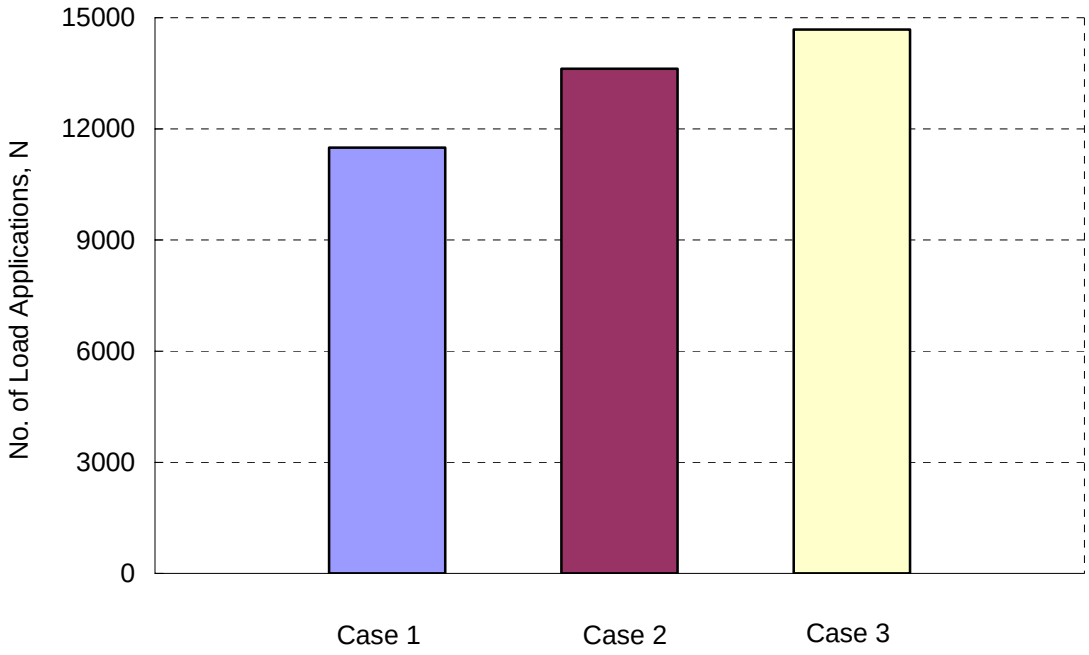

Figure 6-33 Loading Cycles to create 0.4 inch crack in the Local Model

6.2.6 Summary of Multi-scale Analysis

The effects of microstructure to the stress distribution were evaluated using the multi-scale model. The load cycles needed to create crack in the local model were calculated using the Florida HMA fracture mechanic. The key points of the multi-scale analysis are summarized as follows:

- The microstructure characteristics of the OGFC, such as the particle gap, film thickness, mastic modulus, has large effects on the stress distribution in the structure.

- The multi-scale analysis shows that the bond and film between the OGFC and underlying layer will increase the load cycles 53% to 56% to create the same size crack.

6.3 Summary

In the modeling analysis, a continuum model and a multi-scale model were developed. The continuum model and multi-scale model were used to capture the stress in the pavement structures. The Florida HMA fracture mechanics model was implemented to calculate the load cycles needed to crack the structure. The primary findings are summarized as follows:

- Continuum model shows that the OGFC layer without any bond on dense graded asphalt concrete will accelerate the cracking propagation, instead of helping structure to increase the resistance to top-down cracking.
- However, if the OGFC is bonded to the underlying layer, the load cycles will increase 25% to 41% to create a same size crack in the dense graded asphalt concrete.
- Multi-scale model analysis results indicate that the adding of bond and film will increase 53% to 56% load cycles to create a same size crack in the local model, which means the adding of bond and film will increase the cracking resistance of the structure.
- The continuum and multi-scale analysis shows high agreements with the experimental results, which was presented in Chapter 5 that the bond show 17% to 60% improvement in both crack initiation and total failure life.

CHAPTER 7
CLOSURE

7.1 Summary and Findings

This study was conducted to investigate the effects of OGFC and interface condition on top-down cracking resistance of asphalt pavement. A new dog-bone direct tension test (DBDT) was conceived, developed and validated for asphalt mixtures. Resilient modulus, creep, and strength tests were performed at multiple temperatures on dense graded and open graded asphalt mixtures with the newly developed DBDT and existing Superpave IDT. Also, a composite specimen (OGFC on HMA) direct tension test and continuum and micro-mechanics based FEM models were developed to evaluate OGFC and interface conditions on top-down cracking performance.

From individual mixture tests, the tensile properties of dense and open graded asphalt mixtures were successfully obtained with the DBDT developed, as well as with the Superpave IDT. Both tests provided reasonable and consistent test results with respect to temperature and aging. Findings associated with tension testing may be summarized as follows:

- Both Superpave IDT and DBDT test clearly showed that open graded asphalt mixture had much lower resilient modulus and failure limits (strength, failure strain, and fracture energy) than dense graded asphalt mixture.
- Resilient modulus values obtained from both Superpave IDT and DBDT were almost identical, indicating that elastic response due to rapid and repeated loading can be reliably obtained regardless of testing mode, i.e. indirect or direct.

- Absolute value and rate of creep compliance were highly correlated between Superpave IDT and DBDT but were slightly lower for Superpave IDT than for DBDT, which can be attributed to the higher confinement in Superpave IDT. It indicates that uniaxial stresses in the surface course (no confinement) accelerate tension-induced damage accumulation relative to uniaxial stresses at the bottom of the structural layer (with confinement).
- Non-uniform stress states induced in both Superpave IDT and DBDT result in the unique advantage that the failure plane is known a priori, so that tensile failure limits can be measured directly on the failure plane. This advantage mitigates the effects of non-homogeneous damage and macrocrack that might be induced in the asphalt mixture during testing using a uniform stress distribution.
- It appears that although tensile strength and failure strain between Superpave IDT and DBDT are different due to strain rate, the resulting fracture energy from the two tests is the same. This supports previous work indicating that fracture energy is a fundamental property of asphalt mixture.

Findings from tests on composite mixture may be summarized as follows:

- Results from constant displacement rate tests indicated that constant stroke rate strength tests were either too fast to identify the crack initiation point or too slow such that cracks initiated from the dense-graded side.
- Tests on asymmetric composite specimens without interlayer under repeated loading show that damage starts to accumulate in the OGFC right after loading but little or no damage is induced in dense-graded mixture until cracks propagate into

it. This indicated that significant bending was still prevalent in the asymmetric specimen.

- Symmetrical composite specimen configuration was successfully used to remove the bending induced in the asymmetric composite specimen during pulling.
- Test results show that the use of polymer modified (Novabond tack) can significantly improve cracking resistance of pavements with OGFC.

The primary findings from numerical analysis are summarized as follows:

- Continuum modeling shows that the OGFC with conventional tack only exhibited poor top-down cracking performance.
- Partial or full saturation of OGFC with a bonding agent (Novabond tack) resulted in significantly improved cracking performance.
- Multi-scale model analysis also indicated that introduction of a bonding agent (Novabond tack) and resulting film between OGFC and HMA will significantly increase cracking resistance.

7.2 Conclusion

A comprehensive evaluation of the fracture resistance of open graded asphalt mixture and bonded interface was completed. The following conclusions were based on the above findings and results:

- Open graded friction course mixture appears to reduce the cracking performance of asphalt pavement. One of potential reason is that the thresholds of fracture energy and dissipated creep strain energy for open graded asphalt mixture shows considerably lower values than dense graded asphalt mixture. This results in lower

energy ratio and less number of load cycles to create a certain length of crack obtained by HMA fracture mechanics model.

- Both Superpave IDT and the new DBDT test developed in this study provide suitable and accurate tensile properties of asphalt mixture, including open graded asphalt mixture. Thus, continued use of Superpave IDT is recommended because it is much more practical. However, a creep adjustment for values obtained from Superpave IDT should be considered for mechanisms involving uniaxial stress states. DBDT creep compliance is more appropriate for uniaxial stress states, while Superpave IDT creep compliance is more appropriate for stress states involving confinement.
- Excellent agreement in fracture energy was observed between Superpave IDT and DBDT, indicating that fundamental properties can be accurately determined using either test. This further supports that fracture energy is in fact independent of stress state, loading conditions, and specimen geometry. It is thus the most appropriate and necessary property to evaluate mixture fracture potential.
- Experimental and numerical analysis results indicate that the use of traditional open graded asphalt mixture with conventional tack coat only, appears to reduce the fracture resistance of asphalt pavement.
- Experimental and numerical analysis also indicated that OGFC performance may be improved if a polymer modified bonding agent such as Novabond tack were used.
- There are some advantages of using multi-scale analysis over other methods such as continuum analysis, because it provides a framework to optimize the amount of

bond for OGFC with underlying structural layer and is more helpful in achieving understanding with respect to cracking mechanism of the asphalt pavement.

7.3 Recommendations

Based on extensive evaluation throughout this study, the following section will present recommendations for further investigation of effect of the open graded friction course and interface condition on the top-down cracking resistance of flexible pavement system.

- The new DBDT test system and direct tension test for composite specimen developed in this study were evaluated with only laboratory produced specimens. Laboratory specimens were also used for evaluation of fracture resistance of open graded asphalt mixture and bonded interface. To acquire more insight into the crack behavior of asphalt pavement, there is need to evaluate the fracture properties of field cores gathered from various sections. Two field cores would be required for the preparation of one symmetrical composite specimen.
- Aging conditioning procedures that may capture the characteristics of OGFC and bonded interface need to be developed for more accurate and reasonable evaluation. Age hardening certainly has an influence on cracking performance of asphalt pavement and need to be properly taken into account when assessing the tensile properties of asphalt mixtures.
- Healing characteristics were also not evaluated in this study. Healing is probably one of most critical issues that need further investigation when evaluating the cracking behavior of asphalt mixtures. The physical difference of open graded asphalt mixture might result in different healing characteristics than that of dense

graded asphalt mixture. Current deficiencies in evaluating asphalt mixture can be compensated for if healing characteristics are fully integrated when evaluating asphalt mixture.

- One of the primary functions of open graded friction course is to drain the pavement quickly during rainfall events. Thus, these mixtures and bonded interface could be more affected by damage induced by water and should have suitable moisture resistance. To evaluate the moisture resistance, there is need to develop proper moisture conditioning.
- Finally, a rational design specification of open graded asphalt mixtures which integrates tensile properties needs to be developed. The design specification should be practical and feasible. It should also be integrated with pavement design and analysis process as well as address and optimize their fracture resistance and performance characteristics.

LIST OF REFERENCES

AAPA, "National Asphalt Specifications," Second Edition, Kew Victoria, Australia, 2004.

AASHTO, "Standard Method of Test for Bulk Specific Gravity of Compacted Bituminous Mixtures Using Saturated Surface-Dry Specimens," AASHTO T 166, Washington, D. C., 2001.

AASHTO, "Standard Method of Test for Percent Air Voids in Compacted Dense and Open Bituminous Paving Mixtures," AASHTO T 269, Washington, D. C., 2001.

AASHTO, "Standard Practice for Mixture Conditioning of Hot Mix Asphalt," AASHTO PP2, Washington, D. C., 2001.

ADINA User's Manual-Version 8.3, ADINA R&D, INC., Watertown, MA, 2005.

Alvarez, A. E., Martin, A. E., Estakhri, C. K., Button, J. W., Glover, C. J., and Jung, S. H., "Synthesis of Current Practrice on the Design, Construction, and Maintenance of Porous Friction Courses," FHWA/TX-06/0-5262-1, Texas Department of Transportation, Texas Transportation Institute/Texas A&M University, College Station, TX, July 2006.

Alvarez, A. E., Martin, A. E., Estakhri, C. K., Button, J. W., Kraus, Z., Prapaitrakul, N., and Glover, C. J., "Evaluation and Recommeded Improvements for Mix Design of Permeable Friction Courses," FHWA/TX-08/0-5262-3, Texas Department of Transportation, Texas Transportation Institute/Texas A&M University, College Station, TX, December 2008.

Asahi, M. and Kawamura, K., "Activities of Porous Asphalt on Expressway," Proceeding of Road Engineering Association of Asia and Australasia, Tokyo, Japan, 2000.

ASTM, "Standard Practice for Open-Graded Friction Course (OGFC) Mix Design," ASTM D 7064, West Conshohocken, PA, 2004.

ASTM, "Standard Test Method for Bulk Specific Gravity and Density of non-absorptive compacted bituminous Mixtures," ASTM D 2726, West Conshohocken, PA, 2002.

ASTM, "Standard Test Method for Bulk Specific Gravity and Density of Compacted Bituminous Mixtures Using Automatic Vacuum Sealing Method," ASTM D 6752, West Conshohocken, PA, 2002.

Baladi, G. Y., Schorsch, M., and Svasdisant, T., "Determination of Top-Down Cracks in Bituminous Pavements," MDOT-PRCE-MSU-2003-110, Michigan Department of Transportation, MI, 2002.

Bartley Consultants Ltd., "Survey of New Zealand Roading Authorities Regarding Pavement Engineering Issues," Transfund Research Report No. 143, 1999.

Bell, C. A., AbWahab, Y., and Cristi, M. E., "Investigation of Laboratory Aging Procedures for Asphalt-Aggregate Mixtures," In Transportation Research Record: Journal of the Transportation Research Board, No. 1323, National Research Council, National Academy Press, Washington, D. C., pp. 32-46, 1991.

Bensalem, A., Brown, A. J., Nunn, M. E., Merrill, D. B., and Lloyd, W. G., "Finite Element Modeling of Fully Flexible Pavement: Surface Cracking and Wheel Interaction," 2nd International Symposium on 3D Finite Element for Pavement Analysis, Design, and Research, Charleston, WV, pp. 103-113, October 2000.

Birgisson, B., Roque, R., Varadhan, A., Thai, T., and Jaiswal, L., "Evaluation of Thick Open Graded and Bonded Friction Courses for Florida," Final Report of Florida Department of Transportation, University of Florida, Gainesville, FL, March 2006.

Bolzan, P. E. and Huber, G., "Direct Tension Test Experiments," SHRP-A-641, Strategic Highway Research Program, Transportation Research Board, National Research Council, Washington, D.C. 1993.

Bolzan, P. E., Nicholls, J. C., and Huber, G. A., "Searching for Superior Performing Porous Asphalt Wearing Courses," Transportation Research Board, National Research Council, Washington, D. C., 2001.

Bowskill, G. J. and Colwill, D. M., "Experience with porous asphalt in the United Kingdom" In Proceedings of the European Conference on Porous Asphalt, Madrid, Spain, 1997.

Buchanan, M. S., "An Evaluation of Selected Methods to Determine the Bulk Specific Gravity of Compacted Hot Mix Asphalt (HMA)," Journal of the Association of Asphalt Paving Technologists, Vol. 68, pp. 608-634, 1999.

Buttlar, W. G., Al-Khateeb, G. G., and Bozkurt, D., " Development of a Hollow Cylinder Tensile Tester to Obtain Mechanical Properties of Bituminous Paving Mixtures," Journal of the Association of Asphalt Paving Technologists, Vol. 68, pp. 369-403, 1999.

Buttlar, W. G. and Roque, R., "Development and Evaluation of the Strategic Highway Research Program Measurement and Analysis System for Indirect Tensile Testing at Low Temperatures," In Transportation Research Record: Journal of the Transportation Research Board, No. 1454, National Research Council, National Academy Press, Washington, D. C., pp. 163-171, 1994.

Buttlar, W. G., Wagoner, M. P., You, Z., and Brovold, S. T., " Simplifying the Hollow Cylinder Tensile Test Procedure through Volume-Based Strain," Journal of the Association of Asphalt Paving Technologists, Vol. 73, pp. 367-400, 2004.

Chang, C., Baladi, G. Y. and Wolff, T. F., "Detecting Segregation in Bituminous Pavements," In Transportation Research Record: Journal of the Transportation Research Board, No.

1813, National Research Council, National Academy Press, Washington, D. C., pp. 77-86, 2002.

Chehab, G. R., O'Quinn, E., and Kim, Y. R., "Specimen Geometry Study for Direct Tension Test Based on Mechanical Tests and Air Void Variation in Asphalt Concrete Specimens Compacted by Superpave Gyratory Compactor," In Transportation Research Record: Journal of the Transportation Research Board, No. 1723, National Research Council, National Academy Press, Washington, D. C., pp. 125-132, 2000.

Cooley, L. A., Brwon, E. R., and Watson, D. E., "Evaluation of OGFC Mixtures Containing Cellulose Fibers," NCAT Report 00-05, National Center for Asphalt Technology, Auburn, AL, 2000.

Cooley, L. A., Prowell, B. D., Hainin, M. R., Buchanan, M. S., and Harrington, J., "Bulk Specific Gravity Round Robin Using the Corelok Vacuum Sealing Device," NCAT Report 02-11, National Center for Asphalt Technology, Auburn, AL, 2002.

Crouch, L. K., Copeland, A. R., Walker, C. T., Maxwell, R. A., Duncan, G. M., Goodwin, W. A., Badoe, D. A., Leimer, H. W., "Determining Air Void Content of Compacted Hot-Mix Asphalt Mixtures," In Transportation Research Record: Journal of the Transportation Research Board, No. 1813, National Research Council, National Academy Press, Washington, D. C., pp. 39-46, 2002.

Choubane, B., Sholar, G. A., Musselman, J. A., and Page, G. C., "Long Term Performance Evaluation of Asphalt-Rubber Surface Mixes," Research Report of Florida Department of Transportation 98-431, Gainesville, FL, November 1998.

Dauzats, M. and Rampal, A., "Mechanism of Surface Cracking in Wearing Courses," 6th International Conference Structural Design of Asphalt Pavements, The University of Michigan, Ann Arbor, MI, pp. 232-247, July 1987.

De Beer, M., Fisher, C., and Jootse, F. J., " Determination of Pneumatic Tyre/Pavement Interface Contact Stresses under Moving Loads and Some Effects on Pavement with Thin Asphalt Surfacing Layers," 8th International Conference on Asphalt Pavements, University of Washington, Seattle, WA, pp. 179-227, August 1997.

De Freitas, E. F., Pereira, P., Picado-Santos, L. and Papagiannakis, A. T., "Effect of Construction Quality, Temperature and Rutting on Initiation of Top-Down Cracking," In Transportation Research Record: Journal of the Transportation Research Board, No. 1929, National Research Council, National Academy Press, Washington, D. C., pp. 174-182, 2005.

De Freitas, E. F., Pereira, P., and Picado-Santos, L., "Assessement of Top-Down Cracking Causes in Asphalt Pavements," 3th International Symposium on Maintenance and Rehabilitation of Pavements and Technical Control, Guimaraes, Portugal, 2003.

FAA, "Standards for Specifying Construction of Airports," Advisory Circular No. 150/5370-10B, US Department of Transportation, Washington, D. C., 2005.

FDOT, “Standard Specifications for Road and Bridge Construction,” Florida Department of Transportation, Tallahassee, FL, 2007.

Francken, L., “Fatigue Performance of a Bituminous Road Mix under Realistic Test Conditions,” In Transportation Research Record: Journal of the Transportation Research Board, No. 712, National Research Council, National Academy Press, Washington, D. C., pp. 30-36, 1979.

Gerritsen, A. H., van Gurp, C. A. P. M., van der Heide, J. P. J., Molenaar, A. A. A., and Pronk, A.C., “Prediction and Prevention of Surface Cracking in Asphaltic Pavements,” 6th International Conference Structural Design of Asphalt Pavements, The University of Michigan, Ann Arbor, MI, pp. 378-391, July 1987.

Haas, R. C. G., "A Method for Designing Asphalt Pavements to Minimize Low -Temperature Shrinkage Cracking". The Asphalt Institute Research Report 73-1 (RRR-73-1), January 1973.

Halstead, W. J., “Open-Graded Friction Courses for Highways,” National Cooperative Highway Research Program (NCHRP) Synthesis 49, Transportation Research Board, National Research Council, Washington, D. C., 1978.

Harvey, J., Eriksen, K., Sousa, J., and Monismith, C. L., “Effects of Laboratory Specimen Preparation on Aggregate-Asphalt Structure, Air-Void Content Measurement, and Repetitive Simple Shear Test Results,” In Transportation Research Record: Journal of the Transportation Research Board, No. 1454, National Research Council, National Academy Press, Washington, D. C., pp. 113-122, 1994.

Himeno, K., Ikeda, T., Kamijima, T., and Abe, T., “Distribution of Tire Contact Pressure of Vehicles and Its Influence on Pavement Distress,” 8th International Conference on Asphalt Pavements, University of Washington, Seattle, WA, pp. 129-139, August 1997.

Huber, G., “Performance Survey on Open-Graded Friction Course Mixes,” Synthesis of Highway Practice 284, Transportation Research Board, National Research Council, Washington, D. C., 2000.

Huang, B. and Shu, X., “Laboratory Evaluation of Semi-Circular Bending Tensile Strength Test for HMA Mixtures,” Transportation Research Board, National Research Council, Washington, D. C., 2005.

InstroTek, “Corelok Operator’s Guide,” InstroTek, Raleigh, NC, July 2003.

Jacobs, M. M., “Crack Growth in Asphaltic Mixes,” Ph.D. Dissertation, Delft University of Technology, The Netherlands, 1995.

Jones, R.M., “Mechanics of Composite Materials,” McGraw-Hill, 1980.

Kandhal, P. S., and Mallick, R. B., "Open Graded Asphalt Friction Course: State of the Practice," NCAT Report 98-7, National Center for Asphalt Technology, Auburn, AL, 1998.

Kandhal, P. S., "Design, Construction, and Maintenance of Open-Graded Asphalt Friction Courses," NAPA Information Series 115, National Asphalt Pavement Association, Lanham, MD, 2002.

Khalid, H. and Walsh, C., "A Rational Mix Design Method for Porous Asphalt," 24th European Transport Forum, London, UK, 1996.

Kim, J., "Accurate Determination of Dissipated Creep Strain Energy and Its Effect on Load- and Temperature-Induced Cracking of Asphalt Pavement," Ph.D. Dissertation, University of Florida, Gainesville, FL, 2005.

Kim, Y. R., Daniel, J. S., and Wen, H., "Fatigue Performance Evaluation of WesTrack Asphalt Mixtures Using Viscoelastic Continuum Damage Approach," Final Report of North Carolina Department of Transportation, North Carolina State University, Raleigh, NC, April 2002.

Komoriya, K., Yoshida T. and Nitta, H., "WA-DA-CHI-WA-RE" Surface Longitudinal Cracks on Asphalt Concrete Pavement," Transportation Research Board, National Research Council, Washington, D. C., 2001.

Kowalski, K. J., McDaniel, R. S., Shah, A., and Olek, J., "Long Term Monitoring of the Noise and Friction Properties of PFC, SMA, and DGA Pavements," Transportation Research Board, National Research Council, Washington, D. C., 2009.

Kraemer, C., "Porous asphalt: Past and Present," In Proceedings of the European Conference on Porous Asphalt, Madrid, Spain, 1997.

Li, X. and Marasteanu, M., "Evaluation of the Low Temperature Fracture Resistance of Asphalt Mixtures Using the Semi Circular Bend Test," Journal of the Association of Asphalt Paving Technologists, Vol. 73, pp. 401-426, 2004.

Mallick, R. B., Kandhal, P. S., Cooley, L. A. Jr., and Watson, D. E., "Design, Construction, and Performance of New Generation Open Graded Friction Courses," Journal of the Association of Asphalt Paving Technologists, Vol. 69, pp. 391-422, 2000.

Mallick, R., Kandhal, P., Cooley, A., and Watson, D., "Design, Construction and Performance of New Generation Open-Graded Friction Courses," National Center for Asphalt Technology Report 00-01, NCAT, Auburn, AL, 2000.

Martin, K. L., Davison, C. J., and Bullin, J. A., "Asphalt Aging in Texas Roads and Test Sections," In Transportation Research Record: Journal of the Transportation Research Board, No. 1269, National Research Council, National Academy Press, Washington, D. C., pp. 9-19, 1990.

Matsuno, S. and Nishizawa, T., "Mechanism of Longitudinal Surface Cracking in Asphalt Pavement," 7th International Conference on Asphalt Pavements, Vol. 2, University of Nottingham, UK, pp. 277-291, 1992.

McDaniel, R. S. and Thornton W. D., "Field Evaluation of a Porous Friction Course for Noise Control," Transportation Research Board, National Research Council, Washington, D. C., 2005.

McDaniel, R. S., Thornton, W. D., and Dominguez, J. G., "Field Evaluation of Porous Asphalt Pavement," SQDH 2004-3, Final Report of The Institute for Safe, Quiet, and Durable Highways at the Purdue University, West Lafayette, IN, May 2004.

Molenaar, A. A. A., "Fatigue and Reflective Cracking due to Traffic," Journal of the Association of Asphalt Paving Technologists," Vol. 53, pp. 440-474, 1984.

Myers, L. A., "Development and Propagation of Surface-Initiated Longitudinal Wheel Path Cracks in Flexible Highway Pavements," Ph.D. Dissertation, University of Florida, Gainesville, FL, 2000.

Myers, L. A. and Roque, R., "Top-Down Crack Propagation in Bituminous Pavements and Implications for Pavement Management," Journal of the Association of Asphalt Paving Technologists, Vol. 71, pp. 651-670, 2002.

Myers, L. A., Roque, R. and Birgisson B., "Propagation Mechanisms for Surface-Initiated Longitudinal Wheel Path Cracks," In Transportation Research Record: Journal of the Transportation Research Board, No. 1778, National Research Council, National Academy Press, Washington, D. C., pp. 113-122, 2001.

Myers, L. A., Roque, R., and Ruth, B. E., "Mechanisms of Surface-Initiated Longitudinal Wheel Path Cracks in High-Type Bituminous Pavements," Journal of the Association of Asphalt Paving Technologists, Vol. 67, pp. 401-432, 1998.

Myers, L. A., Roque, R., Ruth, B. E. and Drakos, C. A, "Measurement of Contact Stresses for Different Truck Types to Evaluate Their Influence on Near-Surface Cracking and Rutting," In Transportation Research Record: Journal of the Transportation Research Board, No. 1655, National Research Council, National Academy Press, Washington, D. C., pp. 175-184, 1999.

Nunn, M., "Design of Long-Life Roads for Heavy Traffic," Industry Conference, Australian Asphalt Pavement Association, Surfers Paradise, Queensland, Australia, 1998.

Perez-Jimenez, F. E. and Gordillo, J., " Optimization of Porous Mixes through the Use of Special Binders," In Transportation Research Record: Journal of the Transportation Research Board, No. 1265, National Research Council, National Academy Press, Washington, D. C., pp. 59-68, 1990.

Poulikakos, L. D., Pittet, M., M., Arnaud, Junod, A., Gubler, R., Simond, E., Partl, L., and Dumont, A., and "Mechanical Properties of Porous Asphalt, Recommendations for

Standardization," Swiss Federal Laboratory for Materials Testing and Research (EMPA) and Ecole Polytechnique Federale de Lausanne (EPFL)-Laboratoire des voies de circulation (LAVOC), December 2006.

Raju, S. Kumar, S. S., Reddy, K. S., Bose, S., and Pandey, B. B., "Analysis of Top-Down Cracking Behavior of Asphalt Pavements," Transportation Research Board, National Research Council, Washington, D. C., 2008.

Romanoschi, S. A., "Characterization of Pavement Layer Interfaces," Ph.D. Dissertation, Louisiana State University, Baton Rouge, LA, 1999.

Romeo, E., "Measurement and Prediction of Fundamental Tensile Failure Limits of Hot Mix Asphalt (HMA)," Ph.D. Dissertation, University of Florida, Gainesville, FL, 2008.

Roque, R., Birgisson, B., Drakos, C. A., and Dietrich, B., "Development and Field Evaluation of Energy-Based Criteria for Top-Down Cracking Performance of Hot Mix Asphalt," Journal of the Association of Asphalt Paving Technologists, Vol. 73, pp. 229-260, 2004a.

Roque, R., Birgisson, B., Tia, M., Kim, B., and Cui, Z., " Guidelines for Use of Modifiers in Superpave Mixtures," Final Report of Florida Department of Transportation, University of Florida, Gainesville, FL, January 2004b.

Roque, R. and Buttlar, W. G., "The Development of a Measurement and Analysis System to Accurately Determine Asphalt Concrete Properties Using the Indirect Tensile Mode," Journal of the Association of Asphalt Paving Technologists, Vol. 61, pp. 304-332, 1992.

Roque, R., Buttlar, W. G., Ruth, B. E., Tia, M., Dickson, S. W., and Reid, B., "Evaluation of SHRP Indirect Tension Tester to Mitigate Cracking in Asphalt Pavements and Overlays," Final Report of Florida Department of Transportation, University of Florida, Gainesville, FL, August 1997.

Roque, R., Hardee, H., and Ruth, B. E., "Thermal Rippling of Asphalt Concrete Pavements," Journal of the Association of Asphalt Paving Technologists," Vol. 57, pp. 464-483, 1988.

Roque, R. and Ruth, B. E., "Mechanisms and Modeling of Surface Cracking in Asphalt Pavements," Journal of the Association of Asphalt Paving Technologists," Vol. 59, pp. 396-421, 1990.

Ruiz, A., Alberola, R., Perez, F., and Sanchez, B., "Porous Asphalt Mixtures in Spain," In Transportation Research Record: Journal of the Transportation Research Board, No. 1265, National Research Council, National Academy Press, Washington, D. C., pp. 87-94, 1990.

Sabita, "The Design and Use of Porous Asphalt Mixes," Manual 17, Roggebaai, South Africa, 1995.

Schorsch, M., Chang, C. and Baladi G. Y., "Effects of Segregation on the Initiation and Propagation of Top-Down Cracks," Transportation Research Board, National Research Council, Washington D.C., 2003.

Sedwick, S. C., "Effect of Asphalt Mixture Properties and Characteristics on Surface-Initiated Longitudinal Wheel Path Cracking," Master's Thesis, University of Florida, Gainesville, FL, 1998.

Shashidhar, N., "X-Ray Tomography of Asphalt Concrete," In Transportation Research Record: Journal of the Transportation Research Board, No. 1681, National Research Council, National Academy Press, Washington, D. C., pp. 186-192, 1999.

Suresha, S. N., Varghese, G., and Shankar, A. U. R., "A Comparative Study on Properties of Porous Friction Course Mixes with Neat Bitumen and Modified Binders," International Journal of Construction and Building Materials, Vol. 23, pp. 1211-1217, 2009.

Svasdisant, T., Schorsch, M., Baladi G. Y., and Pinyosunun, S., "Mechanistic Analysis of Top-Down Cracking in Asphalt Pavement," In Transportation Research Record: Journal of the Transportation Research Board, No. 1809, National Research Council, National Academy Press, Washington, D. C., pp. 126-136, 2002.

Swart, J. H., "Experiences with Porous Asphalt in the Netherlands," In Proceedings of the European Conference on Porous Asphalt, Madrid, Spain, 1997.

Tappeiner, W., "Open-Graded Asphalt Friction Course," NAPA Information Series 115, National Asphalt Pavement Association, Lanham, MD, 1993.

Thai, T. T., " Approaches for using Open-Graded Friction Courses for Paving Florida's Highways," Master Thesis, University of Florida, Gainesville, FL, 2005.

TNZ, "Specification for Open Graded Porous Asphalt," SP/SP11 070704, 2007.

Uchida K., Kurokawa, T., Himeno, K. and Nishizawa, T., "Healing Characteristics of Asphalt Mixture under High Temperature Conditions," 9th International Conference on Asphalt Pavements, Copenhagen, 2002.

Uhlmeyer, J. S., Willoughby, K., Pierce, L. M. and Mahoney, J. P., "Top-Down Cracking in Washington State Asphalt Concrete Wearing Courses," In Transportation Research Record: Journal of the Transportation Research Board, No. 1730, National Research Council, National Academy Press, Washington, D. C., pp. 110-116, 2000.

van der Zwan, J. Th., Goeman, Th., Gruis, H. J. A. J., Swart, J. H., and Oldenburger, R. H., "Porous Asphalt Wearing Courses in the Netherlands: State of the Art Review," In Transportation Research Record: Journal of the Transportation Research Board, No. 1265, National Research Council, National Academy Press, Washington, D. C., pp. 95-110, 1990.

van Heystraeten, G. and Moraux, C., "Ten Years' Experience of Porous Asphalt in Belgium," In Transportation Research Record: Journal of the Transportation Research Board, No. 1265, National Research Council, National Academy Press, Washington, D. C., pp. 34-40, 1990.

Varadhan, A., "Evaluation of Open Graded and Bonded Friction Course for Florida," Master's Thesis, University of Florida, Gainesville, FL, 2004.

Verhaeghe, B. M. J. A., Rust, F. C., Vos, R. M., and Visser, A. T., " Properties of Polymer- and Fibre-Modified Porous Asphalt Mixes," 6th Conference on Asphalt Pavements for Southern Africa, Cape Town, South Africa, October 1994.

Voskuilen, J. L. M., Tolman, F., and Rutten, E., "Do Modified Porous Asphalt Mixture Have a Longer Service Life?" 3rd Eurasphalt and Eurobitume Congress, Vienna, Austria, May 2004.

Wagoner, M. P., Buttlar, W. G., Paulino, G. H., and Blankenship, P., "Investigation of the Fracture Resistance of Hot-Mix Asphalt Concrete Using a Disk-Shaped Compact Tension Test," In Transportation Research Record: Journal of the Transportation Research Board, No. 1929, Transportation Research Board of the National Academies, Washington, D.C., pp. 183-192, 2005.

Wagoner, M. P., Buttlar, W. G., Paulino, G. H., and Blankenship, P., "Laboratory Testing Suite for Characterization of Asphalt Concrete Mixtures Obtained from Field Cores," Journal of the Association of Asphalt Paving Technologists, Vol. 75, pp. 815-851, 2006.

Wambura, J. H. , Mania, J., and Smith, H. R., "Kenya Bituminous Materials Study", In Transportation Research Record: Journal of the Transportation Research Board, No. 1681, Transportation Research Board of the National Academies, Washington, D.C., pp. 129-137, 1999.

Wang, H. and Flintsch, G. W., "Investigation of Short and Long-Term Variations of Pavement Surface Characteristics at the Virginia Smart Road," Transportation Research Board, Washington, D. C., 2007.

Wen, H. and Kim, Y. R., "A Simple Performance Test for Fatigue Cracking and Validation with WesTrack Mixtures," In Transportation Research Record: Journal of the Transportation Research Board, No. 1789, National Research Council, National Academy Press, Washington, D. C., pp. 66-72, 2002.

Zhang, Z., "Identification of Suitable Crack Growth Law for Asphalt Mixtures Using the Superpave Indirect Tensile Test (IDT)," Ph.D. Dissertation, University of Florida, Gainesville, FL, 2000.

Zhang, Z., Roque, R., Birgisson, B., and Sangpetngam, B., "Identification and Verification of a Suitable Crack Growth Law," Journal of the Association of Asphalt Paving Technologists, Vol. 70, pp. 206-241, 2001.

APPENDIX A
LABORATORY MIXTURES INFOMATION

Table A-1 JMF for Georgia Granite Dense Gradation

Sieve (mm)	Sieve Size	# 78 Stone	# 89 Stone	W-10 Screenings	Local Sand	JMF
		33%	7%	50%	10%	100%
19.0	3/4”	100.0	100.0	100.0	100.0	100.0
12.5	1/2”	97.0	100.0	100.0	100.0	99.0
9.5	3/8”	59.0	99.7	100.0	100.0	86.5
4.75	# 4	9.0	30.0	100.0	100.0	65.1
2.36	# 8	4.0	4.0	70.0	100.0	46.6
1.18	# 16	2.0	2.0	42.0	100.0	31.8
0.600	# 30	2.0	1.0	25.0	94.0	22.6
0.300	# 50	1.0	1.0	16.0	53.0	13.7
0.150	# 100	1.0	1.0	10.0	11.0	6.5
0.075	# 200	1.0	1.0	7.0	3.0	4.2
0	Pan	0.0	0.0	0.0	0.0	0.0
G_{sb}		2.809	2.799	2.77	2.626	2.770

Table A-2 JMF for Florida Limestone Open Gradation

Sieve (mm)	Sieve Size	S1A	S1B	Screenings	Filler	JMF
		44.7%	49.4%	3.2%	2.7%	100%
19.0	3/4”	100.0	100.0	100.0	100.0	100.0
12.5	1/2”	79.0	100.0	100.0	100.0	90.6
9.5	3/8”	36.0	92.0	100.0	100.0	67.4
4.75	# 4	7.0	26.0	100.0	100.0	21.9
2.36	# 8	3.0	7.0	68.0	100.0	9.7
1.18	# 16	3.0	3.0	67.0	100.0	7.7
0.600	# 30	3.0	3.0	55.0	100.0	7.3
0.300	# 50	3.0	2.0	35.0	100.0	6.1
0.150	# 100	2.0	2.0	14.0	100.0	5.0
0.075	# 200	1.0	1.0	3.0	100.0	3.7
0	Pan	0.0	0.0	0.0	0.0	0.0
G_{sb}		2.425	2.451	2.527	2.600	2.445

Table A-3 JMF for Nova Scotia Granite Open Gradation

Sieve (mm)	Sieve Size	# 7	# 789	Screenings	Hydrated Lime	JMF
		76.7%	11.7%	10.6%	1.0%	100%
19.0	3/4”	100.0	100.0	100.0	100.0	100.0
12.5	1/2”	95.0	100.0	100.0	100.0	96.2
9.5	3/8”	64.0	92.0	100.0	100.0	71.5
4.75	# 4	11.0	20.0	97.0	100.0	22.1
2.36	# 8	3.0	5.0	68.0	100.0	11.1
1.18	# 16	2.0	3.0	43.0	100.0	7.4
0.600	# 30	2.0	3.0	28.0	100.0	5.9
0.300	# 50	2.0	3.0	18.0	100.0	4.8
0.150	# 100	2.0	3.0	11.0	100.0	4.1
0.075	# 200	1.1	2.5	8.0	100.0	3.0
0	Pan	0.0	0.0	0.0	0.0	0.0
G_{sb}		2.627	2.633	2.580	2.600	2.622

Table A-4 Batch Weight for Georgia Granite Dense Gradation

Sieve (mm)	Sieve Size	Retained Weight, g			
		# 78 Stone	# 89 Stone	W-10 Screenings	Local Sand
19.0	3/4"	0.0	1,485.0	1,800.0	4,050.0
12.5	1/2"	44.6	1,485.0	1,800.0	4,050.0
9.5	3/8"	608.9	1,485.9	1,800.0	4,050.0
4.75	# 4	1,351.4	1,705.5	1,800.0	4,050.0
2.36	# 8	1,425.6	1,787.4	2,475.0	4,050.0
1.18	# 16	1,455.3	1,793.7	3,105.0	4,050.0
0.600	# 30	1,455.3	1,796.9	3,487.5	4,077.0
0.300	# 50	1,470.2	1,796.9	3,690.0	4,261.5
0.150	# 100	1,470.2	1,796.9	3,825.0	4,450.5
0.075	# 200	1,470.2	1,796.9	3,892.5	4,486.5
0	Pan	1,485.0	1,800.0	4,050.0	4,500.0
Sum		1,485	315	2,250	450

Table A-5 Batch Weight for Florida Limestone Open Gradation

Sieve (mm)	Sieve Size	Retained Weight, g			
		S1A	S1B	Screenings	Filler
19.0	3/4"	0.0	2,011.5	4,234.5	4,378.5
12.5	1/2"	422.4	2,011.5	4,234.5	4,378.5
9.5	3/8"	1,287.4	2,189.3	4,234.5	4,378.5
4.75	# 4	1,870.7	3,656.5	4,234.5	4,378.5
2.36	# 8	1,951.2	4,078.9	4,280.6	4,378.5
1.18	# 16	1,951.2	4,167.8	4,282.0	4,378.5
0.600	# 30	1,951.2	4,167.8	4,299.3	4,378.5
0.300	# 50	1,951.2	4,190.0	4,328.1	4,378.5
0.150	# 100	1,971.3	4,190.0	4,358.3	4,378.5
0.075	# 200	1,991.4	4,212.3	4,374.2	4,378.5
0	Pan	2,011.5	4,234.5	4,378.5	4,500.0
Sum		2,011.5	2,223.0	144.0	121.5

Table A-6 Batch Weight for Nova Scotia Granite Open Gradation

Sieve (mm)	Sieve Size	Retained Weight, g			
		# 7	# 789	Screenings	Hydrated Lime
19.0	3/4"	0.0	3,451.5	3,978.0	4,455.0
12.5	1/2"	172.6	3,451.5	3,978.0	4,455.0
9.5	3/8"	1,242.5	3,493.6	3,978.0	4,455.0
4.75	# 4	3,071.8	3,872.7	3,992.3	4,455.0
2.36	# 8	3,348.0	3,951.7	4,130.6	4,455.0
1.18	# 16	3,382.5	3,962.2	4,249.9	4,455.0
0.600	# 30	3,382.5	3,962.2	4,321.4	4,455.0
0.300	# 50	3,382.5	3,962.2	4,369.1	4,455.0
0.150	# 100	3,382.5	3,962.2	4,402.5	4,455.0
0.075	# 200	3,413.5	3,964.8	4,416.8	4,455.0
0	Pan	3,451.5	3,978.0	4,455.0	4,500.0
Sum		3,451.5	526.5	477.0	45.0

APPENDIX B
SUPERPAVE IDT TEST RESULTS

Table B-1 Superpave IDT Test Results for Dense Graded Asphalt Mixtures

Types/ Aging Con.	Temp.	m-value	D_1 (1/psi)	St (Mpa)	M_R (Gpa)	FE (kJ/m^3)	$DCSE_f$ (kJ/m^3)	Creep Rate (1/psi-sec)	D(t) (1/GPa)	Failure Strain (με)
Dense (Unmod) ST	-10°C	0.514	3.54E-08	3.51	22.21	0.80	0.52	6.33E-10	0.225	398.41
	0°C	0.529	2.25E-07	3.05	15.28	1.80	1.50	4.59E-09	1.330	870.23
	5°C	0.632	2.27E-07	2.79	13.55	2.70	2.41	1.13E-08	2.673	1289.29
	10°C	0.668	4.77E-07	2.14	10.85	4.20	3.99	3.20E-08	7.055	2566.05
Dense (Unmod) LT	-10°C	0.391	7.19E-08	3.95	22.26	1.00	0.65	4.18E-10	0.204	404.23
	0°C	0.479	1.66E-07	3.56	18.43	1.70	1.36	2.18E-09	0.735	751.07
	5°C	0.490	2.36E-07	3.02	15.66	2.40	2.11	3.41E-09	1.082	1120.48
	10°C	0.532	4.48E-07	2.25	11.99	2.20	1.99	9.43E-09	2.619	1336.78
Dense (Mod) ST	-10°C	0.334	1.57E-07	3.72	21.40	1.10	0.78	5.24E-10	0.282	515.24
	0°C	0.423	3.57E-07	3.20	17.40	2.30	2.01	2.81E-09	1.013	1038.17
	5°C	0.473	5.89E-07	2.81	11.98	4.50	4.17	7.31E-09	2.304	2180.68
	10°C	0.534	7.54E-07	2.23	10.55	5.50	5.26	1.61E-08	4.414	3326.20
Dense (Mod) LT	-10°C	0.306	5.89E-08	3.84	23.88	0.80	0.49	1.49E-10	0.117	348.31
	0°C	0.360	2.27E-07	3.55	17.40	2.40	2.04	9.79E-10	0.443	974.00
	5°C	0.380	3.66E-07	2.99	15.97	3.00	2.72	1.93E-09	0.788	1434.74
	10°C	0.413	5.43E-07	2.59	11.37	3.50	3.21	3.88E-09	1.414	1824.64

Table B-2 Superpave IDT Test Results for Open Graded Asphalt Mixtures

Types/ Aging Con.	Temp.	m-value	D_1 (1/psi)	St (Mpa)	M_R (Gpa)	FE (kJ/m^3)	$DCSE_f$ (kJ/m^3)	Creep Rate (1/psi-sec)	D(t) (1/GPa)	Failure Strain (με)
FC-5 (FLime) ST	-10°C	0.229	3.84E-07	1.97	11.47	0.40	0.23	4.28E-10	0.317	315.03
	0°C	0.400	4.80E-07	1.67	9.84	0.50	0.36	3.06E-09	1.185	448.59
	5°C	0.497	6.20E-07	1.36	8.16	0.90	0.79	9.58E-09	2.879	881.90
	10°C	0.533	5.87E-07	1.45	9.10	1.20	1.08	1.25E-08	3.500	1058.80
FC-5 (FLime) LT	-10°C	0.189	2.65E-07	2.07	14.71	0.30	0.15	1.85E-10	0.180	285.21
	0°C	0.324	4.46E-07	1.93	11.35	0.50	0.34	1.35E-09	0.670	446.92
	5°C	0.421	4.69E-07	1.72	10.35	0.90	0.76	3.62E-09	1.324	773.89
	10°C	0.427	6.26E-07	1.57	10.16	1.10	0.98	5.13E-09	1.824	1013.60
FC-5 (NGran) ST	-10°C	0.292	3.46E-07	1.44	11.06	0.20	0.11	7.63E-10	0.433	259.18
	0°C	0.431	3.72E-07	1.39	9.39	0.40	0.30	3.15E-09	1.135	447.62
	5°C	0.508	6.69E-07	1.36	8.84	0.80	0.70	1.14E-08	3.387	838.63
	10°C	0.557	8.38E-07	1.17	6.93	1.30	1.20	2.19E-08	5.828	1499.10
FC-5 (NGran) LT	-10°C	0.223	4.65E-07	1.44	11.69	0.20	0.11	4.85E-10	0.351	251.72
	0°C	0.355	5.25E-07	1.34	9.25	0.30	0.20	2.17E-09	0.943	400.95
	5°C	0.442	7.13E-07	1.38	8.83	0.90	0.79	6.69E-09	2.275	805.92
	10°C	0.555	7.47E-07	1.27	7.29	1.10	0.99	1.91E-08	5.118	1215.67

APPENDIX C
DBDT TEST RESULTS

Table C-1 DBDT Test Results for Dense Graded Asphalt Mixtures

Types/ Aging Con.	Temp.	m-value	D_1 (1/psi)	St (Mpa)	M_R (Gpa)	FE (kJ/m^3)	$DCSE_f$ (kJ/m^3)	Creep Rate (1/psi-sec)	D(t) (1/GPa)	Failure Strain (με)
Dense (Unmod) ST	-10°C	0.435	7.73E-08	4.81	21.37	0.75	0.41	6.82E-10	0.275	302.11
	0°C	0.545	2.66E-07	4.98	15.12	1.67	1.18	6.23E-09	1.708	612.43
	5°C	0.568	4.39E-07	4.67	13.17	3.24	2.53	1.26E-08	3.261	1051.09
	10°C	0.659	7.14E-07	4.56	10.25	4.38	3.85	4.45E-08	9.850	1449.85
Dense (Unmod) LT	-10°C	0.381	1.11E-07	5.09	24.80	0.86	0.47	5.88E-10	0.272	303.17
	0°C	0.497	1.88E-07	4.97	18.32	1.52	1.07	2.89E-09	0.892	527.24
	5°C	0.524	2.91E-07	4.54	15.52	2.03	1.56	5.69E-09	1.623	756.12
	10°C	0.543	5.04E-07	4.46	11.71	2.30	1.82	1.17E-08	3.162	872.13
Dense (Mod) ST	-10°C	0.326	2.16E-07	6.04	20.88	1.39	0.89	6.70E-10	0.346	403.75
	0°C	0.481	2.36E-07	5.97	16.79	2.76	2.12	3.14E-09	0.996	784.61
	5°C	0.562	3.29E-07	5.86	12.83	4.92	4.25	9.00E-09	2.371	1344.09
	10°C	0.599	4.96E-07	5.48	10.69	7.14	6.57	1.86E-08	4.549	1961.02
Dense (Mod) LT	-10°C	0.322	1.29E-07	5.54	20.61	1.23	0.68	3.83E-10	0.221	386.82
	0°C	0.449	1.87E-07	5.71	17.29	2.28	1.67	1.87E-09	0.651	672.70
	5°C	0.458	2.78E-07	5.45	18.55	3.12	2.56	3.02E-09	1.004	922.83
	10°C	0.466	3.67E-07	5.28	12.15	3.38	2.87	4.26E-09	1.376	1035.28

Table C-2 DBDT Test Results for Open Graded Asphalt Mixtures

Types/ Aging Con.	Temp.	m-value	D_1 (1/psi)	St (Mpa)	M_R (Gpa)	FE (kJ/m^3)	$DCSE_f$ (kJ/m^3)	Creep Rate (1/psi-sec)	D(t) (1/GPa)	Failure Strain (με)
FC-5 (FLime) ST	-10°C	0.230	3.26E-07	3.22	12.78	0.48	0.20	3.69E-10	0.280	266.80
	0°C	0.408	4.21E-07	3.14	9.97	0.82	0.46	2.87E-09	1.069	444.88
	5°C	0.582	4.31E-07	3.04	9.56	1.11	0.84	1.40E-08	3.539	586.09
	10°C	0.616	6.28E-07	2.97	7.29	1.39	1.02	2.72E-08	6.455	764.92
FC-5 (FLime) LT	-10°C	0.268	2.09E-07	2.59	13.97	0.39	0.19	3.55E-10	0.241	271.73
	0°C	0.366	4.00E-07	2.77	11.20	0.50	0.23	1.83E-09	0.775	316.37
	5°C	0.456	4.58E-07	2.77	9.37	0.74	0.51	4.86E-09	1.595	440.72
	10°C	0.471	6.40E-07	2.62	7.78	1.14	0.91	7.77E-09	2.443	598.35
FC-5 (NGran) ST	-10°C	0.330	2.92E-07	2.41	12.17	0.38	0.19	9.38E-10	0.461	277.24
	0°C	0.513	2.74E-07	2.3	8.85	0.39	0.22	4.89E-09	1.429	301.30
	5°C	0.530	6.28E-07	2.22	7.71	0.72	0.53	1.30E-08	3.598	537.53
	10°C	0.614	8.80E-07	2.22	6.03	1.23	0.96	3.77E-08	8.941	905.09
FC-5 (NGran) LT	-10°C	0.245	4.45E-07	2.21	10.83	0.28	0.09	5.94E-10	0.400	228.00
	0°C	0.431	3.94E-07	2.34	9.64	0.41	0.21	3.33E-09	1.169	315.00
	5°C	0.475	7.80E-07	2.65	7.61	0.83	0.55	9.88E-09	3.064	531.66
	10°C	0.609	7.51E-07	2.60	7.23	1.20	0.97	3.08E-08	7.384	742.24

APPENDIX D
CREEP PARAMETERS FROM SUPERPAVE IDT AND DBDT TESTS

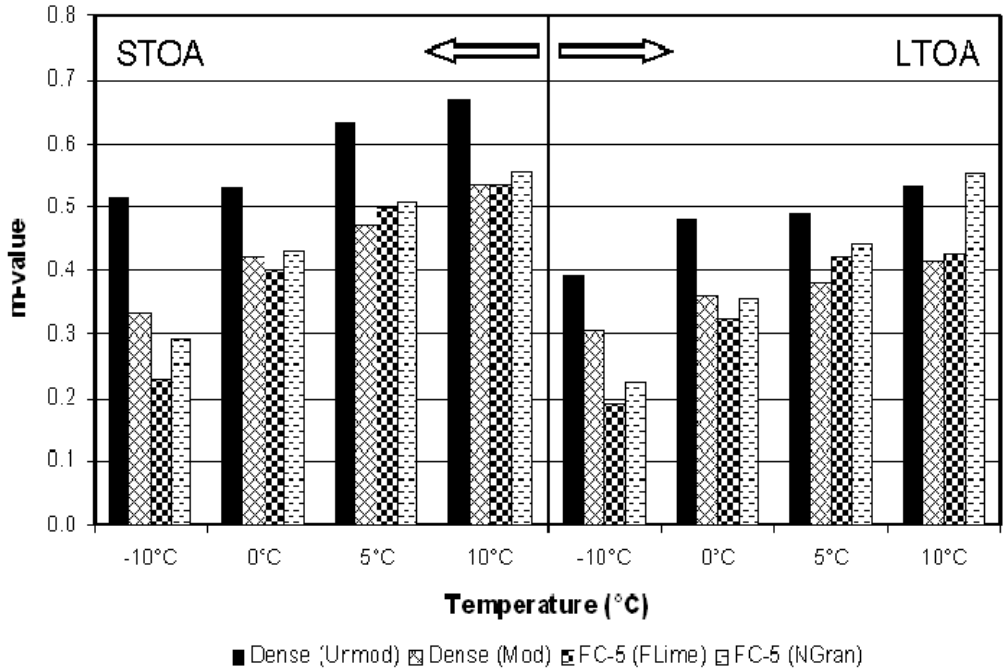

Figure D-1 m-value from IDT Test

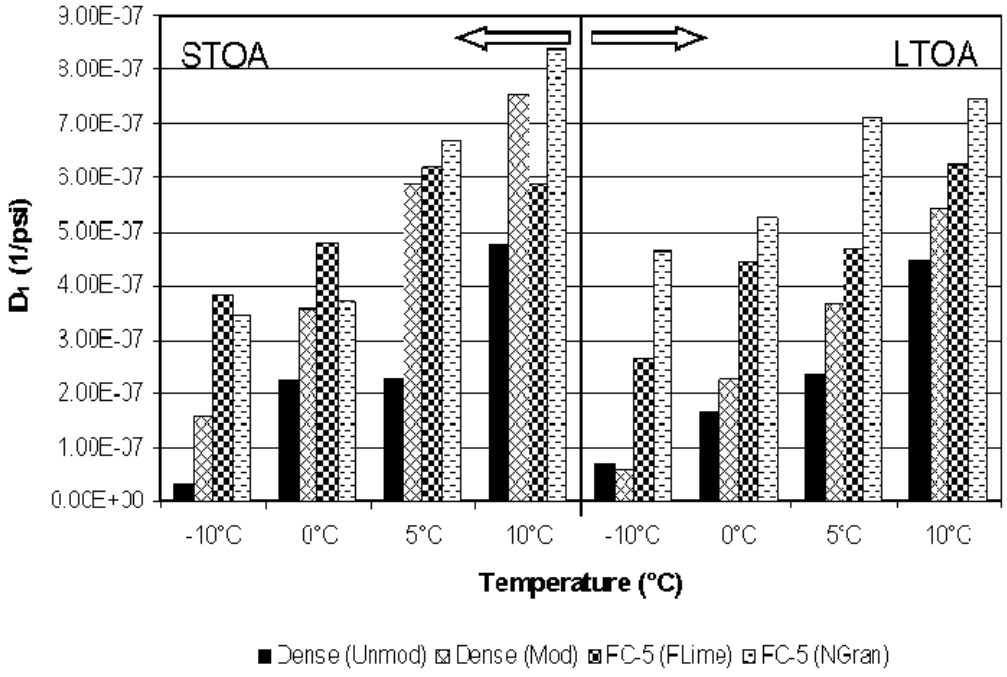

Figure D-2 D_1 from IDT Test

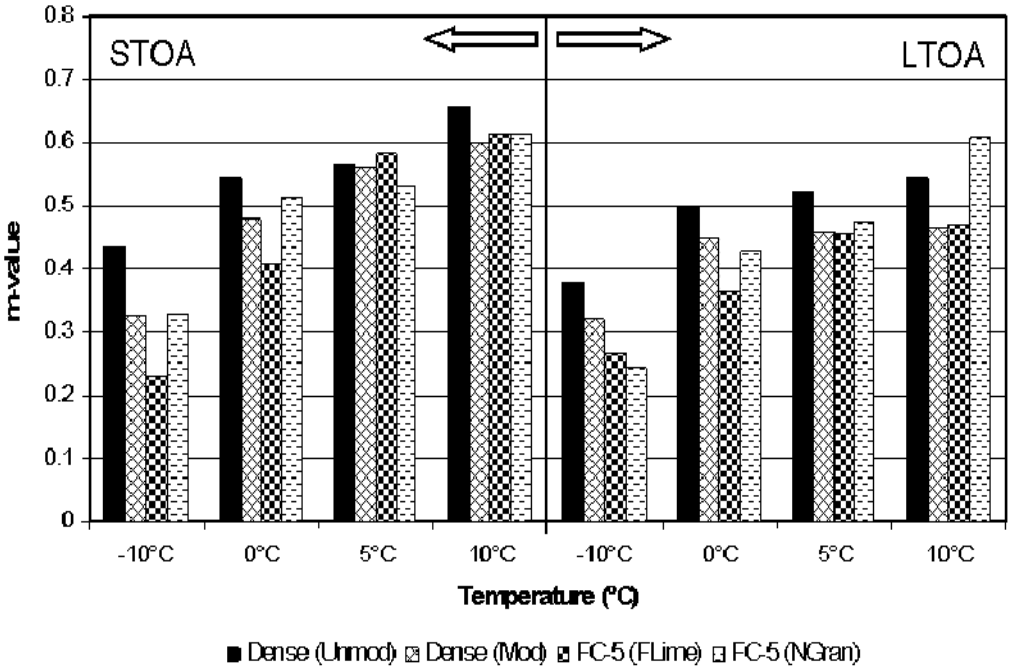

Figure D-3 m-value from DBDT Test

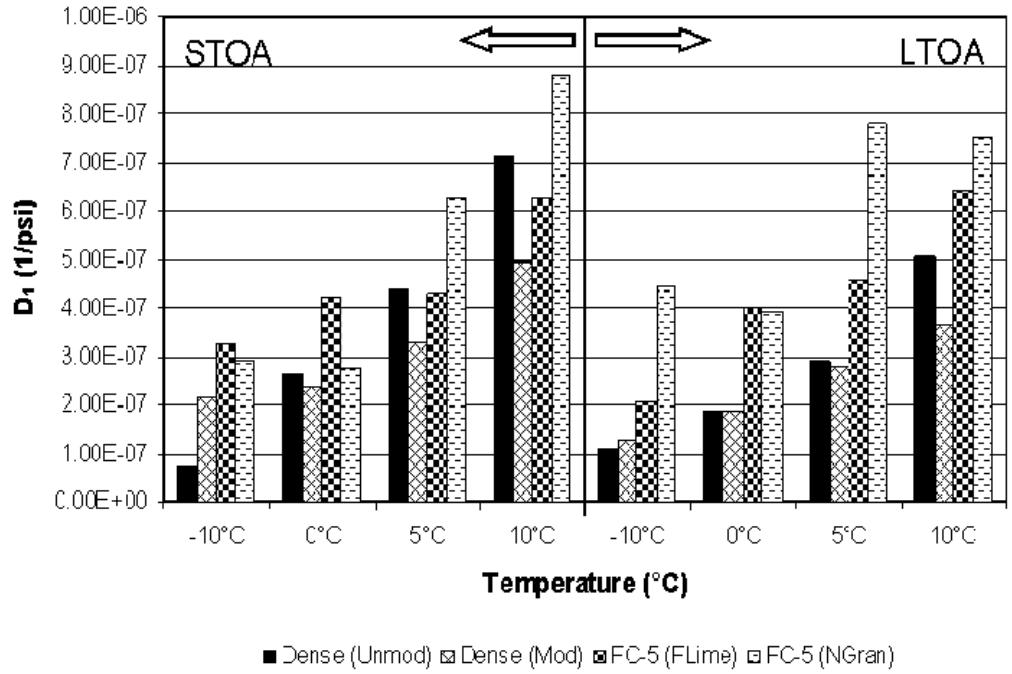

Figure D-4 D_1 from DBDT Test

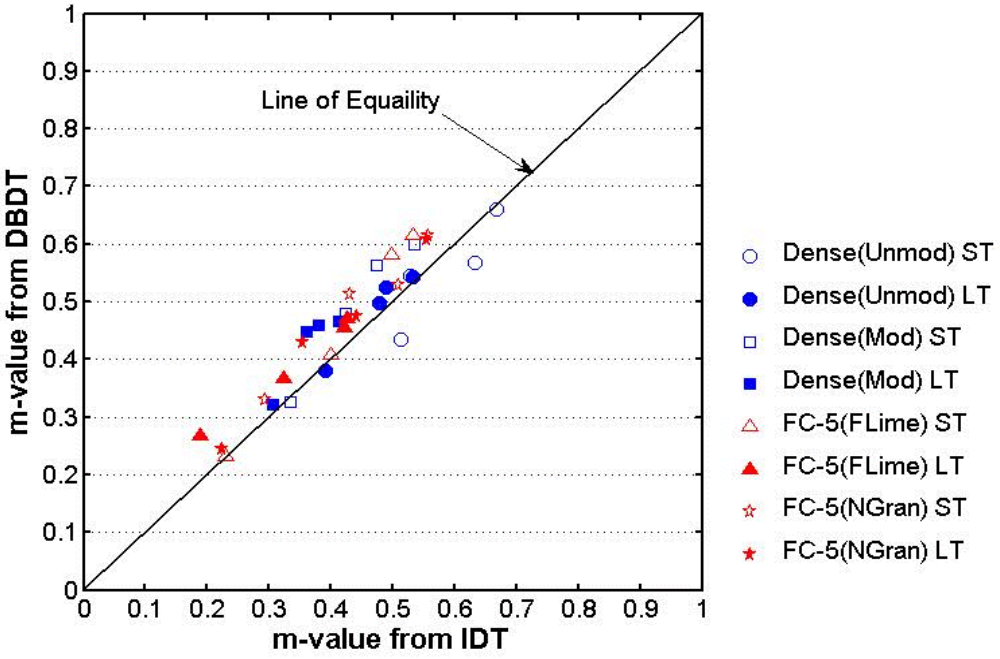

Figure D-5 m-value from IDT and DBDT Tests

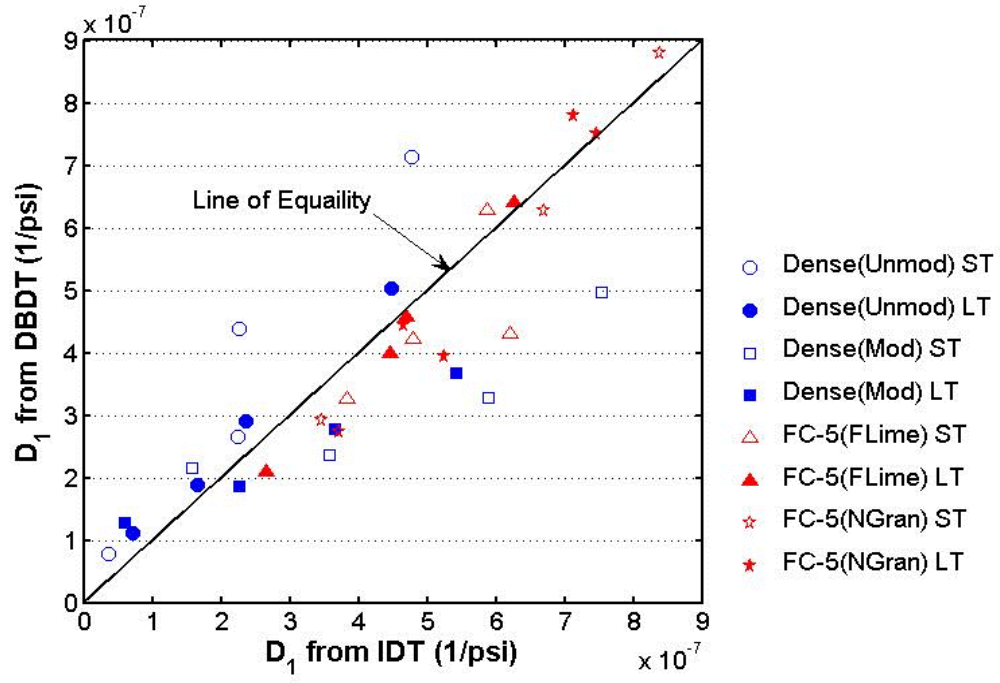

Figure D-6 D_1 from IDT and DBDT Tests

APPENDIX E
CALCULATION OF THE AMOUNT OF INTERLAYER MATERIAL (TACKCOAT/NOVABOND)

Cross section area of the specimen:

$A = \pi r^2 = \pi \times 7.5^2 = 176.71\, cm^2$

$1\ yard^2 = 8361.27\ cm^2; 1\ gallon = 3785.41\, cm^3;$
$1\ gallon/yd^2 = 3785.41\, cm^3 / 8361.27\ cm^2 = 0.453\, cm^3/cm^2$

Mass of asphalt residual painted, $mass = application\ rate \times 0.453 \times 176.71 \times P_b$

$$mass = 80.05 \times application\ rate \times P_b$$

Specific gravity P_b of asphalt residual is around 1.0. Application rate for conventional tack coat is selected as $0.045\ gallon/yd^2$ for open-graded friction course according to 2007 FDOT Standard Specifications for Road and Bridge Construction Section 300. In the emulsion, like RS-1, the amount of asphalt residual (AC-20) determined by distillation is 55%.

Mass of AC-20 applied: $mass = 80.05 \times 0.045 \times 1.0 \times 0.55 = 1.98\ grams$

Application rate for Novabond tack is selected as 0.30 for open graded friction course. In the emulsion, the amount of asphalt residual (SBS polymer modified asphalt) determined by distillation is 63%.

Mass of modified asphalt applied: $mass = 80.05 \times 0.30 \times 1.0 \times 0.63 = 15.2\ grams$

APPENDIX F
EVALUATION OF INTEGRITY OF ASPHALT MIXTURE DUE TO ADDITIONAL COMPACTION

Table F-1 Superpave IDT Test Results

Project Name	m-value	D_1	S_t (Mpa)	M_R (Gpa)	FE (kJ/m^3)	$DCSE_f$ (kJ/m^3)	$DCSE_{MIN}$ (kJ/m^3)	ER	Creep Rate (1/psi-sec)	Creep Rate (1/psi-sec)
50 Gyrations	0.554	5.62E-07	2.77	12.37	4.1	3.8	2.173	1.74	1.43E-08	
100 Gyrations	0.564	4.70E-07	2.80	14.05	3.2	2.9	1.918	1.52	1.30E-08	1.28E-08
150 Gyrations	0.530	5.26E-07	3.00	13.40	5.1	4.8	1.835	2.60	1.08E-08	
No Re-Compaction: Replicate 1	0.474	1.03E-06	2.60	11.21	5.0	4.7	2.458	1.91	1.29E-08	
No Re-Compaction: Replicate 2	0.618	4.17E-07	2.76	12.18	3.5	3.2	2.227	1.43	1.84E-08	1.51E-08
No Re-Compaction: Replicate 3	0.547	5.74E-07	2.67	14.12	3.1	2.8	2.110	1.35	1.37E-08	

Note: 50 gyrations, 100 gyrations, and 150 gyrations denote the additional amount of gyrations applied to compact the Superpave mixture on top of the dense-graded mixture.

APPENDIX G
CALCULATION OF MASS FOR COMPACTION OF OPEN GRADED ASPHALT MIXTURE

Assume compacted open-graded mixture height is H_{OGFC}; air void content is AC_{OGFC}; maximum specific gravity is Gmm_{OGFC}; Mass of open-graded mixture is M_{OGFC}; Gyratory compaction mold inner diameter is D; base material height is H_{base},

$$M_{OGFC} = V_{asphal+aggregate} \times Gmm_{OGFC}$$
$$= \pi \times (D/2)^2 \times H_{OGFC} \times (1 - AC_{OGFC}) \times Gmm_{OGFC}.$$

This compaction is based the compacted specimen height, $H_{OGFC} + H_{base}$, but not the number of gyrations.